frontiers | Research Topics

Genetics, genomics, and breeding of edible mushrooms in Asia

Edited by
Chenyang Huang, Tadanori Aimi and Vikineswary Sabaratnam

Published in
Frontiers in Microbiology
Frontiers in Genetics

ISSN 1664-8714
ISBN 978-2-8325-4692-5
DOI 10.3389/978-2-8325-4692-5

About Frontiers

Frontiers is more than just an open access publisher of scholarly articles: it is a pioneering approach to the world of academia, radically improving the way scholarly research is managed. The grand vision of Frontiers is a world where all people have an equal opportunity to seek, share and generate knowledge. Frontiers provides immediate and permanent online open access to all its publications, but this alone is not enough to realize our grand goals.

Frontiers journal series

The Frontiers journal series is a multi-tier and interdisciplinary set of open-access, online journals, promising a paradigm shift from the current review, selection and dissemination processes in academic publishing. All Frontiers journals are driven by researchers for researchers; therefore, they constitute a service to the scholarly community. At the same time, the *Frontiers journal series* operates on a revolutionary invention, the tiered publishing system, initially addressing specific communities of scholars, and gradually climbing up to broader public understanding, thus serving the interests of the lay society, too.

Dedication to quality

Each Frontiers article is a landmark of the highest quality, thanks to genuinely collaborative interactions between authors and review editors, who include some of the world's best academicians. Research must be certified by peers before entering a stream of knowledge that may eventually reach the public - and shape society; therefore, Frontiers only applies the most rigorous and unbiased reviews. Frontiers revolutionizes research publishing by freely delivering the most outstanding research, evaluated with no bias from both the academic and social point of view. By applying the most advanced information technologies, Frontiers is catapulting scholarly publishing into a new generation.

What are Frontiers Research Topics?

Frontiers Research Topics are very popular trademarks of the *Frontiers journals series*: they are collections of at least ten articles, all centered on a particular subject. With their unique mix of varied contributions from Original Research to Review Articles, Frontiers Research Topics unify the most influential researchers, the latest key findings and historical advances in a hot research area.

Find out more on how to host your own Frontiers Research Topic or contribute to one as an author by contacting the Frontiers editorial office: frontiersin.org/about/contact

Genetics, genomics, and breeding of edible mushrooms in Asia

Topic editors

Chenyang Huang — Institute of Agricultural Resources and Regional Planning, Chinese Academy of Agricultural Sciences, China

Tadanori Aimi — Tottori University, Japan

Vikineswary Sabaratnam — University of Malaya, Malaysia

Citation

Huang, C., Aimi, T., Sabaratnam, V., eds. (2024). *Genetics, genomics, and breeding of edible mushrooms in Asia*. Lausanne: Frontiers Media SA.

doi: 10.3389/978-2-8325-4692-5

Table of contents

frontiers | Frontiers in Microbiology

TYPE Editorial
PUBLISHED 18 March 2024
DOI 10.3389/fmicb.2024.1390845

OPEN ACCESS

EDITED AND REVIEWED BY
John R. Battista,
Louisiana State University, United States

*CORRESPONDENCE
Chenyang Huang
huangchenyang@caas.cn

RECEIVED 24 February 2024
ACCEPTED 05 March 2024
PUBLISHED 18 March 2024

CITATION
Huang C, Sabaratnam V and Aimi T (2024) Editorial: Genetics, genomics, and breeding of edible mushrooms in Asia.
Front. Microbiol. 15:1390845.
doi: 10.3389/fmicb.2024.1390845

Editorial: Genetics, genomics, and breeding of edible mushrooms in Asia

Chenyang Huang[1,2,3]*, Vikineswary Sabaratnam[4] and Tadanori Aimi[5]

[1]Institute of Agricultural Resources and Regional Planning, Chinese Academy of Agricultural Sciences, Beijing, China, [2]State Key Laboratory of Efficient Utilization of Arid and Semi-arid Arable Land in Northern China, Beijing, China, [3]Key Laboratory of Microbial Resources, Ministry of Agriculture and Rural Affairs, Beijing, China, [4]Mushroom Research Centre, Institute of Biological Sciences, Faculty of Science, Universiti Malaya, Kuala Lumpur, Malaysia, [5]Faculty of Agriculture, Tottori University, Tottori, Japan

KEYWORDS

edible mushrooms, Asia, genetics, genomics, breeding

Editorial on the Research Topic
Genetics, genomics, and breeding of edible mushrooms in Asia

Mushrooms are unique, as described by Chang and Miles (1989) in the following quote: "Without leaves, without buds, without flowers, yet, they form fruit; as a food, as a tonic, as a medicine, the entire creation is precious". Influenced by different histories and cultures, Asians prefer to eat edible mushrooms. Consequently, in Asia, both the scale of production and the level of cultivation technology used are very high. The edible mushroom industry in Asia accounts for more than 85% of the world's total production. Research on the genetics, genomics, and breeding of edible mushrooms in Asia is growing rapidly. The theme of this Research Topic is to gather the progress of research conducted on Asian edible mushrooms. It is gratifying that the research on Asian edible mushrooms is conducted in an all-round manner.

In terms of species

Asians not only eat and study button mushrooms, there are more species, but also currently commercially cultivated nearly 100 species of mushrooms. Eight species were studied in this Research Topic: the bulk species are *Pleurotus ostreatus* (Liu et al.), *Pleurotus cornucopiae* (Qi et al.), *Auricularia heimuer* (Qian et al.), and *Auricularia cornea* (Ma et al.); the rare species are morels (*Morchella* spp.) (Chen et al.) and *Hymenopellis radicata* (Cao et al.); the medicinal species are *Ganoderma sichuanense* (Li et al.) and *Inonotus hispidus* (Wang et al.).

From the perspective of the entire industrial chain

This Research Topic consists of five parts. 1. The first part focuses on genomics. Wang et al. present works on genomic comparison between two *Inonotus hispidus* strains isolated from growing in different tree species. Comparative genomics showed that the coding genes and the total number of genes annotated in different databases of *Fraxinus mandshurica* were higher than that of *Morus alba*.

Ma et al. present works on high-quality genome assembly and multi-omics analysis of the pigment synthesis pathway in *Auricularia cornea*. The results showed that there were numerous inversions and translocations between homologous regions of white/purple *A. cornea*. The purple strain synthesized pigment via the shikimate pathway. Cao et al. present works on the population genetic structure of *Hymenopellis radicata* germplasm resources based on genome re-sequencing. 2. The second part deals with development and regulation. Qi et al. present works on milR20 that negatively regulates the development of fruit bodies in *Pleurotus cornucopiae*. The results showed that the function of milR20, which targeted pheromone A receptor *g8971,* was involved in the MAPK signaling pathway. 3. The third part focuses on breeding, Qian et al. present works on interspecies hybridization between *Auricularia cornea* cv. Yu Muer and *Auricularia heimuer* cv. Bai Muer through protoplast fusion. The hybrids and their parents showed significant differences in their colony morphology. Yellowish-white primordia were obtained from two hybrids. In my personal opinion, the genetic stability of the hybrids merits further attention. 4. The fourth part deals with the prevention and control of disease and pests. Li et al. present works on the characterization and fungicide sensitivity of *Trichoderma* species causing green mold of *Ganoderma sichuanense* in China. The results showed that Prochloraz manganese showed the best performance against most *Trichoderma* spp. Liu et al. present works on a lectin gene that is involved in the defense of *Pleurotus ostreatus* against the mite predator *Tyrophagus putrescentiae*. The findings shed light on the molecular mechanisms of *P. ostreatus*' defense against the mite predator. 5. The fifth part discusses continuous cropping obstacles. In response to the hottest species of morels in China, the most complex problem of continuous cropping obstacles is proposed to solve the problem. Chen et al. present works on how dazomet changes microbial communities and improves morel mushroom yield under continuous cropping. The results showed that dazomet improves morel mushroom yield under continuous cropping.

Overall, the research on Asian edible mushrooms has entered a period of full-scale outbreak, and we suggest that more and better research will continue to emerge.

At present, this Research Topic is a microcosm of the research on Asian edible mushrooms. In the future, this Research Topic will be a testimony to it.

References

Chang, S. T., and Miles, P. G. (1989). *Edible Mushrooms and their Cultivation*. Boca Raton, FL: CRC Press Inc.

Author contributions

CH: Conceptualization, Funding acquisition, Validation, Writing—original draft, Writing—review & editing. VS: Validation, Writing—review & editing. TA: Writing—review & editing.

Funding

The author(s) declare that financial support was received for the research, authorship, and/or publication of this article. This study was financially supported by the National Key R&D Program of China (2022YFD1200600) and the China Agriculture Research System (CARS20).

Acknowledgments

We deeply thank all the authors and reviewers who have contributed to this Research Topic.

Conflict of interest

The authors declare that the research was conducted in the absence of any commercial or financial relationships that could be construed as a potential conflict of interest.

Publisher's note

frontiers | Frontiers in Microbiology

TYPE Original Research
PUBLISHED 27 April 2023
DOI 10.3389/fmicb.2023.1191500

OPEN ACCESS

EDITED BY
Chenyang Huang,
Chinese Academy of Agricultural Sciences, China

REVIEWED BY
Lining Wang,
Guangdong Academy of Sciences, China
Yan Zhang,
Chinese Academy of Agricultural Sciences (CAAS), China

*CORRESPONDENCE
Cuixin Li
354802569@qq.com
Shaoxuan Qu
qusx@jaas.ac.cn

†These authors have contributed equally to this work

RECEIVED 22 March 2023
ACCEPTED 13 April 2023
PUBLISHED 27 April 2023

CITATION
Liu J, Li H, Luo X, Ma L, Li C and Qu S (2023) A lectin gene is involved in the defense of *Pleurotus ostreatus* against the mite predator *Tyrophagus putrescentiae*. *Front. Microbiol.* 14:1191500. doi: 10.3389/fmicb.2023.1191500

A lectin gene is involved in the defense of *Pleurotus ostreatus* against the mite predator *Tyrophagus putrescentiae*

Junjie Liu[1†], Huiping Li[2†], Xin Luo[2], Lin Ma[2], Cuixin Li[1*] and Shaoxuan Qu[1,2*]

[1]School of Life Sciences, Southwest Forestry University, Kunming, Yunnan, China, [2]Institute of Vegetable Crops, Jiangsu Academy of Agricultural Sciences, Nanjing, China

The storage mite, *Tyrophagus putrescentiae*, found worldwide in many habitats, is an important pest of edible mushrooms. Excessive chemical spraying for pest control has been linked to environmental pollution, health risks, insecticide resistance development, and food safety. Host resistance can be sustainable and cost-effective and provide effective and economical pest control. Previous studies have reported that the oyster mushroom *Pleurotus ostreatus* has evolved effective defense mechanisms against *T. putrescentiae* attack, but the underlying mechanism remains unclear. Here we report that a lectin gene from *P. ostreatus* mycelia, *Polec2*, induced fungal resistance to mite grazing. *Polec2* belongs to a galectin-like lectin classification, encoding a protein with β-sandwith-fold domain. Overexpression of *Polec2* in *P. ostreatus* led to activation of the reactive oxygen species (ROS)/mitogen-activated protein kinases (MAPKs) signaling pathway, salicylic acid (SA), and jasmonate (JA) biosynthesis. The activation resulted in bursts of antioxidant activities of catalases (CAT), peroxidases (POD), superoxide dismutases (SOD), and increased production of SA, JA, jasmonic acid-isoleucine (JA-Ile) and jasmonic acid methyl ester (MeJA), accompanied by reduced *T. putrescentiae* feeding and suppressed its population. We also provide an overview of the phylogenetic distribution of lectins across 22 fungal genomes. Our findings shed light on the molecular mechanisms of *P. ostreatus*' defense against the mite predator and will be useful in investigating the molecular basis of fungi-fungivory interactions and gene mining for pest-resistance genes.

KEYWORDS

fungal lectin, edible fungi, the storage mite, fungal defense, oyster mushroom

1. Introduction

Organisms have evolved efficient defense mechanisms to protect themselves from biotic and abiotic stresses (Naranjo-Ortiz and Gabaldón, 2019). Innate immunity plays a critical role, and hence con-structs the first defensive line, in animals and pathogens. In modern agriculture, cultivating crop varieties with durable and broad-spectrum resistance is an effective strategy (Li et al., 2003; Dangl et al., 2013; Deng et al., 2017). Currently, pests of edible mushrooms are primarily controlled with pesticides, leading to pest resistance problems, pesticide residues, and food safety risks (Wang et al., 2016). Hence, innate immunity can be used to improve edible mushrooms' recalcitrance to pest attacks (Arthur et al., 2014).

Edible mushroom hosts affect the feeding preference, reproduction, longevity, and life table parameters of pests (Kunzler, 2015). The different cultivars of the oyster mushroom *Pleurotus ostreatus* have a significant effect on the biological parameters of the storage mite, *Tyrophagus putrescentiae*, whose infestation reduces mushroom yield (Qu et al., 2015; Hou et al., 2022). Previous studies have reported that plant nutrients impact insect herbivore performance (Wetzel et al., 2016). In our recent work, *P. ostreatus* was shown to have developed several defense systems against *T. putrescentiae* feeding (Li et al., 2022). Fungus *P. ostreatus* coordinated inducible chemical-based defense responses through the reactive oxygen species (ROS)/mitogen-activated protein kinases (MAPKs) signaling pathway, jasmonate (JA) regulation, specific gene expression and protein synthesis, and anti-mite substance metabolism. Furthermore, upregulated genes were related to terpenoid metabolism, including the P450 family genes and those encoding toxins, such as lectins (Li et al., 2022). Fungal volatile terpenes play an important role in the communications of fungus-mite interactions (Li et al., 2018).

Lectins are a group of carbohydrate-binding proteins that can specifically bind polysaccharides, glycoproteins, and glycolipids on cell surfaces (Ji and Nicolson, 1974). Lectins can recognize exogenous carbohydrates and often exhibit anti-competitor, anti-predator, anti-parasite, and anti-pathogen activities. Mushrooms are rich in lectins. Fungi have massive hemagglutinins (early terminology for lectins). Lectins purified from *Gymnopilus* mushrooms were shown to inhibit *Staphylococcus aureus* and *Aspergillus niger*, suggesting a role for lectin in defense (Alborés et al., 2014; Singh et al., 2020).

In earlier research, lectin proteins AAL, MOA, and TAP1 purified through *in vitro* expression from *Aleuria aurantia*, *Marasmius oreades*, and *Sordaria macrospora*, respectively, demonstrated toxicity against *Aphelenchus avenae* and *Bursaphelenchus okinawaensis*. However, CCL2 and CGL2, which are toxic to the nematode *Caenorhabditis elegans*, did not exhibit the same effect on *A. avenae* (Butschi et al., 2010; Tayyrov et al., 2018; Singh et al., 2020). It is also proposed that lectins are involved in the biological activities of mushrooms, including participation in fungal growth, development, mycorrhiza formation, and defense against predators and parasites (Kawagishi et al., 1997). Previous studies have revealed a linkage of lectins and hemolysins to why *Lepista* and *Cantharellus* mushrooms barely attract insects (Pohleven et al., 2011; Varrot et al., 2013). Lectins are mainly enriched in mushrooms' fruit bodies and sclerotia (Wang et al., 2002). Most of them are expressed in the cytoplasm, but cytoplasmic ligands deficiency makes it hard to correspond with endogenous function (Wohlschlager et al., 2014). Meanwhile, the absence of lectins does not affect fungal development (either by knockout or knockdown), demonstrating that its function is exogenous. Massive structural lectin families from fungal fruit bodies have been characterized, mainly galectin, β-trefoil-type, β-propeller-type, actinoporin-type, cyanovirin-N-type, and immunoglobulin-type. Some of these have been reported to have insecticidal properties (Bleuler-Martínez et al., 2011; Plaza et al., 2015; Bleuler-Martinez et al., 2017; Lebreton et al., 2021; Bleuler-Martinez et al., 2022). Lectins abundant in *P. ostreatus* have been widely reported for their anti-tumor activity (Vajravijayan et al., 2020). Crystals of *P. ostreatus* lectin was first reported with a molecular mass of 293 kDa (Chattopadhyay et al., 1999). Then, the structure and function of a *P. ostreatus* lectin named POL is reported that the protein active site requires two adjacent alcohol groups, one in the axial position of the sugar and the other in the equatorial position of the sugar, adjacent to which a calcium-mediated binding loop can be identified (Vajravijayan et al., 2020). Interestingly, a lectin from *P. ostreatus* named *Plp* has been found to be induced by blue light (Perduca et al., 2020). However, *P. ostreatus* anti-predator lectins remain understood limitedly.

In this work, we investigated the defense mechanism of an anti-predator lectin gene, named *Polec2,* which was significantly up-regulated in *P. ostreatus* mycelium after *T. putrescentiae* feeding (Li et al., 2022). To gain an insight into the molecular and biochemical properties of the oyster mushroom against *T. putrescentiae*, we examined effect of *Polec2* overexpression on the mushroom's defense system. The characteristics of this lectin were compared with those anti-predator lectins characterized previously. These findings unveil an important anti-predator activity of *Polec2* and expand a basis of the mushroom's resistance to *T. putrescentiae*.

2. Materials and methods

2.1. Strains and culture conditions

The dikaryotic *P. osteatus* strain CCMSSC00389 (China Center for Mushroom Spawn Standards and Control, CCMSSC; designated WT hereafter) was grown on potato dextrose agar (PDA) at 25°C under darkness for 7 days. For RNA isolation and RNA Sequencing, the vegetative mycelia of the strain were collected after cultivation in 100 ml PDB (potato dextrose broth) in the dark at 25°C for 7 days. For plasmid construction, preparation, and propagation, Escherichia coli DH5α (Tiangen, Beijing, China) was used and grown in LB medium, supplemented with ampicillin (100 μg/ml) or kanamycin (50 μg/ml) at 37°C for 24 h. *Agrobacterium tumefaciens* strain GV3101 (Tiangen, Beijing, China) was grown on minimal medium (MM) at 28°C for 2 days (Lei et al., 2017). An induction medium (IM) with 100 μg/ml of hygromycin (Hyg, Roche, USA) was used to co-cultivate *A. tumefaciens* and protoplasts of *P. ostreatus*. Transformants of *P. ostreatus* were grown on complete medium (CM) for cultivation at 25°C under darkness for 10 days (Lei et al., 2017). Then, for testing response to *T. putrescentiae* grazing, the WT strain and its transformants were cultivated on PDA within a six-well plate for 5 days or wheat grains with a 25 ml conical flask for 10 days at 25°C (Hou et al., 2022).

2.2. Mite stock

The populations of *T. putrescentiae* were maintained at the Institute of Vegetable Research, Jiangsu Academy of Agricultural Sciences, Nanjing, Jiangsu, China. *T. putrescentiae* was reared in a round plastic transparent box (a diameter of 7 cm) containing the vegetative mycelia of *Lentinula edodes* at 26 ± 1°C and 80 ± 5% relative humidity (RH) (Hou et al., 2022). Two months before the experiment, populations to transferred to wheat grain straws of the WT strain and its transformants at 28°C to assess host suitability.

2.3. *Polec2* gene cloning and transplantation

After 7 days of growth on PDA at 25°C, *P. ostreatus* mycelia were harvested and frozen in liquid nitrogen, and then stored

at −80°C. Total RNA was extracted from 0.1 g of each sample using an SV Total RNA isolation kit (Promega, WI, United States), then reverse transcribed to cDNA with a First-stand cDNA Synthesis Kit (Takara, Beijing, China) as described previously (Hou et al., 2022). The *Polec2* sequence was amplified by an I-5TM 2X high-fidelity master mix polymerase (Tsingke, Beijing, China) using the primers PoLec2-1F (5′-ATGCATGACATTAGTACTTAT-3′) and PoLec2-1R (5′-CTATGCGAG-AGGGATGACTAC-3′) designed from the transcriptome data (accession number: PRJNA665192) of the predicted lectin 2 of *P. ostreatus*. The PCR conditions were as follows: 98°C for 5 min, followed by 30 cycles of denaturation at 98°C for 15 s, annealing at 55°C for 10 s, and elongation at 72°C for 40 s, and a final elongation step at 72°C for 10 min. The PCR product was purified and cloned into the pMD19-T vector and then sequenced (Tsingke, Nanjing, China).

The *Polec2* cDNA was purified by agarose gel electrophoresis and ligated to the pCAMBIA1303 vector (Abcam, Shanghai, China). Protoplasts of *P. ostreatus* were prepared as described (Nurziya et al., 2019). The transformation method of *P. ostreatus* was described performed according to Shi et al. (2012). The stability of transformants was evaluated by the relative expression of *Polec2* using quantitative real-time PCR (qRT-PCR) analysis after they were grown on CM agar without hygromycin for five rounds of cultivation. The qRT-PCR primer pairs of *Polec2* were shown in Supplementary Table S1. The β-actin gene was used as an internal standard.

2.4. Phylogenetic analysis

One hundred thirty seven lectin sequences from 22 mushroom species were obtained from the MycoLec module of UniLectin[1] and the NCBI database[2] (Supplementary Table S2), and clustered using the MAFFT tool with a global matching algorithm (the maximum number of iterative refinements was 1,000) (Yamada et al., 2016). The best-fit algorithm was tested using the Modomatic method integrated into iqTree as WAG+R5 (Yamada et al., 2016), which was then used to calculate the genetic evolution tree in iqTree using the maximum likelihood (ML) method with a Bootstrap value of 5,000 times (Whelan et al., 2015; Minh et al., 2020). Tree files were generated and annotated using the iToL online tool (Letunic and Bork, 2021).

2.5. Antioxidant activity assay

Fresh mycelia of the WT strain and its transformants were collected after cultivation on 100 ml PDB at 25°C for 7 days. Using commercially available detection kits (Webiolotech, Nanjing, China), the total antioxidant catalase (CAT) activity, peroxidase (POD) activity, superoxide dismutase (SOD) activity, H_2O_2 content, and malondialdehyde (MDA) content were measured. These tests were performed using 1.0 g of fresh mycelia of each transformant and were repeated four times. The WT strain was used as a control.

2.6. Analysis of hormone content changes

Mycelial samples fresh weight 1.0 g *per capita* were crushed in liquid nitrogen and stored at −80°C in glass tubes. The production of salicylic acid (SA), methyl salicylate (MeSA), jasmonic acid (JA), 12-oxo-phytodienoic acid (OPDA), jasmonic acid-isoleucine (JA-Ile), jasmonic acid methyl ester (MeJA), indole-3-acetic acid (IAA), 3-indole butyric acid (IBA), abscisic acid (ABA), indole-propionic acid (IPA), and isopentenyladenine (IP) were analyzed using a high-performance liquid chromatography–tandem mass spectrometry (HPLC-MS/MS) method with a QTRAP 6500 triple quadrupole mass spectrometer of AB Sciex (Framingham, MA, United States). The pretreatment and detection procedure of samples were performed as described previously (Webiolotech, Nanjing, China) (Li et al., 2022).

2.7. Expression analysis of Key genes in the immune defense system by qRT-PCR

The expression of 14 key genes in the defensive signaling pathway was analyzed in the transgenic strains using an one-step qRT-PCR kit (Takara, Tokyo, Japan) with the Light-cycling 480 Real-Time System (Roche, Switzerland) (Supplementary Table S2). Total RNA of transgenic strains and subjected to Primer Quest™ Tool[3] for qRT-PCR were designed from the *P. ostreatus* CCMSSC0389, PC15 and PC9 reference genome (PRJNA476433, PRJNA670761 and PRJNA81933) and the transcriptome data in Primer 6.0 software (Supplementary Table S2). The PCR condition used 95°C for 2 min, followed by a cycling program of 95°C for 10 s, 58°C for 30 s, and 72°C for 30 s, and then the productions were heat denatured over a 35°C temperature gradient at 2.2°C/s from 60°C to 95°C (Li et al., 2022). The β-actin gene was used as an internal standard. A standard curve was constructed for every set of primers using a cDNA sample diluted using a 10-fold gradient (Supplementary Table S1). The gene expression levels in the WT strain mycelia were the control. Three biological replicates were analyzed per sample. Relative gene expression levels were computed according to the $2^{-\Delta\Delta CT}$ method described by Winer et al. (1999).

2.8. Assay for *Polec2*-overexpressing strains resistance against *Tyrophagus putrescentiae*

Polec2-overexpressing strains resistance against *T. putrescentiae* was assessed as development, survivor ship and host fitness parameters of *T. putrescentiae* reared on the fresh mycelia using at least six replicates of each strain as previously described (Hubert et al., 2013; Hou et al., 2022). Before the start of these tests, *T. putrescentiae* was exposed to the WT strain and transgenic strains for five generations.

2.9. Statistical analysis

The statistical analysis of experimental data was performed using IBM SPSS 26.0 (IBM Corp., NY, United States). The data were

1 https://www.unilectin.eu/mycolec/

2 http://www.ncbi.nlm.nih.gov

3 https://sg.idtdna.com/pages/tools/primerquest

examined for homogeneity of variance before analysis. Differences in the transgenic strains' hormone level, gene expression, antioxidant activity, and the biological parameters of *T. putrescentiae* were evaluated using a one-way ANOVA test, followed by a Waller-Duncan test ($p = 0.05$).

3. Results

3.1. Sequence analysis, gene structure, and phylogenetic analysis of *Polec2*

A total putative full-length cDNA of *Polec2* was cloned (GenBank accession number: OP751397), encoding a putative protein of 431. *Polec2* has a molecular weight of 45.77 KDa and a predicted pI of 8.39. Based on the phylogenetic relationship, 137 lectins from 22 different species of mushroom-forming fungi, including 12 *Agaricales*, two *Boletales*, one *Cantharellales*, one *Polyporales*, and six *Russulales*, were clustered into 8 different groups in the ML tree (Figure 1). Agaricales display the largest variety, spanning over all of 6 classes of lectins. Strong variations in lectin catalogs from *P. ostreatus* are observed depending on the fungal lineage, with 24 lectins were clustered into 5 different classes. Some lectin classes such as Coprinus-like (CCL-like) β-trefoil-type lectins were frequently identified within two *Pleurotus* species. *Polec2* was classified to the galectin-like class with β-sandwich-fold.

Six groups of these proteins were reported to be involved in the fungal defense of the fungal fruit body, including galectins, Coprinus-like, ricin-like, Clitocybe-like, and fungal fruit body lectins (Varrot et al., 2013; Tayyrov et al., 2018; Bleuler-Martinez et al., 2022; Figure 1). For example, lectins with entomotoxic activity, CNL from *Clitocybe nebularis* is Clitocybe-like lectin family, MPL from *Macrolepiota procera* are ricin-like lectin family, CCL2 from *Coprinopsis cinerea* is galectins lectin family, and XCL from *Xerocomellus chrysenteron* is fungal fruit body lectin family (Wohlschlager et al., 2014; Bleuler-Martinez et al., 2022).

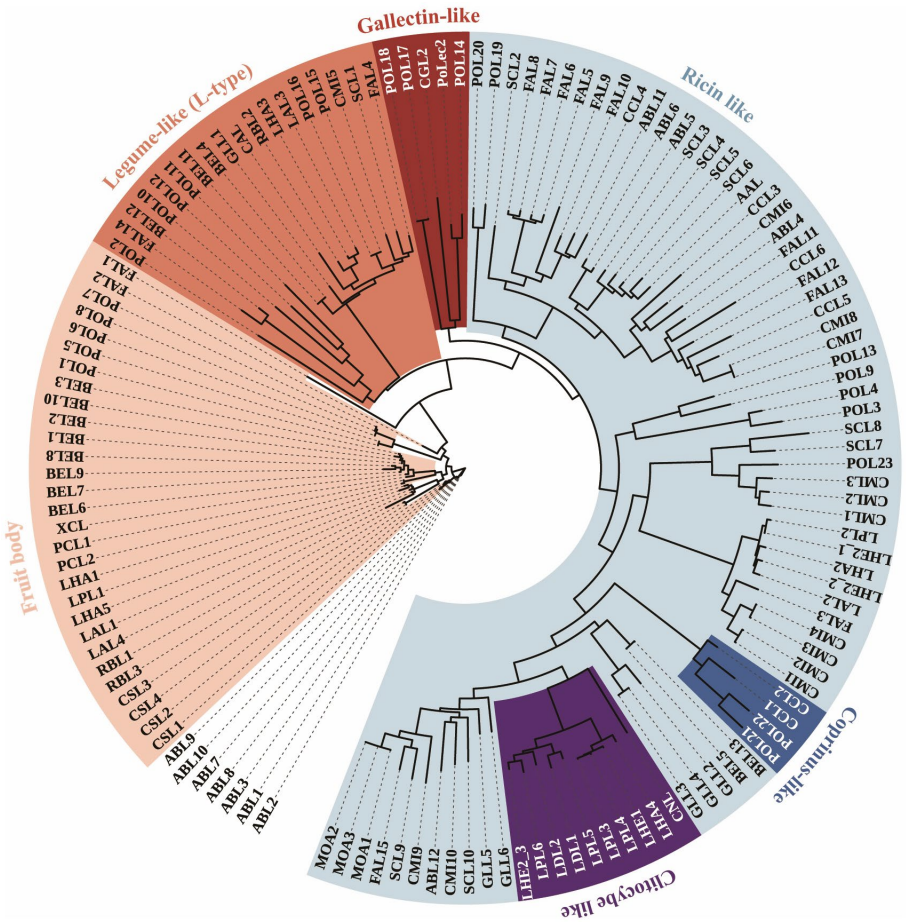

FIGURE 1
Phylogenetic tree of 137 lectin proteins from 22 species in Agaricomycetes. Unrooted phylogenetic tree of lectins protein sequences from *Pleurotus ostreatus* (POL1-23 and PoLec2), *P. cornucopiae* (PCL1 and PCL2), *Agaricus bisporus* (ABL1-8), *Auriculariopsis ampla* (AAL), *Clitocybe nebularis* (CNL), *Coprinellus micaceus* (CML1-10), *C. cinerea* (CCL1-6), *Cubamyces menziesii* (CML1-3), *Cyathus striatus* (CSL1-4), *Flammula alnicola* (FAL1-15), *Schizophyllum commune* (SCL1-10), *Boletus edulis* (BEL1-13), *Xerocomellus chrysenteron* (XCL), *Cantharellus anzutake* (CAL), *Ganoderma leucocontextum* (GLL1-6), *Lactarius akahatsu* (LAL1-4), *L. deliciosus* (LDL1 and LDL2), *L. hatsudake* (LHA1-5), *L. hengduanensis* (LHE1 and LHE2_1-LHE2_3), *L. pseudohatsudake* (LPL1-6), *Macrolepiota procera* (MOA1 and MOA2), and *Russula brevipes* (RBL1-3). The outer ring indicates the classes of lectins, including Galectins (shaded in red), Coprinus-like (shaded in blue), Ricin-like (shaded in cyan), Clitocybe-like (shaded in purple), Legume-like (shaded in orange), and Fungal fruit body (shaded in pink) lectins. The tree is displayed using the iTOL web server.

Furthermore, the ricin-like lectin family is the major group (46.7%) of 137 proteins, those mostly contain β-trefoil fold structures from *Schizophyllum commune*, *Coprinellus micaceus*, *Flammula alnicola*, etc., in more closely related branches, which are likely to be of value in providing potential insecticidal activity. Structurally, POL21 and POL22 from *P. ostreatus* had higher homologies to CCL2, having potential for entomotoxic activity that remains to be verified.

3.2. Regulation of antioxidant enzyme activities

Subsequently, we obtained five stable transformants from six overexpressing strains (named L1 to L6) of *Polec2* in *P. ostreatus* by the *Agrobacterium*-mediated transformation. According to the qRT-PCR analysis, the transformants all showed significantly elevated *Polec2* expression relative to the WT strain, with L1, L2 and L6 being most upregulated (Figure 2A). These three transformants were further used to evaluate their bioactivity, including hormone level, gene expression, and antioxidant activity.

ROS is important in various biological functions, including cell survival, cell growth, proliferation, differentiation, signaling, immune response, and other physiological responses (Zuo et al., 2015). Three key antioxidant enzymes involved in the biosynthesis and degradation of ROS were measured to investigate the antioxidative effects of *Polec2*. For L1 and L6 strains, SOD, POD, and CAT activities of fresh mycelium significantly increased than those in WT strain ($F_{3,15} = 178.2–1116.1$, $p < 0.001$) (Figure 2C). An increase in the content of H_2O_2 ($F_{3,15} = 65.9$, $p < 0.001$) was also observed (Figure 2B). MDA is one of the most significant byproducts of membrane lipid peroxidation, and its activity was strongly activated in the transformants ($F_{3,15} = 18.7$, $p < 0.01$), which subtly indicated the membrane systems' greater stress resistance (Figure 2C). In addition, we investigated the expression levels of the key genes involved in the ROS metabolism, including the NADPH oxidases catalytic subunits coding genes, *nox1* and *nox2*, and the catalase genes *cat1* and *cat2*. Compared to unaffected *nox1* expression, the expression of *nox2* was abolished in three transformants, accompanied by differential downregulation of *cat1* and *cat2* (Figure 2D). Compared with L1 and L6 strains, CAT activities of L2 strain showed no difference with WT (Figure 2C).

Furthermore, *Polec2* overexpression activated gene expression in the mitogen-activated protein kinases (MAPK) pathway (Figure 2E). MAPK kinases HOG1 and MPK1, and guanine nucleotide exchange factors *pho1*, *scf3*, and *cdc24* were all significantly increased in the transformant L1, ranging from 2.54 to 8.0-fold, whereas *mpk1*, *hog1*, *pho1*, and *scf3* were not significantly changed in the transformant L2 and L6 (Figure 2E). The relative expression of serine/threonine-protein kinases PKH1 was all significantly increased in the three transformants. ROS/MAPKs signaling pathway plays an important role in direct anti-fungivory defenses of the oyster mushroom.

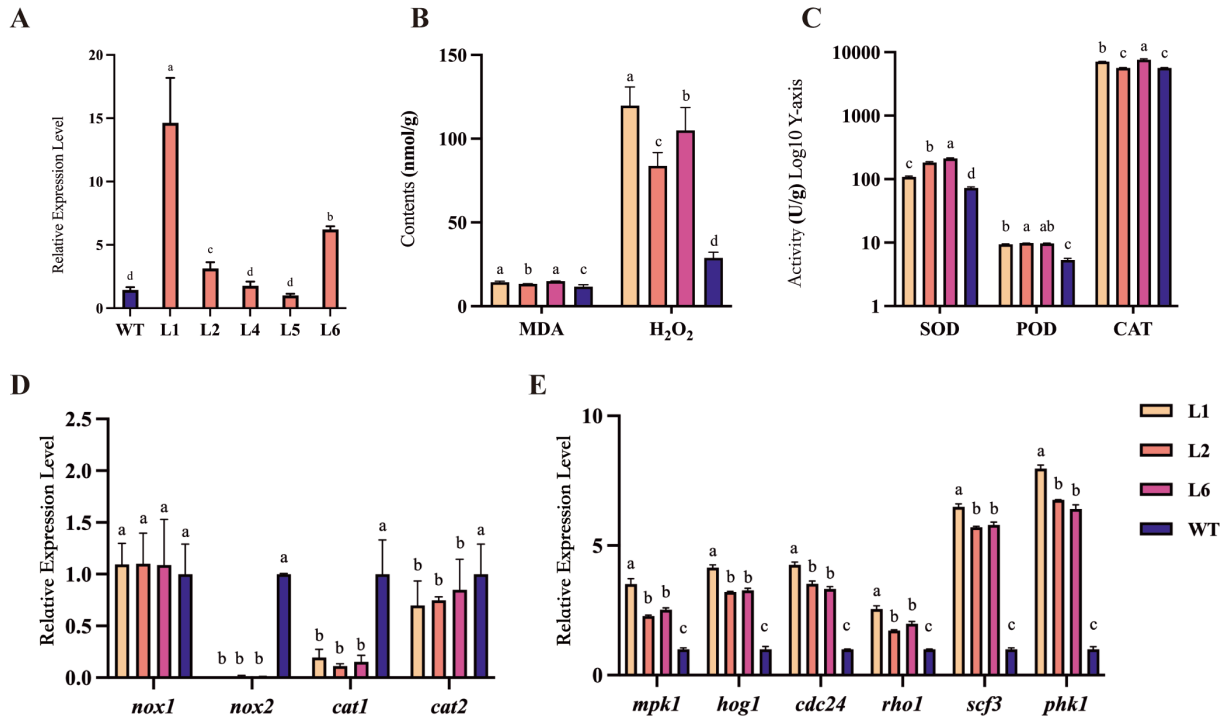

FIGURE 2
The changes of antioxidant enzyme activities in *Polec2* overexpressing strains. **(A)** Relative expressions of *Polec2* in the six transformants (L1 to L6) after grown on complete medium without hygromycin for five rounds of cultivation. **(B)** Change in malondialdehyde (MDA) and hydrogen peroxide (H_2O_2) contents. **(C)** Change in superoxide dismutase (SOD), peroxidase (POD), and catalase (CAT) activities. **(D)** Expression analysis of genes in the reactive oxygen species (ROS) metabolism, including the NADPH oxidases catalytic subunits genes *nox1* and *nox2*, and the catalase genes *cat1* and *cat2*. **(E)** Expression analysis of genes in the mitogen-activated protein kinases (MAPK) signaling pathway, including MAPKs genes *hog1* and *mpk1*, serine/threonine-protein kinases *Pkh1*, and guanine nucleotide exchange factors *pho1*, *scf3*, and *cdc24*. Letters indicate significant differences from the WT strain ($p<0.05$, Waller-Duncan test).

3.3. Activation of salicylic acid- and jasmonic acid-signaling pathways in *Polec2* overexpressing strains

To examine the effect of *Polec2* on *P. ostreatus* defense against *T. putrescentiae*, we measured the levels of JA, JA-Ile, OPDA, MeJA, SA, MeSA, IAA, ABA, IBA, IPA, and IP in *Polec2* overexpressing strains. Compared with the WT strain, the levels of SA, JA, JA-Ile, MeJA, IP and IPA were significantly higher ($F_{3,15} = 16.705–252.359$, $p < 0.0001$), whereas the levels of MeSA, OPDA, IAA, IBA, and ABA were significantly lower ($F_{3,15} = 23.828–2053.547$, $p < 0.0001$, respectively; Figure 3A). Moreover, the level of SA rose over 50-fold. The expression of the SA- and JA-signaling pathways proteins, and phenylalanine ammonia-lyase 1 (PAL1) were significantly up-regulated (4.33-fold, 12.47-fold, and 1.77-fold, respectively), whereas PAL2 not increased in the transformants. Lipoxygenase 1 and 2 (LOX1 and LOX2) were not induced (Figure 3B). In contrast, *Polec2* overexpression strongly strengthens SA- and JA-dependent defense of *P. ostreatus*.

3.4. *Polec2*-overexpressing strains resistance analysis

To investigate how *Polec2* influences *T. putrescentiae* feeding, growth, development and population increase, infestation tests were performed on L1, L2 and L6 transformants. The mycelium of the WT strain was almost depleted after 48 h of *T. putrescentiae* feeding, but the mycelium of the transformants L1, L2 and L6 had only small holes (Figure 4A). By careful examination, we could see that the mites are buried and are feeding on the area where the mycelium nuclei have twisted into clusters. The mites could be seen feeding on the mycelium that had knotted into clusters but became entangled, then died (Figure 4B). On the contrary, the white mycelium of WT strain was significantly reduced and sparse after 48 h of mite feeding (Figure 4A). However, we found that the mites could complete the life history in the transformants, and the total developmental stages were not significantly different from the WT strain (Table 1). Instead of growth, the hatchability and survival of *T. putrescentiae* were significantly reduced (by 12–22%) (Table 1). The rate of population increase of *T. putrescentiae* was estimated and incubated in 25 ml culture flasks with 0.25 g grains of tested strains for 21 d at 25°C and 85% RH. The population rate of increase was strongly negative for the transformants, about 25% of that for the WT strain (Figure 4C).

4. Discussion

Fungi are eukaryotic organisms that absorb nutrients and can be found in any ecological niche. Fungi have been studied in the

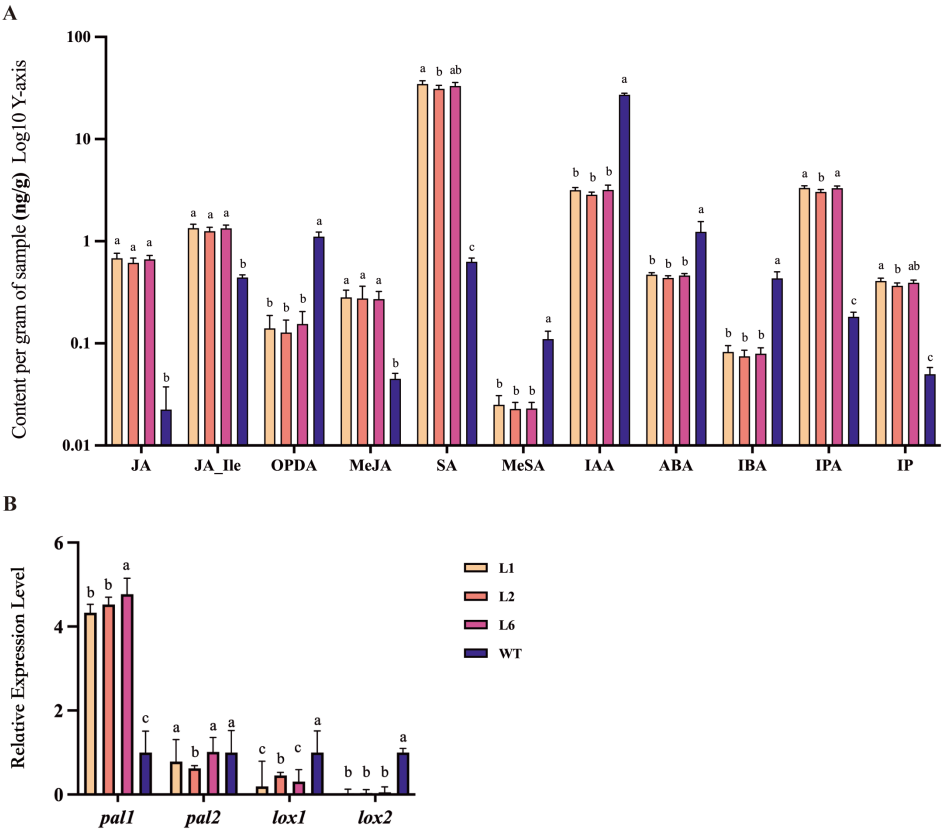

FIGURE 3
The changes of hormone levels in *Polec2* overexpressing strains (L1, L2 and L6). **(A)** Change in different hormone levels (using a log scale), including the production of salicylic acid (SA), methyl salicylate (MeSA), jasmonic acid (JA), 12-oxo-phytodienoic acid (OPDA), jasmonic acid-isoleucine (JA-Ile), jasmonic acid methyl ester (MeJA), indole-3-acetic acid (IAA), 3-indole butyric acid (IBA), abscisic acid (ABA), in-dolepropionic acid (IPA), and isopentenyladenine (IP). **(B)** Expression analysis of genes in the SA- and JA-signaling pathways, including two phenylalanine ammonia-lyases *pal1* and *pal2* for SA biosynthesis and two Lipoxygenases *lox1* and *lox2* for JA biosynthesis. Letters indicate significant differences from the WT strain ($p<0.05$, Waller-Duncan test).

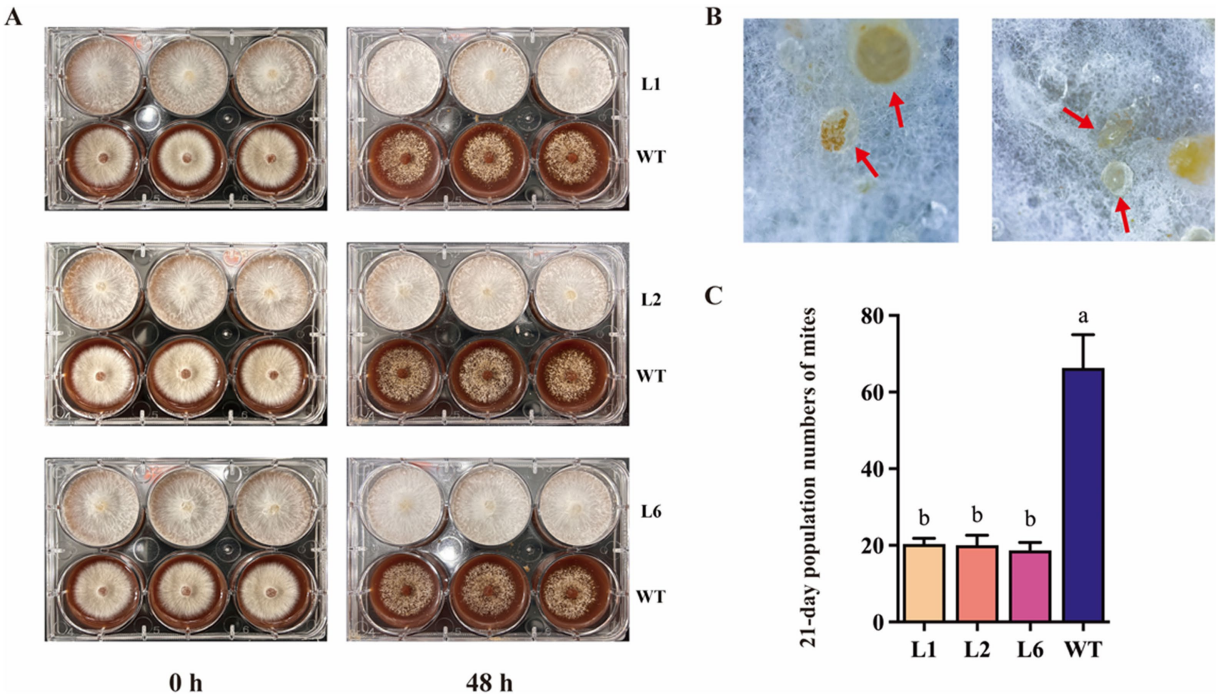

FIGURE 4
Polec2 overexpressing strains resistance to *T. putrescentiae*. **(A)** Infestation tests in *Polec2* overexpressing strains (framed into blue square). **(B)** *T. putrescentiae* (red arrow) was buried in the mycelium of *Polec2* overexpressing strains. **(C)** The 21-day population numbers of *T. putrescentiae* feeding on *Polec2* overexpressing strains (L1, L2 and L6). Letters indicate significant differences from the WT strain ($p<0.05$, Waller-Duncan test).

TABLE 1 The developmental durations (days) for *T. putrescentiae* reared on *Polec2* overexpressing strains at 25°C and 85% RH.

Strains	Egg	Larva	Deutonymph	Tritonymph	Total	Hatchability	Mortality
L1	2.51 ± 0.77	2.5 ± 0.68a	3.11 ± 1.4	2.26 ± 0.79ab	10.54 ± 0.94	82.43 ± 3.82b	82.39 ± 3.08b
L2	3.12 ± 3.3	1.91 ± 0.89ab	3.31 ± 3.56	1.1 ± 2.41b	9.99 ± 1.54	85.33 ± 6.91b	79.41 ± 2.79b
L6	2.1 ± 0.58	1.77 ± 0.53ab	2.28 ± 0.96	3.5 ± 1.25a	10.03 ± 1.47	85.73 ± 3.08b	76.31 ± 2.16b
WT	2.28 ± 0.5	1.54 ± 1.27b	3.32 ± 0.77	2.36 ± 1.35ab	9.96 ± 2.1	98.54 ± 1.84a	98.43 ± 2.61a

Values are presented as mean ± SD.
Means within a column followed by the same letter are significantly different (Waller-Duncan test: $p < 0.05$).

laboratory as model systems in every aspect of the biological sciences due to their simple and rapid life cycles, yet complex genetics, metabolism, and morphology (Biedermann and Vega, 2020). Fungi frequently use predation, parasitism, and antagonism to suppress their competitors, including agricultural pests (Ambethgar, 2009). Most fungi used to control agricultural pests are Hyphomycetes, capable of infecting and killing insects and are thus referred to entomopathogenic fungi (Shamshad, 2010). Conversely, some pests can destroy edible fungal production, which is already a significant economic crop worldwide (Qu et al., 2015; Panevska et al., 2019). To avoid harmful chemicals, further research is needed on integrated pest management in mushrooms, biological control, and in-depth insight into edible fungal defense mechanisms.

As a part of their chemical defense, edible fungi have been shown to produce terpenoids, glycans, aegerolysins, lectins, and other substances (Kunzler, 2015; Lebreton et al., 2021; Li et al., 2022). Several aegerolysins have been found to have insecticidal activity in *Pleurotus* mushrooms, including ostreolysin A (OlyA) and pleurotolysin A (PlyA), pleurotolysin B (PlyB), and erylysin A (EryA) with the membrane-attack-complex/ perforin domain, which can bind to insect cells and artificial lipid membranes and toxicity to western corn root-worm larvae and adults and Colorado potato beetle larvae (Wohlschlager et al., 2014; Panevska et al., 2019). More than 13 types of lectins have been found in the genome of *P. ostreatus*, including the AAL-like lectin, oyster lectin, fungal fruit body lectin, and Ricin B lectin (Perduca et al., 2020). Here, our study showed strong variations in lectin catalogs from *P. ostreatus*, and found new classes including CCL-like β-trefoil-type and galectin-like class with β-sandwich-fold lectins. Significantly, CCL-like β-trefoil-type lectins in other fungi species have previously been reported to have resistance against predators and parasites (Bleuler-Martinez et al., 2017; Vajravijayan et al., 2020; Lebreton et al., 2021).

In the present study, *Polec2* was proven to activate ROS/MAPK signaling and reinforce SA- and JA-dependent defense of *P. ostreatus* against *T. putrescentiae*. After overexpression of *Polec2* (more than 5-fold), two of the signaling events were the activations of ROS and MAPKs. As a result of an increase in generation of ROS,

ROS-scavenging proteins such as protein SOD, CAT and POD were induced upon cell damage. Furthermore, MDA content are essential biological parameters for evaluating the degree of oxidative cell damage (Mittler et al., 2011; Hernández-Oñate et al., 2012). These results indicate that overexpression of *Polec2* could significantly induce the accumulation of MDA content and decrease electrolyte permeability. NADPH oxidases (Noxs) have a variety of functions in plants and animals, including response to wounding, predators, and programed cell death (PCD), where ROS produced by Noxs forms a gradient of H_2O_2, indicating that it serves as propagation signal (Mittler et al., 2011). The advantage of ROS includes the capacity of the cell to rapidly produce and scavenge different forms of ROS in a simultaneous manner, enabling rapid and dynamic changes in ROS levels. Different organisms generate ROS at different levels and could leak or actively transport ROS such as H_2O_2 into their environment, it is possible that another advantage of ROS as signaling molecules in early stages of evolution was the sensing and/or communication between different organisms (Mittler et al., 2011). In fungi, wounding causes two of three Noxs (*nox1*, *nox2*, and *noxR*) dependent ROS production in the fungus *Trichoderma atroviride*, and *noxR* protein regulates Nox1 according to gene-replacement experiments (Hernández-Oñate et al., 2012; Medina-Castellanos et al., 2014). Fungi contain from one to three Nox genes, depending on the species (Aguirre et al., 2005). We discovered that one of two Nox genes, Nox1, had the potential ability to regulate ROS production in *P. ostreatus*, but this conclusion need further investigation. These findings suggested that, as in plants and animals, changes in intracellular redox status may act as signal molecules in a conserved defense-response mechanism in fungi (Aguirre and Lambeth, 2010). Activation of MAPKs signaling confirms its important role in the oyster mushroom defense, which could involve signaling multiple defense responses, including the biosynthesis/signaling of defense hormones, ROS generation, defense gene activation, and antibiotic substance production (Li et al., 2022). And then SA and JA biosynthesis and metabolism were found to both strongly increase in *Polec2* transgenic strains when compared to the WT strain. SA and JA have been discovered to be crucial components of *P. ostreatus*' defense systems against *T. putrescentiae* attack in earlier investigations (Li et al., 2022). In particular, endogenous and exogenous JA can influence the expression of genes involved in the biosynthesis of terpenoids and steroids to produce the metabolism of anti-mite substances (Li et al., 2022). Overall, our results show that *Polec2* actives the ROS, MAPK, SA, and JA signaling pathways to defend against *T. putrescentiae* infestation. In this study, we discovered that rearing *T. putrescentiae* on *Polec2* transgenic strains significantly reduced hatchability, survival, and population increase, indicating stronger resistance to *T. putrescentiae*.

According to these observations, *Polec2* expression could be beneficial in efforts to control *T. putrescentiae* without using other inputs or causing environmental damage. This study also presents a method for elucidating resistance mechanisms in edible fungi, providing a resistance-conferring gene for breeding mite-resistant mushroom varieties in pest control. Interestingly, *P. ostreatus* appeared to produce some sticky particles that limited the action of *T. putrescentiae* and caused its death, though the underlying mechanism is unknown and should be investigated in future work.

Data availability statement

The original contributions presented in the study are included in the article/Supplementary material, further inquiries can be directed to the corresponding authors.

Author contributions

CL and SQ: conceptualization. HL: methodology. JL and XL: software. JL: writing original draft preparation. SQ: writing review and editing. LM: project administration. SQ and LM: funding acquisition. All authors have read and agreed to the published version of the manuscript.

Funding

This research was funded by the National Natural Science Foundation of China (32001911), the China Agriculture Research System of MOF and MARA (CARS-20), and Biological Quality Engineering Project (503190106).

Conflict of interest

The authors declare that the research was conducted in the absence of any commercial or financial relationships that could be construed as a potential conflict of interest.

Publisher's note

Supplementary material

The Supplementary material for this article can be found online at: https://www.frontiersin.org/articles/10.3389/fmicb.2023.1191500/full#supplementary-material

References

Aguirre, J., and Lambeth, J. D. (2010). Nox enzymes from fungus to fly to fish and what they tell us about Nox function in mammals. *Free Radic. Biol. Med.* 49, 1342–1353. doi: 10.1016/j.freeradbiomed.2010.07.027

Aguirre, J., Ríos-Momberg, M., Hewitt, D., and Hansberg, W. (2005). Reactive oxygen species and development in microbial eukaryotes. *Trends Microbiol.* 13, 111–118. doi: 10.1016/j.tim.2005.01. 007

Alborés, S., Mora, P., Bustamante, M. J., Cerdeiras, M. P., and Franco Fraguas, L. (2014). Purification and applications of a lectin from the mushroom Gymnopilus spectabilis. *Appl. Biochem. Biotechnol.* 172, 2081–2090. doi: 10.1007/s12010-013-0665-5

Ambethgar, V. (2009). Potential of entomopathogenic fungi in insecticide resistance management (IRM): a review. *J. Biopest.* 2, 177–193. doi: 10.57182/jbiopestic.2.2.177-193

Arthur, C. M., Cummings, R. D., and Stowell, S. R. (2014). Using glycan microarrays to understand immunity. *Curr. Opin. Chem. Biol.* 18, 55–61. doi: 10.1016/j.cbpa.2013.12.017

Biedermann, P. H. W., and Vega, F. E. (2020). Ecology and evolution of insect-fungus mutualisms. *Annu. Rev. Entomol.* 65, 431–455. doi: 10.1146/annurev-ento-011019-024910

Bleuler-Martínez, S., Butschi, A., Garbani, M., Wälti, M. A., Wohlschlager, T., Potthoff, E., et al. (2011). A lectin-mediated resistance of higher fungi against predators and parasites. *Mol. Ecol.* 20, 3056–3070. doi: 10.1111/j.1365-294X.2011.05093.x

Bleuler-Martinez, S., Stutz, K., Sieber, R., Collot, M., Mallet, J. M., Hengartner, M., et al. (2017). Dimerization of the fungal defense lectin CCL2 is essential for its toxicity against nematodes. *Glycobiology* 27, 486–500. doi: 10.1093/glycob/cww113

Bleuler-Martinez, S., Varrot, A., Olieric, V., Schubert, M., Vogt, E., Fetz, C., et al. (2022). Structure-function relationship of a novel fucoside-binding fruiting body lectin from Coprinopsis cinerea exhibiting nematotoxic activity. *Glycobiology* 32, 600–615. doi: 10.1093/glycob/cwac020

Butschi, A., Titz, A., Wälti, M. A., Olieric, V., Paschinger, K., Nöbauer, K., et al. (2010). Caenorhabditis elegans N-glycan core beta-galactoside confers sensitivity towards nematotoxic fungal galectin CGL2. *PLoS Pathog.* 6:e1000717. doi: 10.1371/journal.ppat.1000717

Chattopadhyay, T. K., Lisgarten, J. N., Brechtel, R., Rüdiger, H., and Palmer, R. A. (1999). Crystallization of Pleurotus ostreatus (oyster mushroom) lectin. *Acta Crystallogr. D Biol. Crystallogr.* 55, 1589–1590. doi: 10.1107/s0907444999007945

Dangl, J. L., Horvath, D. M., and Staskawicz, B. J. (2013). Pivoting the plant immune system from dissection to deployment. *Science* 341, 746–751. doi: 10.1126/science.1236011

Deng, Y., Zhai, K., Xie, Z., Yang, D., Zhu, X., Liu, J., et al. (2017). Epigenetic regulation of antagonistic receptors confers rice blast resistance with yield balance. *Science* 355, 962–965. doi: 10.1126/science.aai8898

Hernández-Oñate, M. A., Esquivel-Naranjo, E. U., Mendoza-Mendoza, A., Stewart, A., and Herrera-Estrella, A. H. (2012). An injury-response mechanism conserved across kingdoms determines entry of the fungus Trichoderma atroviride into development. *Proc. Natl. Acad. Sci. U. S. A.* 109, 14918–14923. doi: 10.1073/pnas.1209396109

Hou, Z. Q., Liu, J. J., Li, H. P., Luo, X., Ma, L., and Qu, S. X. (2022). Biological parameters and host preference of Tyrophagus putrescentiae (Schrank) on different Pleurotus ostreatus cultivars. *Syst. Appl. Acarol.* 27, 1–8. doi: 10.11158/saa.27.1.1

Hubert, J., Pekar, S., Aulicky, R., Nesvorna, M., and Stejskal, V. (2013). The effect of stored barley cultivars, temperature and humidity on population increase of Acarus siro, Lepidoglyphus destructor and Tyrophagus putrescentiae. *Exp. Appl. Acarol.* 60, 241–252. doi: 10.1007/s10493-012-9639-5

Ji, T. H., and Nicolson, G. L. (1974). Lectin binding and perturbation of the outer surface of the cell membrane induces a transmembrane organizational alteration at the inner surface. *Proc. Natl. Acad. Sci. U. S. A.* 71, 2212–2216. doi: 10.1073/pnas.71.6.2212

Kawagishi, H., Mitsunaga, S.-I., Yamawaki, M., Ido, M., Shimada, A., Kinoshita, T., et al. (1997). A lectin from mycelia of the fungus Ganoderma lucidum. *Phytochemistry* 44, 7–10. doi: 10.1016/s0031-9422(96)00492-x

Kunzler, M. (2015). Hitting the sweet spot-glycans as targets of fungal defense effector proteins. *Molecules* 20, 8144–8167. doi: 10.3390/molecules20058144

Lebreton, A., Bonnardel, F., Dai, Y. C., Imberty, A., Martin, F. M., and Lisacek, F. (2021). A comprehensive phylogenetic and bioinformatics survey of lectins in the fungal kingdom. *J. Fungi (Basel)* 7:453. doi: 10.3390/jof7060453

Lei, M., Wu, X., Zhang, J., Wang, H., and Huang, C. (2017). Establishment of an efficient transformation system for Pleurotus ostreatus. *World J. Microbiol. Biotechnol.* 33:214. doi: 10.1007/s11274-017-2378-3

Letunic, I., and Bork, P. (2021). Interactive tree of life (iTOL) v5: an online tool for phylogenetic tree display and annotation. *Nucleic Acids Res.* 49, W293–W296. doi: 10.1093/nar/gkab301

Li, C. P., Cui, Y. B., Wang, J., Yang, Q. G., and Tian, Y. (2003). Acaroid mite, intestinal and urinary acariasis. *World J. Gastroenterol.* 9, 874–877. doi: 10.3748/wjg.v9.i4.874

Li, H. P., Liu, J. J., Hou, Z. Q., Luo, X., Lin, J. S., Jiang, N., et al. (2022). Activation of mycelial defense mechanisms in the oyster mushroom Pleurotus ostreatus induced by Tyrophagus putrescentiae. *Food Res. Int.* 160:111708. doi: 10.1016/j.foodres.2022.111708

Li, H. P., Yang, W. J., Qu, S. X., Pei, F., Luo, X., Mariga, A. M., et al. (2018). Variation of volatile terpenes in the edible fungi mycelia Flammulina velutipes and communications in fungus-mite interactions. *Food Res. Int.* 103, 150–155. doi: 10.1016/j.foodres.2017.10.031

Medina-Castellanos, E., Esquivel-Naranjo, E. U., Heil, M., and Herrera-Estrella, A. (2014). Extracellular ATP activates MAPK and ROS signaling during injury response in the fungus Trichoderma atroviride. *Front. Plant Sci.* 5:659. doi: 10.3389/fpls.2014.00659

Minh, B. Q., Schmidt, H. A., Chernomor, O., Schrempf, D., Woodhams, M. D., von Haeseler, A., et al. (2020). IQ-TREE 2: new models and efficient methods for phylogenetic inference in the genomic era. *Mol. Biol. Evol.* 37, 1530–1534. doi: 10.1093/molbev/msaa015

Mittler, R., Vanderauwera, S., Suzuki, N., Miller, G. A. D., Tognetti, V. B., Vandepoele, K., et al. (2011). ROS signaling: the new wave? *Trends Plant Sci.* 16, 300–309. doi: 10.1016/j.tplants.2011.03.007

Naranjo-Ortiz, M. A., and Gabaldón, T. (2019). Fungal evolution: major ecological adaptations and evolutionary transitions. *Biol. Rev. Camb. Philos. Soc.* 94, 1443–1476. doi: 10.1111/brv.12510

Nurziya, Y., Zhao, M. R., Lou, Y., Hao, J. Z., Wei, P., Jia, W. J., et al. (2019). Preparation of protoplast mononuclear strain of Pleurotus ostreatus and analysis of its culture characteristics. *Xinjiang Agr. Sci.* 56, 731–739. doi: 10.6048/j.issn.1001-4330.2019.04.016

Panevska, A., Hodnik, V., Skočaj, M., Novak, M., Modic, S., Pavlic, I., et al. (2019). Pore-forming protein complexes from Pleurotus mushrooms kill western corn rootworm and Colorado potato beetle through targeting membrane ceramide phosphoethanolamine. *Sci. Rep.* 9:5073. doi: 10.1038/s41598-019-41450-4

Perduca, M., Destefanis, L., Bovi, M., Galliano, M., Munari, F., Assfalg, M., et al. (2020). Structure and properties of the oyster mushroom (Pleurotus ostreatus) lectin. *Glycobiology* 30, 550–562. doi: 10.1093/glycob/cwaa006

Plaza, D. F., Schmieder, S. S., Lipzen, A., Lindquist, E., and Kunzler, M. (2015). Identification of a novel nematotoxic protein by challenging the model mushroom Coprinopsis cinerea with a fungivorous nematode. *G3 (Bethesda)* 6, 87–98. doi: 10.1534/g3.115.023069

Pohleven, J., Brzin, J., Vrabec, L., Leonardi, A., Cokl, A., Strukelj, B., et al. (2011). Basidiomycete Clitocybe nebularis is rich in lectins with insecticidal activities. *Appl. Microbiol. Biotechnol.* 91, 1141–1148. doi: 10.1007/s00253-011-3236-0

Qu, S. X., Li, H. P., Ma, L., Song, J. D., Hou, L. J., and Lin, J. S. (2015). Temperature-dependent development and reproductive traits of Tyrophagus putrescentiae (Sarcoptiformes: acaridae) reared on different edible mushrooms. *Environ. Entomol.* 44, 392–399. doi: 10.1093/ee/nvu064

Shamshad, A. (2010). The development of integrated pest management for the control of mushroom sciarid flies, Lycoriella ingenua (Dufour) and Bradysia ocellaris (Comstock), in cultivated mushrooms. *Pest Manag. Sci.* 66, 1063–1074. doi: 10.1002/ps.1987

Shi, L., Fang, X., Li, M., Mu, D., Ren, A., Tan, Q., et al. (2012). Development of a simple and efficient transformation system for the basidiomycetous medicinal fungus Ganoderma lucidum. *World J. Microbiol. Biotechnol.* 28, 283–291. doi: 10.1007/s11274-011-0818-z

Singh, R. S., Walia, A. K., and Kennedy, J. F. (2020). Mushroom lectins in biomedical research and development. *Int. J. Biol. Macromol.* 151, 1340–1350. doi: 10.1016/j.ijbiomac.2019.10.180

Tayyrov, A., Schmieder, S. S., Bleuler-Martinez, S., Plaza, D. F., and Künzler, M. (2018). Toxicity of potential fungal defense proteins towards the fungivorous nematodes Aphelenchus avenae and Bursaphelenchus okinawaensis. *Appl. Environ. Microbiol.* 84, e02051–e02018. doi: 10.1128/AEM.02051-18

Vajravijayan, S., Pletnev, S., Luo, Z., Pletnev, V. Z., Nandhagopal, N., and Gunasekaran, K. (2020). Crystallographic and calorimetric analysis on Pleurotus ostreatus lectin and its sugar complexes - promiscuous binding driven by geometry. *Int. J. Biol. Macromol.* 152, 862–872. doi: 10.1016/j.ijbio-mac.2020.02.294

Varrot, A., Basheer, S. M., and Imberty, A. (2013). Fungal lectins: structure, function and potential applications. *Curr. Opin. Struct. Biol.* 23, 678–685. doi: 10.1016/j.sbi.2013.07.007

Wang, T., Song, W., and Li, Y. B. (2016). Study on the characteristics and countermeasures of export technical barriers of edible fungi in our country. *Qual. Assur. Saf. Crop. Foods* 01, 61–66. doi: 10.4236/oalib.1103154

Wang, M., Trigueros, V., Paquereau, L., Chavant, L., and Fournier, D. (2002). Proteins as active compounds involved in insecticidal activity of mushroom fruitbodies. *J. Econ. Entomol.* 95, 603–607. doi: 10.1603/0022-0493-95.3.603

Wetzel, W. C., Kharouba, H. M., Robinson, M., Holyoak, M., and Karban, R. (2016). Variability in plant nutrients reduces insect herbivore performance. *Nature* 539, 425–427. doi: 10.1038/nature 20140

Whelan, S., Allen, J. E., Blackburne, B. P., and Talavera, D. (2015). ModelOMatic: fast and automated model selection between RY, nucleotide, amino acid, and codon substitution models. *Syst. Biol.* 64, 42–55. doi: 10.1093/sysbio/syu062

Winer, J., Jung, C. K. S., Shackel, I., and Williams, P. M. (1999). Development and validation of real-time quantitative reverse transcriptase-polymerase chain reaction for monitoring gene expression in cardiac myocytesin vitro. *Anal. Biochem.* 270, 41–49. doi: 10.1006/abio.1999.4085

Wohlschlager, T., Butschi, A., Grassi, P., Sutov, G., Gauss, R., Hauck, D., et al. (2014). Methylated glycans as conserved targets of animal and fungal innate defense. *Proc. Natl. Acad. Sci. U. S. A.* 111, E2787–E2796. doi: 10.1073/pnas.1401176111

Wohlschlager, T., Butschi, A., Zurfluh, K., Vonesch, S. C., auf dem Keller, U., Gehrig, P., et al. (2011). Nematotoxicity of Marasmius oreades agglutinin (MOA) depends on glycolipid binding and cysteine protease activity. *J. Biol. Chem.* 286, 30337–30343. doi: 10.1074/jbc.M111.258202

Yamada, K. D., Tomii, K., and Katoh, K. (2016). Application of the MAFFT sequence alignment program to large data-reexamination of the usefulness of chained guide trees. *Bioinformatics* 32, 3246–3251. doi: 10.1093/bioinformatics/btw412

Zuo, L., Zhou, T., Pannell, B. K., Ziegler, A. C., and Best, T. M. (2015). Biological and physiological role of reactive oxygen species-the good, the bad and the ugly. *Acta Physiol (Oxf.)* 214, 329–348. doi: 10.1111/apha.12515

frontiers | Frontiers in Microbiology

TYPE Original Research
PUBLISHED 04 May 2023
DOI 10.3389/fmicb.2023.1177820

OPEN ACCESS

EDITED BY
Liping Zeng,
University of California,
Riverside, United States

REVIEWED BY
Wenxia He,
University of North Carolina at Chapel Hill,
United States
Ning Ding,
Lanzhou University, China
Shuangshuang Wang,
East China Normal University, China

*CORRESPONDENCE
Lijiao Zhang
✉ zhanglijiao@caas.cn

RECEIVED 02 March 2023
ACCEPTED 10 April 2023
PUBLISHED 04 May 2023

CITATION
Qi Y, Huang C, Zhao M, Wu X, Li G, Zhang Y and Zhang L (2023) milR20 negatively regulates the development of fruit bodies in *Pleurotus cornucopiae*. *Front. Microbiol.* 14:1177820. doi: 10.3389/fmicb.2023.1177820

milR20 negatively regulates the development of fruit bodies in *Pleurotus cornucopiae*

Yuhui Qi[1,2,3], Chenyang Huang[1,2,3], Mengran Zhao[1,2,3], Xiangli Wu[1,2,3], Guangyu Li[1,2,3], Yingjie Zhang[1,2,3,4] and Lijiao Zhang[1,2,3]*

[1]Institute of Agricultural Resources and Regional Planning, Chinese Academy of Agricultural Sciences, Beijing, China, [2]Key Laboratory of Microbial Resources, Ministry of Agriculture and Rural Affairs, Beijing, China, [3]State Key Laboratory of Efficient Utilization of Arid and Semi-arid Arable Land in Northern China, Beijing, China, [4]College of Life Sciences, Shanxi Normal University, Taiyuan, China

The mechanism underlying the development of fruit bodies in edible mushroom is a widely studied topic. In this study, the role of milRNAs in the development of fruit bodies of *Pleurotus cornucopiae* was studied by comparative analyses of the mRNAs and milRNAs at different stages of development. The genes that play a crucial role in the expression and function of milRNAs were identified and subsequently expressed and silenced at different stages of development. The total number of differentially expressed genes (DEGs) and differentially expressed milRNAs (DEMs) at different stages of development was determined to be 7,934 and 20, respectively. Comparison of the DEGs and DEMs across the different development stages revealed that DEMs and its target DEGs involved in the mitogen-activated protein kinase (MAPK) signaling pathway, protein processing in endoplasmic reticulum, endocytosis, aminoacyl-tRNA biosynthesis, RNA transport, and other metabolism pathways, which may play important roles in the development of the fruit bodies of *P. cornucopiae*. The function of milR20, which targeted pheromone A receptor *g8971* and was involved in the MAPK signaling pathway, was further verified by overexpression and silencing in *P. cornucopiae*. The results demonstrated that the overexpression of milR20 reduced the growth rate of mycelia and prolonged the development of the fruit bodies, while milR20 silencing had an opposite effect. These findings indicated that milR20 plays a negative role in the development of *P. cornucopiae*. This study provides novel insights into the molecular mechanism underlying the development of fruit bodies in *P. cornucopiae*.

KEYWORDS

milR20, fruit body development, *Pleurotus cornucopiae*, comparative transcriptome, MAPK signaling pathway

1. Introduction

MicroRNAs (miRNAs) are small non-coding RNA molecules that are 18–24 nt long, play important regulatory roles in gene regulation, and influence various biological processes in plants and animals. Numerous miRNAs of plants and animals have been identified to date. The first miRNA-like fungal RNAs (milRNAs) were discovered in *Neurospora crassa* (Lee et al., 2010) and the milRNAs have been subsequently identified in other filamentous fungi and basidiomycetes (Kang et al., 2013; Wang et al., 2021). The characteristics of fungal milRNAs are

similar to those of plant and animal miRNAs. For instance, the miRNA precursors of plants and animals have a typical hairpin structure that is similar to those of fungi. However, the biosynthesis mechanism of fungal miRNAs are different from the animal and plant miRNAs. The milRNAs of *N. crassa* are produced by four different mechanisms that include a distinct combination of factors, including Dicers, Argonaute protein QDE-2, the exonuclease QIP, and the RNAse III domain-containing MRPL3 protein. While the miRNA in animals and plants were produced by Dicer-like enzymes or Drosha proteins in miRNA maturation (Jones-Rhoades et al., 2006; Lee et al., 2010).

The majority of recent studies on miRNAs are primarily focusing on the miRNAs of animals or plants, and there is a scarcity of research on fungal miRNAs. The miRNA-mediated post-transcriptional regulation of genes is a novel gene regulation strategy that is used to regulate the expression of protein-coding genes by targeting mRNAs *via* cleavage or translational repression. Our current understanding of target recognition by miRNAs suggests that the mRNA sequence is complementary to bases 2–8 of miRNAs (referred to as the seed sequence) in the majority of miRNA-mediated silencing complexes (miRISCs). The seed region has the highest complementarity to the 3′-untranslated region (UTR) of the mRNA of the target gene, and previous studies have demonstrated that various miRNAs with numerous functions regulate multiple target genes *via* different mechanisms (Kiriga et al., 2020). The recent advancements in sequencing technologies and bioinformatics tools have facilitated the identification of milRNAs in various fungi (Zhou J. H. et al., 2012; Mu et al., 2015; Li et al., 2016). However, there is a scarcity of information regarding the functions and target recognition mechanism of fungal milRNAs.

Understanding the regulatory mechanisms of fungal milRNAs may aid in breeding novel varieties of edible mushroom. *Pleurotus cornucopiae* is one of the most extensively cultivated mushrooms in China, and has a high nutritional and medicinal value. The mechanism underlying the development of fruiting bodies is a complex process that is regulated by both genetics and environment, and has been a topic of immense interest in recent years. Numerous genes that play an important role in the development of mushrooms have been identified and characterized. For instance, it has been demonstrated that the genes that encode the FvHmg1 and LFC1 transcription factors negatively regulate the fruit body development of *Flammulina velutipes* (Wu et al., 2020; Meng et al., 2021). Additionally, genes encoding SsNox2 NADPH oxidases contribute to the generation of reactive oxygen species (ROS), which are essential for the sclerotia development of *Sclerotinia sclerotiorum* (Kim et al., 2011). Glutathione peroxidase (GPX), which aids in maintaining ROS homeostasis, has a complex influence on the growth of the filamentous fungi *Hypsizygus marmoreus* (Zhang J. J. et al., 2020). Additionally, the genes encoding protein kinases in the mitogen-activated protein kinase (MAPK) signaling pathway play an important role in cellular regulation in fungi by regulating phosphorylation and dephosphorylation. A previous study on *Metarhizium robertsii* revealed that the MAPK signaling cascade plays a regulatory role in the formation of conidia and stress tolerance (Chen et al., 2016). The SakA response factor of *Aspergillus nidulans* can transmit osmotic and oxidative stress signals to the MAPK signaling pathway and regulate the growth, development, and stress response of *A. nidulans* (Lara-Rojas et al., 2011). Another study reported that the adenosine cyclase of the cyclic adenosine monophosphate (cAMP) signal transduction pathway aids in the transformation of yeast morphology to mycelial morphology, and plays a crucial role in mycelial growth (Rocha et al., 2001).

Recent studies have demonstrated that small RNAs play vital roles in fungal development. For instance, it has been demonstrated that milR4 and milR16 mediate the development of fruiting bodies in *Cordyceps militaris*. The disruption of milR4 results in the non-formation of fruiting bodies while the disruption of milR16 results in the formation of abnormal fruiting bodies with pale yellow-colored primordia (Shao et al., 2019). In contrast, the overexpression of *Po-MilR-1* in *P. ostreatus* results in slow mycelial growth and formation of abnormal pilei with irregular edges (Xu et al., 2021). However, only one milRNA of *P. ostreatus* that plays a vital role in mycelial growth has been identified and purified to date. Therefore, the potential roles of milRNAs in the development of fruiting bodies of *P. cornucopiae* is poorly understood to date owing to the scarcity of information, and further studies are necessary in this regard.

In this study, the genes encoding the Dicer, argonaute (AGO), and RNA-dependent RNA polymerase (RDRP) proteins of *P. cornucopiae* were identified and their expression profiles were determined at different developmental stages. The milRNAs related to the development of *P. cornucopiae* were determined by small RNA sequencing and *in silico* analyses. The potential targets of the milRNAs in the genome of *P. cornucopiae* were additionally detected, and the expression and functions of these target genes were determined by transcriptome sequencing and bioinformatics analyses. The theoretically predicted milRNAs and their gene targets were experimentally validated by quantitative real-time PCR (qRT-PCR) and dual-luciferase activity assay. Finally, one milRNA of *P. cornucopiae* was identified, and its functions in the development of fruiting bodies of *P. cornucopiae* were determined by overexpression and silencing. The results are anticipated to provide a foundation for research on milRNA function and the application of milRNAs in the development of edible mushrooms.

2. Materials and methods

2.1. Strains and media

The CCMSSC 00406 strain of *P. cornucopiae* was obtained from the China Center for Mushroom Spawn Standards and Control. The fungal mycelia were inoculated on potato dextrose agar (PDA) at 28°C for 6 days. The cottonseed hull culture medium was used to the mushroom production experiment according to our previous study (Qiu et al., 2018). The samples of mycelia, primordia, and caps of fruiting bodies, denoted as M, P, and C, were collected and stored at −80°C after freezing with liquid nitrogen.

2.2. Identification of RDRP, Dicer, and AGO proteins

The amino acid sequences of the proteins which were functionally annotated as RDRP, Dicer, and AGO proteins were derived from the genome of *P. cornucopiae*. The sequences were subjected to domain analyses using the conserved domain database of NCBI for determining protein function. The sequences of the RDRP, Dicer, and AGO proteins of other fungi were retrieved from GenBank, and

aligned to the corresponding proteins of *P. cornucopiae* with CLUSTALW (Thompson et al., 1994; Hu et al., 2013; Wang et al., 2021). A phylogenetic tree was constructed using the maximum likelihood method based on the Tamura-Nei model and 1,000 bootstrap replicates with the MEGA software, version 5.0 (Kumar et al., 2016) for analyzing the relationships between the RDRP, Dicer, and AGO proteins of *P. cornucopiae* and those of other fungi in literature.

2.3. Deep sequencing of mRNAs and small RNAs

Comparative mRNA and milRNA analyses were performed using the CCMSSC 00406 strain of *P. cornucopiae*. Samples of the different developmental stages, including M, P, and C, of CCMSSC 00406 were collected in three biological replicates and subjected to mRNA and small RNA sequencing. The total RNA was extracted from all the samples using TRIzol reagent (Invitrogen, Carlsbad, United States), according to the manufacturer's instructions, and subsequently treated with RNase-free DNase I (TaKaRa, Shiga, Japan) for removing the genomic DNA. The concentration of the RNA was evaluated using a NanoDrop 2000 spectrophotometer (ThermoFisher, Waltham, United States), and the integrity of the RNA was detected using an Agilent 2100 Bioanalyzer (Agilent, Palo Alto, United States). The cDNA libraries were constructed according to the protocol for library construction and sequenced on an Illumina NovaSeq 6000 platform (Illumina, San Diego, United States). The small RNAs were isolated from the total RNA by polyacrylamide gel electrophoresis (PAGE) with a 6% Tris, boric acid, and EDTA (TBE)—urea denaturing gel, and ligated to specific 5′ and 3′ adaptors. The cDNA libraries were sequenced on an Illumina HiSeq2500 platform following reverse transcription and appropriate amplification and purification.

2.4. Bioinformatics analyses of mRNAs and small RNAs

The clean data (clean reads) were obtained from the raw RNA-seq data by removing the reads containing adapters, poly-N, and low quality reads. The HISAT2 software was used for mapping the reads to the reference genome.[1] The genes were annotated by BLAST search against using the NCBI non-redundant protein sequence (NR), Gene Ontology (GO; Tatusov et al., 2000), Kyoto Encyclopedia of Genes and Genomes (KEGG; Kanehisa et al., 2004), KOG (Koonin et al., 2004), and protein family (Pfam) databases. The expression levels of the genes were estimated by fragments per kilobase of transcript per million fragments mapped (FPKM). The genes that were differentially expressed among the different developmental stages were determined using the DESeq2 tool, with a false discovery rate (FDR) of <0.05. The differentially expressed genes (DEGs) were subjected to GO and KEGG pathway enrichment analyses, and the 20 most enriched pathways with the lowest Q values were selected (Mao et al., 2005).

The high-quality small RNA sequence reads (clean reads) were filtered from the total reads by removing the low-quality reads, reads containing adaptor sequences, and sequences smaller than 18 nt or longer than 30 nt. The clean reads were subsequently aligned to the genome of *P. cornucopiae* using the Bowtie software (Langmead et al., 2009). The different non-coding RNAs, including rRNAs, snRNAs, tRNAs, and snoRNAs, were identified using the Bowtie software, and subsequently removed. The remaining unannotated small RNAs were analyzed for detecting the known miRNAs from miRBase, and the miRDeep2 tool was used for predicting the novel milRNAs (Friedlander et al., 2012). The Randfold software was used for predicting the secondary structures of the novel milRNAs. The expression of the milRNAs in different developmental stages was calculated using the transcripts per million (TPM) normalization method (Fahlgren et al., 2007). The milRNAs that were differentially expressed in the M, P, and C at the different developmental stages were identified using the DESeq tool (Zeng et al., 2018). The target genes of the milRNAs were predicted based on the milRNA sequence information using the TargetFinder,[2] miRanda (Enright et al., 2003), and RNAhybrid (Rehmsmeier et al., 2004) webtools, as previously described.

2.5. Analysis of the expression of milRNAs and mRNAs related to the development of fruiting bodies

The expression levels of the milRNAs were quantified by stem-loop real-time PCR, using 5S rRNA as the internal control for each sample (Zhou Q. et al., 2012). The stem-loop primers in the reverse transcription kit and the upstream primers used for qRT-PCR were designed using miRNA design software.[3] The first-strand cDNA was synthesized using a miRNA first Strand cDNA Synthesis Kit (Vazyme, Nanjing, China), according to the manufacturer's instructions. The miRNA Universal SYBR qPCR Master Mix (Vazyme, Nanjing, China) and an ABI 7500 real-time PCR amplifier (Applied Biosystems, Foster City, CA, United States) were used for qRT-PCR, as described in our previous study. The expression of the target genes of the milRNAs was detected using glyceraldehyde-3-phosphate dehydrogenase (GAPDH) as the internal control for each sample, as previously described (Hou et al., 2021). The relative expression levels of the milRNAs and their target genes in the different stages were quantified using the comparative threshold cycle (CT) $2^{-\triangle\triangle CT}$ method. The primers used for qRT-PCR amplification of the milRNAs are enlisted in Supplementary Table S1.

2.6. Dual-luciferase activity assay

A ~ 200 bp sequence near the binding site of the wild-type (WT) *g8971* and mutant *g8971* genes were synthesized and inserted into the pmirGLO vector. Briefly, HEK293T cells were co-transfected with 0.2 μg of the luciferase reporter vector (g8971-WT or g8971-MT) and

1 https://www.ncbi.nlm.nih.gov/nuccore/WQMT00000000.2/

2 http://targetfinder.org

3 https://www.vazyme.com

10 ng of milR-20-mimic or mimic NC together with the renilla luciferase construct using lipofectamine TM 2000 (Invitrogen), according to the manufacturer's instructions (Grentzmann et al., 1998). The HEK293T cells were collected 48 h post-transfection, and the activities of luciferase and renilla luciferase were measured using a Dual-Luciferase® Reporter Assay System (Promega, Wisconsin, United States) according to the instructions provided (Cai et al., 2017). Five biological repetitions of the experiment were averaged and analyzed using Student's *t* test.

2.7. Overexpression and silencing of milR20

For the overexpression of milR20, a precursor of milR20 was amplified using the WT genomic DNA as the template, and inserted by homologous recombination into a pCAMBIA1300 vector containing the gpd promoter of *P. ostreatus*. MilR20 was silenced using the short tandem target mimic (STTM) technology; STTM contains two target mimic (TM) sequences and a 48 nt-long specific linker sequence. The TM sequence corresponds to the sequence that is complementary to milR20 and possesses a tri-nucleotide that is inserted between the 10 and 11th bases of milR20. The STTM sequence was subsequently ligated to the pCAMBIA1300 vector.

All the recombinant plasmids were verified by sequencing and transfected into WT cells by *Agrobacterium tumefaciens*-mediated transformation (ATMT), as previously described. The strains in which milR20 was overexpressed and silenced were detected by PCR for cloning the *hpt* gene. The expression levels of milR20 following overexpression and silencing were quantified by qRT-PCR. The diameters of the colonies of the WT strain and the strains in which milR20 was overexpressed (OE-milR20) and silenced (STTM-milR20) were measured using the cross method for determining the mycelial growth rate. The WT, OE-milR20, and STTM-milR20 strains were separately inoculated on a culture medium for analyzing the primordial formation time, the developmental cycle of the fruiting bodies, and the spore print.

2.8. Statistical analysis

All statistical analyses were performed using the SPSS 26.0 software (SPSS Inc., Chicago, United States). The data are presented as mean ± SEM values. Statistical significance was defined as *($p < 0.05$), **($p < 0.01$), and ***($p < 0.001$). The GraphPad Prism 8.0.1 software (GraphPad Software Inc., San Diego, United States) and Excel 2010 software (Microsoft, Redmond, WA, SA, United States) were used for drawing figure.

3. Results

3.1. mRNA sequencing and analyses

The expression profiles of the genes expressed in the M, P, and C stages across the three different developmental stages were determined using mRNA-seq. Three biological replicates were sequenced for each tissue type and a total of approximately 428 million clean reads were obtained from all the samples after filtering the low-quality reads. The number of reads in the samples ranged from 39 to 65 million. The reads were mapped to the genome of *P. cornucopiae*; approximately 32–53 million reads (80–82% of the total reads) mapped to the genome of *P. cornucopiae* (Supplementary Table S2). The Pearson correlation coefficients results indicated that the reproducibility between biological replicates was high enough for subsequent studies (Supplementary Figure S1).

In order to identify the genes that are involved in the development of *P. cornucopiae*, the DEGs among the different developmental stages were identified using the following criteria: FDR ≤ 0.05 and fold change (FC) ≥ 1.5. The number of DEGs in the M vs. P, M vs. C, and P vs. C comparison groups was determined to be 4,819, 7,017, and 2,917, respectively (Figure 1A). A total of 7,934 DEGs were identified from all the comparison groups, of which the number of DEGs in the M vs. C comparison group was highest. This indicated that the number of genes differentially expressed between the different intervals was higher than that between adjacent stages, and this finding was consistent with the organizational difference.

The DEGs were subjected to GO and KEGG pathway enrichment analyses. The results of GO enrichment analysis revealed that the DEGs in the M vs. C, P vs. C, and M vs. P comparison were significantly enriched in 46, 54, and 47 GO terms ($p < 0.05$), respectively. The significantly GO terms in the overlapped groups and the top 10 most significantly enriched GO terms in a single group were present. In biological process, the significantly enriched GO terms shared in M vs. C and P vs. C were gluconeogenesis, glycolytic, nitrogen compound metabolic process, and carbohydrate transport. The significantly enriched GO terms shared in M vs. P and M vs. C were histidine biosynthetic process, translation, and reciprocal meiotic recombination. The significantly enriched GO terms shared in M vs. C, P vs. C and M vs. P were oxidation-reduction process. The significantly enriched GO terms in single group were translational elongation, response to stress, transmembrane transport etc. In molecular function, the significantly enriched GO terms in different group were ATPase activity, oxidoreductase activity, transporter activity, and signal transducer activity etc. In cellular component, the significantly enriched GO terms in different stage were mitochondrion, ribosome, intergral component of membrane etc. These findings indicated that the DEGs involved in energy metabolic process, signal transduce process, and DEGs located to mitochondrion and membrane could play a role in the development of fruiting bodies in *P. cornucopiae* (Figure 1B). The total 7,934 DEGs from all three comparison group were used for KEGG analysis and 20 most enriched KEGG pathways were present. The results revealed that the DEGs were enriched in the MAPK signaling pathway, metabolism, cell cycle, and protein processing endoplasmic reticulum terms (Figure 1C). These findings indicated that the DEGs that were involved in these pathways could play a key role in the development of *P. cornucopiae*.

3.2. Identification and analysis of the genes involved in milRNA biogenesis and function

RNA-dependent RNA polymerase, AGO, and Dicer proteins play a key role in milRNA biogenesis and function in eukaryotes. Therefore, the presence of these proteins could indicate that *P. cornucopiae* contains miRNAs. Therefore, the genes encoding RDRP, AGO, and Dicer proteins were identified in the genome of *P. cornucopiae* by

10.3389/fmicb.2023.1177820

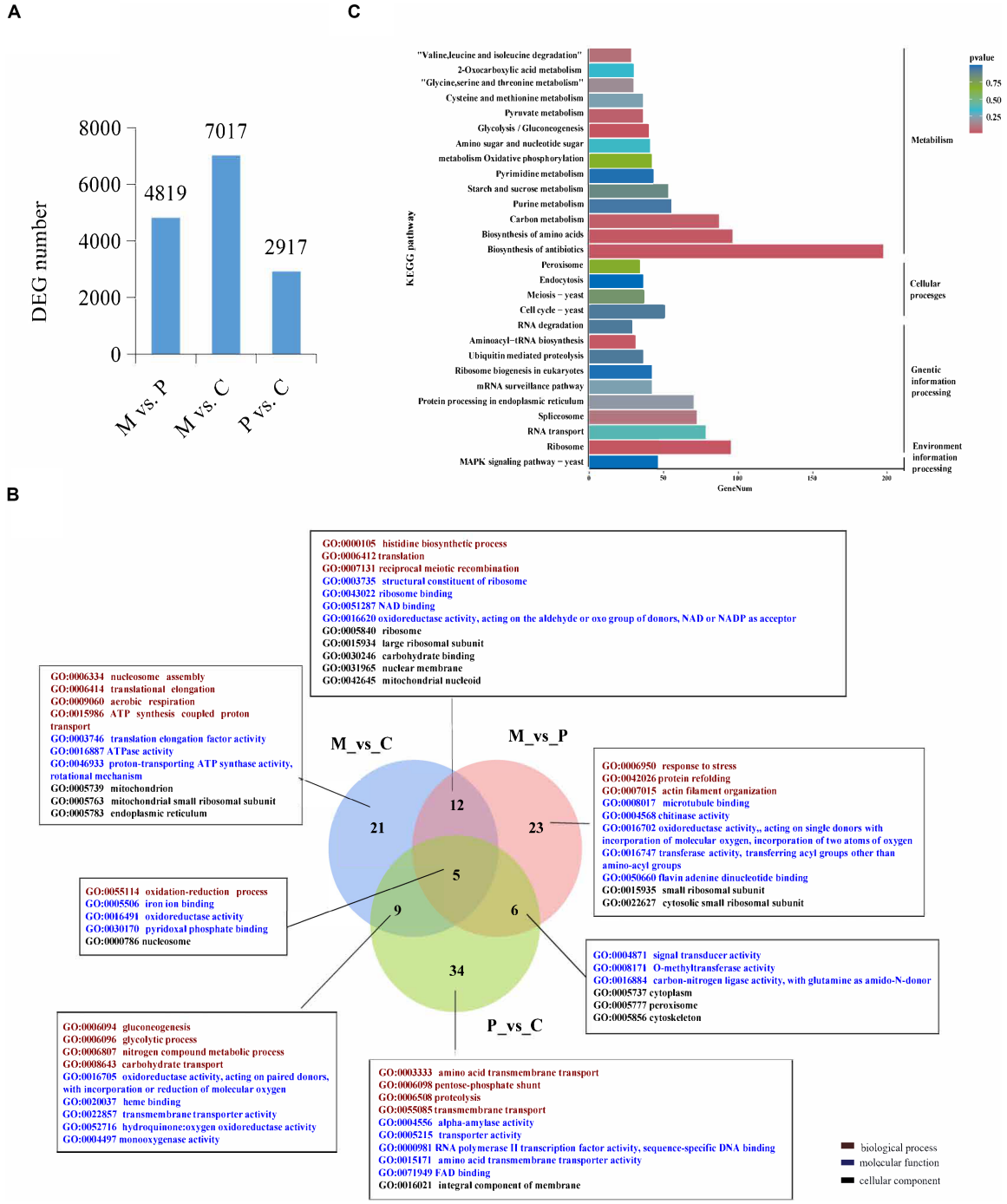

FIGURE 1
Analysis of the differentially expressed genes (DEGs) across the different developmental stages. **(A)** The number of DEGs among the different developmental stages. **(B)** Venn diagram depicting the GO term that the DEGs enriched in all three comparative groups. GO terms in figure are all significantly enriched terms with p <0.05. **(C)** KEGG enrichment analyses of the DEGs among the different developmental stages.

BLASTp. A total of five homologs of AGO (KAG9218964.1, KAG9218965.1, KAG9225438.1, KAG9226743.1, and KAG9226008.1), three homologs of RDRP (KAG9223309.1, KAG9222124.1, and KAG9222908.1), and four homologs of Dicer (KAG9225908.1, KAG9221133.1, KAG9221142.1, and KAG9219090.1), which shared the best sequence homology with the genome sequence of *P. cornucopiae*, were identified. In order to ensure that these proteins were indeed homologs of Dicer, AGO, and RDRP proteins, the conserved domains in these predicted protein sequences were predicted by searching against the NCBI database. The results demonstrated that all the five homologs of AGO contained the N-terminal domain (ArgoN), Argonaute Linker 1 domain (Arg), Piwi AGO and Zwille (PAZ), and Piwi domains. The three homologs of RDRP contained the RDRP domain, while the four homologs of Dicer contained the ribonuclease III domain (Ribonuclease III) and a conserved Dicer dimerization domain (Figure 2A). The results of

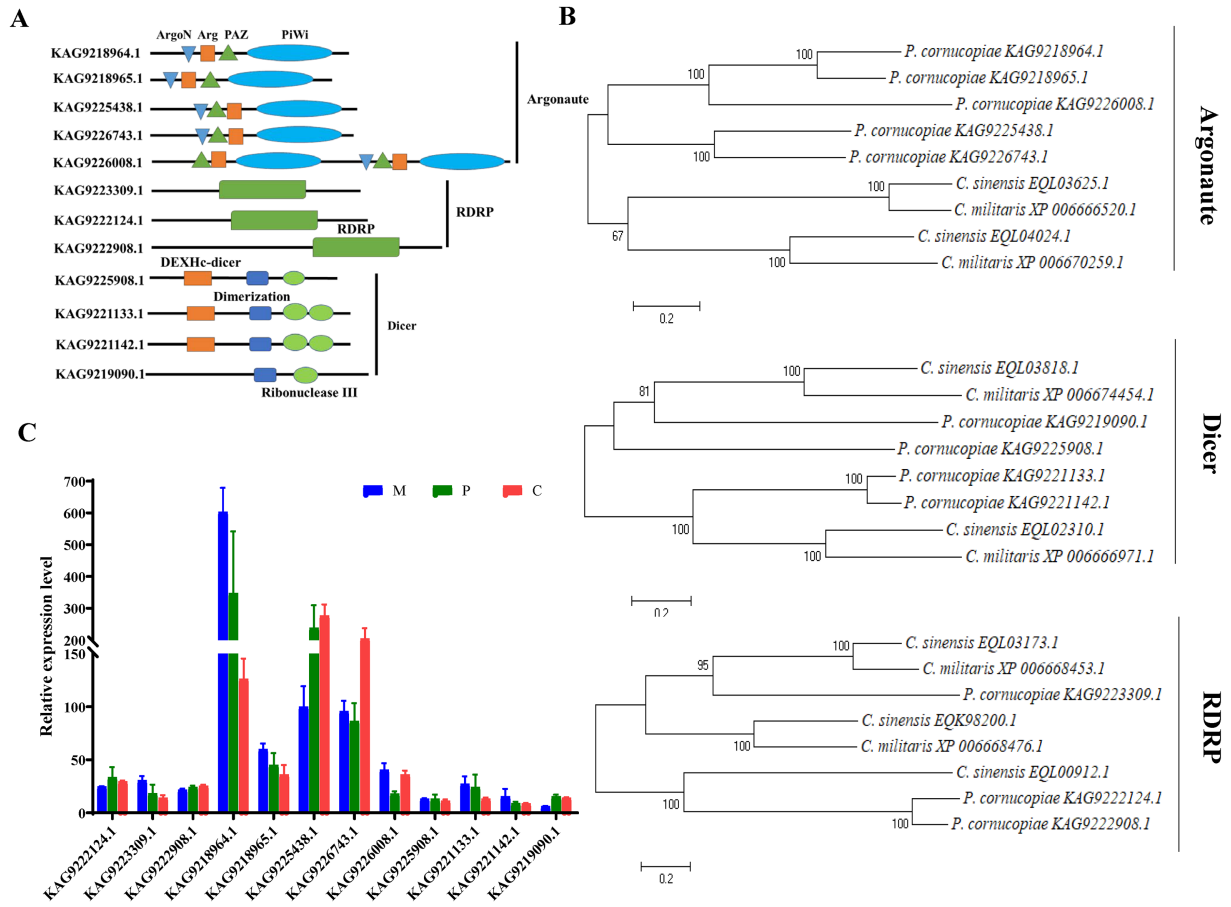

FIGURE 2
Analysis of the Dicer, RDRP, and AGO proteins of *Pleurotus cornucopiae* and other fungi. **(A)** Conserved domain analysis of the Dicer, RDRP, and AGO proteins of *P. cornucopiae*. **(B)** Phylogenetic analysis of the Dicer, RDRP, and AGO proteins of *P. cornucopiae* and other fungi. **(C)** Expression levels of the genes determined from the transcriptome data during the different developmental stages of *P. cornucopiae*. The data are expressed as the mean±standard error (SE) of the data obtained from three replicates.

phylogenetic analysis demonstrated that the sequences of the RDRP, AGO, and Dicer proteins of *P. cornucopiae* were highly homologous to those of *C. sinensis* and *C. militaris* (Figure 2B). These findings suggested that *P. cornucopiae* possesses functional milRNA machinery.

In order to further explore the possible role of milRNAs in the developmental process of *P. cornucopiae*, the expression levels of RDRP, AGO, and Dicer at the different developmental stages were analyzed from the transcriptome data. The results demonstrated that the expression levels of AGO were higher than that of the other genes at each of the developmental stages. The expression levels of the genes encoding RDRP, AGO, and Dicer proteins varied across the different developmental stages of *P. cornucopiae* (Figure 2C), which suggested that the expression and functions of milRNAs were various during development.

3.3. Sequencing and analyses of the milRNAs in the different development stages

In order to identify the milRNAs that are related to the development of fruiting bodies in *P. cornucopiae*, the small RNAs in the M, P, and C stages were subjected to sequencing, which was performed in triplicate. The samples of M tissues were denoted as M-1, M-2, and M-3, while the samples of P tissues were denoted as P-1, P-2, and P-3, and the samples of C tissues were denoted as C-1, C-2, and C-3. Approximately 20 million raw reads were obtained from each sample. Approximately 10 million clean reads with lengths varying between 18 and 30 nt were obtained after filtering the low-quality reads and trimming the 3′-specific adaptors, and the remaining small RNAs were annotated. The clean reads were aligned to the genome of *P. cornucopiae*, and the results demonstrated that the 2–6 million reads included various small ncRNAs, including rRNAs, tRNAs, and snoRNAs, which accounted for 21.35–60.19% of the total clean reads obtained from the different developmental stages. The 4–8 million unannotated clean reads were subsequently analyzed for further prediction of milRNAs, which accounted for 39.64–77.94% of the total clean reads obtained from the different developmental stages (Supplementary Table S3).

A total of 32 milRNAs were finally identified from the different developmental stages of *P. cornucopiae*, and 31, 26, and 30 milRNAs were identified from the M, P, and C stages, respectively (Supplementary Figure S2). The milRNAs were denoted as milR1–milR32 (Supplementary Table S4). Analysis of the length distribution

of the milRNAs revealed that the lengths of the mature milRNAs ranged from 18 to 25 nt. The majority of these milRNAs were 18–22 nt long, and accounted for 93.75% of the total mature milRNAs, which was higher than the number of milRNAs with other lengths (Figure 3A). The results of nucleotide bias analysis revealed that the nucleotides at the 5′-terminus had a strong preference for uracil (U) in the milRNAs that were 18–22 nt long, which was similar to that observed in animals and plants. However, the milRNAs that were 24–25 nt long were enriched in adenine (A) at the 5′-end (Figure 3B).

The abundance of milRNAs was normalized according to the TPM normalization method. Of the 32 milRNAs, 25 were expressed in all the three developmental stages, while the other seven milRNAs were expressed in one or two of the developmental stages (Supplementary Figure S2). The heatmap in Figure 3C demonstrates that the expression patterns of the milRNAs varied across the different development stages and nine of these milRNAs were highly expressed during the entire development of *P. cornucopiae*. The findings suggested that the milRNAs that were expressed at high levels in all the three developmental stages could play a crucial role in the development of *P. cornucopiae*.

To explore the milRNAs that are related to the development of fruiting bodies in *P. cornucopiae*, we analyzed the differentially expressed milRNAs (DEMs) across the three developmental stages. $p < 0.05$ was regarded as the threshold for determining the significant differences in milRNA expression. The results demonstrated that 13, 13, and 6 milRNAs were significantly different expressed in the M vs. P, M vs. C, and P vs. C comparison groups, respectively. A total 20 DEMs were identified in the three comparison groups, of which three DEMs were common between the M vs. C and P vs. C comparison groups, and could play an important role in the development of fruiting bodies (Figure 4A). Analysis of the expression levels of the DEMs in the different comparison groups revealed that the number of DEMs downregulated was higher than that of upregulated in the C vs. P comparison group, while the number of upregulated DEMs was approximately equal to that of the downregulated DEMs in the M vs. P and P vs. C comparison group (Supplementary Table S5; Figure 4B). These results indicated that the DEMs that were downregulated along the development of the fruiting body could play a more crucial role in the development of *P. cornucopiae*.

In order to elucidate the potential functions of the DEMs in the development of *P. cornucopiae*, the target genes of milRNAs were predicted using the TargetFinder, miRanda, and RNAhybrid software, as previously described. A total 17 milRNAs in the 20 DEMs were predicted to target 44 genes. The findings revealed that some of the DEMs could regulate several target genes and more than one milRNA could regulate the same target gene (Supplementary Table S5), which was consistent with the reports of previous studies on plant and animal miRNAs. These target genes were subjected to functional enrichment analyses using the GO and KEGG databases. The findings demonstrated that 41 of the target genes of DEMs were functionally annotated. The results of GO enrichment analysis revealed that the target genes were primarily enriched in the transporter activity,

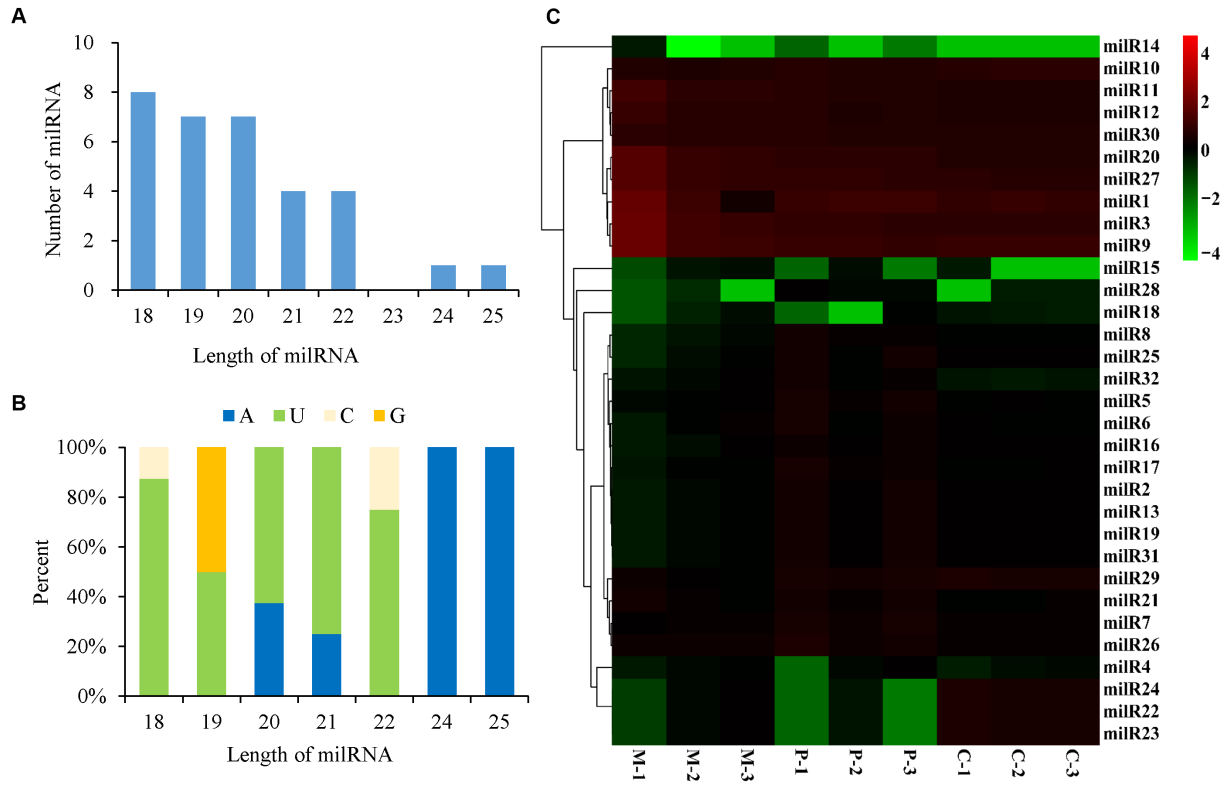

FIGURE 3
Characteristics and expression levels of the milRNAs in the three developmental stages of *Pleurotus cornucopiae*. **(A)** Length distribution of the milRNAs of *P. cornucopiae*. **(B)** 5′-terminal nucleotide bias of the milRNAs of *P. cornucopiae*. **(C)** Heatmap depicting the expression levels of the milRNAs in the three development stages.

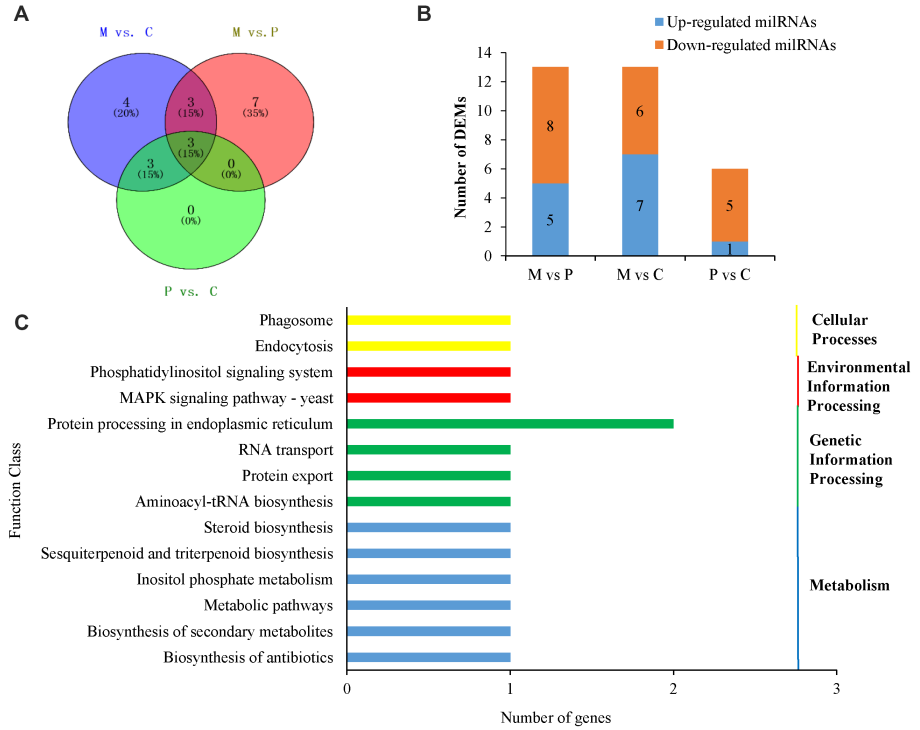

FIGURE 4
Analyses of DEMs. **(A)** Venn diagram depicting the DEMs among the different developmental stages. **(B)** Expression of DEMs in the different comparison groups. **(C)** Results of KEGG pathway analysis of the target genes of DEMs.

receptor activity, and catalytic activity terms in the molecular function category; the signaling pathways, cellular processes, and response to stimulus terms in the biological process category; and the organelles and membranes terms in the cellular component category (Supplementary Figure S3). The results of KEGG enrichment analysis demonstrated that the target genes were enriched in different pathways, including the phosphatidylinositol signaling system, endocytosis, MAPK signaling pathway, protein processing in endoplasmic reticulum, and other metabolic pathways (Figure 4C).

3.4. Correlation analysis of milRNAs and mRNAs

The Venn diagram depicting the DEGs and the target genes of DEMs indicated that 29 of the 44 target genes of the DEMs were differentially expressed across the different developmental stages (Figure 5A). Of these, only seven DEGs could be mapped by KEGG pathway analyses, and were found to be enriched in the MAPK signaling pathway, phosphatidylinositol signaling system, protein processing in endoplasmic reticulum, and other metabolic pathways that may play crucial roles in the growth and development of *P. cornucopiae* (Table 1). For instance, the findings revealed that the *g4622* gene was involved in the phosphatidylinositol signaling system, *g9630* was enriched in endocytosis, *g8971* was enriched in the MAPK signaling pathway, and the remaining genes were involved in other pathways.

MiRNAs are important regulators of gene expression and act *via* degradation or translational repression of target mRNAs (Zdanowicz et al., 2009). Correlation analysis of expression profiles of milRNAs and their targets showed that only milR20 and milR14 had the relative opposite expression trend to their targets in partial development stage (Figures 5B,C), while other miRNA-target did not (Figures 5D–F). The results demonstrated that milR14 could play a minor role in the development of fruiting bodies because it was not expressed in the P and C stages. However, the stage-specific expression pattern of milR14 suggest it may have important function during stage M development. However, the expression of milR20 was downregulated from the P to the C stage, while the expression of its target gene, *g8971*, was upregulated from the P to the C stage. These result indicated that *g8971* may be the target of milR20. milR20 was highly expressed in the three development stage with the expression level higher than 40,000, and it was a DEM from the M vs. C and P vs. C comparison group with the expression level decreased from M to C stage. The predict target of milR20, *g8971*, was DEGs at different developmental stages, and encodes a pheromone receptor that involved in the MAPK signal pathway which plays an important role in the development. These results therefore indicated that milR20 could negatively regulate the development of fruit bodies in *P. cornucopiae*.

In this study, qRT-PCR analysis was also performed for validating the expression profiles of the miRNA-target modules of interest, namely, milR20 and *g8971*. The expression pattern of milR20 and its target gene, *g8971*, obtained by RT-qPCR analysis was similar to that determined by high-throughput sequencing, and the findings revealed that the expression of milR20 tended to decrease from stages P to C (Supplementary Figure S4), while the expression level of *g8971* increased from stage P to C. The findings revealed that the milR20 had

10.3389/fmicb.2023.1177820

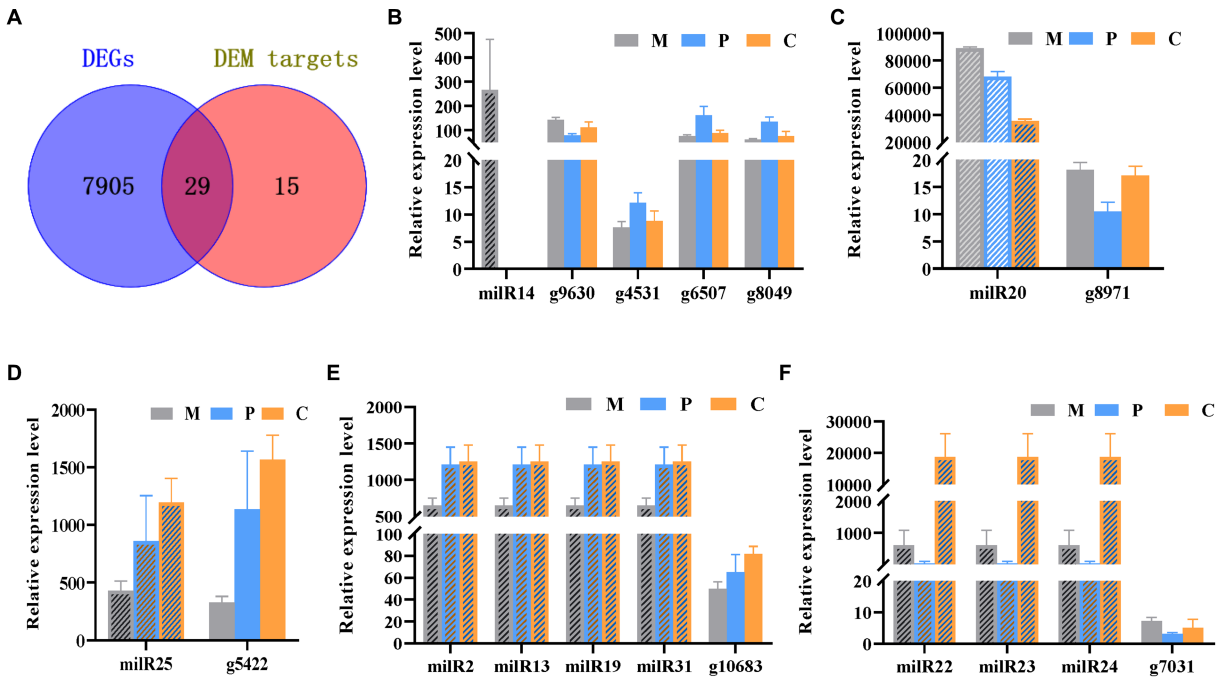

FIGURE 5
Integrated analyses of mRNA and milRNA data. **(A)** Venn diagram depicting the DEGs in the different stages of development and DEM targets. **(B–F)** Analysis of the expression levels of the DEMs and their targets DEGs.

TABLE 1 Enriched KEGG pathways of target DEGs of DEMs.

milRNA	Target	KEGG pathway	Target gene annotation
milR14	g9630	Endocytosis (ko04144)	Putative GTPase activating protein
milR14	g8049	RNA transport (ko03013)	Eukaryotic initiation factor 4E
milR14	g6507	Aminoacyl-tRNA biosynthesis (ko00970)	Arginine-tRNA ligase
milR14	g4531	Biosynthesis of antibiotics (ko01130)	Squalene/phytoene synthase
milR19	g10683	Protein processing in endoplasmic reticulum (ko04141)	Uncharacterized J domain-containing protein
milR20	g8971	MAPK signaling pathway (ko04011)	Pheromone A receptor
milR25	g5422	Protein processing in endoplasmic reticulum (ko04141)	Hsp70 protein

opposite expression trend to *g8971* from stage P to C. So milR20 was selected for further analyses.

3.5. milR20 targets *g8971* and inhibits its expression

The results of prediction using the RNAhybrid software revealed that milR20 targeted the 848–868 nt region of the *g8971* gene (Figure 6A). Dual-luciferase reporter assays were performed for elucidating the targeting relationship between milR20 and its target gene, *g8971*. The WT *g8971* reporter vector (g8971-WT) and the mutant plasmids (g8971-MT) were constructed, and co-transfection experiments were performed. The results of the dual-luciferase assay demonstrated that milR20 significantly reduced the relative luciferase activity of g8971-WT. However, there was no significant effect on the relative luciferase activity of g8971-MT. These findings therefore indicated that milR20 could negatively regulate the expression of *g8791* by directly binding to and targeting *g8971* (Figure 6B).

3.6. Functional analysis of milR20 by STTM-mediated silencing and overexpression

In this study, the copy number of milR20 in the genome of *P. cornucopiae* was first determined by comparing the milRNA sequence with the genome using the BLASTn program. The results demonstrated that there was only one copy of milR20 in the genome. The precursor sequence of milR20 (pre-milR20) was identified and analyzed using the miRDeep2 software. A 250 bp-long sequence of

10.3389/fmicb.2023.1177820

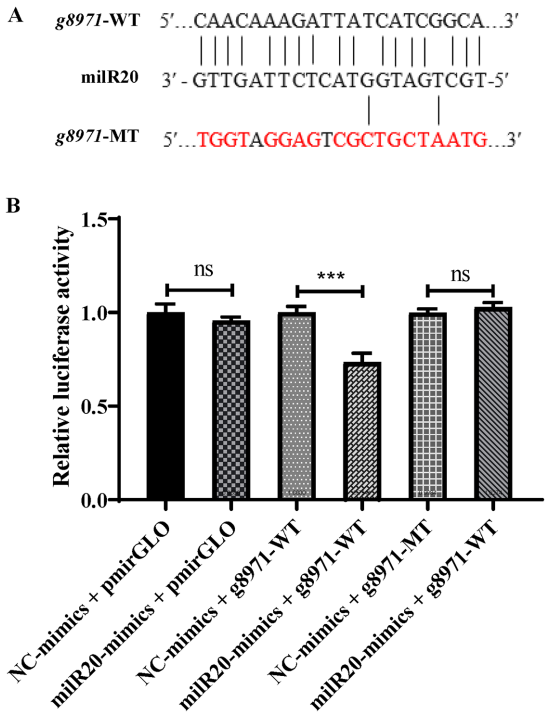

FIGURE 6
Verification of the targeting relationship between milR20 and *g8971*. **(A)** The specific binding sites of milR20 in the sequence of *g8971* are depicted, and the mutation sites were designed based on this sequence. The sequences in red represent the mutation sites. **(B)** The activity of luciferase was measured by dual-luciferase reporter assays. The activities of luciferase of g8971-WT decreased markedly in cells transfected with miR-milR20 compared to that of the control. The values are depicted as the mean±SE; ***$p<0.001$.

pre-milR20 was obtained and represented as hairpin structures, which verified that milR20 was a real milRNA (Supplementary Figure S5).

In order to explore whether milR20 has any role in the development of *P. cornucopiae*, milR20 was separately silenced and overexpressed and the phenotypic effects were analyzed. STTM-mediated silencing has been shown to be an effective tool for inhibiting the activity of endogenous mature miRNAs in plants. In this study, we designed milR20 STTM constructs containing two same non-cleavable milRNA binding sites (highlighted in blue in Figure 7A), and linked by a 48–88 nt spacer (colored in yellow). We generated transgenic strains in which milR20 was overexpressed or silenced with STTM. Analysis of the expression levels of milR20 in the M stage of the transgenic strains revealed that the expression of milR20 increased significantly in the OE-milR20 strain compared to that in the WT, while its expression in the STTM-milR20 strain (32–75%) decreased significantly compared to that of the WT (Figure 7B).

The effect of milR20 on the development of *P. cornucopiae* was detected by analyzing the mycelial growth of the WT and mutant strains that had been incubated on PDA plates. The rate of mycelial growth in the OE-milR20 strain was significantly lower than that of the WT strain; however, the rate of mycelial growth in the STTM-milR20 strain was significantly higher than that of the WT strain (Figures 7C,D). These findings indicated that milR20 may play a negative role in mycelial growth.

The effect of milR20 on the development of the fruiting bodies of *P. cornucopiae* was subsequently detected by cultivating the mutant and WT strains on cultivation substrates. The time required for the formation of primordia was initially analyzed statistically. The primordia appeared on the 28th to the 29th day in all the strains, and there were no significant differences between the mutants and WT with respect to the time required for the formation of primordia. This finding indicated that milR20 had no influence on the formation of primordia (Supplementary Figure S6). Analysis of the morphology of the fruiting bodies revealed that the developmental cycle of the fruiting bodies was prolonged in the OE-milR20 strain that overexpressed milR20, compared to that of the WT. However, the developmental cycle of the fruiting bodies was slightly shortened in the STTM-milR20 strain compared to that of the WT. Analysis of the spore morphology revealed that the spore print density of the OE-milR20 strain did not exhibit significant alterations compared to that of the WT, while the quantity of spores produced by the STTM-milR20 strain increased slightly (Figure 7C). Detection of the expression levels of the target *g8971* gene of milR20 revealed that *g8971* was downregulated in the OE-milR20 strain, while there was no significant difference in the expression of *g8971* in the STTM-milR20 strain (Figure 7E). These results indicated that milR20 may negatively regulate the development of the fruiting bodies of *P. cornucopiae* by inhibiting the expression of *g8971*.

4. Discussion

Previous studies have demonstrated that miRNAs have an important role in the development of plant and animals. The development of high-throughput sequencing technologies has enabled the identification of milRNAs from various species of fungi in recent years. However, there is a scarcity of information regarding the functions of milRNAs in fungi. *Pleurotus cornucopiae* is an important mushroom that has been used for studying the functions of milRNAs in fungal development. AGO, Dicer, and RDRP proteins are key components of miRNA maturation and function in *N. crassa* and are conserved in *C. militaris* and other fungal species that have been reported to possess milRNAs (Lee et al., 2010; Yang et al., 2013; Shao et al., 2019; Wang et al., 2021). The present study demonstrated that the AGO, Dicer, and RDRP proteins of these fungal species were closely related to those of *P. cornucopiae*, which indicated that mechanisms of milRNA biogenesis also exist in *P. cornucopiae*. The number of genes encoding Dicer, AGO, and RDRP proteins vary across different fungal species, and the expression patterns of these homologs vary across the different developmental stages (Lee et al., 2010; Shao et al., 2019, 2020; Wang et al., 2021). This suggests that the homologs of genes encoding Dicers, AGOs, and RDRPs may play different roles during the formation of mature milRNAs from dsRNAs, and the expression and functions of milRNAs also vary during development. In this study, the expression level of genes encoding Dicers, AGOs, and RDRPs were analyzed by transcriptome analysis across the different developmental stages of *P. cornucopiae*. All the genes were expressed at different developmental stages, and there were

10.3389/fmicb.2023.1177820

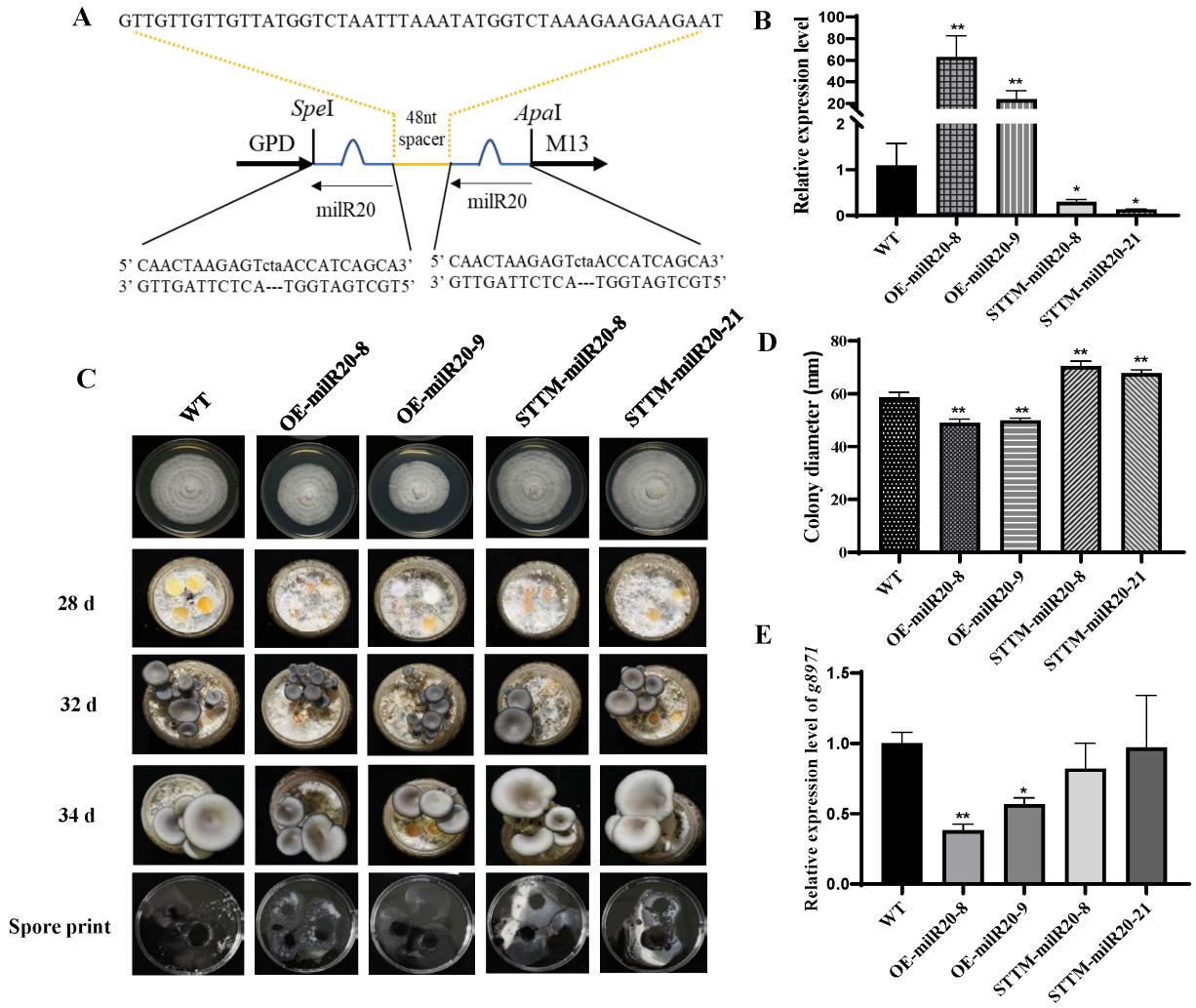

FIGURE 7
Effect of milR20 on the development of *Pleurotus cornucopiae*. **(A)** Schematic representation of the structure of the STTM plasmids that were used for silencing milR20. A target mimic with an unmodified central sequence (highlighted in blue) that was complementary to the central portion of milR20 and had a trinucleotide bulge was inserted at the cleavage site located at 10–11nt of the miRNA. **(B)** Analysis of the relative expression levels of the WT and mutants by qRT-PCR. **(C)** Phenotype of the WT and mutant strains at different developmental stages. **(D)** Statistics of the colony diameter of the WT and milR20-recombinant strains under normal temperature, determined using SPSS. **(E)** Detection of the expression levels of the target *g8971* gene of milR20 in the WT and mutant strains by qRT-PCR; * and ** indicate significant difference at $p<0.05$ and $p<0.01$, respectively.

variations in the expression patterns, which suggested that the homologs of genes encoding Dicers, AGOs, and RDRPs may function in a coordinated manner to regulate the expression and function of milRNAs during the development of *P. cornucopiae*.

The results of mRNA analysis demonstrated that the DEGs among the different development stages were mainly enriched in the signaling and growth terms in the biological process category of GO, and in the MAPK signaling pathway of KEGG. These findings indicated that the genes that were involved in the MAPK signaling pathway could be involved in the development of *P. cornucopiae*, and this finding was consistent with the results of previous studies on plants (Yi et al., 2016; Xiao et al., 2017; Chen et al., 2021). MAPK cascades are known to transmit extracellular signals to intracellular targets and play a crucial role in regulating several fundamental processes, including proliferation, differentiation, and cellular response to diverse extrinsic stresses (Guo et al., 2020).

In this study, the results of milRNA analysis demonstrated that a total of 32 milRNAs were identified in the M, P, and C stages, and the majority of these milRNAs were expressed at all the stages. However, the expression levels of the milRNAs varied across the three developmental stages. A total of 20 milRNAs were differently expressed in the three M vs. P, M vs. C, and P vs. C comparison groups, of which the number of downregulated DEMs was higher than the number of upregulated DEMs. These results indicated that the downregulated milRNAs could play a vital role in the development of *P. cornucopiae*. MiRNAs are important regulators of gene expression and function *via* degradation or translational repression of the target mRNAs (Moran et al., 2017). Integrated analysis of the milRNAs and mRNAs revealed that the target DEGs of the DEMs mapped to the MAPK signaling pathway, and this finding was consistent with the results of mRNA analysis. These results indicated that the milRNAs which regulated the MAPK signaling pathway could play a significant

role in the development of *P. cornucopiae*, and was consistent with the findings of previous studies which reported that miRNAs regulate the activity of the MAPK cascade and influence cellular proliferation in animals (Chen et al., 2017; Xiao et al., 2018; Xu et al., 2018; Safa et al., 2020; Zhang H. et al., 2020).

Correlation analysis of the milRNA expression profiles and their target genes revealed that only a small number of the milRNA-mRNA pairs exhibited an opposite expression pattern in the different developmental stages. These results indicated that the expression of the majority of target genes was possibly not negatively regulated by the milRNAs. Previous studies have also demonstrated an incoherent regulation between miRNAs/milRNAs and their target genes (Shao et al., 2019). This could be attributed to the fact that milRNAs primarily mediate gene regulation by repressing mRNA translation in fungi and not *via* mRNA degradation. Considering the complex regulatory network of gene expression, this could be alternatively explained by the fact that the expression of target genes can also be regulated by other genes, including genes encoding transcription factors, and competing endogenous RNAs that competitively bind to miRNAs (Kartha and Subramanian, 2014).

In this study, the results of the dual-luciferase activity assay and qRT-PCR results revealed that milR20 targeted the *g8971* and inhibited the expression of *g8971*. The expression of milR20 was downregulated in both the M vs. C and P vs. C comparison groups, and the target gene of milR20, *g8971*, was invovled in the MAPK signaling pathway and could play a vital role in the development of *P. cornucopiae*. Therefore, the functions of milR20 in the development of *P. cornucopiae* were subsequently analyzed using overexpressing and silencing by short tandem target mimic (STTM) technology in this study.

The STTM technology mimics the binding of target miRNAs to RNA-induced silencing complex (RISC) to inhibit the functions of target miRNAs (Teotia et al., 2016). This method has been proven to be an effective and stable tool for blocking the activity of endogenous mature miRNAs in plants (Jia et al., 2015; Zhang et al., 2017). In this study, the expression levels of milR20 decreased significantly in the STTM-milR20 strain, indicating that the STTM technology can also be used to effectively silence fungal milRNAs. The mycelial growth rates and the development of fruit body in the OE-milR20 strain were reduced and prolonged, while those of the STTM-milR20 strain were the opposite in comparison to that of the WT strain. The expression level of *g8971* in the OE-milR20 were significantly decreased, while no significant difference in STTM-miR20 strains. These could be explained by the expression fold change difference of milR20 in different strains or the regulation of *g8971* by other genes. These findings indicated that milR20 could negatively regulate the growth of *P. cornucopiae* by repressing the expression of *g8971* regulating the MAPK signaling pathway.

Data availability statement

The original sequence data of transcriptome can be found at the following link: https://www.ncbi.nlm.nih.gov/bioproject/PRJNA943625 and the milRNA sequence data can be found at the following link: https://www.ncbi.nlm.nih.gov/bioproject/PRJNA944818. Other data presented in this study are available in Supplementary material.

Author contributions

LZ designed the study and prepared the manuscript. YQ performed the experiments and analyzed the data. YQ, CH, MZ, XW, GL, YZ, and LZ discussed the results. All authors contributed to the article and approved the submitted version.

Funding

This study was financially supported by the China Agriculture Research System (CARS20), Fundamental Research Funds for Central Nonprofit Scientific Institution (No. 1610132020004), National Key R&D Program of China (2022YFD1200600), and the Beijing Agriculture Innovation Consortium (BAIC03).

Conflict of interest

The authors declare that the research was conducted in the absence of any commercial or financial relationships that could be construed as a potential conflict of interest.

Publisher's note

Supplementary material

The Supplementary material for this article can be found online at: https://www.frontiersin.org/articles/10.3389/fmicb.2023.1177820/full#supplementary-material

References

Cai, B. L., Li, Z. H., Ma, M. T., Wang, Z. J., Han, P. G., Abdalla, B. A., et al. (2017). LncRNA-Six1 encodes a micropeptide to activate Six1 in cis and is involved in cell proliferation and muscle growth. *Front. Physiol.* 8:230. doi: 10.3389/fphys.2017.00230

Chen, J., Wang, L., and Yuan, M. (2021). Update on the roles of rice MAPK cascades. *Int. J. Mol.Sci.* 22:1679. doi: 10.3390/ijms22041679

Chen, P., Xu, W., Luo, Y., Zhang, Y., He, Y., Yang, S., et al. (2017). MicroRNA 543 suppresses breast cancer cell proliferation, blocks cell cycle and induces cell apoptosis via direct targeting of ERK/MAPK. *Onco. Targets. Ther.* 10, 1423–1431. doi: 10.2147/OTT.S118366

Chen, X. X., Xu, C., Qian, Y., Liu, R., Zhang, Q. Q., Zeng, G. H., et al. (2016). MAPK cascade-mediated regulation of pathogenicity, conidiation and tolerance to abiotic stresses in the entomopathogenic fungus *Metarhizium robertsii*. *Environ. Microbiol.* 18, 1048–1062. doi: 10.1111/1462-2920.13198

Enright, A. J., John, B., Gaul, U., Tuschl, T., Sander, C., and Marks, D. S. (2003). MicroRNA targets in *Drosophila*. *Genome Biol.* 5:R1. doi: 10.1186/gb-2003-5-1-r1

Fahlgren, N., Howell, M. D., Kasschau, K. D., Chapman, E. J., Sullivan, C. M., Cumbie, J. S., et al. (2007). High-throughput sequencing of *Arabidopsis* microRNAs: evidence for frequent birth and death of MIRNA genes. *PLoS One* 2:e219. doi: 10.1371/journal.pone.0000219

Friedlander, M. R., Mackowiak, S. D., Li, N., Chen, W., and Rajewsky, N. (2012). miRDeep2 accurately identifies known and hundreds of novel microRNA genes in seven animal clades. *Nucleic Acids Res.* 40, 37–52. doi: 10.1093/nar/gkr688

Grentzmann, G., Ingram, J. A., Kelly, P. J., Gesteland, R. F., and Atkins, J. F. (1998). A dual-luciferase reporter system for studying recoding signals. *RNA* 4, 479–486.

Guo, Y. J., Pan, W. W., Liu, S. B., Shen, Z. F., Xu, Y., and Hu, L. L. (2020). ERK/MAPK signalling pathway and tumorigenesis. *Exp. Ther. Med.* 19, 1997–2007. doi: 10.3892/etm.2020.8454

Hou, L., Zhao, M., Huang, C., He, Q., Zhang, L., and Zhang, J. (2021). Alternative oxidase gene induced by nitric oxide is involved in the regulation of ROS and enhances the resistance of *Pleurotus ostreatus* to heat stress. *Microb. Cell Factories* 20:137. doi: 10.1186/s12934-021-01626-y

Hu, Y., Stenlid, J., Elfstrand, M., and Olson, A. (2013). Evolution of RNA interference proteins dicer and argonaute in *Basidiomycota*. *Mycologia* 105, 1489–1498. doi: 10.3852/13-171

Jia, X., Bi, Y., Li, J., Xie, Q., Yang, H., and Liu, W. (2015). Cellular microRNA miR-26a suppresses replication of porcine reproductive and respiratory syndrome virus by activating innate antiviral immunity. *Sci. Rep.* 5:10651. doi: 10.1038/srep10651

Jones-Rhoades, M. W., Bartel, D. P., and Bartel, B. (2006). MicroRNAs and their regulatory roles in plants. *Annu. Rev. Plant Biol.* 57, 19–53. doi: 10.1146/annurev.arplant.57.032905.105218

Kanehisa, M., Goto, S., Kawashima, S., Okuno, Y., and Hattori, M. (2004). The KEGG resource for deciphering the genome. *Nucleic Acids Res.* 32, 277D–2280D. doi: 10.1093/nar/gkh063

Kang, K., Zhong, J., Jiang, L., Liu, G., Gou, C. Y., Wu, Q., et al. (2013). Identification of microRNA-like RNAs in the filamentous fungus *Trichoderma reesei* by solexa sequencing. *PLoS One* 8:e76288. doi: 10.1371/journal.pone.0076288

Kartha, R. V., and Subramanian, S. (2014). Competing endogenous RNAs (ceRNAs): new entrants to the intricacies of gene regulation. *Front. Genet.* 5:8. doi: 10.3389/fgene.2014.00008

Kim, H. J., Chen, C. B., Kabbage, M., and Dickman, M. B. (2011). Identification and characterization of *Sclerotinia Sclerotiorum* NADPH oxidases. *Appl. Environ. Microbiol.* 77, 7721–7729. doi: 10.1128/Aem.05472-11

Kiriga, W. J., Chunyi, Z., Jun, L., and Huan, W. (2020). Plant non-coding RNAs: origin, biogenesis, mode of action and their roles in abiotic stress. *Int. J. Mol. Sci.* 21:8401. doi: 10.3390/ijms21218401

Koonin, E. V., Fedorova, N. D., Jackson, J. D., Jacobs, A. R., Krylov, D. M., Makarova, K. S., et al. (2004). A comprehensive evolutionary classification of proteins encoded in complete eukaryotic genomes. *Genome Biol.* 5:R7. doi: 10.1186/gb-2004-5-2-r7

Kumar, S., Stecher, G., and Tamura, K. (2016). MEGA7: molecular evolutionary genetics analysis version 7.0 for bigger datasets. *Mol. Biol. Evol.* 33, 1870–1874. doi: 10.1093/molbev/msw054

Langmead, B., Trapnell, C., Pop, M., and Salzberg, S. L. (2009). Ultrafast and memory-efficient alignment of short DNA sequences to the human genome. *Genome Biol.* 10:R25. doi: 10.1186/gb-2009-10-3-r25

Lara-Rojas, F., Sanchez, O., Kawasaki, L., and Aguirre, J. (2011). *Aspergillus nidulans* transcription factor AtfA interacts with the MAPK SakA to regulate general stress responses, development and spore functions. *Mol. Microbiol.* 80, 436–454. doi: 10.1111/j.1365-2958.2011.07581.x

Lee, H. C., Li, L., Gu, W., Xue, Z., Crosthwaite, S. K., Pertsemlidis, A., et al. (2010). Diverse pathways generate microRNA-like RNAs and dicer-independent small interfering RNAs in fungi. *Mol. Cell* 38, 803–814. doi: 10.1016/j.molcel.2010.04.005

Li, B., Cheng, X. S., Zhang, T., Liu, L. L., Nie, Z. M., and Sheng, Q. (2016). The identification of microRNAs in *Ganoderma lingzhi sporocarp*. *Mycoscience* 57, 271–278. doi: 10.1016/j.myc.2016.03.004

Mao, X., Cai, T., Olyarchuk, J. G., and Wei, L. (2005). Automated genome annotation and pathway identification using the KEGG Orthology (KO) as a controlled vocabulary. *Bioinformatics* 21, 3787–3793. doi: 10.1093/bioinformatics/bti430

Meng, L., Lyu, X. M., Shi, L. L., Wang, Q. J., Wang, L., Zhu, M. J., et al. (2021). The transcription factor FvHmg1 negatively regulates fruiting body development in winter mushroom *Flammulina velutipes*. *Gene* 785:145618. doi: 10.1016/j.gene.2021.145618

Moran, Y., Agron, M., Praher, D., and Technau, U. (2017). The evolutionary origin of plant and animal microRNAs. *Nat. Ecol. Evol.* 1:27. doi: 10.1038/s41559-016-0027

Mu, D. S., Li, C. Y., Shi, L., Zhang, X. C., Ren, A., and Zhao, M. W. (2015). Bioinformatic identification of potential MicroRNAs and their targets in the Lingzhi or Reishi medicinal mushroom *Ganoderma lucidum* (higher basidiomycetes). *Int. J. Med. Mushrooms* 17, 783–797. doi: 10.1615/IntJMedMushrooms.v17.i8.80

Qiu, Z., Wu, X., Gao, W., Zhang, J., and Huang, C. (2018). High temperature induced disruption of the cell wall integrity and structure in *Pleurotus ostreatus* mycelia. *Appl. Microbiol. Biotechnol.* 102, 6627–6636. doi: 10.1007/s00253-018-9090-6

Rehmsmeier, M., Steffen, P., Hochsmann, M., and Giegerich, R. (2004). Fast and effective prediction of microRNA/target duplexes. *RNA* 10, 1507–1517. doi: 10.1261/rna.5248604

Rocha, C. R. C., Schroppel, K., Harcus, D., Marcil, A., Dignard, D., Taylor, B. N., et al. (2001). Signaling through adenylyl cyclase is essential for hyphal growth and virulence in the pathogenic fungus *Candida albicans*. *Mol. Biol. Cell* 12, 3631–3643. doi: 10.1091/mbc.12.11.3631

Safa, A., Abak, A., Shoorei, H., Taheri, M., and Ghafouri-Fard, S. (2020). MicroRNAs as regulators of ERK/MAPK pathway: a comprehensive review. *Biomed. Pharmacother.* 132:110853. doi: 10.1016/j.biopha.2020.110853

Shao, Y., Tang, J., Chen, S., Wu, Y., Wang, K., Ma, B., et al. (2019). milR4 and milR16 mediated fruiting body development in the medicinal fungus *Cordyceps militaris*. *Front. Microbiol.* 10:83. doi: 10.3389/fmicb.2019.00083

Shao, J., Wang, L., Liu, Y., Qi, Q., Wang, B., Lu, S., et al. (2020). Identification of milRNAs and their target genes in *Ganoderma lucidum* by high-throughput sequencing and degradome analysis. *Fungal Genet. Biol.* 136:103313. doi: 10.1016/j.biopha.2020.110853

Tatusov, R. L., Galperin, M. Y., Natale, D. A., and Koonin, E. V. (2000). The COG database: a tool for genome-scale analysis of protein functions and evolution. *Nucleic Acids Res.* 28, 33–36. doi: 10.1093/nar/28.1.33

Teotia, S., Singh, D., Tang, X. Q., and Tang, G. L. (2016). Essential RNA-based technologies and their applications in plant functional genomics. *Trends Biotechnol.* 34, 106–123. doi: 10.1016/j.tibtech.2015.12.001

Thompson, J. D., Higgins, D. G., and Gibson, T. J. (1994). Improving the sensitivity of progressive multiple sequence alignment through sequence weighting, position-specific gap penalties and weight matrix choice. *Nucleic Acids Res.* 22, 4673–4680. doi: 10.1093/nar/22.22.4673

Wang, G., Li, M., Zhang, C., Zhan, N., Cheng, H., Gao, Y., et al. (2021). Identification of microRNA-like RNAs in *Cordyceps guangdongensis* and their expression profile under differential developmental stages. *Fungal Genet. Biol.* 147:103505. doi: 10.1016/j.fgb.2020.103505

Wu, T. J., Hu, C. C., Xie, B. G., Wei, S. L., Zhang, L., Zhu, Z. X., et al. (2020). A putative transcription factor LFC1 negatively regulates development and yield of winter mushroom. *Appl. Microbiol. Biotechnol.* 104, 5827–5844. doi: 10.1007/s00253-020-10642-8

Xiao, X., Tang, Z., Li, X., Hong, Y., Li, B., Xiao, W., et al. (2017). Overexpressing OsMAPK12-1 inhibits plant growth and enhances resistance to bacterial disease in rice. *Funct. Plant Biol.* 44, 694–704. doi: 10.1071/Fp16397

Xiao, S., Yang, M., Yang, H., Chang, R., Fang, F., and Yang, L. (2018). miR-330-5p targets SPRY2 to promote hepatocellular carcinoma progression via MAPK/ERK signaling. *Oncogene* 7:90. doi: 10.1038/s41389-018-0097-8

Xu, M., Li, J., Wang, X., Meng, S., Shen, J., Wang, S., et al. (2018). MiR-22 suppresses epithelial-mesenchymal transition in bladder cancer by inhibiting snail and MAPK1/slug/vimentin feedback loop. *Cell Death Dis.* 9:209. doi: 10.1038/s41419-017-0206-1

Xu, D. Y., Zhou, Q. X., Yan, B. Y., and Ma, A. M. (2021). Identification and physiological function of one microRNA (Po-MilR-1) in oyster mushroom *Pleurotus ostreatus*. *Mycoscience* 62, 182–188. doi: 10.47371/mycosci.2021.01.004

Yang, Q., Li, L., Xue, Z., Ye, Q., Zhang, L., Li, S., et al. (2013). Transcription of the major neurospora crassa microRNA-like small RNAs relies on RNA polymerase III. *PLoS Genet.* 9:e1003227. doi: 10.1371/journal.pgen.1003227

Yi, J., Lee, Y. S., Lee, D. Y., Cho, M. H., Jeon, J. S., and An, G. (2016). OsMPK6 plays a critical role in cell differentiation during early embryogenesis in *Oryza sativa*. *J. Exp. Bot.* 67, 2425–2437. doi: 10.1093/jxb/erw052

Zdanowicz, A., Thermann, R., Kowalska, J., Jemielity, J., Duncan, K., Preiss, T., et al. (2009). Drosophila miR2 primarily targets the m(7)GpppN cap structure for translational repression. *Mol. Cell* 35, 881–888. doi: 10.1016/j.molcel.2009.09.009

Zeng, W., Wang, J., Wang, Y., Lin, J., Fu, Y., Xie, J., et al. (2018). Dicer-like proteins regulate sexual development via the biogenesis of perithecium-specific micrornas in a plant pathogenic fungus *Fusarium graminearum*. *Front. Microbiol.* 9:818. doi: 10.3389/fmicb.2018.00818

Zhang, J. J., Hao, H. B., Wu, X. L., Wang, Q., Chen, M. J., Feng, Z. Y., et al. (2020). The functions of glutathione peroxidase in ROS homeostasis and fruiting body development in *Hypsizygus marmoreus*. *Appl. Microbiol. Biotechnol.* 104, 10555–10570. doi: 10.1007/s00253-020-10981-6

Zhang, J., Liu, H., Lin, H., Li, S. C., Tao, H. H., Zhang, L., et al. (2017). Sp1 is a competitive endogenous RNA of Klf4 during odontoblast differentiation. *Int. J. Biochem. Cell B.* 85, 159–165. doi: 10.1016/j.biocel.2017.02.008

Zhang, H., Sun, P., Wang, Y. L., Yu, X. F., and Tong, J. J. (2020). MiR-214 promotes proliferation and inhibits apoptosis of oral cancer cells through MAPK/ERK signaling pathway. *Eur. Rev. Med. Pharmacol. Sci.* 24, 3710–3716. doi: 10.26355/eurrev_202004_20834

Zhou, J. H., Fu, Y. P., Xie, J. T., Li, B., Jiang, D. H., Li, G. Q., et al. (2012). Identification of microRNA-like RNAs in a plant pathogenic fungus *Sclerotinia sclerotiorum* by high-throughput sequencing. *Mol. Gen. Genomics.* 287, 275–282. doi: 10.1007/s00438-012-0678-8

Zhou, Q., Wang, Z., Zhang, J., Meng, H., and Huang, B. (2012). Genome-wide identification and profiling of microRNA-like RNAs from *Metarhizium anisopliae* during development. *Fungal Biol.* 116, 1156–1162. doi: 10.1016/j.funbio.2012.09.001

frontiers | Frontiers in Microbiology

TYPE Correction
PUBLISHED 12 July 2023
DOI 10.3389/fmicb.2023.1236756

OPEN ACCESS

APPROVED BY
Frontiers Editorial Office,
Frontiers Media SA, Switzerland

*CORRESPONDENCE
Lijiao Zhang
✉ zhanglijiao@caas.cn

RECEIVED 08 June 2023
ACCEPTED 30 June 2023
PUBLISHED 12 July 2023

CITATION
Qi Y, Huang C, Zhao M, Wu X, Li G, Zhang Y and Zhang L (2023) Corrigendum: milR20 negatively regulates the development of fruit bodies in *Pleurotus cornucopiae*. *Front. Microbiol.* 14:1236756. doi: 10.3389/fmicb.2023.1236756

Corrigendum: milR20 negatively regulates the development of fruit bodies in *Pleurotus cornucopiae*

Yuhui Qi[1,2,3], Chenyang Huang[1,2,3], Mengran Zhao[1,2,3], Xiangli Wu[1,2,3], Guangyu Li[1,2,3], Yingjie Zhang[1,2,3,4] and Lijiao Zhang[1,2,3]*

[1]Institute of Agricultural Resources and Regional Planning, Chinese Academy of Agricultural Sciences, Beijing, China, [2]Key Laboratory of Microbial Resources, Ministry of Agriculture and Rural Affairs, Beijing, China, [3]State Key Laboratory of Efficient Utilization of Arid and Semi-arid Arable Land in Northern China, Beijing, China, [4]College of Life Sciences, Shanxi Normal University, Taiyuan, China

KEYWORDS

milR20, fruit body development, *Pleurotus cornucopiae*, comparative transcriptome, MAPK signaling pathway

A corrigendum on
milR20 negatively regulates the development of fruit bodies in *Pleurotus cornucopiae*

by Qi, Y., Huang, C., Zhao, M., Wu, X., Li, G., Zhang, Y., and Zhang, L. (2023). *Front. Microbiol.* 14:1177820. doi: 10.3389/fmicb.2023.1177820

In the published article, there was an error in Figure 5 as published. The gene in Figure 5E was displayed as "g3400". The correct statement is "g10683". The gene in Figure 5F was displayed as "g3400". The correct statement is "g7031". The corrected Figure 5 and its caption appear below.

In the published article, there was an error in the Funding statement. The names of the first two funding bodies were incorrectly presented as "Fundamental Research Funds for China Agriculture Research System" and "Central Nonprofit Scientific Institution". The correct Funding statement appears below.

Funding

This study was financially supported by the China Agriculture Research System (CARS20), Fundamental Research Funds for Central Nonprofit Scientific Institution (No. 1610132020004), National Key R&D Program of China (2022YFD1200600), and the Beijing Agriculture Innovation Consortium (BAIC03).

The authors apologize for this error and state that this does not change the scientific conclusions of the article in any way. The original article has been updated.

Publisher's note

10.3389/fmicb.2023.1236756

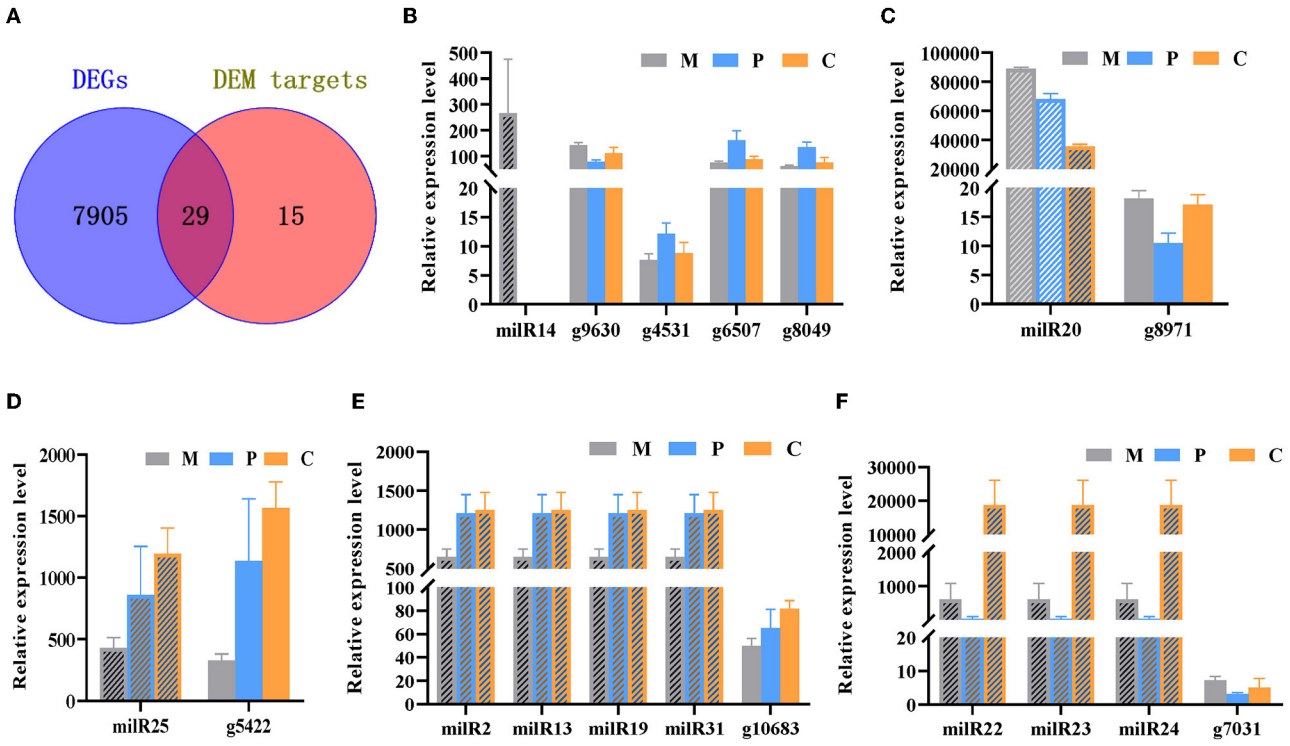

FIGURE 5
Integrated analyses of mRNA and milRNA data. **(A)** Venn diagram depicting the DEGs in the different stages of development and DEM targets. **(B–F)** Analysis of the expression levels of the DEMs and their targets DEGs.

frontiers | Frontiers in Microbiology

TYPE Original Research
PUBLISHED 15 June 2023
DOI 10.3389/fmicb.2023.1211795

OPEN ACCESS

EDITED BY
Chenyang Huang,
Chinese Academy of Agricultural Sciences, China

REVIEWED BY
Yan Zhang,
Shandong Agricultural University, China
Yongxin Tao,
Fujian Agriculture and Forestry University, China
Mingwen Zhao,
Nanjing Agricultural University, China

*CORRESPONDENCE
Fangjie Yao
✉ yaofj@aliyun.com

†These authors have contributed equally to this work and share first authorship

RECEIVED 25 April 2023
ACCEPTED 22 May 2023
PUBLISHED 15 June 2023

CITATION
Ma X, Lu L, Yao F, Fang M, Wang P, Meng J, Shao K, Sun X and Zhang Y (2023) High-quality genome assembly and multi-omics analysis of pigment synthesis pathway in *Auricularia cornea*.
Front. Microbiol. 14:1211795.
doi: 10.3389/fmicb.2023.1211795

High-quality genome assembly and multi-omics analysis of pigment synthesis pathway in *Auricularia cornea*

Xiaoxu Ma[1,2†], Lixin Lu[1†], Fangjie Yao[1,3*], Ming Fang[1], Peng Wang[4], Jingjing Meng[1], Kaisheng Shao[2], Xu Sun[2] and Youmin Zhang[1]

[1]Lab of Genetic Breeding of Edible Fungi, Horticultural, College of Horticulture, Jilin Agricultural University, Changchun, China, [2]Guizhou Academy of Agricultural Sciences, Guizhou Key Laboratory of Edible Fungi Breeding, Guiyang, China, [3]Country Engineering Research Centre of Chinese Ministry of Education for Edible and Medicinal Fungi, Jilin Agricultural University, Changchun, China, [4]Economic Plants Research Insitute, Jilin Academy of Agricultural Sciences, Changchun, China

Owing to its great market potential for food and health care, white *Auricularia cornea*, a rare edible fungus, has received increased attention in recent years. This study presents a high-quality genome assembly of *A. cornea* and multi-omics analysis of its pigment synthesis pathway. Continuous Long Reads libraries, combined with Hi-C-assisted assembly were used to assemble of white *A. cornea*. Based on this data, we analyzed the transcriptome and metabolome of purple and white strains during the mycelium, primordium, and fruiting body stages. Finally, we obtained the genome of *A.cornea* assembled from 13 clusters. Comparative and evolutionary analysis suggests that *A.cornea* is more closely related to *Auricularia subglabra* than to *Auricularia heimuer*. The divergence of white/purple *A.cornea* occurred approximately 40,000 years ago, and there were numerous inversions and translocations between homologous regions of the two genomes. Purple strain synthesized pigment via the shikimate pathway. The pigment in the fruiting body of *A. cornea* was γ-glutaminyl-3,4-dihydroxy-benzoate. During pigment synthesis, α-D-glucose-1P, citrate, 2-Oxoglutarate, and glutamate were four important intermediate metabolites, whereas polyphenol oxidase and other 20 enzyme genes were the key enzymes. This study sheds light on the genetic blueprint and evolutionary history of the white *A.cornea* genome, revealing the mechanism of pigment synthesis in *A.cornea*. It has important theoretical and practical implications for understanding the evolution of basidiomycetes, molecular breeding of white *A.cornea*, and deciphering the genetic regulations of edible fungi. Additionally, it provides valuable insights for the study of phenotypic traits in other edible fungi.

KEYWORDS

***Auricularia cornea*, genome, transcriptome, metabolome, shikimate pathway, GDHB pigment**

Introduction

Auricularia cornea, which belongs to the genus *Auricularia* Bull. ex Juss. (Basidiomycota), is a highly nutritious, medicinally valuable fungus that can be used as both medicine and food (Baldrian and Lindahl, 2011). The rare white variety has great market potential due to its popularity. Genomic information is the basis for studying *A. cornea* color inheritance. It is also an important resource for studies including gene mapping, genetic diversity analysis, classification and phylogeny, germplasm evaluation, and molecular marker-assisted breeding (Wu et al., 2015; Cao et al., 2016). However, while the lack of a chromosome-level genome significantly limits *A. cornea* research and development, it also causes low integrity in the assembly of genome sequencing results used for research, limits polymorphic sites, and fails to reveal all genetic information characteristics. Therefore, insights into the basic genome structure of *A. cornea* are required to obtain a chromosome-level genome.

Over 30 edible fungi, including *Auricularia heimuer*, *Gloeostereum incarnatum*, *Agaricus bisporus*, *Flammulina velutipes*, *Pleurotus ostreatus*, and *Ganoderma lucidum*, have had their genomes sequenced and assembled, thanks to advances in sequencing techniques. These reference genomes are now important resources for studies regarding molecular marker-assisted breeding, population genetics, and comparative genomes (Morin et al., 2012; Young-Jin et al., 2014; Zhu et al., 2015; Qu et al., 2016; Yuan et al., 2019; Fang et al., 2020; Jiang et al., 2021). Although *A. cornea* sequencing and assembly have been completed, having a 78.50 M genome size and 51 contigs (Dai et al., 2019). Notably, current second- and third-generation sequencing methods can only assemble the genome to a contig/scaffold level, but the Hi-C method extends the draft genome. The latter involves sequencing DNA fragments after cross-linking and enrichment based on linear distances and close spatial structures. The analyzed sequencing data can reveal the interactions between DNA segments, deduce the genome 3D spatial structure, and determine the possible regulation between genes in order to construct a genome close to the chromosomal level. In addition to acquiring a chromosome-level genome, Hi-C-assisted assembly can improve the quality and continuity of the assembled genome by error correction, further optimizing the assembly results by determining whether the genome contains redundancy. As for giga-genome and polyploidy species, Hi-C can achieve effective mounting and haplotype analysis to produce a high-quality reference genome (Zhang et al., 2019).

Except for the high-quality genome analysis, the end products of the cellular regulatory process, known as metabolites, can sufficiently explain the phenotypic changes of a biological system but inadequately analyze metabolite diversity and the genetic mechanism. Therefore, synergistic analysis based on transcriptomics and metabolomics can provide accurate information regarding the gene–metabolite interaction and build a regulatory network for corresponding metabolites, thereby facilitating the study of gene function and metabolic pathways. The association analysis of transcriptome and metabolome was extensively used to elaborate the genetic and regulatory mechanisms of plants' metabolites (Cho et al., 2016; Hu et al., 2016; Wang et al., 2017; Li et al., 2018; Tingting et al., 2019). It has only been published in a few studies involving edible fungi, such as the anti-browning mechanism in *A. bisporus*, β-glucoside inhibitor in increasing cold-resistance of *Volvaria volvacea*, and high-temperature stress on *Lentinus edodes* (Zhao et al., 2019; Cai et al., 2021; Gong et al., 2022).

The color of *A. cornea*'s purple fruiting body varies from dark to light, showing a series of continuous changes. This indicates that the purple fruiting body of *A. cornea* is regulated by multiple genes in the pigment synthesis process, which presents a quantitative trait with continuous change. The white strain's fruiting body is completely white, which could be caused by the deletion or mutation of one or more key enzyme genes in the pigment synthesis pathway, which blocks the entire pathway and results in no pigment synthesis. A previous study demonstrated that the key enzyme influencing pigment synthesis in *A. cornea* was identified as glutamine-dependent amidotransferase (Gn-AT), which was also hypothesized to be the key enzyme for the synthesis of the pigment γ-glutamine-4-hydroxy-benzoate (GHB) (Wang et al., 2019). However, the complete pigment synthesis pathway, major genes involved in this pathway, and melanin type contained in *A. cornea* pigment remain unclear.

In this study, two sequencing models (Continuous Long Reads (CCS) Library and Circular Consensus Sequencing (CCS) Library) combined with Hi-C-assisted assembly were used to perform high-throughput sequencing on the white *A. cornea* genome to assemble the genome at the chromosome level. At various growth stages, the transcriptome and metabolome of the white strain ACW001 and purple strain ACP004 were compared and analyzed using a high-quality reference genome. Through multi-omics association, the coexpression of differentially expressed genes and metabolites was effectively analyzed in order to provide accurate information and construct a pigment synthesis model for the interaction between pigment synthesis genes and metabolites. Understanding the pathway and mechanism of pigment synthesis and its varieties can lay a solid foundation for the efficient breeding of white *A. cornea* and for the color genetic study of other edible fungi.

Results and analysis

Genome sequencing and Hi-C-assisted assembly

16 Gb raw data were generated from PacBio Sequel and Illumina NovaSeq PE150. After selection, assembly, and optimization, 79.01 Mb genome sequences comprising 28 contigs were obtained (Figure 1). Hi-C captured 24,808,063 pairs of reads that could pair with the genome, 17,376,358 valid read pairs were obtained after HiCUP quality control, and the reads were aligned to 23 contigs. Because the intra-chromosome interaction probability markedly exceeded that of inter-chromosome, different contigs were divided into different chromosomes, and 23 contigs were clustered into clusters resembling chromosomes. 99.63% of assembled sequences were mounted to 13 clusters; the N50 value was 6.03 Mb and N90 value was 4.56 Mb (Table 1). On the same chromosome, the interaction probability decreased as the interaction distance increased and the contigs could be ordered and oriented. In addition, a collinearity analysis of the existing genetic linkage and physical maps was performed (Supplementary Figure S1). BUSCO evaluation showed that only 26 of 1,764 single-copy genes were missing, with a 98.53% assembly integrity, exceeding the 97.60% of the Basidiomycota database and 98.30% of the fungal database (Manni et al., 2021a,b). The assembled genome is larger than *A. heimuer* (49.76 Mb) and *Auricularia polytricha* (38.69 Mb) of *Auricularia*, and similar to

10.3389/fmicb.2023.1211795

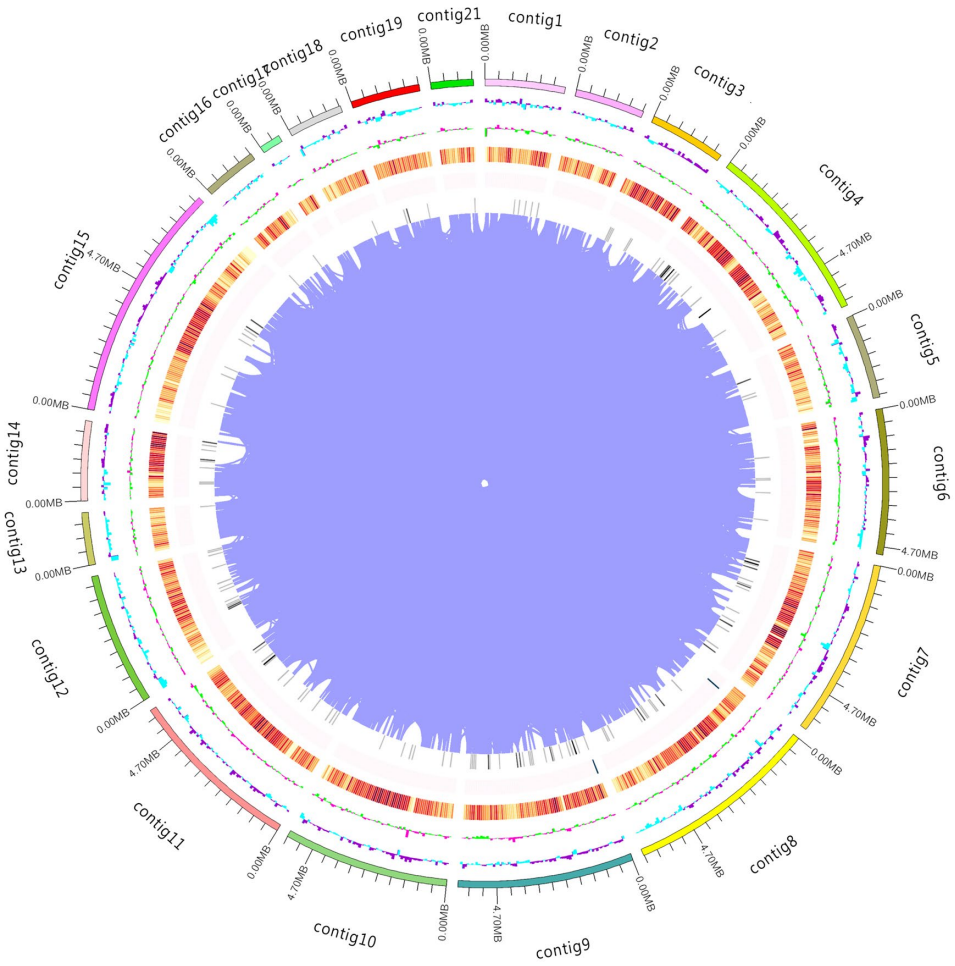

FIGURE 1
Whole genome map. The outermost circle represents the genomic sequence position coordinates. Moving from outer to inner, the next circles represent the genomic GC content, GC skew value, gene density (coding genes, rRNA, snRNA, and tRNA densities are counted separately, with darker colors indicating higher gene density in the window), and chromosome duplication.

TABLE 1 Assembly results of CLR and CCS.

Assembly feature	CCS Library	CLR Library
Assembly size (Mb)	79.01	78.24
Number of contigs	28	70
Contig N50 (bp)	5,662,720	23,93,831
Longest contig (bp)	8,179,760	5,514,487
Number of clusters	13	13
Assembly of genome (%)	99.63	74.35
GC (%)	59.06	59.65
Repeat region of assembly (%)	5.74	5.17
Number of predicted gene models	18,574	19,133
Average gene length (bp)	1,310	1,274

Auricularia subglabra (74.92 Mb). The current *A. cornea* genome had 23 fewer contigs than the previously disclosed genome, with higher N50 and N90 values and comparable guanine–cytosine (GC) content, suggesting that the current genome has higher quality and completeness.

Genome annotation

A total of 28,142 repetitive sequences were predicted, with a combined length of 4.75 megabases (Mb), accounting for 5.74% of the genome. Numerous transposable elements were identified, with long

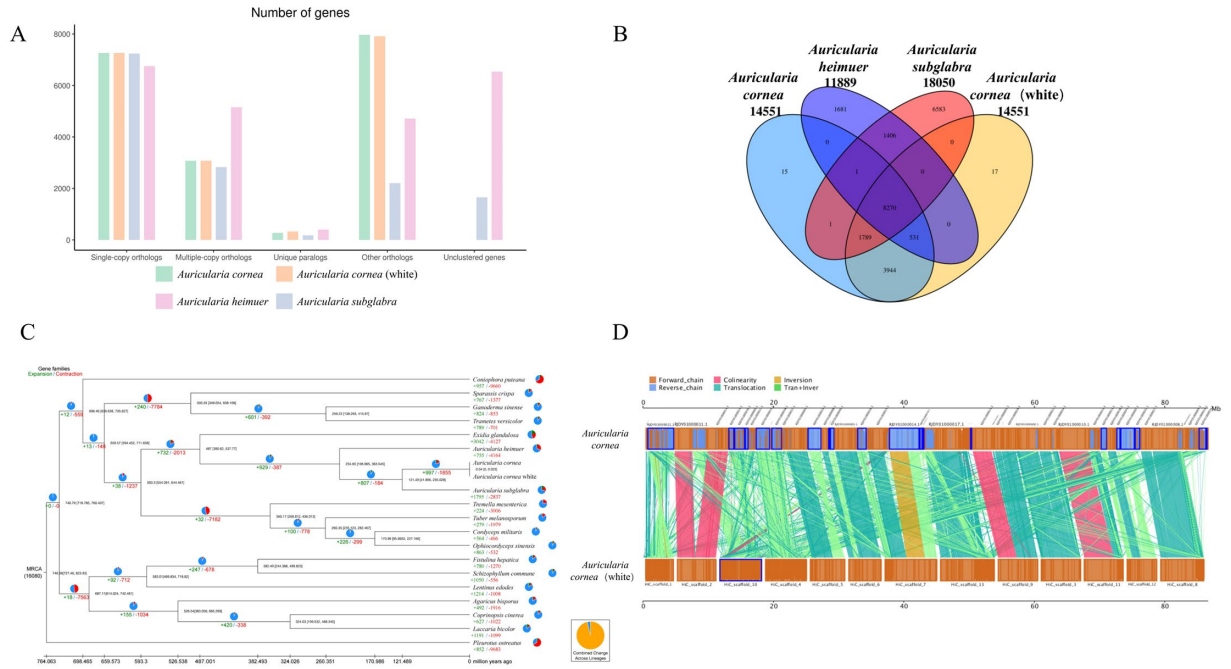

FIGURE 2
Genomic analyses. **(A)** Orthologous genes in the genomes of *A. cornea*, *A. cornea* white, *A. subglabra* and *A. heimuer*. **(B)** Unique and shared gene families among the four genomes. **(C)** Phylogenetic tree of 20 edible fungi. **(D)** The genome collinearity analysis of the *A. cornea*.

terminal repeat sequences (LTRs) being the most abundant, occupying 2.49% (2.06 Mb) of the genome, followed by long interspersed nuclear elements (LINEs), which accounted for 0.25% (0.21 Mb) of the genome. The proportion of LTRs in white *A. cornea* was significantly different from that in purple *A. cornea* (10.33%). These differences may be due to natural selection, species lifestyle, and ecological niche (Lan and Constabel, 2011), and could be an important factor causing the variations between white and purple *A. cornea*. A total of 9,423 simple sequence repeat (SSR) loci were detected, with a similar SSR locus density to black wood ear. The number of 3-base repeat units was the highest, which was 4,677, representing 49.63% of the total SSR repeat units.

To avoid the impact of repetitive sequences on the quality of gene prediction, we masked these regions during gene prediction. Using the Augustus program, we predicted a total of 18,574 coding genes, with a combined length of 24.33 Mb and an average length of 1,310 (bp). The coding regions accounted for 29.41% of the entire genome. Of these genes, 14,616 (78.69%) were supported by transcripts with a coverage of >80%. To gain a better understanding of the functions of the predicted genes, we compared them against eight widely used functional databases. Our results showed that 15,933 (86.20%) of the predicted genes had putative functions in these databases. Specifically, 14,844 (79.92%) had homologs in the Non-Redundant Protein Database (Nr), 9,278 (49.95%) were known proteins in the Gene Ontology (GO) database, 14,486 (77.99%) were known proteins in the Kyoto Encyclopedia of Genes and Genomes (KEGG), 1,929 (10.39%) were known proteins in the Cluster of Orthologous Groups of proteins (KOG) database, 2,763 (14.88%) were known proteins in the SwissProt database, 9,278 (49.95%) were known proteins in the Pfam database, 809 (4.36%)were known proteins in the Carbohydrate-active enzymes (CAZy)database, contained 893 CAZyme modules, and 475 (2.56%) were known proteins in the Transporter Classification Database (TCDB). Furthermore, we identified a total of 2.36 Mb of non-coding RNAs (ncRNAs), which accounted for 2.99% of the assembled genome. Among them, 211 were transfer RNAs (tRNAs), and 906 were ribosomal RNAs (rRNAs).

Secondary metabolic gene cluster analysis

The *A. cornea* genome contains 32 secondary metabolic gene clusters, including 20 terpene synthases, 1 type I polyketide synthase (PKS), 2 indole synthases, 1 nonribosomal peptide synthase, and 8 nonribosomal peptide synthases-like. While the most prevalent secondary metabolites of fungi are polyketides, a group of compounds synthesized by PKSs, quinones are common polyketide fungal pigments produced via the polyketide pathway (Feng et al., 2015). Therefore, type I PKS significantly contributes to fungal polyketide synthesis, and its gene cluster contains 9 genes located on contig 15.

Comparison and evolutionary analysis

To study the evolution of the gene family of white *A. cornea*, we compared the protein sequences with three other *Auricularia* species (Purple *A. cornea*, *A. heimuer* and *A. subglabra*) and 16 other edible fungi. A total of 1,997 homologous gene families were conserved in all compared genomes (Figure 2A). In the four *Auricularia* species genomes, there were approximately 8,270 conserved homologous gene families. Furthermore, we found 15 and 17 specific homologous gene families for white/purple *A. cornea*, respectively (Figure 2B). Functional analysis indicated that these

specific genes are associated with carbon source degradation and secondary metabolite metabolism. We then performed phylogenetic evolutionary analysis of 641 conserved single-copy homologous genes in all edible mushrooms, and the phylogenetic tree of 19 species showed that the *Auriculariales* clustered together on the same branch. *A. cornea* was closer to *A. subglabra* than to *A. heimuer* in terms of genetics (Figure 2C), which is consistent with previous reports. These results indicate that our phylogenetic tree accurately reflects the evolutionary relationship. The divergence time between *Auriculariales* and other orders was about 487 (390.62–537.77) Mya, and the divergence time between *A. cornea* and *A. subglabra* within the *Auriculariales* was about 121.49 (41.90–235.03) Mya. Based on the divergence time of white/purple *A. cornea*, it can be inferred that about 40,000 years ago, the purple *A. cornea* may have been affected by environmental factors or natural mutations that damaged the pigment synthesis pathway, resulting in the white mutant.

In the evolutionary process of *A. cornea*, contraction of gene families is more common than expansion, and a total of 997 gene families have been expanded in *A. cornea*. The number of contracted gene families in *A. cornea* (1,855) is much smaller than in the same genus *A. heimuer* (4,164) and *A. subglabra* (2,837). Functional analysis shows that these contracted gene families are mainly related to degradation metabolism, immune system, sorting, and degradation. These genes play a critical role in adapting to harsh environments and substrate degradation, leading to the widespread distribution of *A. cornea* in *Auricularia*.

We conducted a whole-genome collinearity analysis between *A. cornea* and purple *A. cornea* and found numerous inversions and translocations between homologous regions of the two genomes (Figure 2D). For instance, we observed a translocation between scaffold 7 of white *A. cornea* and contig14 of purple *A. cornea*, as well as an inversion and translocation between scaffold 1 of white *A. cornea* and contig21 of purple *A. cornea*. However, only a few regions showed highly conserved syntenic blocks shared between the two genomes, such as scaffold 2 of white *A. cornea* and contig11 and contig13 of purple *A. cornea*. These findings suggest that a series of chromosome fusions or breakages may have occurred during the long evolutionary history of *A. cornea*, resulting in the observed genomic diversity. This genomic diversity may play a crucial role in various aspects of the organism's biology, including morphological formation, lifestyle, and environmental adaptation.

The pigment of *Auricularia cornea* is synthesized by shikimate pathway

Color is an important agronomic trait of *A. conrea*. In order to clarify the regulation gene and pathway of pigment synthesis, we conducted an RNA-seq experiment on the mycelium period (Mycelium as control treatment: WCK and PCK), primordium period (The 8th day of fruiting: W08 and P08), and fruiting body period (The 15th day of fruiting: W15 and P15) of white strains ACW001(W) and purple strains ACP004(P) based on the ACW001-33 genome. Pigment synthesis-related regulatory genes were selected by combining phenotypic differences with gene expression levels. Based on expression information, principal component analysis (PCA) was performed (Figure 3A), and we calculated the Pearson correlation coefficient of every two samples (Figure 3B), excluding two samples with low repeatability, and DEGs in purple and white strains were then analyzed (Figures 3C,D).

Morphological observation of *A. cornea* at different stages revealed that pigment secretion began in the primordium period. From the mycelium to fruiting body period, purple parents underwent a color change, whereas white parents remained unaltered. Therefore, we selected the intersection of upregulated DEGs in W08 *VS* P08, W15 *VS* P15, and PCK *VS* P15 and non-DEGs in WCK *VS* PCK and WCK *VS* W15 to perform KEGG annotation analysis (Figure 3E). The enrichment analysis revealed that the pathways of ubiquinone and other terpenoid-quinone biosynthesis, glycolysis, pentose phosphate, and TCA cycle were significantly enriched (Figure 3F). Another gene set enrichment analysis (GSEA) performed using the two sample gene sets of PCK *VS* P08 and PCK *VS* P15 from the purple strains. The pathways of glycolysis, phenylalanine, tyrosine, and tryptophan were significantly upregulated during purple strain development (Figure 3G). Eleven core genes enriched by GSEA included phosphate synthase, farnesyl pyrophosphate synthase, polyphenol oxidases (PPO: PPO1, PPO2, and TYPR), glutamic oxaloacetate aminotransferase (GOT), aromatic amino acid aminotransferases (AMT and ARO), alcohol dehydrogenases (TDH and ADHT), and aldolase A (ALDA). It was found that the pigment synthesis pathway related to KEGG enrichment and GSEA analysis results is the Shikimate pathway, Shikimate was synthesized via glycolysis and the pentose phosphate pathway, and the enriched core genes were also related to these pathways. Therefore, *A. cornea* pigment was preliminarily inferred to be synthesized via the shikimate pathway.

The pigment of *Auricularia cornea* is composed of GDHB

The shikimate pathway synthesizes various pigments, with PPO participating in all pigment syntheses of this pathway, suggesting that transcriptome analysis cannot reveal the specific PPO participation in melanin synthesis. Therefore, we used nontargeted LC–MS to identify the fruiting body metabolites of ACW001 and ACP004, obtaining 899 and 715 metabolites in the positive and negative ion modes, respectively. Under the two ion modes, PCA analysis and the OPLS-DA score plot demonstrated excellent separation effects, effectively differentiating the white and purple strains (Figures 4A,B). The prediction values of the OPLS-DA analysis exceeded 0.9, indicating a reliable result. According to the screening criteria (variable importance in projection [VIP] ≥ 1 and T-test $p < 0.05$), 81 (39 upregulated and 42 downregulated) and 69 (47 upregulated and 22 downregulated) differential metabolites (DEMs) were identified under positive and negative ion modes, respectively (Supplementary Tables S1, S2). When plotted on the VIP chart (Figure 4C) of OPLS-DA, the VIP data corresponding to the DEMs (MS2 levels) in the top 15 differential VIP values in each comparison group showed that glutamate and glutamine in the purple strains were significantly upregulated. Malate, citrate, 2-Oxoglutarate, tyrosine, alanine, and phenylalanine changed synergistically with glutamate and glutamine, as determined by the Pearson correlation coefficients of all DEMs in pairs (Figure 4D). Notably, these metabolites are important in the TCA cycle and shikimate pathway, the TCA cycle generates glutamine, which is a precursor substance for the synthesis of γ-glutaminyl-3,4-dihydroxy-benzoate (GDHB) pigments. The GDHB pigment synthesis pathway is a branch of the shikimate pathway. Many compounds involved in the GDHB pigment synthesis pathway carry glutamine groups, and no other melanin precursor substances have

10.3389/fmicb.2023.1211795

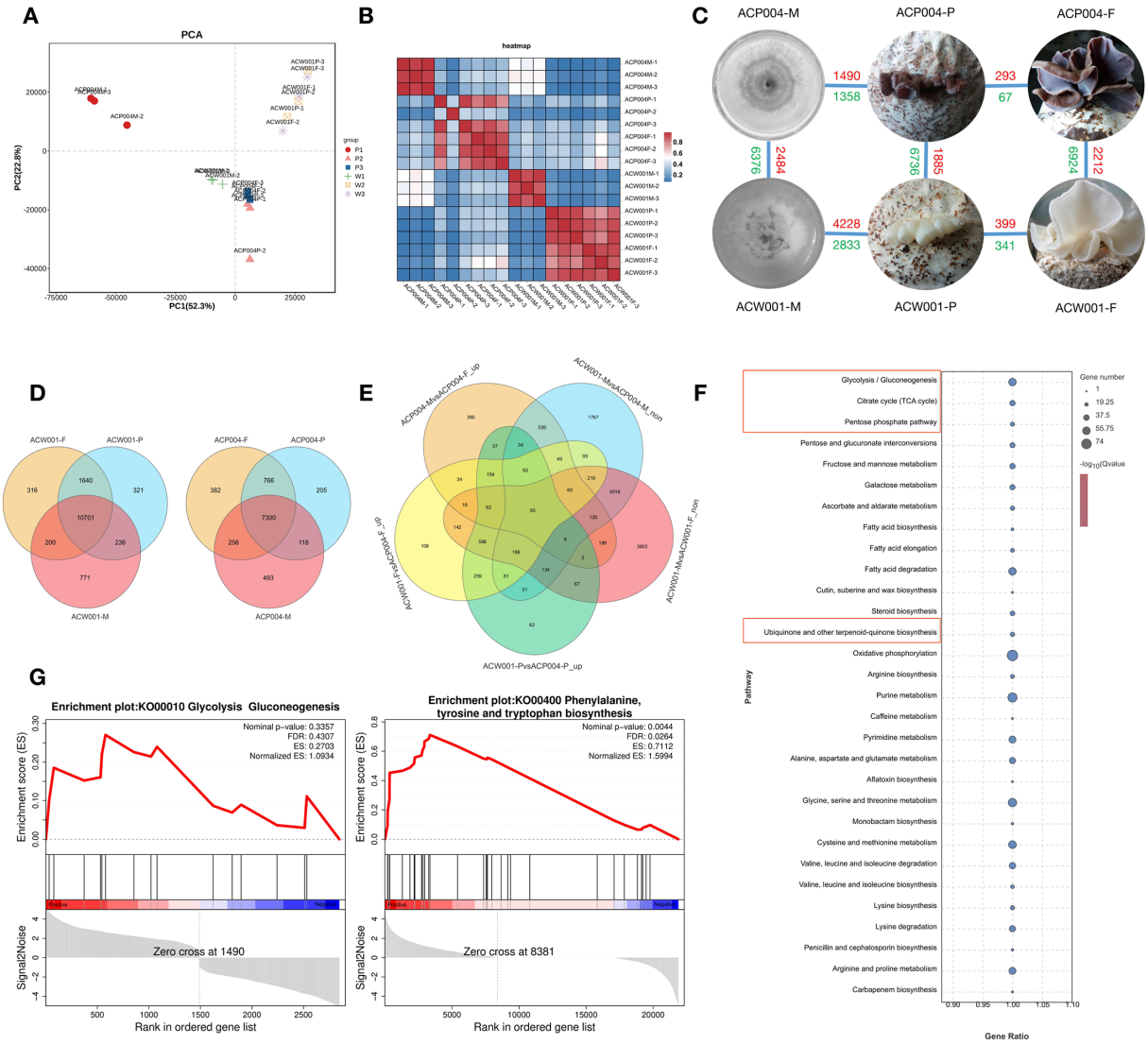

FIGURE 3
Transcriptome-based analysis of genes involved in pigment synthesis. **(A)** PCA analysis, the more similar the sample composition is, the closer the distance in the PCA plot. **(B)** Correlation heat map: repeatability between repeated samples can be investigated. **(C)** DEG distribution in each sample, red represents upregulation and green represents downregulation. **(D)** Venn diagram of differential genes during the three development periods of purple and white strains. **(E)** Venn diagram of targeted genes. **(F)** KEGG enrichment bubble diagram. The red boxes represent the pathways associated with predicted pigment synthesis. **(G)** GESA enrichment ES curves. The gene enriched when ES reached the highest score is the major gene of the pathway.

been found. Therefore, it is inferred that *A. cornea* pigment is a single type of pigment synthesized by the GDHB pathway.

Transcriptome and metabolome association analysis of pigment synthesis pathway

Transcription and metabolism do not happen independently in the biological system, we performed KEGG pathway model analyze related to pigment synthesis based on gene expression level and metabolite abundance to further explain the regulatory mechanism between gene expression and metabolism. It was significantly enriched with glycolysis and the shikimate pathway ($p < 0.05$), indicating a strong consistency between transcriptome and metabolome results. The metabolic biomarker changes associated with shikimate synthesis and metabolism are shown in the network chart (Figure 5A, Orange). Purple strains synthesized phosphoenolpyruvate (PEP) and D-erythrose-4P via glycolysis and the pentose phosphate pathway, followed by shikimate polymerization with the action of DAHP synthase, and pigment synthesis via the shikimate pathway.

Key metabolites and gene screening in pigment synthesis pathway

Data of gene expression level and metabolite abundance were used to build the O2PLS (bidirectional orthogonal projections to

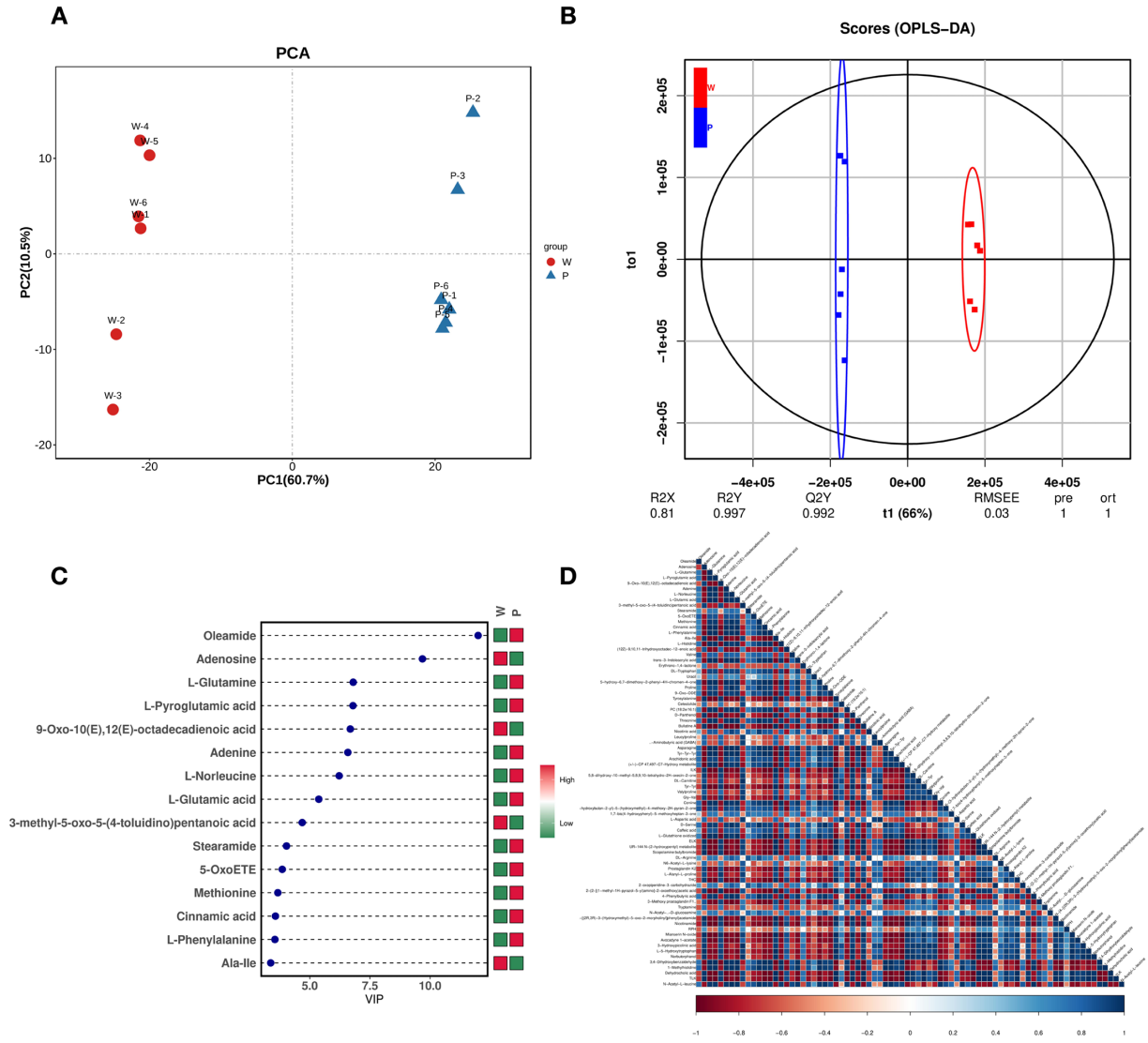

FIGURE 4
Metabolome-based analysis of metabolites associated with pigment synthesis. **(A)** PCA analysis, PC1 describes the most obvious features in the multidimensional data matrix, and PC2 describes the most significant features in the data matrix except PC1. **(B)** OPLS-DA, use the classification effect of R2X, R2Y, Q2 models. **(C)** DEM VIP map, color on the right side indicates the abundance of each metabolite in different groups, red represents upregulated, and green represents downregulated. The higher the VIP values, the more they contribute to distinguishing samples. The metabolites with VIP exceeding 1 have significant differences. **(D)** DEM heat map, each row and column represents the sample, and the darker the color, the stronger the correlation between the two samples.

latent structures) loading diagram model (Figure 5B). Citrate (Com_18_neg) and 2-Oxoglutarate (Com_24_neg) in the TCA cycle were positively correlated with A02009 (Aldolase A, ALDA). ALDA participated in the glycolytic pathway; β-D-fructose-1,6P generated glyceraldehyde-3P and finally synthesized acetyl-CoA. ALDA was also implicated in the pigment synthesis pathway in the transcriptome GSEA analysis. Then, construct the correlation coefficient model based on gene expression level and metabolite abundance: After calculating the Pearson correlation coefficients of gene expression level and metabolite abundance, the data of the top 250 DEGs and DEMs with absolute values of correlation coefficients exceeding 0.99 were selected to draw a network diagram (Figure 5C). 2 DEMs (α-D-glucose-1P and glutamate) involving 16 DEGs (Table 2) were closely associated with pigment synthesis. These DEMs and DEGs were responsible for central regulation in pigment synthesis.

Key gene validation in the pigment synthesis pathway

The strain AC31 (Obtained by monosporal hybridization between ACW001 and ACP004, the color of the fruiting body is pink), white parent ACW001, and purple parent ACP004 were selected for the RT-qPCR analysis of the 17 putative genes (Figure 6, The primer sequence is shown in Supplementary Table S3). The results showed that 15 of the 17 pigment synthesis-associated genes were significantly more expressed in the purple and pink strains than in the white strains. Genes Aromatase1 (ARO1:A03568), ARO8 (A10754) had high expression levels in all strains, without a significant difference. AROs ficantly enriched in GSEA, indicating their important roles in the pathway, despite the absence of a significant expression level differential between the different color

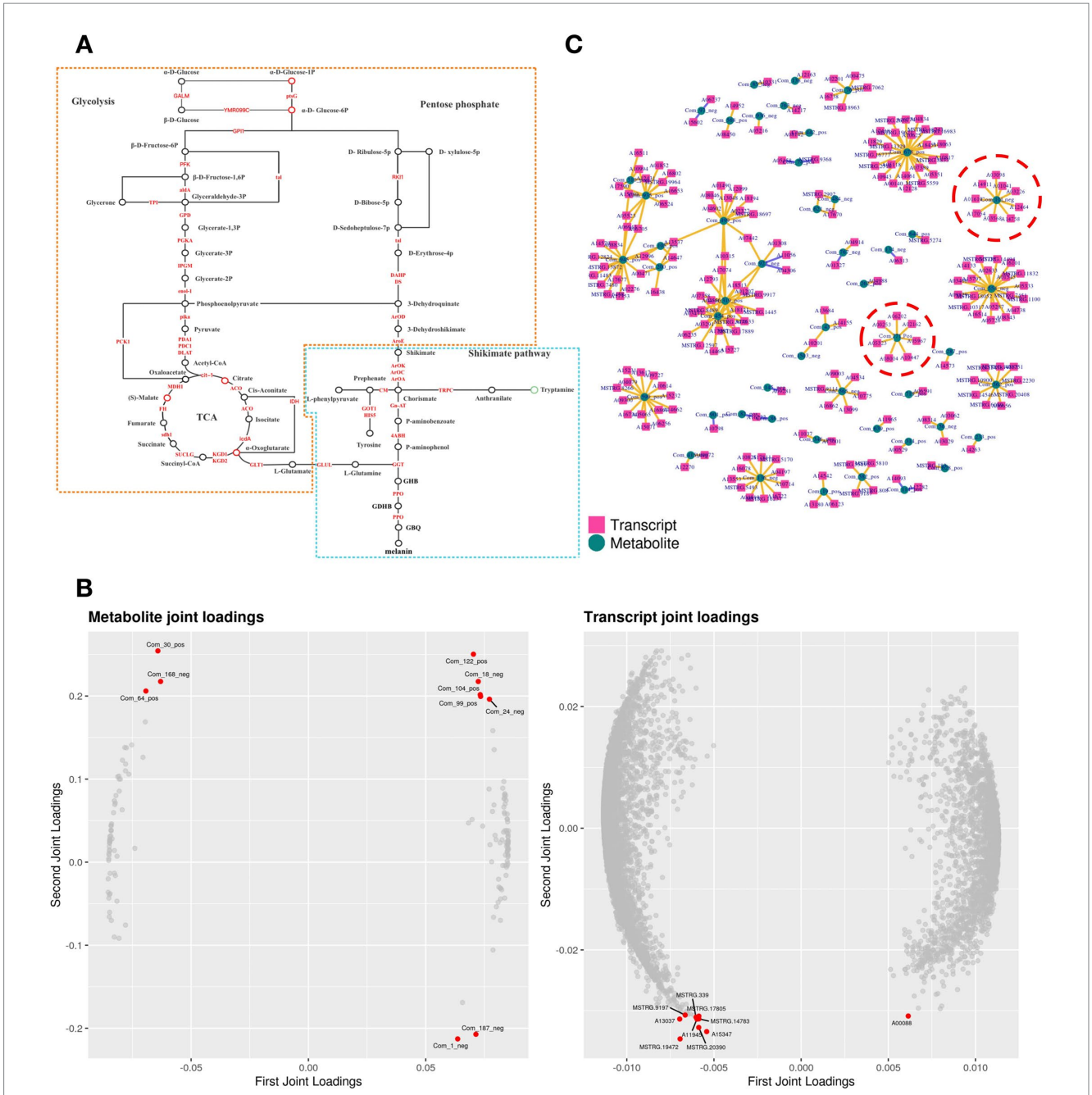

FIGURE 5
Conjoint analysis model of transcriptome and metabolome. **(A)** Pathway analysis of pigment synthesis. The yellow part is the shikimate pathway, and the blue part is the GDHB pigment synthesis pathway. **(B)** O2PLS loading diagram model. The left side is the metabolomic loading map, and the right side is the transcriptomic loading map. **(C)** Pearson correlation coefficient model. Inside red circles are DEMs and DEGs related to pigment synthesis.

strains. The RT-qPCR results demonstrated the accuracy of the association analysis.

Discussion

Effects of different sequencing modes on genome assembly

Although both the CLR and CCS libraries can produce high-quality draft genomes, their assembly integrity and accuracy differ significantly. As seen in Table 1, the genomic sizes under these two modes are similar, but the CCS genome contains only 28 contigs. We also observed that CCS assembled more precisely based on the size of contig N50 and the longest contig. The two modes had similar GC content, indicating a high-accuracy sequence. In addition, the Hi-C-assisted assembly exhibited significant differences. Although both modes anchored the genome sequences to 13 clusters, CLR sequence anchoring accounted for only 74.35%, with 21 of 70 contigs engaging in clustering. In contrast, the CCS mode reached 99.63% on anchoring, with 23 of the 28 contigs engaging in clustering. Notably, when performing clustering, one

TABLE 2 Statistics of genes related to pigment synthesis.

Gene ID	EC number	Symbol	Gene ID	EC number	Symbol	Gene ID	EC number	Symbol
A01041	5.1.3.15	YMR099C	A01610	4.1.1.49	PCK1	A03568	2.6.1.57	ARO1
A03098	5.1.3.3	GALM	A06202	1.1.1.41	IDH1	A17054	2.6.1.9	ARO8
A03226	4.1.2.13	fba	A02162	1.1.1.42	icdA	A05690	1.14.18.1	PPO1
A12464	4.2.1.11	Enol-1	A00253	1.2.4.2	KGD1	A12376	1.14.18.1	PPO2
A14758	2.7.1.40	pkiA	A05967	2.3.1.61	KGD2	A01747	1.14.18.1	TYRP
A14911	2.3.1.12	Dlat	A05323	1.1.1.37	MDH1	A02009	1.2.1.3	ALDA
A10447	1.4.1.14	GOGAT	A08004	1.3.5.1	sdh1			

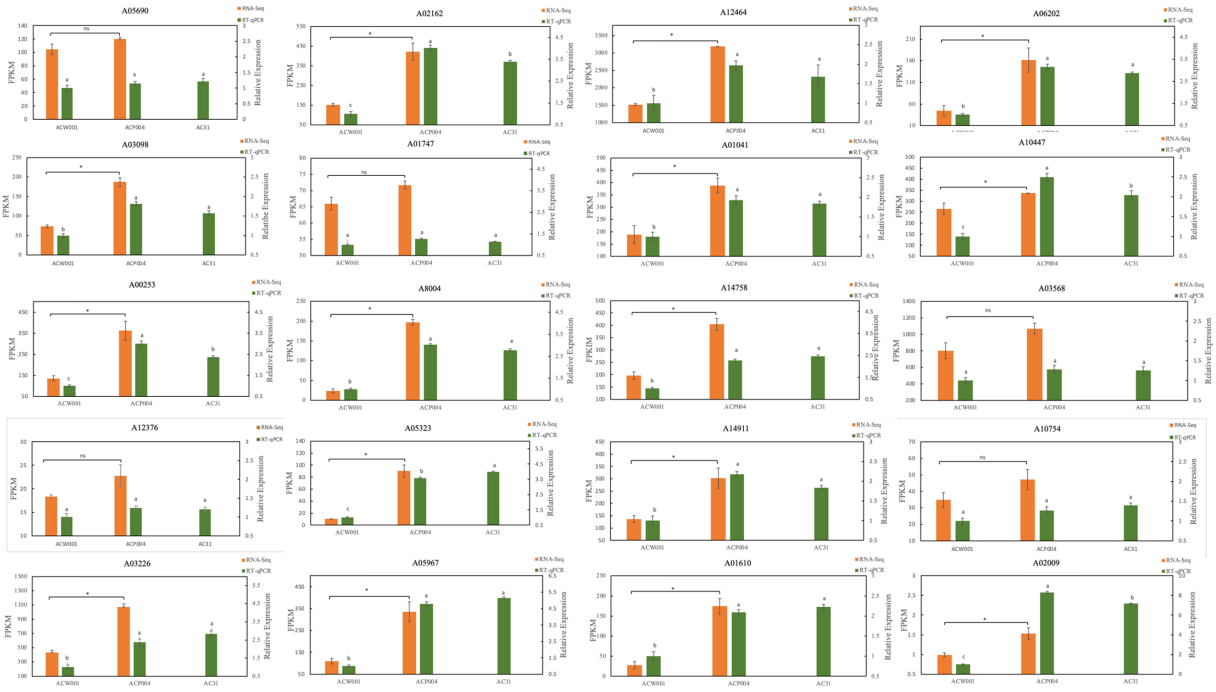

FIGURE 6
RT-qPCR map of 20 pigment synthesis-related genes. ACW001 is the reference strain. The 20 genes included 17 candidate genes and 3 PPOs.

contig appeared in two clusters in the CLR genome, indicating an obvious assembly error. The two modes were similar in repetitive sequences and gene prediction. Overall, CCS obviously outperforms CLR in the genomic sequencing of *A. cornea*. CCS has been widely used in plant and animal genome sequencing but not yet in edible fungi (Rhein, 2021). While the *A. cornea* genome results demonstrated that CCS is suitable for edible fungi and offers greater benefits, they also provided a high-quality genome reference for *A. cornea* and insights into the whole-genome sequencing of other edible fungi.

The importance of GSEA analysis

Transcriptome analysis revealed that the detection rate of all ACP004 samples was approximately 50% relative to the reference genome, but that of all ACW001 samples was approximately 70%, indicating that ACP004 differed significantly from the reference genome in terms of gene composition and sequences. Notably, GO and KEGG enrichment analyses of gene expression differences may miss some color regulatory genes, as the color difference is likeliest due to changes in gene sequences rather than gene expression levels. Therefore, the search for target genes in this study was based on GSEA analysis, which analyzed the gene sets at different periods of purple parents with color changes. GSEA is not limited to DEGs, as it can also include genes that are easily missed in GO/KEGG but have important biological meaning from the perspective of gene set enrichment (Subramanian et al., 2005, 2007; Tarca et al., 2013). This makes our analysis results more accurate.

Prediction of pigment synthesis pathways

The GDHB pathway is a branch of the shikimate pathway. For instance, chorismate is synthesized via the shikimate pathway,

forming para-aminobenzoic acid under Gn-AT catalyzation (Massière and Badet-Denisot, 1998), which is then oxidized and decarboxylated by 4ABH to yield aminophenol (Weijn et al., 2013). Aminophenol and glutamine under GGT catalyzation yield GHB (Jolivet et al., 1999), which is then oxidized by PPO to form GDHB and re-oxidized by PPO to form stable glutaminy-benzoquinone (GBQ), which finally polymerizes melanin (Figure 5A Blue). We used ultraviolet spectrophotometer and infrared spectroscopy scanning to extract and purify the pigment from *A. cornea* in the early stage, and it was found that the main compound group composed of *A. cornea* pigment is pyrocatechol (Fan et al., 2019). This is consistent with the chemical group composition of GDHB, which also indicates that our analysis results are accurate. The type of pigment in *A. cornea* is the same as that in *A. bisporus* (Hans and Dora, 1981), and GHB and GDHB are also present in other types of edible fungi (Mcmorris and Turner, 1983). Therefore, GDHB may be a natural precursor of melanin in many other species of the Basidiomycotina, whose main phenolic oxidase is PPO (Bell and Wheeler, 1986). Of course, all genes in the pigment synthesis pathway are important, and any mutation or deletion of genes may interrupt pigment synthesis (Wang et al., 2019). Subsequent experiments can change the color of fruiting bodies by inhibiting key genes with higher expression levels.

PPOs and are key enzyme genes in the pigment synthesis pathway

Three types of PPOs have been found in *A. cornea*, namely PPO1 (A05690), PPO2 (A12376) and TYPR (A01747). PPO is essential for pigment synthesis in animals, plants, and fungi because it can catalyze monophenolase hydroxylation and oxidize o-diphenol to o-quinone; quinones are subsequently oxidized to derivatives. O-quinone and other quinones, amino acids, and proteins form pigments through nonenzymatic polymerization (Lan and Constabel, 2011; Aleksandar et al., 2015). PPO is also a key enzyme in the GDHB pigment synthesis pathway that oxidizes GHB to GDHB and GBQ. However, these three types of PPOs were not enriched in the association analysis model because PPOs expression levels were high in all strains and there was no significant difference. This led to the omission of PPOs based on differential gene association analysis. In this study, PPOs were significantly enriched in GSEA analysis, and PPOs expression in purple strains began to increase significantly during the primordium stage, coinciding with pigment secretion. Therefore, it is inferred that PPOs are the key enzymes involved in pigment synthesis. The RT qPCR results showed that there was no significant difference in the expression levels of the three PPOs among different colored strains, but the expression levels were high (Figure 6), which is consistent with our analysis results. It is currently unknown whether all three types of PPOs are involved in pigment synthesis, research has shown that PPOs not only regulate pigment synthesis, but also participate in defense mechanisms against stress (Boss et al., 1995), which may be the reason for the high expression levels of all three types of PPOs.

Materials and methods

Test strains

The test strains were wild white strain ACW001 and wild purple strain ACP004, both collected from Henan Province, China. ACW001-33 was the monospore collected from ACW001 and used for whole-genome sequencing. The above strains were stored at the Engineering Research Center for Edible and Medicinal Fungi of Jilin Agricultural University, China.

DNA preparation and sequencing

As the test strain, ACW001-33 was extracted using CTAB and stored at −80°C for future use. Sequencing was performed using the CLR and CCS libraries. The one with better results and accuracy was finally selected. 20 Kb SMRT Bell library and 350 bp small fragment library were constructed on PacBio Sequel and Illumina NovaSeq PE150. After the library test, different libraries were sequenced according to the effective concentration and the amount of output data. Genome assembly and correction of reads were performed with SMRT Link v5.0.1 (Ardui et al., 2018). The reads were aligned to the assembled genome sequence, and the GC bias of the genome was summarized by computing the GC content and coverage depth of the reads in the assembled sequence.

Hi-C-assisted assembly

Samples were first cross-linked using formaldehyde for library sequencing. Following quality control and filtration of hic tags with HiCUP, valid reads for interaction analysis were aligned to the reference genome (Lieberman-Aiden et al., 2009). The number of reads with interactions between contigs was counted, which was also considered the number of interactions. Contigs were clustered according to this number, and sequencing and orientation were then performed based on the interaction intensity of every two contigs and the position of the interacting read alignment. Genome sequences were clustered, ordered, and oriented with ALLHiC, and contig orientation was corrected with hic-hicker (Ryo and Shinichi, 2020).

Genomic component analysis

Repetitive sequence

Interspersed repeat sequences were predicted using Repeat Masker, and tandem repeat sequences were searched by TRF (Tandem repeats finder) (Benson, 1999). An SSR search was used for detecting genome-wide SSR loci and designing primers.

Encoding gene

Augustus prediction was performed *because* the *A. cornea* genome has no transcriptome data or adjacent reference sequence (Stanke et al., 2008). Based on the final assembly result (≥500 bp), ORF (Open Reading Frame) prediction and filtration were performed.

Noncoding RNA

tRNA prediction was performed using tRNAscan-SE (Lowe and Eddy, 1997). rRNA was predicted using rRNAmmer (Lagesen et al., 2007). Predictions of sRNA, snRNA, and miRNA were similar.

Gene function analysis

Regarding coding sequences, we performed functional annotations on different databases, including frequently used KEGG, KOG, Pfam, CAZy, NR, GO, Swiss-Prot, and TCDB, as well as a pathogenicity-specific database. BLAST was used to compare putative genes with each functional database. For the BLAST results of each sequence, the comparison result with the highest score was selected (default: identity ≥40%, coverage ≥40%) for annotation. We also analyzed effectors, including secretory protein, cellular pigment P450, and secondary metabolic gene clusters. A signal peptide prediction tool SignalP was used to predict secretory protein, detect the presence of signal peptides and transmembrane results, and predict whether the protein sequence was secreting protein (Petersen et al., 2011). Annotation was performed using the cytochrome database P450. Predictive analysis of secondary metabolic gene clusters was performed using antiSMASH (Medema et al., 2011).

Phylogenetic development, evolutionary, and whole-genome collinearity analysis

OrthoMCL (v.2.0.9) (Li et al., 2003) was used to identify homologous gene families based on the genome sequences and protein files of 20 species, including *A. cornea*, *A. heimuer*, and *A. subglabra* downloaded from NCBI. Shared single-copy genes were selected and aligned using Clustal Omega (Sievers and Higgins, 2018). A genome-based phylogenetic tree was constructed using the maximum likelihood (ML) algorithm in RAxML (Stamatakis, 2014). Computational Analysis of Gene Family Evolution (CAFE) 3.1 (De Bie et al., 2006) was used to predict the expansion and contraction of homologous gene families, and a value of p of <0.05 was considered significant. Positively selected genes were determined using the branch-site model in the CodeML tool of PAML (Gao et al., 2019). To determine large-scale collinearity relationships between genomes, the MUMmer software (Version 3.23) was used to align the target and reference genomes. LASTZ (Version 1.03.54) was then used to confirm local positional arrangements and search for regions of translocation (Translocation/Trans), inversion (Inversion/Inv), and translocation+inversion (Trans+Inv).

Transcriptomic analysis of different color strains

Data from three different development stages of the white strain ACW001 and purple strain ACP004, including the mycelium period, primordium period (8 days), and fruiting body period (15 days), were collected for total RNA extraction and sequencing. Raw reads were first subjected to quality control with fastp to exclude poor-quality data (Chen et al., 2018). Clean reads were then obtained, which were aligned to the ACW001-33 genome by HISAT2 (Kim et al., 2015). Based on the alignment results, we reconstructed a transcript using Stringtie and calculated all gene expression levels in each sample using RSEM (Pertea et al., 2015). The expression level was displayed with raw reads count and FPKM for subsequent analysis of differences between samples and groups. Finally, by screening the significantly different genes, the selected genes were analyzed by KEGG and GO enrichment to identify pigment synthesis-related pathways and key pigment synthesis-responsible genes (Love et al., 2014).

Metabonomic analysis of different color strains

The fruiting bodies of ACW001 and ACP004 were collected for nontargeted LC–MS metabolite detection. Both positive and negative ion modes were used in the subsequent data analysis during detection. Multivariate data analysis was performed using R language gmodels (v2.18.1) for PCA analysis and the ropls package for OPLS-DA analysis (Warnes, 2007; Julien and Douglas, 2013). We combined the VIP value of OPLS-DA and p-value of the T-test to screen DEMs between comparison groups (Saccenti et al., 2014). Finally, we performed KEGG enrichment and topology analyses of DEMs.

Data availability statement

The datasets presented in this study can be found in online repositories. The names of the repository/repositories and accession number(s) can be found at: https://www.ncbi.nlm.nih.gov/, PRJNA943604, https://www.ncbi.nlm.nih.gov/, PRJNA944815.

Author contributions

PW and FY: conceptualization. PW and XM: methodology and formal analysis. MF: software and data curation. XS, LL, and MF: validation. XM and FY: investigation. FY: resources, project administration, and funding acquisition. XM: writing—original draft preparation and visualization. YZ: writing—review and editing. KS, LL, and FY: supervision. All authors have read and agreed to the published version of the manuscript.

Funding

This work was supported in part by funds from the China Agriculture Research System, grant number CARS-20 and the Guizhou Key Laboratory of Edible fungi breeding (No. [2019]5105-2001 and No. [2019]5105–2005).

Acknowledgments

The authors thank the reviewers for their valuable suggestions.

Conflict of interest

The authors declare that the research was conducted in the absence of any commercial or financial relationships that could be construed as a potential conflict of interest.

Publisher's note

All claims expressed in this article are solely those of the authors and do not necessarily represent those of their affiliated organizations, or those of the publisher, the editors and the reviewers. Any product that may be evaluated in this article, or claim that may be made by its manufacturer, is not guaranteed or endorsed by the publisher.

Supplementary material

The Supplementary material for this article can be found online at: https://www.frontiersin.org/articles/10.3389/fmicb.2023.1211795/full#supplementary-material

References

Aleksandar, B., Matthias, P., Christian, M., Florime, Z., and Annette, R. (2015). The structure of a plant Tyrosinase from walnut leaves reveals the importance of "substrate-guiding residues" for enzymatic specificity. *Angew. Chem. Int. Ed.* 54, 14677–14680. doi: 10.1002/anie.201506994

Ardui, S., Ameur, A., Vermeesch, J. R., and Hestand, M. S. (2018). Single molecule real-time (SMRT) sequencing comes of age: applications and utilities for medical diagnostics. *Nucleic Acids Res.* 46, 2159–2168. doi: 10.1093/nar/gky066

Baldrian, P., and Lindahl, B. R. (2011). Decomposition in forest ecosystems: after decades of research still novel findings. *Fungal Ecol.* 4, 359–361. doi: 10.1016/j.funeco.2011.06.001

Bell, A. A., and Wheeler, M. H. (1986). Biosynthesis and functions of fungal Melanins. *Annu. Rev. Phytopathol.* 24, 411–451. doi: 10.1146/annurev.py.24.090186.002211

Benson, G. (1999). Tandem repeats finder: a program to analyze DNA sequences. *Nucleic Acids Res.* 27, 573–580. doi: 10.1093/nar/27.2.573

Boss, P., Gardner, R., Bart-Jan, J., and Ross, G. (1995). An apple polyphenol oxidase cDNA is up-regulated in wounded tissues. *Plant Mol. Biol.* 27, 429–433. doi: 10.1007/BF00020197

Cai, Z. X., Chen, M. Y., Lu, Y. P., Guo, Z. J., Zeng, Z. H., Zheng, H. Q., et al. *Metabolomics and Transcriptomics unravel the mechanism of browning resistance in Agaricus bisporus*. New York: Cold Spring Harbor Laboratory. (2021).

Cao, T. X., Cui, B. K., Yuan, Y., and Dai, Y. C. (2016). Genetic diversity and relationships of 24 strains of genus Auricularia (Agaricomycetes) assessed using SRAP markers. *Int. J. Med. Mushrooms* 18, 945–954. doi: 10.1615/IntJMedMushrooms.v18.i10.100

Chen, S., Zhou, Y., Chen, Y., and Gu, J. (2018). Fastp: an ultra-fast all-in-one FASTQ preprocessor. *Bioinformatics* 34, i884–i890. doi: 10.1093/bioinformatics/bty560

Cho, K., Cho, K., Sohn, H., Ha, I. J., Hong, S., Lee, H., et al. (2016). Network analysis of the metabolome and transcriptome reveals novel regulation of potato pigmentation. *J. Exp. Bot.* 67, 1519–1533. doi: 10.1093/jxb/erv549

Dai, Y., Li, X., Song, B., Sun, L., Yang, C., Zhang, X., et al. (2019). Genomic analyses provide insights into the evolutionary history and genetic diversity of *Auricularia* species. *Front. Microbiol.* 10:2255. doi: 10.3389/fmicb.2019.02255

De Bie, T., Cristianini, N., Demuth, J. P., and Hahn, M. W. (2006). CAFE: a computational tool for the study of gene family evolution. *Bioinformatics* 22, 1269–1271. doi: 10.1093/bioinformatics/btl097

Fan, X., Yao, F., Wang, W., Fang, M., and Wang, P. (2019). Study on the extraction process and physicochemical properties of black pigment from *Auricularia cornea*. *J. Mol. Sci.* 35, 484–491. doi: 10.13563/j.cnki.jmolsci.2019.06.006

Fang, M., Wang, X., Chen, Y., Wang, P., Lu, L. L., Lu, J., et al. (2020). Genome sequence analysis of *Auricularia heimuer* combined with genetic linkage map. *J Fungi (Basel)* 6:6. doi: 10.3390/jof6010037

Feng, P., Shang, Y., Cen, K., and Wang, C. (2015). Fungal biosynthesis of the bibenzoquinone oosporein to evade insect immunity. *Proc. Natl. Acad. Sci. U. S. A.* 112, 11365–11370. doi: 10.1073/pnas.1503200112

Gao, F., Chen, C., Arab, D. A., Du, Z., He, Y., and Ho, S. Y. W. (2019). EasyCodeML: a visual tool for analysis of selection using CodeML. *Ecol. Evol.* 9, 3891–3898. doi: 10.1002/ece3.5015

Gong, M., Wang, Y., Su, E., Zhang, J., Tang, L., Li, Z., et al. (2022). The promising application of a β-glucosidase inhibitor in the postharvest management of *Volvariella volvacea*. *Postharvest Biol. Technol.* 185:111784. doi: 10.1016/j.postharvbio.2021.111784

Hans, S., and Dora, M. R. (1981). The biosynthesis and possible function of γ-glutaminyl-4-hydroxybenzene in *Agaricus bisporus*. *Phytochemistry* 20, 2347–2352. doi: 10.1016/S0031-9422(00)82663-1

Hu, C., Li, Q., Shen, X., Quan, S., Lin, H., Duan, L., et al. (2016). Characterization of factors underlying the metabolic shifts in developing kernels of colored maize. *Sci. Rep.* 6:35479. doi: 10.1038/srep35479

Jiang, W. Z., Yao, F. J., Fang, M., Lu, L. X., Zhang, Y. M., Wang, P., et al. (2021). Analysis of the genome sequence of strain GiC-126 of *Gloeostereum incarnatum* with genetic linkage map. *Mycobiology* 49, 406–420. doi: 10.1080/12298093.2021.1954321

Jolivet, S., Pellon, G., Gelhausen, M., and Arpin, N. (1999). γ-L-[3H]-Glutaminyl-4-[14C]hydroxybenzene (GHB): biosynthesis and metabolic fate after applying on *Agaricus bisporus* 50, 581–587.

Julien, B., and Douglas, N. R. (2013). A consensus orthogonal partial least squares discriminant analysis (OPLS-DA) strategy for multiblock Omics data fusion. *Anal. Chim. Acta* 769, 30–39. doi: 10.1016/j.aca.2013.01.022

Kim, D., Langmead, B., and Salzberg, S. (2015). HISAT: a fast spliced aligner with low memory requirements. *Nat. Methods* 12, 357–360. doi: 10.1038/nmeth.3317

Lagesen, K., Hallin, P., Rødland, E. A., Stærfeldt, H.-H., Rognes, T., and Ussery, D. W. (2007). RNAmmer: consistent and rapid annotation of ribosomal RNA genes. *Nucleic Acids Res.* 35, 3100–3108. doi: 10.1093/nar/gkm160

Lan, T. T., and Constabel, C. P. (2011). The polyphenol oxidase gene family in poplar: phylogeny, differential expression and identification of a novel, vacuolar isoform. *Planta* 234, 799–813. doi: 10.1007/s00425-011-1441-9

Li, Y., Fang, J., Qi, X., Lin, M., Zhong, Y., Sun, L., et al. (2018). Combined analysis of the fruit Metabolome and Transcriptome reveals candidate genes involved in flavonoid biosynthesis in *Actinidia arguta*. *Int. J. Mol. Sci.* 19:1471. doi: 10.3390/ijms19051471

Li, L., Stoeckert, C. J. Jr., and Roos, D. S. (2003). OrthoMCL: identification of ortholog groups for eukaryotic genomes. *Genome Res.* 13, 2178–2189. doi: 10.1101/gr.1224503

Lieberman-Aiden, E., van Berkum, N. L., Williams, L., Imakaev, M., Ragoczy, T., Telling, A., et al. (2009). Comprehensive mapping of long-range interactions reveals folding principles of the human genome. *Science* 326, 289–293. doi: 10.1126/science.1181369

Love, M. I., Huber, W., and Anders, S. (2014). Moderated estimation of fold change and dispersion for RNA-seq data with DESeq2. *Genome Biol.* 15:550. doi: 10.1186/s13059-014-0550-8

Lowe, T. M., and Eddy, S. R. (1997). tRNAscan-SE: a program for improved detection of transfer RNA genes in genomic sequence. *Nucleic Acids Res.* 25, 955–964. doi: 10.1093/nar/25.5.955

Manni, M., Berkeley, M. R., Seppey, M., Simao, F. A., and Zdobnov, E. M. (2021a). BUSCO update: novel and streamlined workflows along with broader and deeper phylogenetic coverage for scoring of eukaryotic, prokaryotic, and viral genomes. *Mol. Biol. Evol.* 38, 4647–4654. doi: 10.1093/molbev/msab199

Manni, M., Berkeley, M. R., Seppey, M., and Zdobnov, E. M. (2021b). BUSCO: assessing genomic data quality and beyond. *Curr. Protoc.* 1:e323. doi: 10.1002/cpz1.323

Massière, F., and Badet-Denisot, M. A. (1998). The mechanism of glutamine-dependent amidotransferases. *Cell. Mol. Life Sci.* 54, 205–222. doi: 10.1007/s000180050145

Mcmorris, T. C., and Turner, W. B. (1983). Fungal metabolites II. *Mycologia* 64:464. doi: 10.2307/3757861

Medema, M. H., Blin, K., Cimermancic, P., de Jager, V., Zakrzewski, P., Fischbach, M. A., et al. (2011). antiSMASH: rapid identification, annotation and analysis of secondary metabolite biosynthesis gene clusters in bacterial and fungal genome sequences. *Nucleic Acids Res.* 39, W339–W346. doi: 10.1093/nar/gkr466

Morin, E., Kohler, A., Baker, A. R., Foulongne-Oriol, M., Lombard, V., Nagy, L. G., et al. (2012). Genome sequence of the button mushroom *Agaricus bisporus* reveals mechanisms governing adaptation to a humic-rich ecological niche. *Proc. Natl. Acad. Sci. U. S. A.* 109, 17501–17506. doi: 10.1073/pnas.1206847109

Pertea, M., Pertea, G., Antonescu, C., Chang, T., Mendell, J., and Salzberg, S. (2015). StringTie enables improved reconstruction of a transcriptome from RNA-seq reads. *Nat. Biotechnol.* 33, 290–295. doi: 10.1038/nbt.3122

Petersen, T. N., Brunak, S., von Heijne, G., and Nielsen, H. (2011). SignalP 4.0: discriminating signal peptides from transmembrane regions. *Nat. Methods* 8, 785–786. doi: 10.1038/nmeth.1701

Qu, J., Zhao, M., Hsiang, T., Feng, X., Zhang, J., and Huang, C. (2016). Identification and characterization of small noncoding RNAs in genome sequences of the edible fungus *Pleurotus ostreatus*. *Biomed. Res. Int.* 2016, 2503023–2503029. doi: 10.1155/2016/2503023

Rhein, H. S. (2021). Four chromosome scale genomes and a pan-genome annotation to accelerate pecan tree breeding. *Nat. Commun.* 12:4125.

Ryo, N., and Shinichi, M. (2020). HiC-hiker: a probabilistic model to determine contig orientation in chromosome-length scaffolds with hi-C. *Bioinformatics* 13, 3966–3974. doi: 10.1093/bioinformatics/btaa288

Saccenti, E., Hoefsloot, H., Smilde, A. K., Westerhuis, J. A., and Hendriks, M. (2014). Reflections on univariate and multivariate analysis of metabolomics data. *Metabolomics* 10, 361–374. doi: 10.1007/s11306-013-0598-6

Sievers, F., and Higgins, D. G. (2018). Clustal omega for making accurate alignments of many protein sequences. *Protein Sci.* 27, 135–145. doi: 10.1002/pro.3290

Stamatakis, A. (2014). RAxML version 8: a tool for phylogenetic analysis and post-analysis of large phylogenies. *Bioinformatics* 30, 1312–1313. doi: 10.1093/bioinformatics/btu033

Stanke, M., Diekhans, M., Baertsch, R., and Haussler, D. (2008). Using native and syntenically mapped cDNA alignments to improve de novo gene finding. *Bioinformatics* 24, 637–644. doi: 10.1093/bioinformatics/btn013

Subramanian, A., Kuehn, H., Gould, J., Tamayo, P., and Mesirov, J. P. (2007). GSEA-P: a desktop application for gene set enrichment analysis. *Bioinformatics* 23, 3251–3253. doi: 10.1093/bioinformatics/btm369

Subramanian, A., Tamayo, P., Mootha, V. K., Mukherjee, S., Ebert, B. L., Gillette, M. A., et al. (2005). Gene set enrichment analysis: a knowledge-based approach for interpreting genome-wide expression profiles. *Proc. Natl. Acad. Sci. U. S. A.* 102, 15545–15550. doi: 10.1073/pnas.0506580102

Tarca, A. L., Bhatti, G., and Romero, R. (2013). A comparison of gene set analysis methods in terms of sensitivity, prioritization and specificity. *PLoS One* 8:e79217. doi: 10.1371/journal.pone.0079217

Tingting, D., Rongpeng, H., Jiawen, Y., Mingku, Z., Yi, Z., Ying, G., et al. (2019). Anthocyanins accumulation and molecular analysis of correlated genes by metabolome and transcriptome in green and purple asparaguses (*Asparagus officinalis*, L.). *Food Chem.* 271, 18–28. doi: 10.1016/j.foodchem.2018.07.120

Wang, Z., Cui, Y., Vainstein, A., Chen, S., and Ma, H. (2017). Regulation of fig (*Ficus carica* L.) fruit color: Metabolomic and Transcriptomic analyses of the flavonoid biosynthetic pathway. *Front. Plant Sci.* 8:8. doi: 10.3389/fpls.2017.01990

Wang, P., Yao, F. J., Lu, L. L., Fang, M., Zhang, Y. M., Kong, X. H., et al. (2019). Map-based cloning of genes encoding key enzymes for pigment synthesis in *Auricularia cornea*. *Fungal Biol.* 123, 843–853. doi: 10.1016/j.funbio.2019.09.002

Warnes, G. R. (2007). *Gmodels: Various R programming tools for model fitting.* gmodels: Various R Programming Tools for Model Fitting.

Weijn, A., BastiaanNet, S., Wichers, H. J., and Mes, J. J. (2013). Melanin biosynthesis pathway in *Agaricus bisporus* mushrooms. *Fungal Genet. Biol.* 55, 42–53. doi: 10.1016/j.fgb.2012.10.004

Wu, F., Yuan, Y., Rivoire, B., and Dai, Y. C. (2015). Phylogeny and diversity of the Auricularia mesenterica (Auriculariales, Basidiomycota) complex. *Mycol. Prog.* 14:42. doi: 10.1007/s11557-015-1065-8

Young-Jin, P., Hun, B. J., Seonwook, L., Changhoon, K., Hwanseok, R., Hyungtae, K., et al. (2014). Whole genome and global gene expression analyses of the model mushroom flammulina velutipes reveal a high capacity for lignocellulose degradation. *PLOS ONE* 9:e93560. doi: 10.1371/journal.pone.0093560

Yuan, Y., Wu, F., Si, J., Zhao, Y. F., and Dai, Y. C. (2019). Whole genome sequence of *Auricularia heimuer* (Basidiomycota, Fungi), the third most important cultivated mushroom worldwide. *Genomics* 111, 50–58. doi: 10.1016/j.ygeno.2017.12.013

Zhang, X., Zhang, S., Zhao, Q., Ming, R., and Tang, H. (2019). Assembly of allele-aware, chromosomal-scale autopolyploid genomes based on hi-C data. *Nature Plants* 5, 833–845. doi: 10.1038/s41477-019-0487-8

Zhao, X., Chen, M., Zhao, Y., Zha, L., Yang, H., and Wu, Y. (2019). GC(−)MS-based nontargeted and targeted metabolic profiling identifies changes in the Lentinula edodes Mycelial Metabolome under high-temperature stress. *Int. J. Mol. Sci.* 20:330. doi: 10.3390/ijms20092330

Zhu, Y., Xu, J., Sun, C., Zhou, S., Xu, H., Nelson, D. R., et al. (2015). Chromosome-level genome map provides insights into diverse defense mechanisms in the medicinal fungus Ganoderma sinense. *Sci. Rep.* 5:11087. doi: 10.1038/srep11087

frontiers | Frontiers in Genetics

TYPE Original Research
PUBLISHED 13 July 2023
DOI 10.3389/fgene.2023.1221491

OPEN ACCESS

EDITED BY
Chenyang Huang,
Chinese Academy of Agricultural Sciences, China

REVIEWED BY
Bing Wen Gong,
Huazhong Agricultural University, China
Ake Liu,
Changzhi University, China
Youjin Deng,
Fujian Agriculture and Forestry University, China

*CORRESPONDENCE
Haiying Bao,
baohaiying@jlau.edu.cn

RECEIVED 12 May 2023
ACCEPTED 03 July 2023
PUBLISHED 13 July 2023

CITATION
Wang Q, Bao H and Li Z (2023), Genomic comparison between two *Inonotus hispidus* strains isolated from growing in different tree species.
Front. Genet. 14:1221491.
doi: 10.3389/fgene.2023.1221491

Genomic comparison between two *Inonotus hispidus* strains isolated from growing in different tree species

Qingchun Wang[1,2], Haiying Bao[1,2]* and Zhijun Li[1,2]

[1]Key Laboratory for Development and Utilization of Fungi Traditional Chinese Medicine Resources, Jilin Agricultural University, Changchun, Jilin, China, [2]Key Laboratory of Edible Fungal Resources and Utilization (North), Ministry of Agriculture and Rural Affairs, Jilin Agricultural University, Changchun, Jilin, China

Inonotus hispidus mainly growing in broad-leaved trees, including *Morus alba*, *Fraxinus mandshurica*, and *Ulmus macrocarpa* etc. The fruiting body of *I. hispidus* growing in *M. alba* (hereafter as MA) is used as a traditional Chinese medicine "*Sanghuang*". However, differences between the genetic material basis of *I. hispidus* growing in other tree species have not been reported. Therefore, in this paper, the genomic comparison between MA and *I. hispidus* growing in *F. mandshurica* (hereafter as FM) were studied. The whole genome of MA monokaryon was sequenced by Illumina combined with Pac Bio platform. Next, genome assembly, genome component prediction and genome functional annotation were performed. Comparative genomics analysis was performed between FM monokaryon and MA monokaryon, using MA as the reference. The results showed that, MA had 24 contigs with a N50 length of 2.6 Mb. Specifically, 5,342, 6,564, 1,595, 383 and 123 genes were annotated from GO, KEGG, KOG, CAZymes and CYP450, respectively. Moreover, comparative genomics showed that, the coding genes and total number of genes annotated in different databases of FM were higher than that of MA. This study provides a foundation for the medicinal application of FM as MA from the perspective of genetic composition.

KEYWORDS

***Inonotus hispidus*, whole genome sequencing, comparative genomic, CAZymes, functional annotation**

1 Introduction

Edible and medicinal fungus *Inonotus hispidus* (Bull.: Fr.) P. Karst belongs to Basidiomycota, Agaricomycetes, Hymenochaetales, Hymenochaetaceae, and *Inonotus*. It is distributed in China, Korea, Japan, Germany, Russia, Canada and other countries. Recent international medical studies reported that its pharmacological activities include anti-tumor, anti-oxidation, anti-inflammatory, liver protection, bacteriostasis, anti-virus, hypolipidemic and immune enhancement (Awadh et al., 2003; Benarous et al., 2015; Gründemann et al., 2016; Angelini et al., 2019; Li et al., 2019; Liu et al., 2019; Yang et al., 2019; Yang et al., 2020; Li and Bao, 2022a; Zhang et al., 2022a; Yang et al., 2022; Machado-Carvalho et al., 2023; Saka et al., 2023; Tang et al., 2023). *I. hispidus* has an excellent development space as medical and functional food in future. Its main hosts were *M. alba*, *F. mandshurica*, *U. macrocarpa*, *Z. jujuba* and *M. pumila* (Dai et al., 2000). FM is mainly distributed in Northeast China (Dai et al., 2000), whereas MA is prevalent in Northeast, Northwest, North,

East and Southwest of China (Bao et al., 2020). According to the morphological characteristics, habitat and herbal research of MA, some Chinese scholars believe that the MA was positive source of traditional Chinese medicine "*Sanghuang*" (Bao et al., 2020). Historically, MA has been used as "*Sanghuang*" in both "The Ancient Course of the Yellow River" and southern Xinjiang regions. The types and enrichment degrees of chemical metabolites in the fruiting bodies of *I. hispidus* growing in five different tree species were reported to be significantly different using non-targeted metabolomics (Li and Bao, 2022b).

Previous research on *I. hispidus* has primarily focused on exploring the chemical composition, pharmacological action and domesticated culture, with little emphasis on whole genome sequencing. The rapid development of sequencing technology has greatly helped to solve the complex problems in the fungi biology. As of June 2023, 2,426 fungal genome projects had been completed and published on the JGI website (https://mycocosm.jgi.doe.gov/fungi/fungi.info.html), as well as *S. sanghuang* (Jiang et al., 2021), *I. hispidus* (Zhang et al., 2022b; Tang et al., 2022) and *G. lucidum* (Liu et al., 2012). These findings reveal novel insights for understanding gene network control, metabolite synthesis pathways, edible and medicinal fungal cultivation and breeding, contributing to large-scale fungi industrialization development bottleneck. As a result, there is no comprehensive explanation for the whole genome sequence and functional gene coding of *I. hispidus* growing in diverse tree species. This makes it difficult to elucidate the internal mechanism of different hosts at the molecular and genetic levels.

In order to establish a high-quality reference genome of MA and to facilitate subsequent analyses of its genome function and genetic material, as well as to determine whether FM has the value of development and utilization like MA. Therefore, in this study, the whole genome sequencing of MA would be carried out based on the SMRT (https://www.pacb.com/support/sofware-downloads/) (Ardui et al., 2018) and Illumina sequencing. The resulting genomic data of MA would be compared with the sequencing assembly, genome prediction, functional annotation and comparative genome analysis of FM. Furthermore, the similarities and differences in genetic material and metabolites of MA and FM would be explored, which would provide an important theoretical basis to research for transcriptomics, proteomics, metabolomics and development of *I. hispidus* growing in various tree species.

2 Materials and methods

2.1 Materials

In this study, *I. hispidus* growing in two different trees were collected from the field. MA (Figure 1A) was collected from Xiajin Ancient Mulberry Garden, Xiajin County, Shandong Province, China, 10 August 2020 (36°59′N, 115°11′E). FM (Figure 1B) was collected from Jingyuetan National Forest Park, Changchun City, Jilin Province, China, on 11 August 2020 (43°79′N, 125°46′E). The voucher specimen is deposited in the Herbarium of Mycology of Jilin Agricultural University (HMJAU), MA under No.58767 and FM under No.58769. We get the monokaryons of MA and FM by single spore isolation and used for whole genome sequencing. Then, we cultured the MA and FM monokaryon in PDA medium (Potato

FIGURE 1
Fruiting bodies of *I. hispidus*. growing in two different trees. **(A)** Fruiting bodies of MA. **(B)** Fruiting bodies of FM.

200 g, Dextrose 20 g, Agar 20 g) in the dark at 28°C for 14 days. We verified isolation of MA and FM monokaryon were using an Axio Imager A2 fluorescence microscope (Zeiss). Subsequently, all samples were stored at −80°C until they were ready for genome-wide analysis.

2.2 Genome sequencing

2.2.1 Extraction of genome DNA

Genomic DNA of MA and FM were extracted with the GP1 extraction method (Zhong et al., 2016). Added 25 mL GP1 lysate to the monokaryon of MA and FM, and immediately added 500 μL β-mercaptoethanol, mixed upside down, and lysed in a 65°C water bath for 30 min. Centrifuging at 12,000 rpm for 10 min, drawing the supernatant into a new 50 mL centrifuge tube; the equal volume of phenol, chloroform, isoamyl alcohol (25:24:1) was added to each tube, and the mixture was shaken and mixed for 5 min. Then centrifugation at 10°C, 12,500 rpm for 8 min, transfer the uppermost aqueous phase to a new 50 mL centrifuge tube. And added a double volume of chloroform, isoamyl alcohol and the mixture was inverted or shaken for 5 min; and the supernatant was transferred to a new 50 mL centrifuge tube after centrifugation at 10°C and 12,500 rpm for 8 min. The total volume of 3/4 volume of precooled isopropanol was added, mixed upside down for 10 times, incubated in dry ice at −80°C for at least 20 min, then centrifuged at 10°C, 12,000 rpm for 10 min, and the supernatant was discarded; each tube was added with 5 mL of new 75% alcohol to wash the precipitate, and centrifuged at 10°C, 12,000 rpm for 5 min to discard the supernatant carefully. Then 5 mL of 75% ethanol was added to wash the precipitate, and centrifuged at 10°C and 12,000 rpm for 3 min to discard the supernatant carefully. And centrifuge at 12,000 rpm for 2 min, absorb the liquid in the tube, and dry the

fume hood for 3–5 min; then 200–400 μL of EB was added to dissolve the DNA, and 2 μL of RNase A was digested at 37°C for 25 min. Finally, the DNA sample of MA and FM were purified with the PowerClean Pro DNA, respectively. To ensure that the harvested DNA was detected by agarose gel electrophoresis and quantified by Qubit® 2.0 fluorescence meter (Thermo Scientific).

2.2.2 Library construction

Libraries for SMRT (Ardui et al., 2018) sequencing was constructed with an insert size of 20 kb using the SMRT bell TM Template kit (version 1.0.). Briefly, the process was that fragment and concentrate DNA, repair DNA damage and ends, prepare blunt ligation reaction, purify SMRT bell Templates with 0.45X AMPure PB Beads, size-selection using the BluePippin System, repair DNA damage after size-selection. Finally, the library quality was assessed using the Qubit® 2.0 Fluorometer (Thermo Scientific) and the insert fragment size was determined using the Agilent 2100 (Agilent Technologies).

A total amount of 1 μg DNA per sample was used as input material for the DNA sample preparations. Sequencing libraries were generated using NEBNext® Ultra™ DNA Library Prep Kit for Illumina (NEB, United States) following manufacturer's protocol and index codes were added to attribute sequences to each sample. Briefly, the DNA sample was fragmented by sonication to a size of 350 bp, then DNA fragments were end-polished, a-tailed, and ligated with the full-length adaptor for Illumina sequencing with further PCR amplification. Finally, PCR products were purified (AMPure XP system) and libraries were analyzed for size distribution by Agilent2100 Bioanalyzer and quantified using real-time PCR.

2.2.3 Sequencing

The whole genome of MA was sequenced using Illumina Nova Seq PE150 and Pac Bio Sequel, and FM using Illumina Nova Seq PE150. All of the above were sequenced at the Beijing Novogene Bioinformatics Technology Co., Ltd., China.

2.3 Genome assembly

The genome of MA and FM were obtained by assembling the clean data from the second-generation Illumina Nova Seq PE150 system by SOAP *de novo* software (Li et al., 2008). The gap close software was used to fill the gap in preliminary assembly results and removed the same lane pollution by filtering the reads with low sequencing depth (less than 0.35 of the average depth) to obtain the final assembly result of MA and FM. Then, fragments below 500 bp were filtered out and the final result was counted for genome prediction of MA and FM.

All of the data obtained from the Illumina Nova Seq PE150 system will pave the way for the Pac Bio Sequel genomic information of MA. In order to ensure the accuracy of the subsequent analysis results of MA, after filtering the low-quality reads (less than 500 bp) to obtain clean data, which from the Pac Bio Sequel platform were preliminary assembled using SMRT Link version 5.0.1 (Ardui et al., 2018). The long reads of MA were selected (more than 6,000 bp) as the seed sequence, and the other shorter reads were aligned to the seed sequence by Blasr. Then, by the variant Caller module of the SMRT Link software, the arrow algorithm was used to correct and count the variant sites in the initial genome sequence of MA. Finally, the integrity of sequence assembly of MA was evaluated by BUSCO (Benchmarking Universal Single Copy Orthologs, version 2.0) (Simão et al., 2015).

2.4 Genome component prediction and function annotation

Following the assembly process, bioinformatics software was employed to analyzed the genome components of MA and FM. Genome prediction predicts the number of coding genes, repeat sequences and non-coding RNAs. The obtained MA and FM genome-wide data were subjected to Augustus 2.7 program (Keller et al., 2011) *ab initio* prediction. The interspersed repetitive sequences, tandem repeat sequences, transfer RNA (tRNA) and rRNA were predicted by Repeat Masker (Saha et al., 2008) (http://www.repeatmasker.org/), TRF (Maddi et al., 2022) (Tandem repeats finder), tRNAscan-SE (Chan et al., 2021) and rRNAmmer (Lagesen et al., 2007) software, respectively. The sRNA, snRNA and miRNA were predicted by BLAST against the Rfam (Kalvari et al., 2018) database.

Genome function annotation results of MA and FM were compared using functional databases, including Gene Ontology (GO) (http://www.ebi.ac.uk/GOA, accessed on 7 August 2021) (Ashburner et al., 2000), Kyoto Encyclopedia of Genes and Genomes (KEGG) (https://www.kegg.jp/, accessed on 7 August 2021) (Kanehisa et al., 2006), Clusters of Orthologous Groups (KOG) (http://www.ncbi.nlm.nih.gov/COG, accessed on 7 August 2021) (Galperin et al., 2015), Non-Redundant Protein Database (NR) (ftp://ftp.ncbi.nlm.nih.gov/blast/db/, accessed on 7 August 2021) (Li et al., 2002), Transporter Classification Database (TCDB) (http://www.tcdb.org, accessed on7 August 2021) (Saier et al., 2021), Cytochromes P450 (CYP450) (http://drnelson.utmem.edu/CytochromeP450.html, accessed on 7 August 2021) (Kohler et al., 2015), Swiss-Prot (http://www.expasy.org/sprot/and http://www.ebi.ac.uk/swissprot/, accessed on 7 August 2021) (Bairoch and Apweiler, 2000) and Protein Families Database of Alignments and Hidden Markov Models (Pfam) (http://pfam.xfam.org/, accessed on 7 August 2021) (Eddy, 1998). A whole genome Blast (Reiner et al., 2018) search (E-value less than $1e^{-5}$, minimal alignment length percentage larger than 40%) was performed against above eight databases. The predict secretory protein, gene cluster of secondary metabolites and carbohydrate-active enzyme were predicted using the Carbohydrate-active Enzyme Database (CAZymes) (http://www.cazy.org/, accessed on 7 August 2021) (Cantarel et al., 2008), Signal P database (Petersen et al., 2011) and antiSMASH (Blin et al., 2021) database.

2.5 Comparative genomics analysis

Genomic alignment between the sample of FM genome and reference genome of MA were performed by MUMmer (Marçais et al., 2018) and LASTZ (Aljouie and Zhong, 2020) tools. Genomic synteny was analyzed based on the alignment results. InDels, SNPs and SVs were found by the genomic

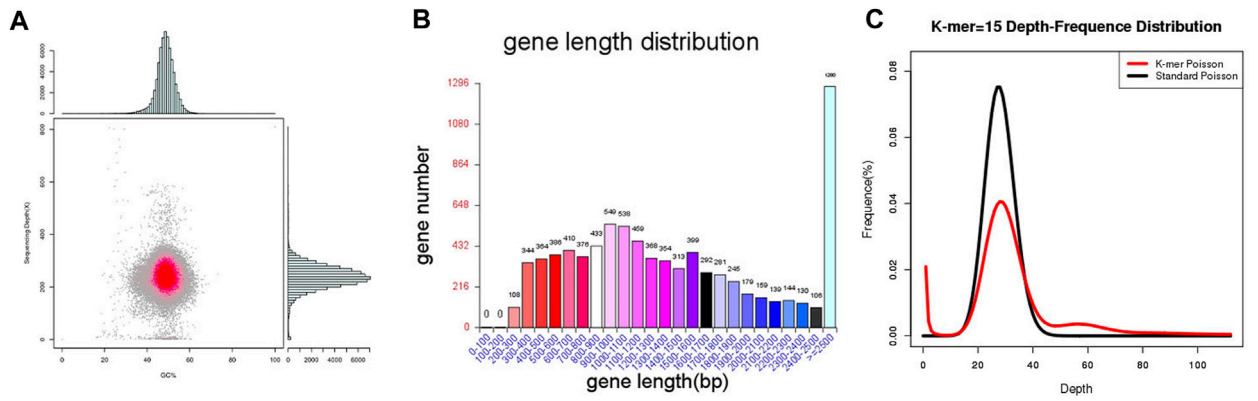

FIGURE 2
Genome sequencing, assembly and prediction of MA. **(A)** Statistical chart of correlation analysis between MA GC content and sequencing depth. The horizontal axis represents the GC content, the vertical axis represents the sequencing depth, the right is the sequencing depth distribution, and the upper is the GC content distribution. **(B)** The gene length distribution of MA. The horizontal axis shows the gene length, and the vertical axis shows the corresponding gene number. **(C)** K-mer analysis diagram of MA.

alignment results among samples by the MUMmer and LASTZ. Comparative analysis of genome sequence, component predictions and genome function annotations were the same as Sections 2.2–2.4.

3 Results

3.1 Genome sequence and component prediction

Through the Pac Bio Sequel platform, it was found that MA generated 817,989 Mb Pac Bio-data. The 34.14 Mb genome sequence was assembled from 24 contigs with N50 length was 2.6 Mb. Of the 24 contigs, the longest one was 4.5 Mb in length. The analysis of GC content and read coverage depth of the MA assembly sequence revealed no significant contamination of the sample DNA. However, scattered points were observed in the region with a GC content ranging from 20% to 40%. These anomalies could potentially be attributed to the presence of mitochondrial DNA in the fungal genomic samples (Figure 2A). The sequence and feature summary of MA *de novo* assembly results demonstrated that high-quality sequence have been obtained (Supplementary Table S1). Using BUSCO software, we identified 94.8% (277/290) of well-known fungal complete and single-copy in MA assembly, which further illustrated a high accuracy and integrity of MA monokaryon (Supplementary Table S2). This Whole Genome Shotgun project has been deposited in GenBank under the accession number JASXRQ000000000. The final genome assembly results and related data of MA were submitted to the NCBI Bio Project PRJNA973857, Bio Sample SAMN35152529 and SRA accession number was SUB13375186, respectively.

MA had a total number of 8,356 protein-coding genes were predicted with a total gene length of 12,839,852 bp, accounting for 37.61% of the whole genome size (34,136,716 bp); and an average gene length of coding genes was 1,537 bp, most of which ranged from 300 bp to 1,700 bp (Table 1; Figure 2B). In the prediction of repeat sequences, the interspersed and repeats were 2,761 and 5,626, respectively. For interspersed, the LTRs, DNAs, LINEs, SINEs and rolling circles contained 1,901, 493, 3,146 and 33, respectively. Moreover, 14 unknowns with a total length of 1,371 bp are to be further explored. For repeats, the TRs, minisatellite DNAs and microsatellite DNAs contained 3,045, 1,985 and 596, respectively (Supplementary Table S3). Regarding RNAs, 88 tRNAs, 9 rRNAs and 13 snRNAs were predicted (Supplementary Table S4). Based on the aforementioned information, the detailed circular genome diagram information of MA was visually represented using Circos (Krzywinski et al., 2009) software (Figure 3).

TABLE 1 Statistics of gene prediction results of MA.

Parameter	Value
Genome size	34,136,716 bp
Gene number	8,356
Gene total length	12,839,852 bp
GC content (%)	51.62
Gene length/Genome (%)	37.61
Gene average length	1,537 bp
Gene internal length	21,296,864 bp
Gene internal GC content	46.59

3.2 Genome function annotation

3.2.1 Gene general annotation

Different public databases were used to predict the number of genes enriched in each functional category (Supplementary Table

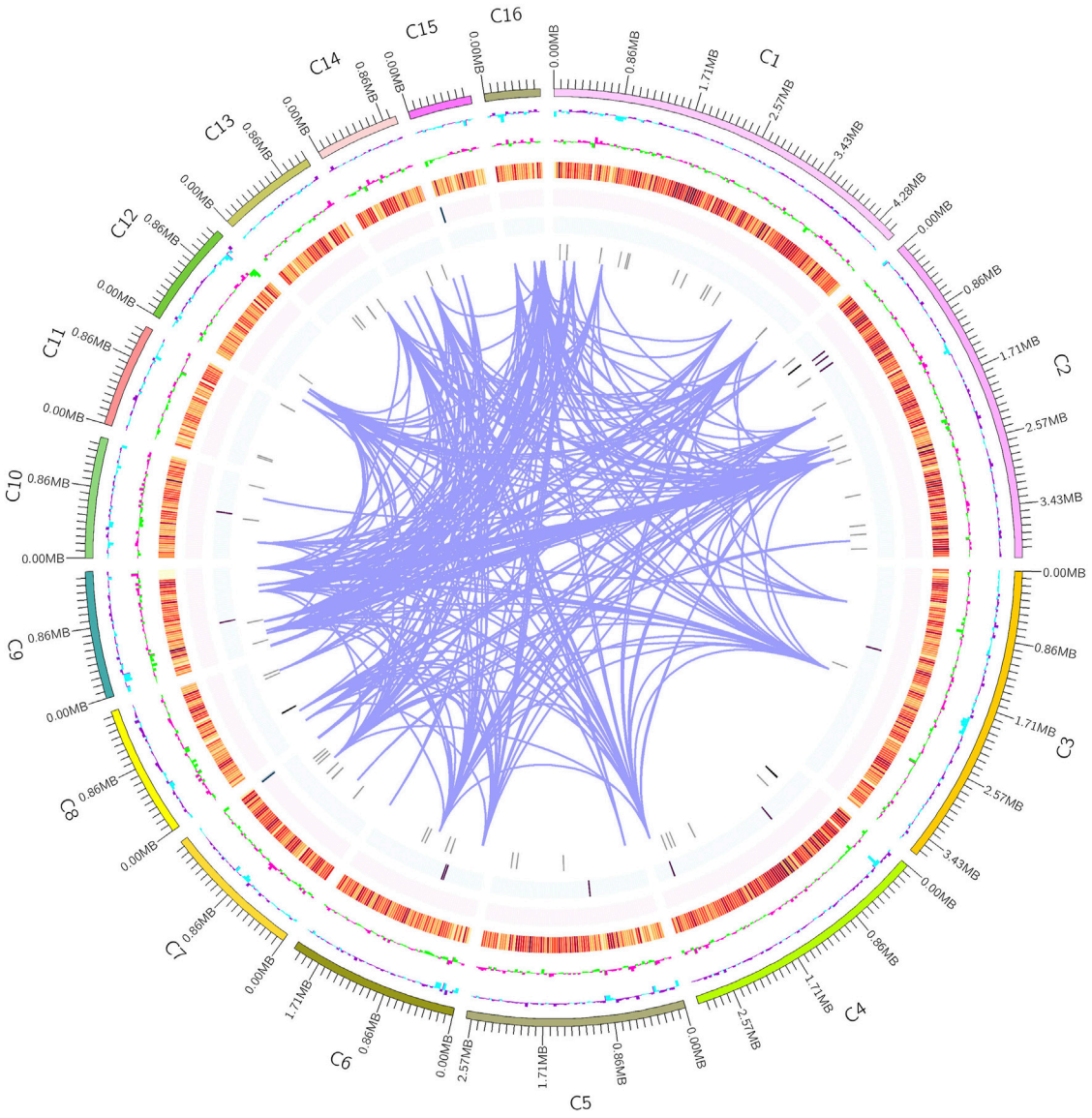

FIGURE 3
Circular whole genome diagram of MA. The outermost layer is the position coordinates. From the outer circle to the inner circle is GC content (purple: > mean value, blue: < mean value). GC skew (the specific algorithm= (G–C)/(G + C); pink: > 1, green: < 1). Gene density (four circles were taken inward from orange, representing the numerical value of coding genes, rRNA, snRNA, and tRNA, respectively). Genome chromosome duplication (regions with similarity greater than 90% of 8 kb sequences were connected by purple lines).

S5). According to the GO database, MA obtained 5,342 genes accounted for 17.60% of the genome and were classified into 3 categories and 48 subcategories. There were mainly distributed in six functional subcategories, binding (2,877), metabolic process (2,790), cellular process (2,781), catalytic activity (2,403), cell (1,724) and cell part (1,724) (Figure 4A).

MA had 6,564 genes were annotated in the KEGG database, among them 1,864 genes were enriched in 366 KEGG pathways (Figure 4B). The most and least enriched functional annotations were metabolism (1,813) and environmental information processing (241), respectively; with the top three coding genes being global and overview maps (693), translation (284) and carbohydrate metabolism (253) (Supplementary Table S6). There were 107 metabolism pathways, with purine metabolism (59), oxidative phosphorylation (56), pyrimidine metabolism (51), amino sugar and nucleotide sugar metabolism (46), starch and sucrose metabolism (43), pyruvate metabolism (37), glycolysis/gluconeogenesis (36), cysteine and methionine metabolism (34) and arginine and proline metabolism (33) and so on. Furthermore, the main enriched signaling pathways were MAPK signaling pathway-yeast (54), mTOR signaling pathway (43), PI3K-Akt signaling pathway (29), Ras signaling pathway (27), MAPK signaling pathway (25), FoxO signaling pathway (24) and other effective pathways (Supplementary Table S7).

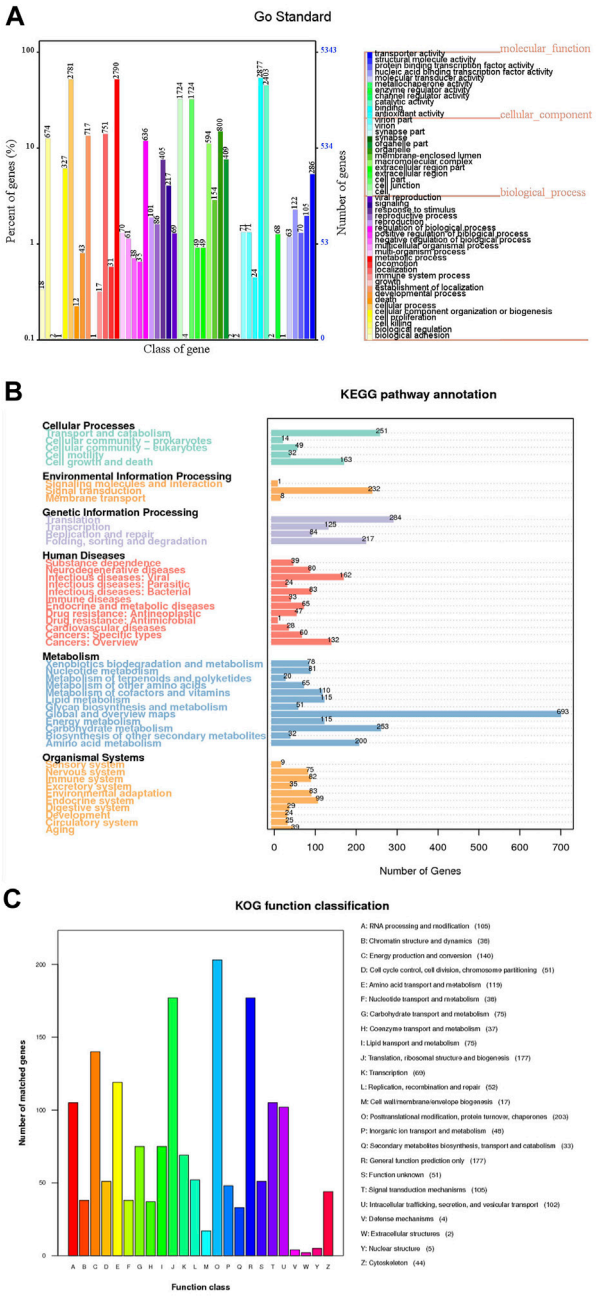

FIGURE 4
Different public database gene annotation map of MA. **(A)** GO annotation. The horizontal axis represents the GO functional classification on the sample annotation, the right vertical axis represents the number of genes on the annotation, and the left vertical axis represents the percentage of the number of genes on the annotation to all coding genes. **(B)** KEGG (Level 1) annotation. The number on the bar graph represents the number of genes on the annotation. **(C)** KOG annotation. The horizontal axis represents the KOG functional type, and the vertical axis represents the number of genes on the annotation.

The data with the KOG protein database to obtain the phylogenetic relationship classification of fungal complete genome-encoded proteins (Figure 4C). There were 1,595 genes annotated in the KOG database. Posttranslational modification, protein conversion, and chaperones (203) coding genes were the most abundant. The abundant number of classes in the KOG groups were translation, ribosomal structure and biogenesis (177), general function prediction only (177), energy production and conversion (140) and amino acid transport and metabolism (119).

3.2.2 Gene special annotations

We used multiple databases, including NR, Pfam, Swiss-prot, TCDB, CAZymes, secretory proteins, CYPs and gene clusters of secondary metabolites to further elucidated the genomic functions of MA. In MA, 7,177 (23.67%) genes were assigned to the NR database. The top three species were *S. baumii*, *F. mediterranea* and *P. pouzarii* (Supplementary Table S8). A total of 5,342 genes of MA were annotated to the Pfam database. Moreover, 6.89% (2,090) of the predicted genes were annotated to the Swiss-prot database. There were 365 (4.37%) genes annotated in TCDB database. Among TCDB, the order of proportion from large to small were the primary active transporters (122, 33.42%), electrochemical potential-driven transporters (119, 32.60%), incompletely characterized transport systems (45, 12.32%), channels/pores (42, 11.50%), accessory factors involved in transport (29, 7.95%), group transporters (8, 2.19%) and transmembrane electron carriers were not included.

The genome of macrofungus contains CAZymes that play an essential role in facilitating the acquisition of complex carbohydrate metabolism. There were 418 genes annotated in CAZymes database (Table 2). Most of these genes encode glycoside hydrolases (GHs) (185, 44.26%), glycosyltransferases (GTs) (79, 18.90%), auxiliary activity (AAs) (63, 15.07%), carbohydrate-binding modules (CBMs) (47, 11.24%), carbohydrate esterases (CEs) (33, 7.89%) and polysaccharide lyases (PLs) (11, 2.63%). From the CAZymes database, a total of 148 CAZymes families were detected in MA monokaryon (Supplementary Table S9). In the MA genome, GHs were distributed in 65 families; among the main enzymes of lignocellulose degradation, cellulase identified 12 families with GH1-GH3, GH-7, GH9, GH10, GH12, GH51, GH74, AA9 and AA16. Hemicellulose was mainly distributed in 15 families with GH1-3, GH6-7, GH9, GH12, GH17, GH27, GH29-31, GH35, GH51 and GH74. Pectinase was mainly distributed in GH2-3, GH9, GH12, GH28, GH53, GH74, GH78, PL14, CE8 and other 10 families. Ligninase was mainly distributed in AA1-2 2 families. CBMs include CBM1, CBM12, CBM13, CBM20, CBM21 and CBM50 families. CEs were divided into CE1, CE4, CE8-9, CE12 and CE15-16 8 families. PLs were mainly distributed in 8 families with PL14, PL35 and PL38 (Supplementary Table S10).

Next, 467, 1,291 and 333 proteins with signal peptide structure, transmembrane structure and signal peptide structure without transmembrane structure were obtained of MA, respectively. A total of 123 genes from MA were assigned to encode CYPs. The highest (84, 68.29%) had E-class P450 group I annotations (Table 2). Moreover, 20 genes were involved in the "Metabolism of xenobiotics by cytochrome P450" (Supplementary Table S11) and 18 genes were involved in the KEGG sub-pathway "Drug metabolism-cytochrome P450" (Supplementary Table S12). A total of 15 gene clusters were

10.3389/fgene.2023.1221491

TABLE 2 Comparative analysis of genomic components and comparison of different databases for MA and FM.

Characteristic	Type	Gene number	
		MA	FM
Comparison results for genomic components	Genome size (bp)	34,136,716	31,430,498
	Gene number	8,356	9,167
	Gene total length (bp)	12,839,852	12,719,201
	Gene average length (bp)	1,537	1,387
	Gene length/Genome (%)	37.61%	40.47%
Comparison results for TCDB database	Channels/pores	42	38
	Electrochemical potential-driven transporters	119	118
	Primary active transporters	122	127
	Group translocators	8	8
	Transmembrane electron carriers	0	0
	Accessory factors involved in transport	29	33
	Incompletely characterized transport systems	45	50
Comparison results for CAZymes database	Glycoside hydrolases (GHs)	185	192
	Glycosyltransferases (GTs)	79	90
	Auxiliary activity (AAs)	63	64
	Carbohydrate-binding modules (CBMs)	47	50
	Carbohydrate esterases (CEs)	33	27
	Polysaccharide lyases (PLs)	11	12
Comparison results for secretory protein prediction	Signal protein	467	558
	TMHMM protein	1,291	1,551
	Secreted protein	333	384
Comparison results for cytochromes P450 database	P450, CYP52	4	5
	E-classP450, CYP2D	1	1
	Undeterminded	15	22
	CytochromeP450	9	14
	E-classP450, group I	84	82
	E-classP450, group IV	7	8
	Pisatindemethylase-like	3	3
Comparison results for gene clusters of secondary metabolites	Terpene	8	11
	NRPS-like, T1PKS	2	2
	NRPS	1	1
	NRPS-like	3	4
	T1PKS	1	1

obtained from MA, which were 8 terpenes, 1 NRPS, 1 T1PKS and 5 other clusters. Additionally, we detected the MA gene in the "Terpenoid backbone biosynthesis (map 00900)" pathway and found 12 key enzymes distributed in the MVA pathway (Table 3). Hexaprenyl-diphosphate synthase, prenylcysteine oxidase/farnesylcysteine lyase, farnesyl diphosphate synthase and protein farnesyltransferase/geranylgeranyltransferase type-1 subunit alpha was encoded by double-copy genes. In contrast, the other 8 enzymes were encoded by a single-copy gene (Supplementary Table S13).

TABLE 3 Core enzymes involved in terpenoid biosynthesis of MA.

Gene name and definition	EC No.	KO term	Gene ID
hexPS, COQ1; hexaprenyl-diphosphate synthase	2.5.1.82, 2.5.1.83	K05355	A1965
PCYOX1, FCLY; prenylcysteine oxidase/farnesylcysteine lyase	1.8.3.5, 1.8.3.6	K05906	A2517
DHDDS, RER2, SRT1; ditrans, polycis-polyprenyl diphosphate synthase	2.5.1.87	K11778	A3541
HMGCR; hydroxymethylglutaryl-CoA reductase (NADPH)	1.1.1.34	K00021	A3675
FDPS; farnesyl diphosphate synthase	2.5.1.1, 2.5.1.10	K00787	A4491
E2.3.3.10; hydroxymethylglutaryl-CoA synthase	2.3.3.10	K01641	A4708
E2.3.1.9, atoB; acetyl-CoA C-acetyltransferase	2.3.1.9	K00626	A5693
STE24; STE24 endopeptidase	3.4.24.84	K06013	A7679
FNTB; protein farnesyltransferase subunit beta	2.5.1.58	K05954	A7968
MVD, mvaD; diphosphomevalonate decarboxylase	4.1.1.33	K01597	A8252
FNTA; protein farnesyltransferase/geranylgeranyltransferase type-1 subunit alpha	2.5.1.58 2.5.1.59	K05955	A1633
E2.7.4.2, mvaK2; phosphomevalonate kinase	2.7.4.2	K00938	A1934

3.3 Comparative genomics analysis

3.3.1 Comparative analysis of genome sequence and component prediction

Comparative genomic analysis of genome sequence, it was found that raw reads, clean reads and filtered reads of FM were 5,595, 4,507 Mb and 46.14%, respectively, above numbers were all higher than ones of MA. Then, the number and the depth of K-mer of FM were also higher than those of MA (Figure 2C), and the former number was 885,330,899 and the latter number was 22.92. But the number of revised size and repeat rate of FM were lower than ones of MA (Supplementary Table S1). By comparing the genome component analysis, it was demonstrated that the genome size, gene total length and gene average length of FM were lower than those of MA, which were 31,430,498, 12,719,201, and 1,387 bp, respectively. Genome component prediction comparison showed that protein-coding genes of FM were higher than MA, reaching 9,167 (Table 2). However, the repeat sequences results of FM were lower than those of MA (Supplementary Table S3), contained only 71 tRNAs (Supplementary Table S4).

3.3.2 Comparative analysis of genome function annotation

The numerical comparison of MA and FM in the GO functional database showed that more genes were enriched in binding, metabolic process and cellular process, and they were annotated to three types of biological functions, indicating high similarity. Compared with MA, FM lacked three subcategories such as growth, synapse and synapse part. And a total number of 5,555 genes were obtained of FM, accounting 17.55% for all the genes, and it was found that cellular component and molecular function were higher than MA, while biological process was lower than MA (Supplementary Figure S1A). Compared with KEGG annotations of MA and FM, the results indicated that the total number of FM (6,943, 21.93%) genes were higher than that of MA and also categorized into 6 levels and 46 categories; and the number of FM genes associated with most genome functions was not significantly different from the number of genes for MA. In addition, its metabolism is also mainly related to global and overview maps (724), carbohydrate metabolism (256), amino acid metabolism (203), energy metabolism (125) and lipid metabolism (123) (Supplementary Figure S1B). However, due to the preliminary nature of the FM measurement, a more in-depth exploration is required to elucidate specific metabolic pathways and identify enriched genes, which can be further compared with MA. In view of MA and FM in the KOG functional database also have high similarity. The number of genes annotated by MA were less than that of FM genome (1,641), but there was no difference in KOG types (Supplementary Figure S1C).

Given that the TCDB database annotation, the total number of FM genes were higher than MA, reaching 374. There was no markedly difference in types (Table 2). Like MA, primary active transporters (127, 33.95%) were the most enriched (Table 2). FM contained more CAZymes genes, reaching 394. Among them, glycoside hydrolases (GHs) (192, 48.73%), glycosyltransferases (GTs) (90, 22.84%), auxiliary activity (AAs) (64, 16.24%), carbohydrate-binding modules (CBMs) (50, 12.69%) and polysaccharide lyases (PLs) (12, 3.05%) were higher than MA, but carbohydrate esterases (CEs) (33, 8.38%) was lower than MA (Table 2). In addition, the total number of FM secretory protein prediction were higher than that of MA (Table 2).

Cytochromes P450 database comparison showed that, E-class P450 group I (82, 60.74%) were high expression enrichment in FM genome, followed by Undeterminded (22, 16.30%) and Cytochrome P450 (14, 10.37%) (Table 2). There were 19 gene clusters of secondary metabolites annotated in FM, including 11 terpenes and 4 NRPS-likes. Both samples contained five kinds of gene clusters of secondary metabolites, further revealing high similarity; it also contains two NRPS-like, T1PKS genes, one NRPS gene and one T1PKS gene. The comparative analysis of the above genome functional annotations will provide a potential reference for whether FM is as medicinal as MA (Table 2).

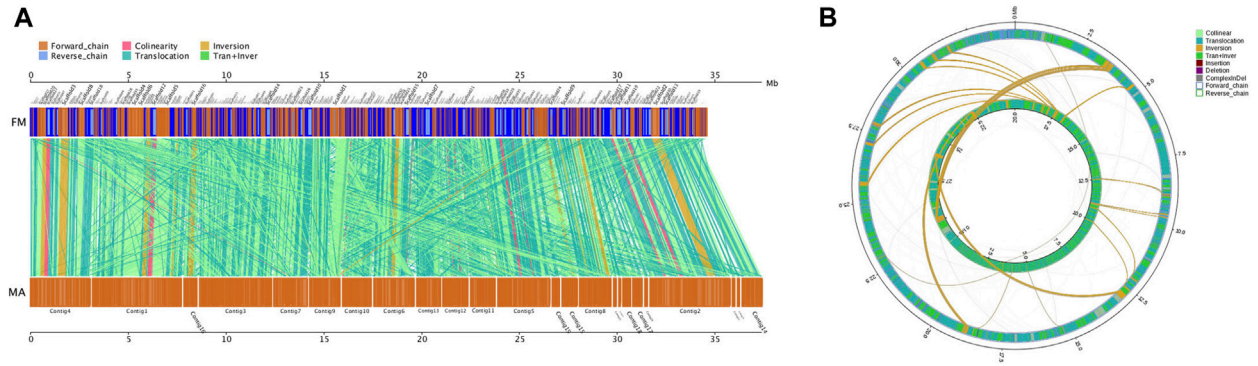

FIGURE 5
Comparative genomics analysis of MA and FM. **(A)** Parallel collinearity comparison between MA and FM. **(B)** Genome-wide structural variation type pairing map. The inner ring and the outer ring were FM and MA, respectively.

3.3.3 Collinearity, InDel, SNP, and SV analysis

The results of collinearity analysis between MA and FM showed that, the total base length of the MA sequence was 29,119,278 bp, which accounted for 92.65% of the total gene length of 31,430,498 bp. There were 6,499 collinearity blocks in MA and FM. MA and FM had many similar translocations, translocation and inversion alignments, indicating that high collinearity relationship between them (Figure 5A; Supplementary Table S14). There were 8,356 InDels, including 275 gene coding regions, 124 insertions and 151 deletions identified between FM and MA. These InDels affected 11 CDS regions, 3 of which led to frameshifts, and 1 InDel resulted in a premature stop (Supplementary Tables S15, S16). There were 228,256 SNPs found between FM and MA, of which 66,280 SNPs occurred in the gene coding regions. The CDS SNPs and intergenic FM were 0, 57, 62, 63, 227, 41,037, 24,834, 66,280 and 161,976, respectively. These values represented 0%, 0.0250%, 0.0272%, 0.0276%, 0.0994%, 17.9785%, 10.8799%, 29.0376% and 70.9624% of the total SNPs (Supplementary Tables S17, S18). FM had 9,020 SVs, of which 3,799 translocations account for 42.1% of the total SVs; 179 inversions account for 1.9%; 3,462 translocations and inversions account for 38.3%; 336 insertions account for 3.7%; 1,143 deletions account for 12.6%; and 98 complex InDels contribute for 1% (Figure 5B; Supplementary Table S19).

4 Discussion

Fungi has been used as functional food and traditional medicine for a long history in China. Among them, "*Sanghuang*" is a well-known edible and medicinal fungus, which is used as health preservation and treatment of diseases. It was recorded in several ancient traditional Chinese herbal books, including *Shennong's Classic of Materia Medica* and *Compendium of Materia Medica* (Bao et al., 2020). At present, the whole genome sequencing of *I. hispidus* growing in different tree species has not been reported. Hence, in this paper, two strains of *I. hispidus* growing in *M. alba* and *F. mandshurica* were chosen to reveal differences of genome sequence and epigenetics. The whole genome of MA monokaryon was sequenced by the combination of the Illumina and Pac Bio platform. Then using MA as a reference, comparative genomics between MA monokaryon and FM monokaryon was analyzed. The result demonstrated that, MA had 8,356 protein-coding genes, 24 contigs with a contig N50 size of 2.6 Mb and a genome-wide map of 34.14 Mb was drawn. The average genome size of most fungi is about 40 Mb (Duan et al., 2022), and the assembled genome size obtained by MA is basically in line with the expected results.

According to the results of genome annotation, MA obtained 30,321 genes from different public databases, but a large number of predicted genes could not match the public database. As we know, KEGG is the essential public database about pathways. On the basis of KEGG functional annotation, MA were primarily connected with carbohydrate metabolism and amino acid metabolism. In light of pathways analysis, the most significant biochemical metabolic pathways and signal transduction pathways of MA were relevant to metabolites. By further analysis of metabolic pathways, MA were found that principally involved in purine metabolism, oxidative phosphorylation, pyrimidine metabolism, amino sugar and nucleotide sugar metabolism, starch and sucrose metabolism, pyruvate metabolism and some other secondary metabolic pathways. There were 31 signal transduction pathways, including MAPK signaling pathway-yeast, mTOR signaling pathway, PI3K-Akt signaling pathway and so on. MA contains 14 xenobiotics biodegradation and metabolisms. It was testified that MA has a strongly primary metabolic process and powerful ability to degrade aromatic compounds. Furthermore, CAZymes as a matrix-degrading enzyme that plays an extremely critical role in maintaining the metabolism and circulation of natural substances. MA had a great deal of genes encoding cellulase, hemicellulase, glucan degradation related enzymes, chitinase (EC 3.2.1.14), α-amylase (EC 3.2.1.-) and peptidoglycan degradation related enzymes. It was announced that MA can not only degrade plant polysaccharides, but also degrade N-acetylamino polysaccharides, and can destroy the integrity of cell wall structure by cooperating with glucanase, cellulase,

peptidoglycanase and chitinase to maintain the growth and senescence of pileus (Ding et al., 2007; Tao et al., 2013). Simultaneously, other cell wall structure-related enzyme genes also further denoted that MA has the potential to specifically degrade the host cell wall to achieve the effect of biocontrol.

In addition, CYPs belong to the heme-containing monooxygenase superfamily. The functional and evolutionary diversity of fungal CYPs makes the classification of fungal CYPs more complex, mainly associated with the biosynthesis and metabolism of fungal endogenous substances such as fatty acids, sterols, terpenes. In the field of pharmacology and therapeutics, the secondary metabolites of medicinal fungi have been reported to have anti-inflammatory and anti-viral effects (Alves et al., 2012; Alves et al., 2013), usually located in the adjacent gene clusters (Keller et al., 2005), and can be found through gene mining. Gene clusters of secondary metabolites with TS, NRPS and PKS. It was found that all known fungal siderophores were synthesized by NRPS (Haas et al., 2008). Like most basidiomycetes, MA contains a small amount of NRPS and T1pks genes, demonstrated that MA has the ability to resist the stress of the external environment and maintain its own growth and metabolism. Among fungi, one of the largest groups of corroborate bioactive natural products were terpenoids, which were composed of isoprene, mainly derived from the mevalonate pathway (Miziorko, 2011; Quin et al., 2014; Adamek et al., 2017), and had a variety of pharmacological activities. For example, the triterpenoid ganoderic acids has been reported to have anti-tumor and immunomodulatory effects (Shi et al., 2010). Twelve key enzymes involved in the MVA pathway were identified from the "Terpenoid backbone biosynthesis (map 00900)" pathway, revealing that the biosynthesis of MA terpenoids is mainly formed by the MVA pathway like most fungi. Among them, lanosterol synthase (LSS) can catalyze the cyclization of (3S)-2,3-0xidosqualene to produce lanosterol. Various enzymes act downstream to convert precursors into ergosterol and other sterols in the fungus. Notably, the catalytic derivatization of these compounds is heavily reliant on the involvement of CYPs enzymes, which play a pivotal role in modifying the lanosterol skeleton (Benveniste, 2004). In the pursuit of identifying potential triterpenoid biosynthesis genes in MA, a single copy of the LSS gene (ERG7; K01852; EC 5.4.99.7) was investigated. Consequently, it is postulated that diverse structural types of sterols and triterpenes may be produced through the action of different enzymes acting upon the LSS gene, as evidenced by the presence of various families of MA CYPs and eight triterpene-related gene clusters.

Moreover, comparative genomics as a research method to comprehend the function, expression mechanism and species evolution of genes by comparing the gene structure and distribution of different genome. During the evolutionary trajectory of fungi, genetic variations such as gene deletions and acquisitions can occur as a result of environmental selection, ultimately influencing the fungal adaptive capacity. In this study, we conducted a comparative analysis of the genome structure and function of FM, utilizing MA as the reference genome. It was worth noting that, the genome composition of FM exhibited distinctions from MA in terms of genome size, the number of coding genes, repeat sequences and non-coding RNAs. These differences suggest that FM may possess enhanced environmental adaptability, implying a potential expansion of its adaptive repertoire throughout its evolutionary history. Comparison of GO, KEGG, KOG and CAZymes results showed that, there was no apparently difference in the function of genes enriched with MA. In accordance with gene clusters, FM contains 11 terpenes. Although, FM and MA types of genome function annotation were high similarity, the specific intrinsic active substances of FM need further exploration. As two common InDels and SNPs markers for genetic polymorphism analysis, it can thorough understand the genetic polymorphism of different species (Santos et al., 2018). A significant number of InDels and SNPs sites were identified between MA and FM, which provided a basis for the subsequent genetic map construction and phylogenetic research of *I. hispidus*. Since accurate screening and functional verification of candidate genes for FM are currently lacking, it is crucial to prioritize comprehensive functional verification of candidate sites. This will enable us to gain clues into the regulatory mechanisms underlying these genes and enhance our understanding of FM genetic characteristics. Through the implementation of gene knock-out experiments, we can examine alterations in the intrinsic activity and ascertain potential significant modifications in the target peak of the active product. The primary objective of the research is to understand the genetic composition of MA and to determine whether FM has the value of development and utilization like MA by comparative genomics analysis. In the future, we would continue to collect *I. hispidus* growing in other tree species and analyze the influence of different tree species on these strains by comparative genomics and transcriptomics.

5 Conclusion

In this study, a comprehensive overview of MA was conducted at the genetic level, and a comparative genomics analysis was performed for FM to compare differences in genetic materials and whether it has potential medicinal value as MA. A 34.14 Mb genome-wide map of MA was drawn by sequencing and assembly. Additionally, 9 major secondary metabolic pathways and 31 signal transduction pathways were obtained in MA. Although, comparative genomics analysis showed that FM had high similarity with MA, the total number of genes annotated in different databases of FM were higher than MA, including 11 terpenes, which provided new insights into the correlation of FM phenotypic characteristics and genetic mechanisms. It also provided a foundation for the development and utilization of *I. hispidus* growing in different tree species from the aspect of genomics research.

Data availability statement

The datasets presented in this study can be found in online repositories. The names of the repository/repositories and accession

number(s) can be found below: NCBI, BioProject ID: PRJNA973857.

Author contributions

QW, HB, and ZL conceived experiments and collected literature. HB survey of resource and shooting sample. QW and ZL data collation and analysis. QW wrote the first draft of this study. All authors contributed to the article and approved the submitted version.

Funding

This study was supported by the National Natural Science Foundation of China (No. 32070021).

Acknowledgments

We thank the National Natural Science Foundation for funding. We also thank the samples provided by Xiajin DeBai *Sanghuang* Biotechnology Co., Ltd., and the experimental platform and technical support provided by the Key Laboratory of Northern Edible Fungi Resources Utilization, Ministry of Agriculture and Rural Affairs of China.

Conflict of interest

The authors declare that the research was conducted in the absence of any commercial or financial relationships that could be construed as a potential conflict of interest.

Publisher's note

All claims expressed in this article are solely those of the authors and do not necessarily represent those of their affiliated organizations, or those of the publisher, the editors and the reviewers. Any product that may be evaluated in this article, or claim that may be made by its manufacturer, is not guaranteed or endorsed by the publisher.

Supplementary material

The Supplementary Material for this article can be found online at: https://www.frontiersin.org/articles/10.3389/fgene.2023.1221491/full#supplementary-material

References

Adamek, M., Spohn, M., Stegmann, E., and Ziemert, N. (2017). Mining bacterial genomes for secondary metabolite gene clusters. *Methods Mol. Biol.* 1520, 23–47. doi:10.1007/978-1-4939-6634-9_2

Aljouie, A., and Zhong, L. (2020). High scoring segment selection for pairwise whole genome sequence alignment with the maximum scoring subsequence and gpus. *Int. J. Comput. Biol. Drug Des.* 13, 71. doi:10.1504/IJCBDD.2020.10026787

Alves, M. J., Ferreira, I. C., Dias, J., Teixeira, V., Martins, A., and Pintado, M. (2013). A review on antifungal activity of mushroom (basidiomycetes) extracts and isolated compounds. *Curr. Top. Med. Chem.* 13, 2648–2659. doi:10.2174/15680266113136660191

Alves, M. J., Ferreira, I. C., Martins, A., and Pintado, M. (2012). Antimicrobial activity of wild mushroom extracts against clinical isolates resistant to different antibiotics. *J. Appl. Microbiol.* 113, 466–475. doi:10.1111/j.1365-2672.2012.05347.x

Angelini, P., Girometta, C., Tirillini, B., Moretti, S., Venanzoni, R., Cipriani, M., et al. (2019). A comparative study of the antimicrobial and antioxidant activities of *Inonotus hispidus* fruit and their mycelia extracts. *Int. J. Food Prop.* 22, 768–783. doi:10.1080/10942912.2019.1609497

Ardui, S., Ameur, A., Vermeesch, J. R., and Hestand, M. S. (2018). Single molecule real-time (SMRT) sequencing comes of age: Applications and utilities for medical diagnostics. *Nucleic Acids Res.* 46, 2159–2168. doi:10.1093/nar/gky066

Ashburner, M., Ball, C. A., Blake, J. A., Botstein, D., Butler, H., Cherry, J. M., et al. (2000). Gene ontology: Tool for the unification of biology. The gene Ontology consortium. *Nat. Genet.* 25, 25–29. doi:10.1038/75556

Awadh, A. N., Mothana, R. A., Lesnau, A., Pilgrim, H., and Lindequist, U. (2003). Antiviral activity of *Inonotus hispidus*. *Fitoterapia* 74, 483–485. doi:10.1016/s0367-326x(03)00119-9

Bairoch, A., and Apweiler, R. (2000). The SWISS-PROT protein sequence database and its supplement TrEMBL in 2000. *Nucleic Acids Res.* 28, 45–48. doi:10.1093/nar/28.1.45

Benarous, K., Bombarda, I., Iriepa, I., Moraleda, I., Gaetan, H., Linani, A., et al. (2015). Harmaline and hispidin from *Peganum harmala* and *Inonotus hispidus* with binding affinity to *Candida rugosa* lipase: *In silico* and *in vitro* studies. *Bioorg Chem.* 62, 1–7. doi:10.1016/j.bioorg.2015.06.005

Benveniste, P. (2004). Biosynthesis and accumulation of sterols. *Annu. Rev. Plant Biol.* 55, 429–457. doi:10.1146/annurev.arplant.55.031903.141616

Blin, K., Shaw, S., Kloosterman, A. M., Charlop-Powers, Z., van, W. G., Medema, M. H., et al. (2021). antiSMASH 6.0: improving cluster detection and comparison capabilities. *Nucleic Acids Res.* 49, W29–W35. doi:10.1093/nar/gkab335

Cantarel, B. L., Coutinho, P. M., Rancurel, C., Bernard, T., Lombard, V., and Henrissat, B. (2008). The carbohydrate-active EnZymes database (CAZy): An expert resource for glycogenomics. *Nucleic Acids Res.* 37, D233–D238. doi:10.1093/nar/gkn663

Chan, P. P., Lin, B. Y., Mak, A. J., and Lowe, T. M. (2021). tRNAscan-SE 2.0: improved detection and functional classification of transfer RNA genes. *Nucleic Acids Res.* 49, 9077–9096. doi:10.1093/nar/gkab688

Dai, Y., Qin, G., and Xu, M. (2000). The forest pathogens of root and butt rot on northeast China. *For. Res.* 13, 15–22. doi:10.13275/j.cnki.lykxyj.2000.01.003

Ding, S., Ge, W., and Buswell, J. A. (2007). Molecular cloning and transcriptional expression analysis of an intracellular beta-glucosidase, a family 3 glycosyl hydrolase, from the edible straw mushroom, *Volvariella volvacea*. *FEMS Microbiol. Lett.* 267, 221–229. doi:10.1111/j.1574-6968.2006.00550.x

Duan, Y., Han, H., Qi, J., Gao, J., Xu, Z., Wang, P., et al. (2022). Genome sequencing of *Inonotus obliquus* reveals insights into candidate genes involved in secondary metabolite biosynthesis. *BMC Genomics* 23, 314. doi:10.1186/s12864-022-08511-x

Eddy, S. R. (1998). Profile hidden Markov models. *Bioinformatics* 14, 755–763. doi:10.1093/bioinformatics/14.9.755

Galperin, M. Y., Makarova, K. S., Wolf, Y. I., and Koonin, E. V. (2015). Expanded microbial genome coverage and improved protein family annotation in the COG database. *Nucleic Acids Res.* 43, D261–D269. doi:10.1093/nar/gku1223

Gründemann, C., Arnhold, M., Meier, S., Bäcker, C., Garcia-Käufer, M., Grunewald, F., et al. (2016). Effects of *Inonotus hispidus* extracts and compounds on human immunocompetent cells. *Planta Med.* 82, 1359–1367. doi:10.1055/s-0042-111693

Haas, H., Eisendle, M., and Turgeon, B. G. (2008). Siderophores in fungal physiology and virulence. *Annu. Rev. Phytopathol.* 46, 149–187. doi:10.1146/annurev.phyto.45.062806.094338

Jiang, J., Wu, S., and Zhou, L. (2021). The first whole genome sequencing of *Sanghuangporus sanghuang* provides insights into its medicinal application and evolution. *J. Fungi (Basel).* 7, 787. doi:10.3390/jof7100787

Kalvari, I., Nawrocki, E. P., Argasinska, J., Quinones-Olvera, N., Finn, R. D., Bateman, A., et al. (2018). Non-coding RNA analysis using the Rfam database. *Curr. Protoc. Bioinforma.* 62, e51. doi:10.1002/cpbi.51

Kanehisa, M., Goto, S., Hattori, M., Aoki-Kinoshita, K. F., Itoh, M., Kawashima, S., et al. (2006). From genomics to chemical genomics: New developments in KEGG. *Nucleic Acids Res.* 34, D354–D357. doi:10.1093/nar/gkj102

Keller, N. P., Turner, G., and Bennett, J. W. (2005). Fungal secondary metabolism - from biochemistry to genomics. *Nat. Rev. Microbiol.* 3, 937–947. doi:10.1038/nrmicro1286

Keller, O., Kollmar, M., Stanke, M., and Waack, S. (2011). A novel hybrid gene prediction method employing protein multiple sequence alignments. *Bioinformatics* 27, 757–763. doi:10.1093/bioinformatics/btr010

Kohler, A., Kuo, A., Nagy, L. G., Morin, E., Barry, K. W., Buscot, F., et al. (2015). Convergent losses of decay mechanisms and rapid turnover of symbiosis genes in mycorrhizal mutualists. *Nat. Genet.* 47, 410–415. doi:10.1038/ng.3223

Krzywinski, M., Schein, J., Birol, I., Connors, J., Gascoyne, R., Horsman, D., et al. (2009). Circos: An information aesthetic for comparative genomics. *Genome Res.* 19, 1639–1645. doi:10.1101/gr.092759.109

Lagesen, K., Hallin, P., Rødland, E. A., Staerfeldt, H. H., Rognes, T., and Ussery, D. W. (2007). RNAmmer: Consistent and rapid annotation of ribosomal RNA genes. *Nucleic Acids Res.* 35, 3100–3108. doi:10.1093/nar/gkm160

Li, Q., Bao, H., Bau, T., Li, Y., Chen, X., and Cao, G. (2019). Chemical composition and anti-inflammatory activity of *Inonotus hispidus*. *J. Jilin Univ. Sci. Ed.* 57, 177–201. (In Chinese). doi:10.1142/S0192415X19500095

Li, R., Li, Y., Kristiansen, K., and Wang, J. (2008). SOAP: Short oligonucleotide alignment program. *Bioinformatics* 24, 713–714. doi:10.1093/bioinformatics/btn025

Li, W., Jaroszewski, L., and Godzik, A. (2002). Tolerating some redundancy significantly speeds up clustering of large protein databases. *Bioinformatics* 18, 77–82. doi:10.1093/bioinformatics/18.1.77

Bao, H., Yang, S., Li, Q., Bau, T., and Li, Y. (2020). Supplementary textual research on "*Sanghuang*". *Journal of Fungal Research*. 15, 264–270. doi:10.13341/j.jfr.2014.1171

Li, Z., and Bao, H. (2022b). Comparative analysis of metabolic compositions and trace elements of *Inonotus hispidus* mushroom grown on five different tree species. *ACS Omega* 7, 9343–9358. doi:10.1021/acsomega.1c06226

Li, Z., and Bao, H. (2022a). Deciphering key regulators of *Inonotus hispidus* petroleum ether extract involved in anti-tumor through whole transcriptome and proteome analysis in H22 tumor-bearing mice model. *J. Ethnopharmacol.* 296, 115468. doi:10.1016/j.jep.2022.115468

Liu, D., Gong, J., Dai, W., Kang, X., Huang, Z., Zhang, H., et al. (2012). The genome of *Ganoderma lucidum* provides insights into triterpenes biosynthesis and wood degradation [corrected]. *PLoS One* 7, e36146. doi:10.1371/journal.pone.0036146

Liu, X., Hou, R., Yan, J., Xu, K., Wu, X., Lin, W., et al. (2019). Purification and characterization of *Inonotus hispidus* exopolysaccharide and its protective effect on acute alcoholic liver injury in mice. *Int. J. Biol. Macromol.* 129, 41–49. doi:10.1016/j.ijbiomac.2019.02.011

Machado-Carvalho, L., Martins, T., Aires, A., and Marques, G. (2023). Optimization of phenolic compounds extraction and antioxidant activity from *Inonotus hispidus* using ultrasound-assisted extraction technology. *Metabolites* 13, 524. doi:10.3390/metabo13040524

Maddi, A. M., Kavousi, K., Arabfard, M., Ohadi, H., and Ohadi, M. (2022). Tandem repeats ubiquitously flank and contribute to translation initiation sites. *BMC Genom Data* 23, 59. doi:10.1186/s12863-022-01075-5

Marçais, G., Delcher, A. L., Phillippy, A. M., Coston, R., Salzberg, S. L., and Zimin, A. (2018). MUMmer4: A fast and versatile genome alignment system. *PLoS Comput. Biol.* 14, e1005944. doi:10.1371/journal.pcbi.1005944

Miziorko, H. M. (2011). Enzymes of the mevalonate pathway of isoprenoid biosynthesis. *Arch. Biochem. Biophys.* 505, 131–143. doi:10.1016/j.abb.2010.09.028

Petersen, T. N., Brunak, S., von, H. G., and Nielsen, H. (2011). SignalP 4.0: Discriminating signal peptides from transmembrane regions. *Nat. Methods* 8, 785–786. doi:10.1038/nmeth.1701

Quin, M. B., Flynn, C. M., and Schmidt-Dannert, C. (2014). Traversing the fungal terpenome. *Nat. Prod. Rep.* 31, 1449–1473. doi:10.1039/c4np00075g

Reiner, J., Pisani, L., Qiao, W., Singh, R., Yang, Y., Shi, L., et al. (2018). Cytogenomic identification and long-read single molecule real-time (SMRT) sequencing of a Bardet-Biedl Syndrome 9 (BBS9) deletion. *NPJ Genom Med.* 3, 3. doi:10.1038/s41525-017-0042-3

Saha, S., Bridges, S., Magbanua, Z. V., and Peterson, D. G. (2008). Empirical comparison of *ab initio* repeat finding programs. *Nucleic Acids Res.* 36, 2284–2294. doi:10.1093/nar/gkn064

Saier, M. H., Reddy, V. S., Moreno-Hagelsieb, G., Hendargo, K. J., Zhang, Y., Iddamsetty, V., et al. (2021). The transporter classification database (TCDB): 2021 update. *Nucleic Acids Res.* 49 (1), D461–D467. doi:10.1093/nar/gkaa1004

Saka, V. P., Chitra, V., and Narayanasamy, D. (2023). Protective role of hispolon and its derivatives against apoptosis in cortical neurons induced by electromagnetic radiation from 4G mobile phone. *J. Biochem. Mol. Toxicol.* 30, e23351. doi:10.1002/jbt.23351

Santos, L. A., Adhikarla, H., Yan, X., Wang, Z., Fouts, D. E., Vinetz, J. M., et al. (2018). Genomic comparison among global isolates of *L. interrogans* serovars copenhageni and icterohaemorrhagiae identified natural genetic variation caused by an Indel. *Front. Cell Infect. Microbiol.* 8, 193. doi:10.3389/fcimb.2018.00193

Shi, L., Ren, A., Mu, D., and Zhao, M. (2010). Current progress in the study on biosynthesis and regulation of ganoderic acids. *Appl. Microbiol. Biotechnol.* 88, 1243–1251. doi:10.1007/s00253-010-2871-1

Simão, F. A., Waterhouse, R. M., Ioannidis, P., Kriventseva, E. V., and Zdobnov, E. M. (2015). BUSCO: Assessing genome assembly and annotation completeness with single-copy orthologs. *Bioinformatics* 31, 3210–3212. doi:10.1093/bioinformatics/btv351

Tang, S., Jin, L., Lei, P., Shao, C., Wu, S., Wang, Y., et al. (2022). Whole-genome assembly and analysis of a medicinal fungus: *Inonotus hispidus*. *Front. Microbiol.* 13, 967135. doi:10.3389/fmicb.2022.967135

Tang, S., Shao, C., Yang, Y., Ren, R., Jin, L., Hu, D., et al. (2023). The antitumor effect of mycelia extract of the medicinal macrofungus *Inonotus hispidus* on HeLa cells via the mitochondrial-mediated pathway. *J. Ethnopharmacol.* 311, 116407. doi:10.1016/j.jep.2023.116407

Tao, Y., Xie, B., Yang, Z., Chen, Z., Chen, B., Deng, Y., et al. (2013). Identification and expression analysis of a new glycoside hydrolase family 55 exo-β-1,3-glucanase-encoding gene in *Volvariella volvacea* suggests a role in fruiting body development. *Gene* 527, 154–160. doi:10.1016/j.gene.2013.05.071

Wang, Z., Feng, X., Liu, C., Gao, J., and Qi, J. (2022). Diverse metabolites and pharmacological effects from the Basidiomycetes *Inonotus hispidus*. *Antibiotics (Basel)* 11, 1097. doi:10.3390/antibiotics11081097

Yang, H., Li, S., Qu, Y., Li, L., Li, Y., and Wang, D. (2022). Anti-colorectal cancer effects of *Inonotus hispidus* (bull: Fr) P. Karst. Spore powder through regulation of gut microbiota-mediated JAK/STAT signaling. *Nutrients* 14, 3299. doi:10.3390/nu14163299

Yang, S., Bao, H., Wang, H., and Li, Q. (2019). Anti-tumour effect and pharmacokinetics of an active ingredient isolated from Inonotus hispidus. *Biol. Pharm. Bull.* 42, 10–17. doi:10.1248/bpb.b18-00343

Zhang, R., Feng, X., Wang, Z., Xie, T., Duan, Y., Liu, C., et al. (2022b). Genomic and metabolomic analyses of the medicinal fungus *Inonotus hispidus* for its metabolite's biosynthesis and medicinal application. *J. Fungi (Basel).* 8, 1245. doi:10.3390/jof8121245

Zhang, Y., Hao, J., Liu, Z., Li, Z., Teng, L., and Wang, D. (2022a). *Inonotus hispidus* protects against hyperlipidemia by inhibiting oxidative stress and inflammation through Nrf2/NF-κB signaling in high fat diet fed mice. *Nutrients* 14, 3477. doi:10.3390/nu14173477

Zhong, Z., Norvienyeku, J., Chen, M., Bao, J., Lin, L., Chen, L., et al. (2016). Directional selection from host plants is a major force driving host specificity in Magnaporthe species. *Sci. Rep.* 6, 25591. doi:10.1038/srep25591

frontiers | Frontiers in Microbiology

TYPE Original Research
PUBLISHED 08 August 2023
DOI 10.3389/fmicb.2023.1200226

OPEN ACCESS

EDITED BY
Vikineswary Sabaratnam,
University of Malaya, Malaysia

REVIEWED BY
Qiang Li,
Chengdu University, China
Guo-Qing Zhang,
Beijing University of Agriculture, China
Fuqiang Yu,
Chinese Academy of Sciences (CAS), China

*CORRESPONDENCE
Ruiying Zhang
✉ zhangruiying@caas.cn

RECEIVED 04 April 2023
ACCEPTED 26 July 2023
PUBLISHED 08 August 2023

CITATION
Chen B, Shao G, Zhou T, Fan Q, Yang N, Cui M, Zhang J, Wu X, Zhang B and Zhang R (2023) Dazomet changes microbial communities and improves morel mushroom yield under continuous cropping.
Front. Microbiol. 14:1200226.
doi: 10.3389/fmicb.2023.1200226

Dazomet changes microbial communities and improves morel mushroom yield under continuous cropping

Bo Chen[1], Gaige Shao[2], Tao Zhou[3], Qinghao Fan[4], Nuolin Yang[4], Man Cui[4], Jinwei Zhang[4], Xiangli Wu[4], Bangxi Zhang[1] and Ruiying Zhang[4]*

[1]Institute of Soil and Fertilizer of Guizhou Province, Guiyang, China, [2]Xi'an Agricultural Technology Extension Center, Xi'an, China, [3]Fruit and Vegetable Workstation of Guizhou Province, Guiyang, China, [4]State Key Laboratory of Efficient Utilization of Arid and Semi-arid Arable Land in Northern China, Institute of Agricultural Resources and Regional Planning, Chinese Academy of Agricultural Sciences, Beijing, China

Morels (*Morchella* spp.) are highly prized and popular edible mushrooms. The outdoor cultivation of morels in China first developed at the beginning of the 21st century. Several species, such as *Morchella sextelata*, *M. eximia*, and *M. importuna*, have been commercially cultivated in greenhouses. However, the detriments and obstacles associated with continuous cropping have become increasingly serious, reducing yields and even leading to a complete lack of fructification. It has been reported that the obstacles encountered with continuous morel cropping may be related to changes in the soil microbial community. To study the effect of dazomet treatment on the cultivation of morel under continuous cropping, soil was fumigated with dazomet before morel sowing. Alpha diversity and beta diversity analysis results showed that dazomet treatment altered the microbial communities in continuous cropping soil, which decreased the relative abundance of soil-borne fungal pathogens, including *Paecilomyces*, *Trichoderma*, *Fusarium*, *Penicillium*, and *Acremonium*, increased the relative abundance of beneficial soil bacteria, including *Bacillius* and *Pseudomonas*. In addition, the dazomet treatment significantly increased the relative abundance of morel mycelia in the soil and significantly improved morel yield under continuous cropping. These results verified the relationship between the obstacles associated with continuous cropping in morels and the soil microbial community and elucidated the mechanism by which the obstacle is alleviated when using dazomet treatment.

KEYWORDS

morel mushroom, *Morchella sextelata*, dazomet, microbial community, continuous cropping obstacle

1. Introduction

True morels (*Morchella* spp., Morchellaceae, Pezizales) are commercially important edible mushrooms with economic and scientific value. They are very popular in most of Asia, Europe and North America due to their delicious taste, special flavor, high nutritional value, low calorific value, and potent health-promoting abilities (Wu et al., 2021). The morels are characterized by the unique honeycomb appearance of the hollow fruiting body. In nature, wild morels are widely

distributed in temperate regions of the Northern Hemisphere, and form fruiting bodies in the spring (Liu et al., 2018).

Over the centuries, various methods of morel cultivation have been attempted. Indoor cultivation of morel first developed in the early 1980s in the United States. In brief, sclerotia are first formed in spawn bags; then, sclerotia are used as spawn to inoculate composted substrates; and finally, fruiting bodies are induced by irrigation (Ower, 1982; Ower et al., 1986, 1988, 1989; Masaphy, 2010; Longley et al., 2019). Because of poor stability and repeatability, this technology has not been widely promoted and commercialized. Even so, this work was still a tremendous breakthrough in the history of morel cultivation.

The outdoor cultivation of morel first developed in China at the beginning of the 21st century. In short, the spawn is composed of vegetative mycelia rather than sclerotia and is inoculated in soil in the greenhouse environment in autumn. When conidia are formed on the soil surface, exogenous nutrient bags are placed in the field to promote the growth of the mycelia. In the early spring of the next year, the vegetative mycelia are stimulated by irrigation to promote differentiation and the formation of primordia (Tan, 2016; Liu et al., 2018). The most important breakthrough in outdoor cultivation has been the invention and application of exogenous nutrient bags. At present, a few morel species, including *Morchella sextelata*, *M. eximia*, and *M. importuna*, etc., have been commercially cultivated using outdoor cultivation techniques in China (Masaphy, 2010; Kuo et al., 2012; Loizides, 2017; Liu et al., 2018). This outdoor cultivation technology has been rapidly and commercially applied on a large scale. In 2020, the annual production of morels in China reached 15,000 tons (fresh weight) and continues to maintain a rapid growth trend (Yu et al., 2022).

In recent years, with the continuous expansion of morel cultivation in China and around the world, outdoor cultivation has often suffered from severe yield reduction and even a failure of fruiting bodies to be produced for unknown reasons (Sambyal and Singh, 2021; Tan et al., 2021; Yu et al., 2022). Some studies have shown that possible reasons leading to the failure of morel fructification include unstable quality of spawn, improper field management practices, unfavorable environmental factors, pathogens, soil characteristics, soil microbial community dynamics, etc. (Zhao et al., 2016; He et al., 2017, 2018; Lan et al., 2020; Wang et al., 2020; Tan et al., 2021; Yu et al., 2022). In fact, the obstacles associated with continuous cropping is also an important reason for the decline in morel yield. The continuous cropping obstacle refers to the phenomenon in which the same crop or a related species is continuously planted in the same plot and the yield and quality are reduced over time, even under normal management conditions (Chen Y. et al., 2022). Many crops, whether perennial or annual, suffer from continuous cropping obstacles (Li et al., 2016). Most edible mushrooms cultivated in farmland soil, such as *Ganoderma lucidum* and *Dictyophora* spp., have also been severely influenced by continuous cropping obstacles (Zhang et al., 2018; Jiang et al., 2021; Lu et al., 2022). The rotation of morel mushrooms and paddy rice is an effective measure to reduce or eliminate this obstacle. However, the application of this crop rotation is limited because most morel is cultivated in dryland greenhouses. To circumvent continuous cropping obstacles, the farmland used for morel cultivation must be changed every year, which greatly increases the cost of morel cultivation. The mechanisms of most continuous cropping obstacles are very complex and are associated with autotoxicity, deterioration of the physicochemical properties of soil, accumulation of soil-borne pathogens, and disruption of the soil microbial community (Xi et al., 2019). To date, the mechanism of continuous cropping obstacles in morel cultivation is not clear.

In recent years, disinfection of soil with fumigants before planting has been an effective and reliable method to prevent and control continuous cropping obstacles related to the soil microbial community (Li Q. et al., 2021). Methyl bromide was once the most commonly used fumigant. However, it has been banned because it destroys the ozone layer. Dazomet is a recently developed broad-spectrum soil fumigant that is usually used to control soil pests, weeds and pathogens in greenhouses, seedling farms and orchards. When dazomet is applied to wet soil, it degrades rapidly and releases methyl isothiocyanate (MITC), formaldehyde, monomethylamine and hydrogen sulfide. MITC is the main active substance. The nonspecific toxicity of MITC is due to its ability to cause perturbation of metal enzymes or thiol-containing proteins, its formation of reactive oxygen species or the metal toxicity it causes due to the chelation of heavy metals (Tilton et al., 2006; Consolazio et al., 2019). The soil retention time of dazomet is short, making it more environmentally benign. With the elimination of methyl bromide, dazomet has been registered in many countries. It has been reported that dazomet has been used in strawberry, tomato, flowers, ginger, cucumber, and other high-value crops (Chen R. et al., 2022). Dazomet impacts both beneficial and harmful soil organisms because it is broad-spectrum, but the severity of the impact varies according to the soil conditions and the species (Wang et al., 2011).

It has been reported that the obstacle associated continuous cropping in morels may be related to changes in the soil microbial community (Liu et al., 2022). To the best of our knowledge, the application of dazomet in the cultivation of edible mushrooms has not been reported. To study the effect of dazomet treatment on the cultivation of morel under continuous cropping, the soil was planted continuously for 1 year and 2 years was fumigated with dazomet before sowing. The growth, fructification, and yield of morel were investigated, and dynamic changes in bacterial and fungal communities were monitored using high-throughput gene sequencing. The results suggested that the dazomet treatments were effective in increasing the yield of morel by changing the microbial community under continuous cropping.

2. Materials and methods

2.1. The morel strain and medium

The experiments were carried out with the *M. sextelata* Qian-Morel 1 cultivar. The spawn and exogenous nutrient bags were provided by Guizhou Lefeng Biotechnology Co., Ltd. The spawn medium consisted of 85% wheat, 5% rice husk, 8% humus, 1% lime and 1% gypsum, with a moisture content of 60%. The medium in exogenous nutrient bags consisted of 89% wheat, 10% rice husk, and 1% lime, and the water content was 60%.

2.2. Experimental design

To test the effect of dazomet fumigation on the continuous cropping obstacle of morel, two experimental sites were selected in

Guizhou Province, one of which was located in Tianba Town, Qixingguan District, and had been planted for 1 years. The other was in Tailai Township, Qianxi City, which had been planted for 2 years. The controls without fumigation and dazomet treatment were established on randomly designed plots, with three replicates for each treatment at each experimental site. The field was plowed with a rotary tiller to a depth of 25 cm. The relative humidity of the soil was adjusted to 65%. The dosage of dazomet (Synwill Co., Ltd) was 60 g/m^2. The dazomet was sprinkled onto the surface of the soil and then evenly mixed with the soil using a small rotary tiller. The field was immediately covered with PE film to maintain the fumes of dazomet in the soil. After 20 days, the film was removed, and the greenhouse was kept ventilated for 15 days. Three independent biological replicates with 200 m^2 each were conducted.

2.3. The cultivation of the morel

The morel was sown on the 35th day after fumigation, and the dosage of spawn was 300 g/m^2. Seven days after sowing, morel mitospores, which was previously considered as asexual conidia (Liu et al., 2023), appeared on the soil surface. On the 10th day, exogenous nutrient bags punched on the side that would be in contact with the soil were placed on the soil surface. Five exogenous nutrient bags were placed per square meter, each containing 400 g of medium. The relative humidity of the soil was maintained at approximately 60%. The exogenous nutrient bags were removed on the 85th day after sowing. The field was irrigated to induce the formation of the primordia. The fruiting bodies were harvested on the 110th day after sowing.

The weight of morels harvested was converted to kg/m^2 according to the area of each replicate. The yield was analyzed using SPSS (version 26.0) through ANOVA. $P < 0.05$ was used as the threshold.

2.4. Soil sampling

To investigate the changes in the soil microbial community, soil samples were collected from the experimental site in Tailai Township, Qianxi City. The soil samples were taken from a depth of 3–5 cm before sowing, at the primordial stage, and before harvest of the fruiting body (Table 1).

TABLE 1 Soil samples used in this study.

Soil sample	Stage of morel cultivation
SCK	Before sowing of the control without fumigation with dazomet
SDT	Before sowing of the dazomet treatment
PCK	Primordial stage of the control
PDT	Primordial stage of the dazomet treatment
FCK	Mature fruit body stage of the control
FDT	Mature fruit body stage of the dazomet treatment

2.5. High-throughput sequencing

The DNA was extracted with the TGuide S96 Magnetic Soil/Stool DNA Kit (Tiangen Biotech (Beijing) Co., Ltd.) according to manufacturer's instructions. The DNA concentration of the samples was measured with the Qubit dsDNA HS Assay Kit and Qubit 4.0 Fluorometer (Invitrogen, Thermo Fisher Scientific, Oregon, United States). The 338F: 5′-ACTCCTACGGGAGGCAGCA-3′ and 806R: 5′-GGACTACHVGGGTWTCTAAT-3′ universal primer set was used to amplify the V3-V4 region of the 16S rRNA gene. The ITS1F: 5′-CTTGGTCATTTAGAGGAAGTAA-3′ and ITS2: 5′-GCTGCGTTCTTCATCGATGC-3′ universal primer set was used to amplify the ITS1 region of the ITS gene. Both the forward and reverse primers were tailed with sample-specific Illumina index sequences to allow for deep sequencing. The total PCR amplicons were purified with Agencourt AMPure XP Beads (Beckman Coulter, Indianapolis, IN) and quantified using the Qubit dsDNA HS Assay Kit and Qubit 4.0 Fluorometer (Invitrogen, Thermo Fisher Scientific, Oregon, United States). After the individual quantification step, amplicons were pooled in equal amounts. For the constructed library, an Illumina NovaSeq 6000 (Illumina, Santiago CA, United States) was used for sequencing.

2.6. Bioinformatic analysis

The bioinformatics analysis of this study was performed with the aid of the BMK Cloud (Biomarker Technologies Co., Ltd., Beijing, China). According to the quality of single nucleotides, raw data were primarily filtered by Trimmomatic (version 0.33) (Edgar, 2013). Identification and removal of primer sequences was performed by Cutadapt (version 1.9.1) (Callahan et al., 2016). PE reads obtained from previous steps were assembled by USEARCH (version 10) (Segata et al., 2011), followed by chimera removal using UCHIME (version 8.1) (Quast et al., 2012). The high-quality reads generated from the above steps were used in the following analysis. Sequences with similarity ≥97% were clustered into the same operational taxonomic unit (OTU) by USEARCH (v10.0) (Edgar, 2013), and the OTUs with relative abundance <0.005% were filtered. Taxonomy annotation of the OTUs was performed based on the Naive Bayes classifier in QIIME2 (Bolyen et al., 2019) using the SILVA database (release 132) (Quast et al., 2012) with a confidence threshold of 70%. The alpha diversity was calculated and displayed by QIIME2 and R software. Beta diversity was determined to evaluate the degree of similarity of microbial communities from different samples using QIIME. Principal coordinate analysis (PCoA), heatmaps, UPGMA and nonmetric multidimensional scaling (NMDS) were used to analyze the beta diversity. Furthermore, we employed linear discriminant analysis (LDA) effect size (LEfSe) (Segata et al., 2011) to test the significant taxonomic differences among groups. A logarithmic LDA score of 4.0 was set as the threshold for discriminative features.

3. Results

3.1. Effects of dazomet treatment on the fructification of morel

After 7 days of sowing, morel mitospores appeared on the soil surface. The number of mitospores was not significantly different

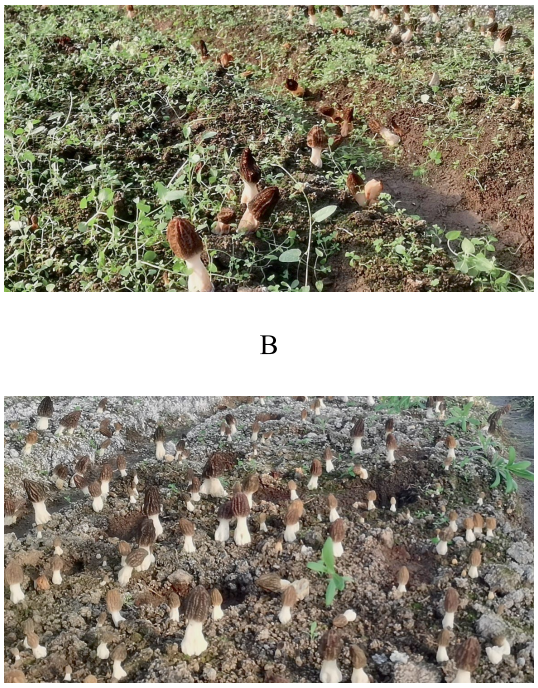

FIGURE 1
Morel fructification of Qianxi experimental sites. **(A)** Morel fructification of the control. **(B)** Morel fructification of the dazomet treatment.

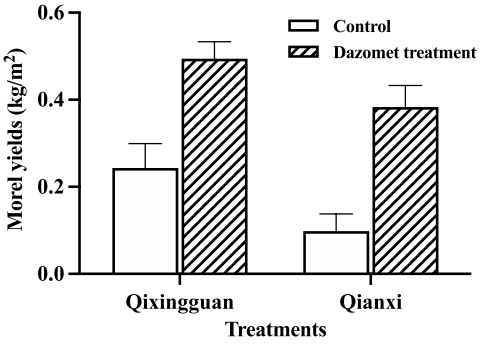

FIGURE 2
The maximum yield of the control without fumigation with dazomet. The Qixingguan experimental site has been cultivated for 1 year, and the Qianxi experimental site has been cultivated continuously for 2 years. Three independent biological replicates are conducted. Error bars indicate the SD (n = 3).

between the control and dazomet treatments. After irrigation, the primordia formed. Compared with the control, the number of primordia and fruiting bodies in the dazomet treatment was significantly higher, and their distribution was more uniform (Figure 1). The sizes and growth rates of the fruiting bodies in the two treatments were similar. There were many weeds in the control, whereas there were almost no weeds in the dazomet treatment, which may be related to the herbicide effect of dazomet (Brosnan and Breeden, 2009; Jeffries et al., 2017). No obvious diseases or pests were found in the control and dazomet treatments.

The maximum yield was calculated by fresh weight. Compared with the control, the yield of fruiting bodies in the dazomet treatment was significantly higher. At the Qixingguan experimental site, which is the second year for continuous cultivation of morel, the yield of the control without fumigation with dazomet was 0.24 kg/m^2, and the yield of the dazomet treatment was twice that of the control. At the Qianxi experimental site, which was undergoing the third year for continuous cultivation of morel, the yield of the control was 0.10 kg/m^2, and the yield of the dazomet treatment was 3 times that of the control (Figure 2). According to the recollection of the farmers, the morel yield in the first year at the Qixingguan experimental site was approximately 0.33 kg/m^2. The maximum yields in the first year and second year at the Qianxi experimental site were approximately 0.48 kg/m^2 and 0.15 kg/m^2, respectively. The results showed that the morel yield decreased year by year under continuous cropping without appropriate treatment. However, the dazomet treatment increased the maximum yield under continuous cropping, which was close to that of the first year.

3.2. High-throughput sequencing results

To understand the mechanism of increasing the morel yield under continuous cropping by fumigation with dazomet, the effect of dazomet treatment on the soil microbial community of the Qianxi experimental site was studied. As described in Table 1, soils were sampled at the sowing, primordium and mature fruit body stages. DNA was extracted from soil samples, and the 16S rDNA V3/V4 region of prokaryotic communities and ITS1 of fungal communities were amplified and sequenced. After quality filtering, a total of 1,082,233 reads for 16S rDNA V3/V4 with a read length of mainly 400–450 bp and 1,384,777 reads for ITS1 with a read length of mainly 220–430 bp across 18 samples were obtained. The rarefaction curves of all samples gradually flattened, which indicated that the sequenced depths were sufficient to reflect the diversity of the samples. After denoising the sequences, 2,305 OTUs for prokaryotic communities and 948 OTUs for fungal communities were generated (Supplementary materials 1, 3). The raw data of 16S rDNA and ITS were uploaded to the Sequence Read Archive (SRA) database of NCB (Accession PRJNA961658).

Venn diagrams of bacterial OTUs are displayed in Figure 3A. A total of 710 OTUs were found to be common to SDT and SCK, with an additional 305 and 426 OTUs exclusive to SCK and SDT. Fifty-seven OTUs were found to be associated with each stage of the control, with an additional 700, 23 and 22 OTUs common to SCK-PCK, PCK-FCK and FCK-SCK, respectively. Venn diagrams of fungal OTUs are displayed in Figure 3B. Seventy-two OTUs were found to be common to SDT and SCK, with an additional 104 and 323 OTUs exclusive to SDT and SCK. Thirty OTUs were found to be associated with each stage of the control, with an additional 125, 21 and 30 OTUs common to SCK-PCK, PCK-FCK and FCK-SCK, respectively. The fungal OTUs in common between SDT and SCK were at 14.29%, which is far less than the overlap of bacteria (49.27%). This indicates that the influence of dazomet treatment before sowing on fungal OTUs is far greater than on bacterial OTUs.

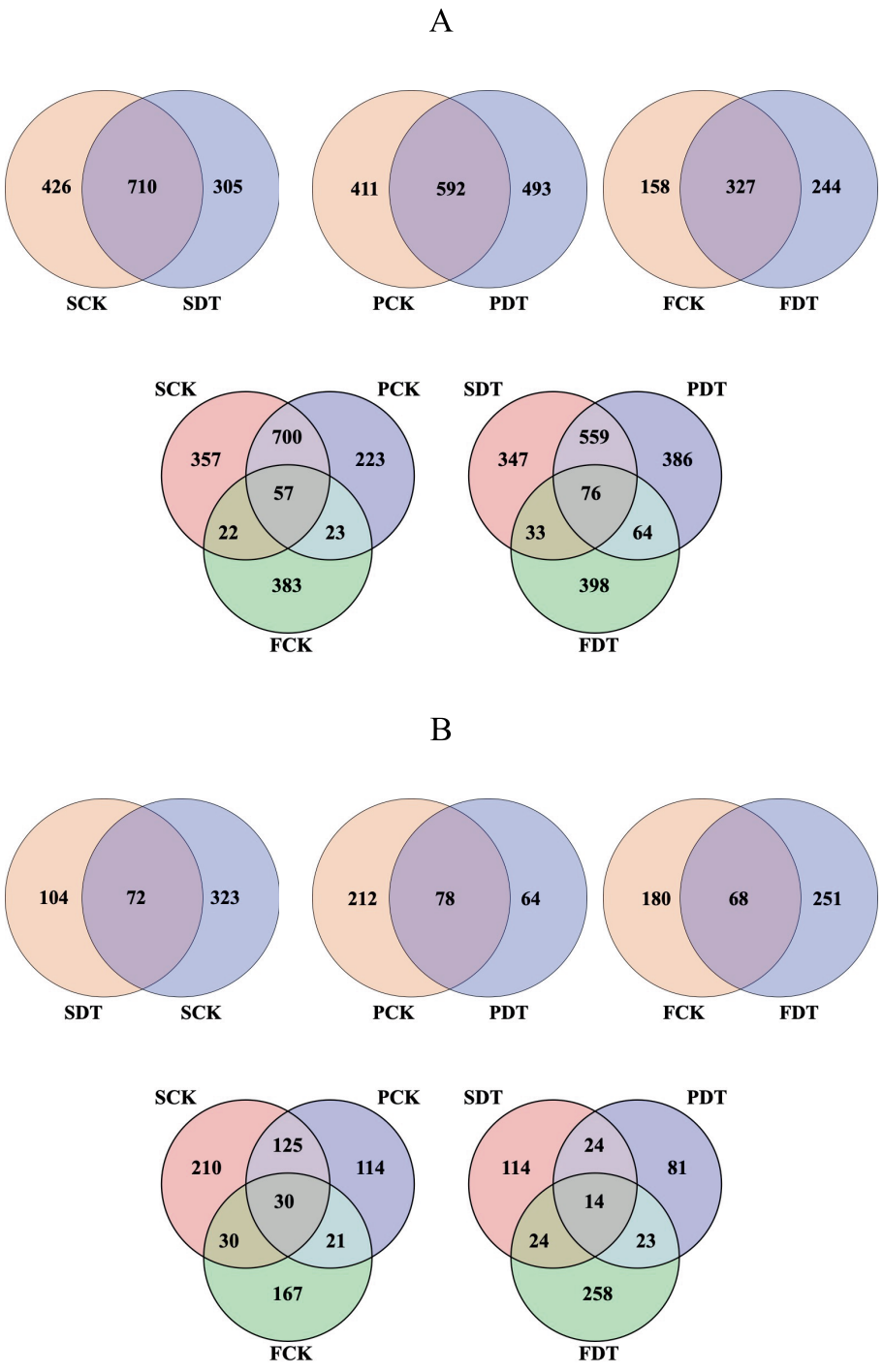

FIGURE 3
Venn diagram of bacterial OTUs **(A)** and fungal OTUs **(B)**.

3.3. Alpha diversity analysis of bacterial and fungal communities

The bacterial alpha diversity Chao1 indices of SCK, SDT, PCK, and PDT were predominantly 500–700, and the Chao1 indices of FCK and FDT were predominantly 250–300 (Figure 4A). The Chao indices of SCK and SDT were not significantly different ($p = 0.16$), but the Shannon index of SDT was significantly lower than that of SCK ($p = 0.0021$) (Figure 4B). This indicates that dazomet treatment before sowing changed the relative abundance rather than the richness of the bacterial community. Compared with those of SCK, SDT, PCK and PDT, the Chao1 and Shannon indices of FCK and FDT were significantly lower. Except for in the dazomet treatment, the cultivation stages also influenced the bacterial community.

For the fungal alpha diversity, the Chao and Shannon indices of SDT were lower than those of SCK, and the patterns of PCK and PDT were

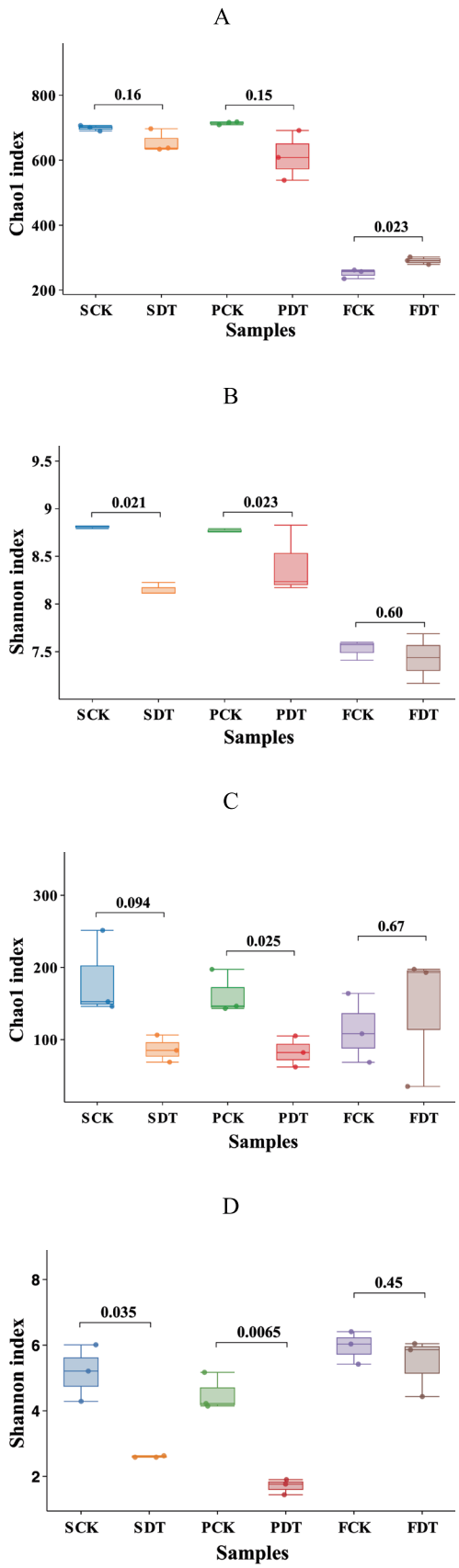

FIGURE 4
The alpha diversity indices of the samples. **(A)** The bacterial Chao index; **(B)** The bacterial Shannon diversity index; **(C)** The fungal Chao index; **(D)** The fungal Shannon diversity index.

similar (Figures 4C,D). This indicates that dazomet treatment before sowing changed both the relative abundance and richness of the fungal community, and the impact of dazomet treatment on the fungal community held to the primordial stage. However, the pattern of the Chao and Shannon indices was remodeled at the fruiting body stage.

3.4. Beta diversity analysis of the prokaryotic and fungal communities

Beta diversity analysis was processed by QIIME software to compare species diversity between different samples. In general, the distance between two dots (samples) indicates similarity between two samples in species composition. The explanatory values of PC1 and PC2 in the bacterial community were 51.07 and 15.99%, respectively (Figure 5A). The PCA grouped 18 samples into 3 clusters by a 95% confidence ellipse. Except for SCK, the clustering of other samples correlated with the cultivation stages of morel. SCK was clustered with PCK and PDT rather than SDT, indicating that SCK contained more bacterial species consistent with those of PCK and PDT. It is inferred that those consistent bacteria may be closely associated with morel cultivation and may have remained from morel cultivation in the last year. SDT formed an independent cluster far from SCK, which shows that dazomet treatment significantly changed the composition of the bacterial community.

The explanatory values of PC1 and PC2 in the fungal community were 54.29 and 28.06%, respectively (Figure 5B). The PCA grouped the 18 samples into 3 clusters by a 95% confidence ellipse. SDT and PDT formed two clusters independently, and SCK, PCK, FCK, and FDT formed a cluster. SDT was far from SCK, indicating that dazomet treatment significantly changed the composition of the fungal community. The distance of PDT from PCK may be the result of the difference between SCK and SDT. The convergence of FDT and FCK may be related to the influence of the morel cultivation stage on the fungal community. SCK, PCK, FCK and FDT shared a common fungal community, which suggests that SCK and PCK retained the fungal community enriched by morel cultivation the previous year.

3.5. Relative abundance of major bacterial and fungal phyla

The bacterial phyla with relative abundances >2% are displayed in Figures 6A,B. Proteobacteria (31.22% ± 2.73%), Acidobacteriota (26.14% ± 1.39%) and Gemmatimonadota (10.50% ± 0.40%) were the dominant bacterial phyla in the SCK. Compared with those of SCK, the relative SDT abundances of Proteobacteria, Acidobacteriota, Methylomirabilota, Myxococcota, Verrucomicrobiota and Nitrospirota increased significantly, and the relative abundances of Actinobacteriota and Firmicutes in SDT decreased significantly. The results show that dazomet treatment changed the relative abundance of the predominant phyla of the soil. Compared with SCK, FCK significantly changed the relative abundances of all 11 predominant phyla. Compared with SDT, FDT significantly changed the relative abundances of 9 bacterial phyla except Verrucomicrobiota and Nitrospirota. Except for

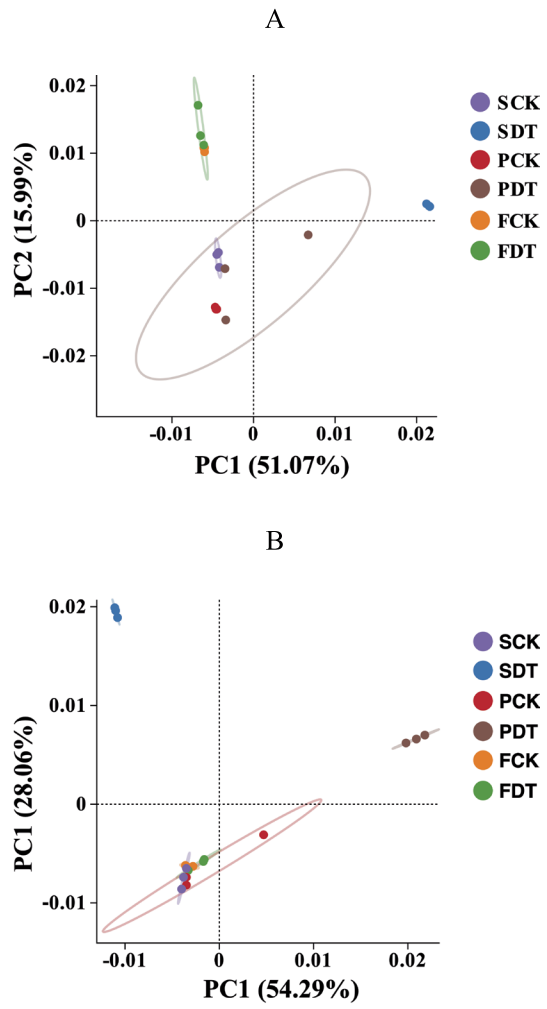

FIGURE 5
Principal component analysis of the prokaryotic community **(A)** and fungal community **(B)**. Each dot represents a sample. The confidence ellipse defines the region that contains 95% of all samples that can be drawn from the underlying Gaussian distribution.

Verrucomicrobiota, FCK and FDT converged in the relative abundance of the other 10 predominant phyla regardless of the difference before the sowing stage. This suggests that morel cultivation also significantly influences the relative abundance of the predominant bacterial phyla.

The fungal phyla with a relative abundance >1% are displayed in Figures 6C,D. Ascomycota (39.56% ± 17.85%) and Basidiomycota (46.53% ± 25.42%) were the dominant fungal phyla in the SCK. Compared with SCK, the relative abundance of Ascomycota was significantly higher, and the relative abundances of Basidiomycota, Mortierellomycota and Chytridiomycota were significantly lower in SDT. This indicates that dazomet treatment also changed the fungal community. Compared with SCK, FCK significantly changed the relative abundances of Ascomycota, Basidiomycota, Mortierellomycota and Chytridiomycota. Compared with SDT, FDT also significantly changed the relative abundances of Ascomycota, Basidiomycota, Mortierellomycota and Chytridiomycota. This indicates that morel cultivation also significantly influences the fungal community.

3.6. Relative abundance of major bacterial and fungal genera

A full list of bacterial OTUs and genera is provided in Supplementary materials 1, 2. The relative abundance of bacterial genera >3% is displayed as a heatmap in Figure 7A. Compared with SCK, the relative abundances of 26 genera, including *Candidatus Udaeobacter*, unclassified *Azospirillales*, *Sphingomonas*, unclassified *Chitinophagaceae*, etc., were significantly lower in SDT. In addition, the relative abundances of those 26 genera in PDT were also significantly lower than those in PCK. This indicates that the influences of dazomet treatment on those 26 genera lasted from the presowing to primordial stages. Compared with SCK, SDT, PCK and PDT, the relative abundances of 34 genera, including unclassified *Sphingomonadaceae*, *Novosphingobium*, *Sulfurimonas*, unclassified *Muribaculaceae*, etc., increases significantly in FCK and FDT. However, the relative abundances of major bacterial genera for FCK and FDT were similar.

A full list of fungal OTUs and genera is provided in Supplementary materials 3, 4. The relative abundance of fungal genera >3% is displayed as a heatmap in Figure 7B. Among 18 samples of 6 treatments, the change in the relative abundance for those 60 dominant genera was not as regular as that of bacteria.

3.7. Indicator genera

Linear discriminant analysis (LDA) effect size (LEfSe) was used to find the dominant indicator genera. By comparing SDT and SCK, the bacterial indicator genera of SCK and SDT are displayed in Figure 8A. The shift in the relative abundance of those indicator genera shows that dazomet treatment not only reduces the relative abundance of SCK indicator genera but also increases the relative abundance of SDT indicator genera (Figure 8B). It is interesting that the indictor genera of SDT were beneficial to edible mushrooms because several studies have demonstrated that *Micromonospora*, *Bacillus*, and *Streptomyces* species function in biocontrol, plant growth promotion, and mushroom composting (Sahin, 2005; Hirsch and Valdés, 2010; Sotoyama et al., 2016; Stanojević et al., 2019; Büchner et al., 2022). Because the SCK indicator genera, including *Candidatus Udaeobacter*, Unclassified *Xanthobacteraceae*, Unclassified *Vicinamibacteraceae*, and unclassified *Vicinamibacterales*, could not be identified accurately, their effects on morel growth could not be determined.

The fungal indicator genera of SCK and SDT are displayed in Figures 8C,D. *Aspergillus* was the fungal indicator genus with the highest relative abundance of 61.33% in SDT, and *Leucoagaricus*, *Agaricus*, and *Mortierella* were the fungal indicator genera in SCK.

3.8. Relative abundance of morel

Morels can produce a large number of fruiting bodies only when they form enough vegetative mycelia. In this study, the relative abundance of morel in soil was analyzed. Morel was not detected in SCK and SDT, indicating that the mycelium of the morel of the last year had completely disappeared before sowing in the current year. The relative abundance of morel was highest at the primordium stage,

10.3389/fmicb.2023.1200226

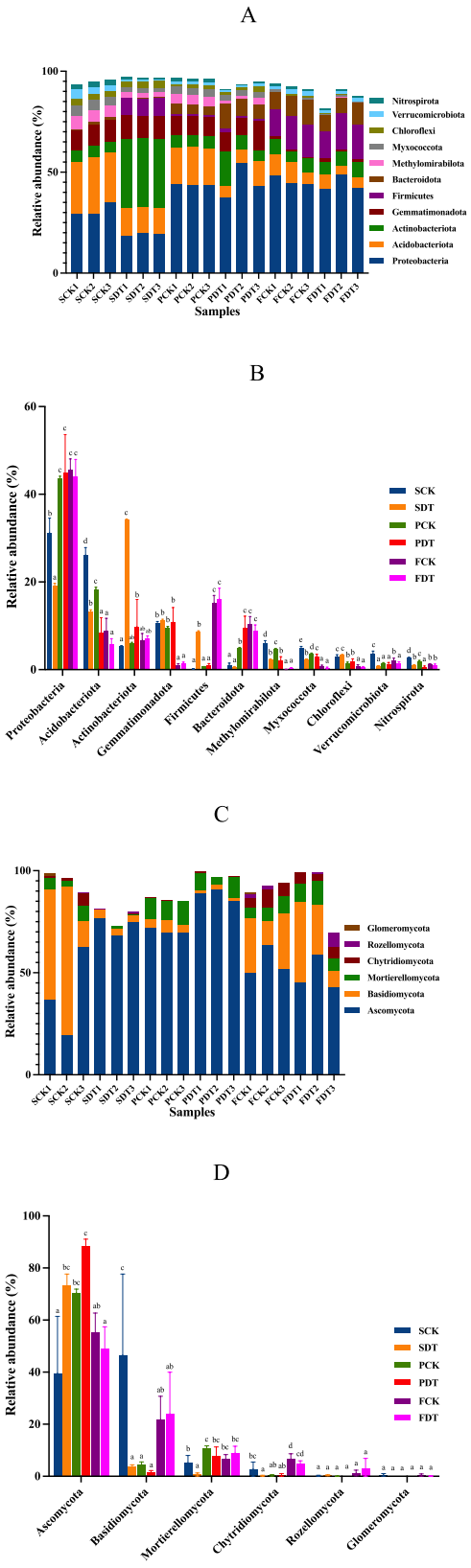

FIGURE 6
The relative abundance of major bacterial and fungal phyla in samples. **(A)** Cumulative relative abundance of bacterial phyla >2% in at least one sample. **(B)** ANOVA of the relative abundance of bacterial phyla. **(C)** Cumulative relative abundance of fungal phyla >1% in at least one sample. **(D)** ANOVA of the relative abundance of fungal phyla.

and it decreased significantly as the fruit body grew and developed. In PCK and PDT, the number of conidia that formed on the soil surface was similar, while the relative abundance of morel in PDT was evidently higher than that in PCK (Figure 9). This indicates that dazomet treatment before sowing improved morel mycelial growth in soil. Therefore, the decrease in the number of primordia and fruiting bodies may be related to the decrease in the relative abundance of morel in soil.

4. Discussion

In this study, we found that dazomet treatment changed soil microbial communities and significantly increased yield under continuous cropping. This result suggested that the obstacle of continuous cropping in morels is closely related to the soil microbial communities.

4.1. The decrease in the relative abundance of soil-borne fungal pathogens

Many continuous cropping obstacles are associated with the accumulation of soil-borne pathogens. Soil-borne pathogens, including *Fusarium*, *Pythium*, *Rhizotonia*, *Cylindrocarpon*, and *Phytophthora*, arising from continuous cropping, cause diseases such as root rot, damping-off and wilt that have a direct cost to crop growth, survival and yield (Ampt et al., 2019; Dignam et al., 2022). For example, *Fusarium oxysporum* is a well-known soilborne plant pathogen that causes severe vascular wilt in economically important crops such as American ginseng, tobacco, watermelon and strawberry (Koike and Gordon, 2015; Lamondia, 2015; Li C. et al., 2021; Wu et al., 2022).

It has been reported that fungi, including *Penicillium*, *Trichoderma*, *Aspergillus*, *Fusarium*, *Botrytis*, and *Clonostachys*, increase in abundance under continuous cropping of morel, and that these fungi may be the main pathogens that cause a reduction in production for continuous *M. sextelata* cultivation (Liu et al., 2022). Nonfructification is sometimes encountered in large-scale morel farming for unknown reasons. It has been suggested that the soils with successful fructification have significantly higher diversity in both the fungal and bacterial communities than those with nonfructification, and most nonfructification soils have been shown to be dominated by a high proportion of certain fungal genera, typically *Acremonium*, *Mortierella*, and *Paecilomyces* (Tan et al., 2021). *Penicillium*, *Trichoderma*, *Aspergillus*, *Fusarium*, *Botrytis*, *Clonostachys*, *Acremonium*, *Mortierella*, and *Paecilomyces* are pathogenic fungi in the production of edible mushrooms and plants. Notably, the pathogenicity of only a few pathogens on morel has been confirmed and reported. Typical diseases include stipe rot disease caused by the *Fusarium incarnatum – F. equiseti* species complex (Guo et al., 2016), pileus rot disease caused by *Diploöspora longispora* (He et al., 2018; Shi et al., 2022; Sun et al., 2023), white mold disease caused by *Paecilomyces penicillatus* (He et al., 2017; Fu et al., 2022), cobweb disease caused by *Cladobotryum protrusum* (Lan et al., 2020), white mildew disease caused by *Aspergillus* sp. (Yu et al., 2020). To the best of our knowledge, none of these soil-borne diseases has been proven to be directly related to the continuous cropping of morel.

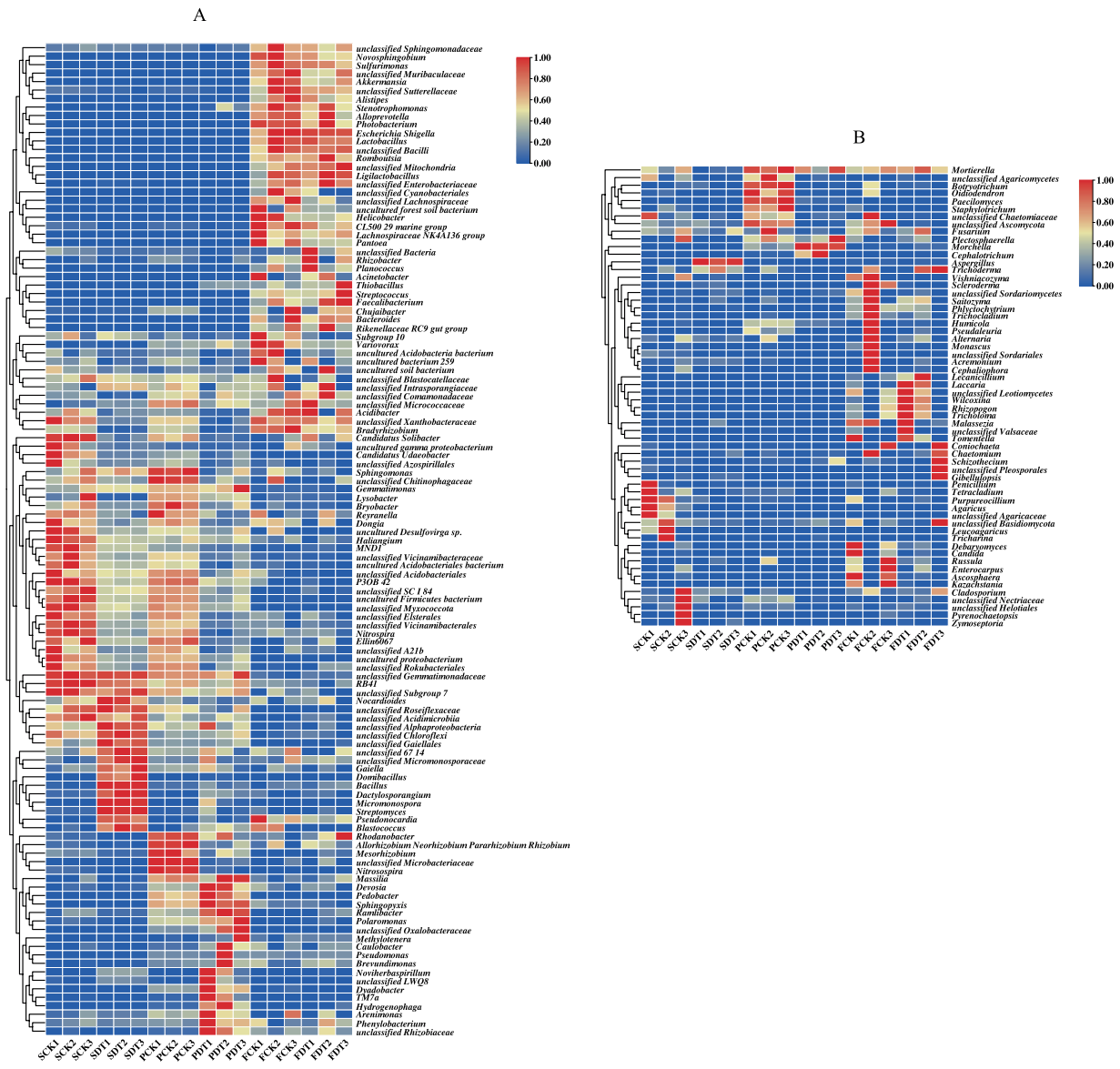

FIGURE 7
Heatmap of dominant bacterial genera **(A)** and dominant fungal genera **(B)**.

In this study, the relative abundance of *Aspergillus* was only 0.3% in SCK. Dazomet treatment increased the relative abundance of *Aspergillus* to 61.3%, which made *Aspergillus* the indicator genus of SDT. After inoculation with morel culture, the relative abundance of *Aspergillus* decreased to 0.1% in PDT and 2.2% in FDT (Figure 10). No white mildew disease was found in the dazomet treatment, which indicates that the effect of *Aspergillus* on morel warrants further study. The relative abundance of *Paecilomyces* was dynamic during morel cultivation, and the highest abundance was at the primordial phase (Figure 7B). The relative abundance of *Paecilomyces* in PCK was 21.9% and that in PDT was 1.8% (Figure 11), which showed that dazomet treatment had a significant effect on the relative abundance of *Paecilomyces*. The main symptom of obstacles associated with continuous cropping of morel is that the number of primordia and fruiting bodies is reduced. However, no obvious white mold disease was found in this study. Perhaps the primordium was too small to make the infection undetectable. It has been reported that once the very young and small morel fruiting bodies are infected by *Paecilomyces*, they stop growing (He et al., 2017). *Trichoderma*, *Fusarium*, *Penicillium*, and *Acremonium* were detected in the control and dazomet treatments. Similar to that of *Paecilomyces*, the relative abundance of these four fungi in PDT was significantly lower than that in PCK as a result of dazomet treatment (Figure 11). It has been reported that Gibberella, Microidium, Sarocladium and Streptomyces accounted for a high proportion in soils with low or no morel yield (Yu et al., 2022). However, those fungi were not detected in this study. In addition, no fungal pathogens *Diploöspora* and *Cladobotryum* were detected in this study. Therefore, the increase in yield by dazomet treatment may be closely related to the decrease in the abundance of *Paecilomyces*, *Trichoderma*, *Fusarium*, *Penicillium*, and *Acremonium*.

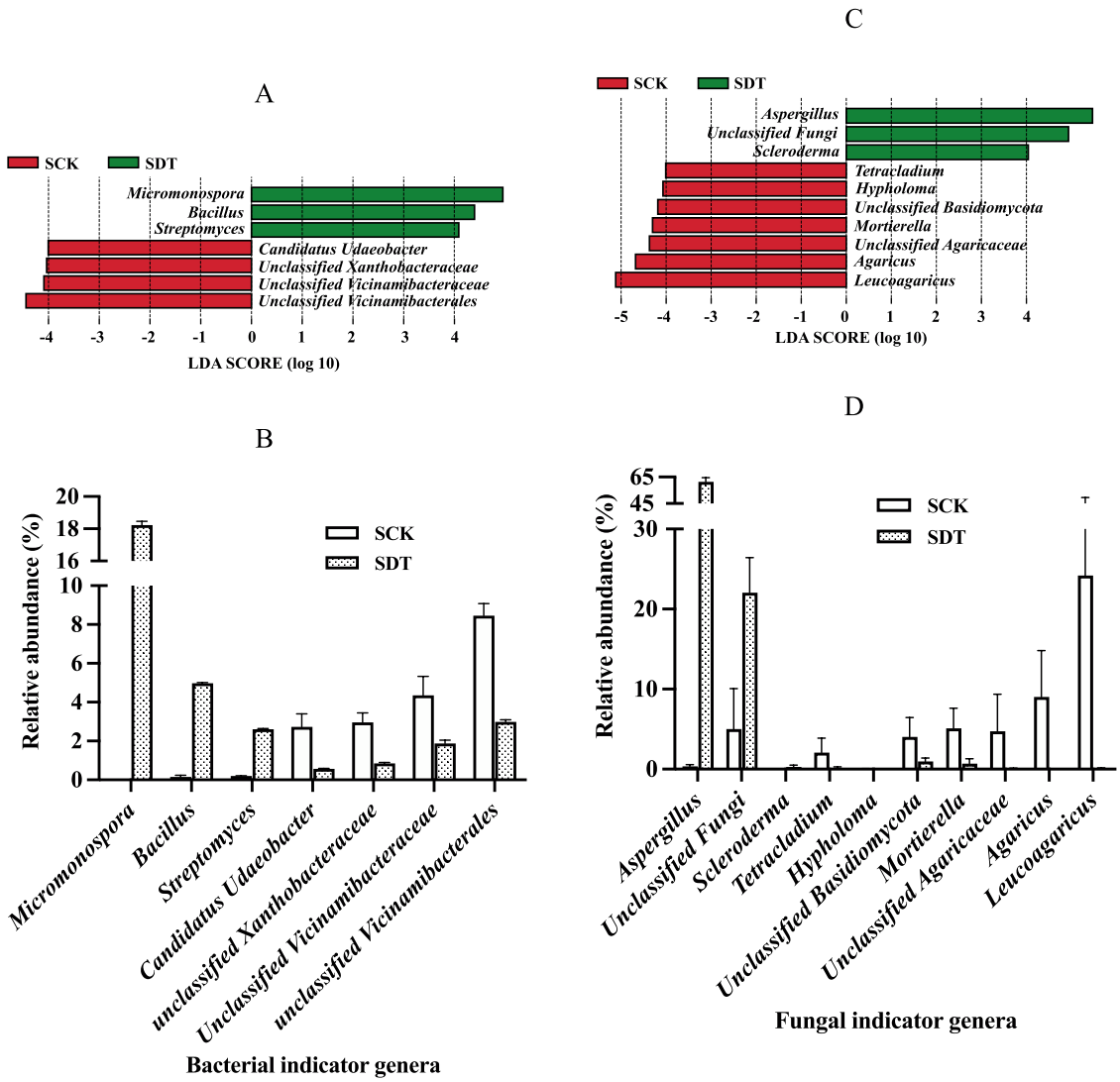

FIGURE 8
The bacterial and fungal indicator genera of SCK and SDT. **(A)** Bacterial indicator genera. **(B)** The relative abundance of bacterial indicator genera. **(C)** Fungal indicator genera. **(D)** The relative abundance of fungal indicator genera. Three independent biological replicates are conducted. Error bars indicate the SD (n = 3).

4.2. The increase in the relative abundance of soil-borne beneficial bacteria

A wide variety of interactions between bacteria and cultivated mushrooms have been described, leading to positive effects on edible mushrooms (Frey-Klett et al., 2011; Carrasco and Preston, 2020; Li et al., 2022). For example, *Pseudomonas* triggers primordium formation in *Agaricus bisporus* by removing inhibitory C8 compounds produced by the mycelium (Noble et al., 2009). *Bacillus* can substantially improve the growth and yield of some edible mushrooms by inhibiting the pathogenic fungi *Trichoderma harzianum* and *Fusarium oxysporum* (Velázquez-Cedeño et al., 2008; Sarwar et al., 2018). The continuous cropping obstacle of *Ganoderma lingzhi* may be related to the decline in the relative abundance of beneficial bacteria such as *Sphingomonas*, *Anaeromyxobacter*, *Bradyrhizobium* and *Dehalococcoides* in the covering soil (Yuan et al., 2021).

The morel can farm *Pseudomonas putida*, including bacterial dispersal, bacterial rearing with fungal exudates, and harvesting and translocation of bacterial carbon. At the same time, *P. putida* can stimulate the formation of sclerotia and improve the stress resistance of morel mycelium (Pion et al., 2013). Additionally, *Pseudomonas* can increase the hydrolysis of organic nitrogen sources by enhancing the activity of proteolytic enzymes produced by the morel and improve biomass for both partners (Lohberger et al., 2019). *Bacillius* was found to substantially affect the growth and development of morel fruiting bodies in recent studies (Longley et al., 2019; Zhang et al., 2019; Liu et al., 2022). *Paenibacillus* may play similar roles to *Bacillus* in morel cultivation (Longley et al., 2019). In addition, some noteworthy bacterial microbes involved in nitrogen fixation and nitrification, such as *Arthrobacter*, *Bradyrhizobium*, *Devosia*, *Pseudarthrobacter*, *Pseudolabrys*, and *Nitrospira*, have been identified in soils with high morel yields (Yu et al., 2022).

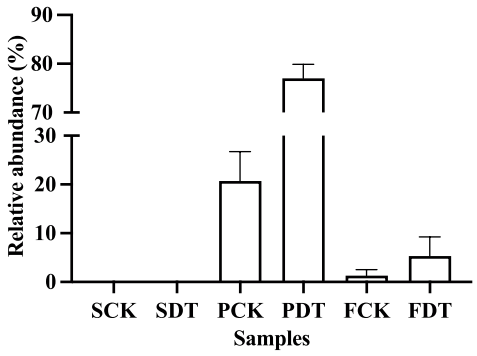

FIGURE 9
The relative abundance of morel in soil samples. Three independent biological replicates are conducted. Error bars indicate the SD (n = 3).

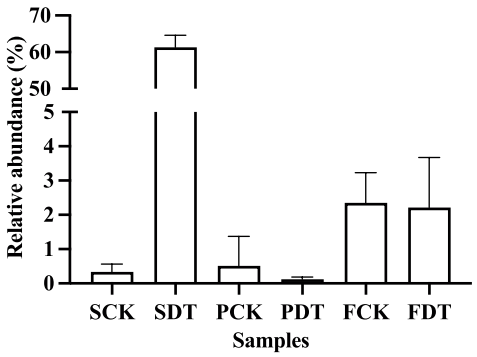

FIGURE 10
The relative abundance of *Aspergillus* in soil samples. Three independent biological replicates are conducted. Error bars indicate the SD (n = 3).

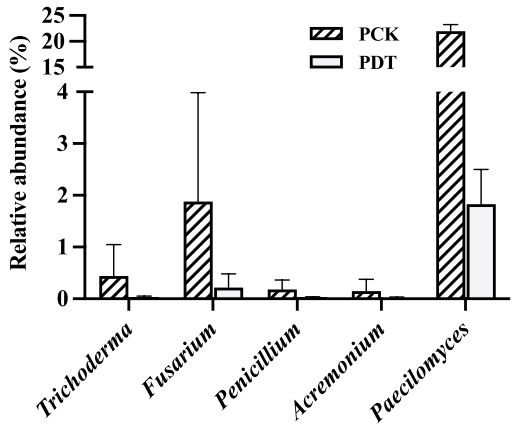

FIGURE 11
The relative abundance of *Trichoderma*, *Fusarium*, *Penicillium*, *Acremonium* and *Paecilomyces* in PCK and PDT. Three independent biological replicates are conducted. Error bars indicate the SD (n = 3).

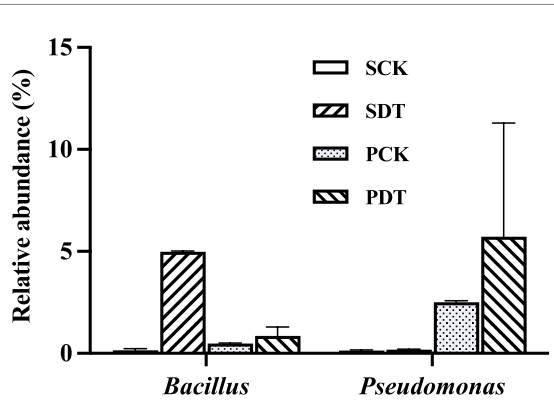

FIGURE 12
The relative abundance of *Bacillus* and *Pseudomonas* in SCK, SDT, PCK, and PDT. Three independent biological replicates are conducted. Error bars indicate the SD (n = 3).

In this study, the relative abundance of *Bacillus* in SDT increased by 32 times compared with that in SCK, and the relative abundance of *Bacillus* in PDT was 79% higher than that in PCK. Similarly, in SDT and PDT, the relative abundance of *Pseudomonas* was significantly higher than that in SCK and PCK, respectively (Figure 12). In addition, *Paenibacillus*, *Devosia*, and *Nitrospira* were also detected in this study, but they were not the dominant genera in the samples (Supplementary material 2). No *Arthrobacter*, *Bradyrhizobium*, *Pseudarthrobacter*, or *Pseudolabrys* were detected in this study. The results showed that dazomet treatment increased the relative abundance of some beneficial bacteria, such as *Bacillus* and *Pseudomonas*, in the soil.

4.3. Restoration of the soil microbial community

Soil microbial diversity is important to sustainable agriculture because microbes can mediate many biochemical processes that support agricultural production. These processes include recycling of plant nutrients, maintenance of soil structure and degradation of agrochemicals (Qin et al., 2017). Soil microbial community structure affects crop health and can also be used as an indicator of soil health (Chen Y. et al., 2022). To date, a number of studies have shown that continuous cropping disrupts the soil microbial community composition (Wu et al., 2022). For instance, the bacterial and fungal diversities were observably altered after the long-term monoculture of *Ganoderma lingzhi* (Yuan et al., 2019, 2021).

As in previous studies (Liu et al., 2017; Benucci et al., 2019; Longley et al., 2019; Orlofsky et al., 2021), the soil microbial communities in this study were dynamic during the cultivation of morel for the control and dazomet treatments. After the long-term monoculture of morel, the disruption of the soil microbial community increases. Soil microbial community disruption negatively affects fructification (Liu et al., 2022; Yu et al., 2022). It has been reported that morel fructification in large-scale cultivation is positively correlated with the diversity and evenness of soil microbial communities (Tan et al., 2021). The principal component analysis (PCA) of bacterial communities showed that SCK, PCK and PDT belonged to one ellipse by 95% confidence, whereas SDT formed an independent cluster far away from the others (Figure 5A). Similar results were obtained for the PCA of the fungal communities (Figure 5B). This result suggested that dazomet treatment partially restored the bacterial and fungal communities from those in continuous cropping soil. Therefore, the increase in yield by dazomet treatment may also be associated with the recovery of microbial communities in continuous cropping soil.

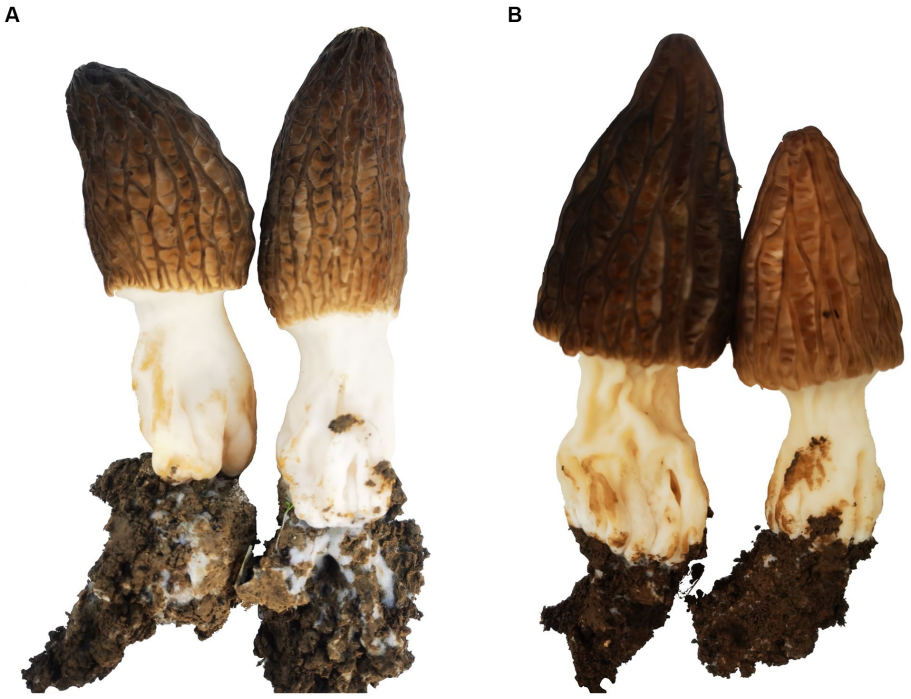

FIGURE 13
Morel fruit bodies cultivated under noncontinuous cropping **(A)** and under continuous cropping **(B)**.

It is well known that rotation with paddy rice can also increase morel yield under continuous cropping. Anaerobic conditions lead to the domination of anaerobic microbes and result in significant changes in soil pH, metal ion availability, and microbial community composition. These changes have negative impacts on soil-borne fungal pathogens (Momma et al., 2013; Khadka and Miller, 2021). In nature, the morel reproduces prolifically in the first year following fires, after which the population rapidly declines (Masaphy and Zabari, 2013; Larson et al., 2016; Miller et al., 2017). This phenomenon may also be related to the soil microbial community, which can be altered by wildfire and stimulates fructification. As mentioned above, the methods to increase the fructification of morel, including dazomet fumigation, rotation with paddy rice, and postfire treatment, could change the soil microbial community. This further suggests the relationship between the obstacle of continuous cropping in morels and soil microbial communities.

Although dazomet fumigation can increase morel yield, the continuous cropping obstacle has not been completely eliminated. We found that there were abundant white hyphae at the bottom of the fruiting bodies growing in the soil for the first time, whereas there was only a small amount of hyphae at the bottom of the fruiting body growing in the continuous cropping soil (Figure 13). The bottoms of the fruiting bodies growing in the soil fumigated with dazomet were similar to those growing in the continuous cropping soil. To completely eliminate continuous cropping obstacles and improve the yield of morel, further research is needed.

5. Conclusion

Our results suggest that dazomet fumigation before inoculation of morel culture decreased the relative abundance of soil-borne fungal pathogens, including *Paecilomyces*, *Trichoderma*, *Fusarium*, *Penicillium*, and *Acremonium*. On the other hand, dazomet treatment increased the relative abundance of beneficial soil bacteria, including *Bacillius* and *Pseudomonas*, which positively affected the growth of mycelia and fructification of the morel. Alpha diversity and beta diversity analysis results showed that dazomet treatment altered the bacterial and fungal communities in continuous cropping soil. The decrease in soil-borne fungal pathogens, the increase in beneficial bacteria and the recovery of the microbial community increased the abundance of morel mycelium, improved the number of primordia and fruiting bodies, and enhanced the yield of the morel under continuous cropping conditions. In summary, dazomet treatment can partially eliminate obstacles associated with continuous cropping and can improve the yield of the morel.

Data availability statement

The datasets presented in this study can be found in online repositories. The names of the repository/repositories and accession number(s) can be found below: BioProject accession number: PRJNA961658.

Author contributions

BC conducted the experiments. GS, TZ, QF, NY, MC, and JZ analyzed the data and wrote the manuscript. XW and BZ reviewed the manuscript. RZ designed the research and supervised the work. All authors contributed to the article and approved the submitted version.

Funding

This work was supported by the Chinese Agriculture Research System (CARS-20); Fundamental Research Funds for Central Nonprofit Scientific Institution (No. 1610132021007); Guizhou Provincial Key Technology R&D Program ([2021]YB201, [2022]YB083, [2023]YB054); Guizhou Provincial Major Scientific and Technological Program ([2019]3007) and Guizhou Province Science and Technology Innovation Ability Pro-motion Special Project ([2021]1).

Conflict of interest

The authors declare that the research was conducted in the absence of any commercial or financial relationships that could be construed as a potential conflict of interest.

Publisher's note

Supplementary material

The Supplementary material for this article can be found online at: https://www.frontiersin.org/articles/10.3389/fmicb.2023.1200226/full#supplementary-material

References

Ampt, E. A., Van Ruijven, J., Raaijmakers, J. M., Termorshuizen, A. J., and Mommer, L. (2019). Linking ecology and plant pathology to unravel the importance of soil-borne fungal pathogens in species-rich grasslands. *Eur. J. Plant Pathol.* 154, 141–156. doi: 10.1007/s10658-018-1573-x

Benucci, G. M. N., Longley, R., Zhang, P., Zhao, Q., Bonito, G., and Yu, F. (2019). Microbial communities associated with the black morel *Morchella sextelata* cultivated in greenhouses. *PeerJ* 7:e7744. doi: 10.7717/peerj.7744

Bolyen, E., Rideout, J. R., Dillon, M. R., Bokulich, N. A., Abnet, C. C., Al-Ghalith, G. A., et al. (2019). Reproducible, interactive, scalable and extensible microbiome data science using QIIME 2. *Nat. Biotechnol.* 37, 852–857. doi: 10.1038/s41587-019-0209-9

Brosnan, J. T., and Breeden, G. (2009). Surface applications of dazomet provide nonselective control of seashore paspalum (*Paspalum vaginatum*) Turf. *Weed Technol.* 23, 270–273. doi: 10.1614/WT-08-147.1

Büchner, R., Vörös, M., Allaga, H., Varga, A., Bartal, A., Szekeres, A., et al. (2022). Selection and characterization of a *Bacillus* strain for potential application in industrial production of white button mushroom (*Agaricus bisporus*). *Agronomy* 12:467. doi: 10.3390/agronomy12020467

Callahan, B. J., Mcmurdie, P. J., Rosen, M. J., Han, A. W., Johnson, A. J. A., and Holmes, S. P. (2016). DADA2: high-resolution sample inference from Illumina amplicon data. *Nat. Methods* 13, 581–583. doi: 10.1038/nmeth.3869

Carrasco, J., and Preston, G. M. (2020). Growing edible mushrooms: a conversation between bacteria and fungi. *Environ. Microbiol.* 22, 858–872. doi: 10.1111/1462-2920.14765

Chen, Y., Du, J., Li, Y., Tang, H., Yin, Z., Yang, L., et al. (2022). Evolutions and managements of soil microbial community structure drove by continuous cropping. *Front. Microbiol.* 13:839494. doi: 10.3389/fmicb.2022.839494

Chen, R., Jiang, W., Xu, S., Fan, H., Chen, X., Shen, X., et al. (2022). An emerging chemical fumigant: two-sided effects of dazomet on soil microbial environment and plant response. *Environ. Sci. Pollut. Res.* 29, 3022–3036. doi: 10.1007/s11356-021-15401-4

Consolazio, N., Lowry, G. V., and Karamalidis, A. K. (2019). Hydrolysis and degradation of dazomet with pyrite: implications for persistence in produced waters in the Marcellus shale. *Appl. Geochem.* 108:104383. doi: 10.1016/j.apgeochem.2019.104383

Dignam, B. E. A., Marshall, S. D. G., Wall, A. J., Mtandavari, Y. F., Gerard, E. M., Hicks, E., et al. (2022). Impacts of soil-borne disease on plant yield and farm profit in dairying soils. *J. Sustain. Agric. Environ.* 1, 16–29. doi: 10.1002/sae2.12009

Edgar, R. C. (2013). UPARSE: highly accurate OTU sequences from microbial amplicon reads. *Nat. Methods* 10, 996–998. doi: 10.1038/nmeth.2604

Frey-Klett, P., Burlinson, P., Deveau, A., Barret, M., Tarkka, M., and Sarniguet, A. (2011). Bacterial-fungal interactions: hyphens between agricultural, clinical, environmental, and food microbiologists. *Microbiol. Mol. Biol. Rev.* 75, 583–609. doi: 10.1128/MMBR.00020-11

Fu, B., Wang, J., Yingmei, L., Zhang, S., Hao, Z., and Zhang, F. (2022). Isolation, identification and biological characteristics of causal pathogen causing pileus rot of cultivated *Morchela importuna*. *Acta Agriculturae Boreali-Ocidentalis Sinica* 31, 640–647.

Guo, M. P., Chen, K., Wang, G. Z., and Bian, Y. B. (2016). First report of stipe rot disease on *Morchella importuna* caused by *Fusarium incarnatum – F. equiseti* species complex in China. *Plant Dis.* 100:2530. doi: 10.1094/PDIS-05-16-0633-PDN

He, P., Li, C., Cai, Y., Zhang, Y., Bian, Y., and Liu, W. (2018). First report of pileus rot disease on cultivated *Morchella importuna* caused by *Diploöspora longispora* in China. *J. Gen. Plant Pathol.* 84, 65–69. doi: 10.1007/s10327-017-0754-3

He, X.-L., Peng, W.-H., Miao, R.-Y., Tang, J., Chen, Y., Liu, L.-X., et al. (2017). White mold on cultivated morels caused by *Paecilomyces penicillatus*. *FEMS Microbiol. Lett.* 364:fnx037. doi: 10.1093/femsle/fnx037

Hirsch, A. M., and Valdés, M. (2010). Micromonospora: an important microbe for biomedicine and potentially for biocontrol and biofuels. *Soil Biol. Biochem.* 42, 536–542. doi: 10.1016/j.soilbio.2009.11.023

Jeffries, M. D., Gannon, T. W., Reynolds, W. C., Yelverton, F. H., and Silcox, C. A. (2017). Herbicide applications and incorporation methods affect dazomet efficacy on bermudagrass. *HortTechnology Hortte* 27, 24–29. doi: 10.21273/HORTTECH03564-16

Jiang, J., Zheng, Q., Liu, K., Ying, G., and Lü, M. (2021). Research progress of continuous cropping obstacle in *Ganoderma lingzhi*. *Edible Med Mushrooms* 29, 112–115.

Khadka, R. B., and Miller, S. A. (2021). Synergy of anaerobic soil disinfestation and *Trichoderma* spp. in *Rhizoctonia* root rot suppression. *Front. Sustain. Food Syst.* 5:645736. doi: 10.3389/fsufs.2021.645736

Koike, S. T., and Gordon, T. R. (2015). Management of *Fusarium* wilt of strawberry. *Crop Prot.* 73, 67–72. doi: 10.1016/j.cropro.2015.02.003

Kuo, M., Dewsbury, D. R., O'donnell, K., Carter, M. C., Rehner, S. A., Moore, J. D., et al. (2012). Taxonomic revision of true morels (*Morchella*) in Canada and the United States. *Mycologia* 104, 1159–1177. doi: 10.3852/11-375

Lamondia, J. A. (2015). *Fusarium* wilt of tobacco. *Crop Prot.* 73, 73–77. doi: 10.1016/j.cropro.2015.03.003

Lan, Y. F., Cong, Q. Q., Wang, Q. W., Tang, L. N., Li, X. M., Yu, Q. W., et al. (2020). First report of *Cladobotryum protrusum* causing cobweb disease on cultivated *Morchella importuna*. *Plant Dis.* 104:977. doi: 10.1094/PDIS-08-19-1611-PDN

Larson, A. J., Cansler, C. A., Cowdery, S. G., Hiebert, S., Furniss, T. J., Swanson, M. E., et al. (2016). Post-fire morel (*Morchella*) mushroom abundance, spatial structure, and harvest sustainability. *For. Ecol. Manag.* 377, 16–25. doi: 10.1016/j.foreco.2016.06.038

Li, C., Chen, G., Zhang, J., Zhu, P., Bai, X., Hou, Y., et al. (2021). The comprehensive changes in soil properties are continuous cropping obstacles associated with American ginseng (*Panax quinquefolius*) cultivation. *Sci. Rep.* 11:5068. doi: 10.1038/s41598-021-84436-x

Li, X., Lewis, E. E., Liu, Q., Li, H., Bai, C., and Wang, Y. (2016). Effects of long-term continuous cropping on soil nematode community and soil condition associated with replant problem in strawberry habitat. *Sci. Rep.* 6:30466. doi: 10.1038/srep30466

Li, Q., Xiang, P., Zhang, T., Wu, Q., Bao, Z., Tu, W., et al. (2022). The effect of phosphate mining activities on rhizosphere bacterial communities of surrounding vegetables and crops. *Sci. Total Environ.* 821:153479. doi: 10.1016/j.scitotenv.2022.153479

Li, Q., Zhang, D., Cheng, H., Song, Z., Ren, L., Hao, B., et al. (2021). Chloropicrin alternated with dazomet improved the soil's physicochemical properties, changed microbial communities and increased strawberry yield. *Ecotoxicol. Environ. Saf.* 220:112362. doi: 10.1016/j.ecoenv.2021.112362

Liu, W., Guo, H., Bi, K., Alekseevna, S. L., Qi, X., and Yu, X. (2022). Determining why continuous cropping reduces the production of the morel *Morchella sextelata*. *Front. Microbiol.* 13:903983. doi: 10.3389/fmicb.2022.903983

Liu, W., He, P., Zhang, J., Wu, L., Er, L., Shi, X., et al. (2023). Ultrastructure and physiological characterization of *Morchella* mitospores and their relevance in the understanding of the morel life cycle. *Microorganisms* 11:345. doi: 10.3390/microorganisms11020345

Liu, Q., Liu, H., Chen, C., Wang, J., Han, Y., and Long, Z. (2017). Effects of element complexes containing Fe, Zn and Mn on artificial morel's biological characteristics and

soil bacterial community structures. *PLoS One* 12:e0174618. doi: 10.1371/journal.pone.0174618

Liu, Q., Ma, H., Zhang, Y., and Dong, C. (2018). Artificial cultivation of true morels: current state, issues and perspectives. *Crit. Rev. Biotechnol.* 38, 259–271. doi: 10.1080/07388551.2017.1333082

Lohberger, A., Spangenberg, J. E., Ventura, Y., Bindschedler, S., Verrecchia, E. P., Bshary, R., et al. (2019). Effect of organic carbon and nitrogen on the interactions of *Morchella* spp. and bacteria dispersing on their mycelium. *Front. Microbiol.* 10:124. doi: 10.3389/fmicb.2019.00124

Loizides, M. (2017). Morels: the story so far. *Field Mycology* 18, 42–53. doi: 10.1016/j.fldmyc.2017.04.004

Longley, R., Benucci, G. M. N., Mills, G., and Bonito, G. (2019). Fungal and bacterial community dynamics in substrates during the cultivation of morels (*Morchella rufobrunnea*) indoors. *FEMS Microbiol. Lett.* 366:fnz215. doi: 10.1093/femsle/fnz215

Lu, M., Liu, M., Chen, G., and Wang, X. (2022). Effects of *Ganoderma lingzhi* continuous monocropping on soil properties and soil nematode community in Jilin, China. *J Jilin Agric. Univ.*

Masaphy, S. (2010). Biotechnology of morel mushrooms: successful fruiting body formation and development in a soilless system. *Biotechnol. Lett.* 32, 1523–1527. doi: 10.1007/s10529-010-0328-3

Masaphy, S., and Zabari, L. (2013). Observations on post-fire black morel ascocarp development in an Israeli burnt forest site and their preferred micro-sites. *Fungal Ecol.* 6, 316–318. doi: 10.1016/j.funeco.2013.02.005

Miller, A. N., Raudabaugh, D. B., Iturriaga, T., Matheny, P. B., Petersen, R. H., Hughes, K. W., et al. (2017). First report of the post-fire morel *Morchella exuberans* in eastern North America. *Mycologia* 109, 710–714. doi: 10.1080/00275514.2017.1408294

Momma, N., Kobara, Y., Uematsu, S., Kita, N., and Shinmura, A. (2013). Development of biological soil disinfestations in Japan. *Appl. Microbiol. Biotechnol.* 97, 3801–3809. doi: 10.1007/s00253-013-4826-9

Noble, R., Dobrovin-Pennington, A., Hobbs, P. J., Pederby, J., and Rodger, A. (2009). Volatile C8 compounds and *Pseudomonads* influence primordium formation of *Agaricus bisporus*. *Mycologia* 101, 583–591. doi: 10.3852/07-194

Orlofsky, E., Zabari, L., Bonito, G., and Masaphy, S. (2021). Changes in soil bacteria functional ecology associated with *Morchella rufobrunnea* fruiting in a natural habitat. *Environ. Microbiol.* 23, 6651–6662. doi: 10.1111/1462-2920.15692

Ower, R. (1982). Notes on the development of the morel ascocarp: *Morchella Esculenta*. *Mycologia* 74, 142–144. doi: 10.1080/00275514.1982.12021480

Ower, R.D., Mills, G.L., and Malachowski, J.A. (1986). Cultivation of Morchella U.S. Patent No: 4594809.

Ower, R.D., Mills, G.L., and Malachowski, J.A. (1988). Cultivation of Morchella U.S. Patent No: 4757640.

Ower, R.D., Mills, G.L., and Malachowski, J.A. (1989). Cultivation of Morchella U.S. Patent No: 4866878.

Pion, M., Spangenberg, J. E., Simon, A., Bindschedler, S., Flury, C., Chatelain, A., et al. (2013). Bacterial farming by the fungus *Morchella crassipes*. *Proc. R. Soc. B Biol. Sci.* 280:20132242. doi: 10.1098/rspb.2013.2242

Qin, S., Yeboah, S., Cao, L., Zhang, J., Shi, S., and Liu, Y. (2017). Breaking continuous potato cropping with legumes improves soil microbial communities, enzyme activities and tuber yield. *PLoS One* 12:e0175934. doi: 10.1371/journal.pone.0175934

Quast, C., Pruesse, E., Yilmaz, P., Gerken, J., Schweer, T., Yarza, P., et al. (2012). The SILVA ribosomal RNA gene database project: improved data processing and web-based tools. *Nucleic Acids Res.* 41, D590–D596. doi: 10.1093/nar/gks1219

Sahin, N. (2005). Antimicrobial activity of *Streptomyces* species against mushroom blotch disease pathogen. *J. Basic Microbiol.* 45, 64–71. doi: 10.1002/jobm.200410427

Sambyal, K., and Singh, R. V. (2021). A comprehensive review on *Morchella importuna*: cultivation aspects, phytochemistry, and other significant applications. *Folia Microbiol.* 66, 147–157. doi: 10.1007/s12223-020-00849-7

Sarwar, A., Brader, G., Corretto, E., Aleti, G., Ullah, M. A., Sessitsch, A., et al. (2018). Qualitative analysis of biosurfactants from *Bacillus* species exhibiting antifungal activity. *PLoS One* 13:e0198107. doi: 10.1371/journal.pone.0198107

Segata, N., Izard, J., Waldron, L., Gevers, D., Miropolsky, L., Garrett, W. S., et al. (2011). Metagenomic biomarker discovery and explanation. *Genome Biol.* 12:R60. doi: 10.1186/gb-2011-12-6-r60

Shi, X., Liu, D., He, X., Liu, W., and Yu, F. (2022). Epidemic identification of fungal diseases in Morchella cultivation across China. *J. Fungi* 8:1107. doi: 10.3390/jof8101107

Sotoyama, K., Akutsu, K., and Nakajima, M. (2016). Biological control of *Fusarium* wilt by *Bacillus amyloliquefaciens* IUMC7 isolated from mushroom compost. *J. Gen. Plant Pathol.* 82, 105–109. doi: 10.1007/s10327-015-0641-8

Stanojević, O., Berić, T., Potočnik, I., Rekanović, E., Stanković, S., and Milijašević-Marčić, S. (2019). Biological control of green mould and dry bubble diseases of cultivated mushroom (*Agaricus bisporus* L.) by *Bacillus* spp. *Crop Prot.* 126:104944. doi: 10.1016/j.cropro.2019.104944

Sun, J., Yu, S., Lu, Y., Liu, H., and Liu, X. (2023). Proposal of a new family *Pseudodiploösporeaceae* fam. nov. (*Hypocreales*) based on phylogeny of *Diploöspora longispora* and *Paecilomyces penicillatus*. *Mycology* 14, 60–73. doi: 10.1080/21501203.2022.2143919

Tan, F. (2016). History, current status and prospect of artificial cultivation of morel mushroom. *Edible Med. Mushrooms* 24, 140–144.

Tan, H., Liu, T., Yu, Y., Tang, J., Jiang, L., Martin, F. M., et al. (2021). Morel production related to soil microbial diversity and evenness. *Microbiol. Spect.* 9:e0022921. doi: 10.1128/Spectrum.00229-21

Tilton, F., La Du, J. K., Vue, M., Alzarban, N., and Tanguay, R. L. (2006). Dithiocarbamates have a common toxic effect on zebrafish body axis formation. *Toxicol. Appl. Pharmacol.* 216, 55–68. doi: 10.1016/j.taap.2006.04.014

Velázquez-Cedeño, M., Farnet, A. M., Mata, G., and Savoie, J.-M. (2008). Role of *Bacillus* spp. in antagonism between *Pleurotus ostreatus* and *Trichoderma harzianum* in heat-treated wheat-straw substrates. *Bioresour. Technol.* 99, 6966–6973. doi: 10.1016/j.biortech.2008.01.022

Wang, X., Peng, J., Sun, L., Bonito, G., Guo, Y., Li, Y., et al. (2020). Genome sequencing of *Paecilomyces penicillatus* provides insights into its phylogenetic placement and mycoparasitism mechanisms on morel mushrooms. *Pathogens* 9:834. doi: 10.3390/pathogens9100834

Wang, F., Wang, Q., Yan, D., Mao, L., Guo, M., Yan, P., et al. (2011). Effects of dimethyl disulfide on microbial communities in protectorate soils under continuous cropping. *Chin. J. Eco Agric.* 19, 890–896. doi: 10.3724/SP.J.1011.2011.00890

Wu, H., Chen, J., Li, J., Liu, Y., Park, H. J., and Yang, L. (2021). Recent advances on bioactive ingredients of *Morchella esculenta*. *Appl. Biochem. Biotechnol.* 193, 4197–4213. doi: 10.1007/s12010-021-03670-1

Wu, X., Wu, C., Lu, D., Wu, Y., Ye, Z., Xia, L., et al. (2022). Variation of soil microbial community and sterilization to *Fusarium oxysporum* f. sp. *Niveum* play roles in slightly acidic electrolyzed water-alleviated watermelon continuous cropping obstacle. *Front. Microbiol.* 13:837121. doi: 10.3389/fmicb.2022.837121

Xi, H., Shen, J., Qu, Z., Yang, D., Liu, S., Nie, X., et al. (2019). Effects of long-term cotton continuous cropping on soil microbiome. *Sci. Rep.* 9:18297. doi: 10.1038/s41598-019-54771-1

Yu, F. M., Jayawardena, R. S., Thongklang, N., Lv, M. L., Zhu, X. T., and Zhao, Q. (2022). Morel production associated with soil nitrogen-fixing and nitrifying microorganisms. *J. Fungi* 8:299. doi: 10.3390/jof8030299

Yu, M., Yin, Q., and He, P. (2020). Isolation and identification of pathogen of morel white rot. *Northern Hortic.* 7, 142–145.

Yuan, Y., Huang, H. C., Ye, L. Y., Fu, J. S., and Wu, X. P. (2019). Analysis of fungal community in continuous cropping soil of *Ganoderma lingzhi*. *Mycosystema* 38, 2112–2121.

Yuan, Y., Li, L., Huang, H., Liu, G., Xie, F., Fu, J., et al. (2021). Analysis of bacterial community in *Ganoderma lingzhi* continuous cropping soil based on 16S rDNA amplicon sequencing. *Chinese Agric. Sci. Bull.* 37, 116–123.

Zhang, Y., Jiang, W., Chang, Y., Niu, R., and Ye, Z. (2018). Isolation, identification and anti-microbial activity of antagonistic bacteria in continuous cropping soil of *Dictyophora*. *Chinese J. Trop. Agric.* 38, 90–94.

Zhang, F., Long, L., Hu, Z., Yu, X., Liu, Q., Bao, J., et al. (2019). Analyses of artificial morel soil bacterial community structure and mineral element contents in ascocarp and the cultivated soil. *Can. J. Microbiol.* 65, 738–749. doi: 10.1139/cjm-2018-0600

Zhao, Y., Chai, H., and Zhang, X. (2016). Predicament and prospect of *Morchella* industrialization in China. *Edible Med. Mushrooms* 24, 133–139.

frontiers | Frontiers in Microbiology

TYPE Original Research
PUBLISHED 19 October 2023
DOI 10.3389/fmicb.2023.1264699

OPEN ACCESS

EDITED BY
Chenyang Huang,
Chinese Academy of Agricultural Sciences, China

REVIEWED BY
Beilei Wu,
Chinese Academy of Agricultural Sciences, China
Vagish Dwibedi,
Chandigarh University, India

*CORRESPONDENCE
Bo Zhang
zhangbofungi@126.com
Xiao Li
lxmogu@163.com
Yu Li
yuli966@126.com

†These authors have contributed equally to this work

RECEIVED 21 July 2023
ACCEPTED 28 September 2023
PUBLISHED 19 October 2023

CITATION
Li X, Sossah FL, Tuo Y, Hu J, Wei Q, Li S, Rong N, Wiafe-Kwagyan M, Li C, Zhang B, Li X and Li Y (2023) Characterization and fungicide sensitivity of *Trichoderma* species causing green mold of *Ganoderma sichuanense* in China. *Front. Microbiol.* 14:1264699. doi: 10.3389/fmicb.2023.1264699

Characterization and fungicide sensitivity of *Trichoderma* species causing green mold of *Ganoderma sichuanense* in China

Xuefei Li[1,2,3†], Frederick Leo Sossah[2,4†], Yonglan Tuo[1,2,3], Jiajun Hu[1,2], Qian Wei[3], Shiyu Li[2,3], Na Rong[2,3], Michael Wiafe-Kwagyan[5], Changtian Li[2], Bo Zhang[1,2,3]*, Xiao Li[1,2,3]* and Yu Li[1,2,3]*

[1]Joint International Research Laboratory of Modern Agricultural Technology, Ministry of Education, Jilin Agricultural University, Changchun, China, [2]Engineering Research Center of Chinese Ministry of Education for Edible and Medicinal Fungi, Jilin Agricultural University, Changchun, China, [3]College of Plant Protection, Jilin Agricultural University, Changchun, China, [4]Coconut Research Programme, Council for Scientific and Industrial Research (CSIR), Oil Palm Research Institute, Kade, Ghana, [5]Department of Plant and Environmental Biology, School of Biological Sciences, College of Basic and Applied Sciences, University of Ghana, Accra, Ghana

Green mold disease, caused by *Trichoderma* spp., is one of the most devastating diseases of mushrooms in China. The application of fungicides remains one of the important control methods among the integrated pest management tools for disease management in mushroom farms. This study aimed to identify *Trichoderma* spp., isolated from *G. sichuanense* fruiting bodies displaying green mold symptoms collected from mushroom farms in Zhejiang, Hubei, and Jilin Province, China, and evaluate their in vitro sensitivity to six fungicides. A total of 47 isolates were obtained and classified into nine *Trichoderma* spp. namely, *T. asperellum*, *T. citrinoviride*, *T. ganodermatiderum*, *T. guizhouense*, *T. hamatum*, *T. harzianum*, *T. koningiopsis*, *T. paratroviride*, and *T. virens*, through morphological characteristics and phylogenetic analysis of concatenated sequences of translation elongation factor 1-alpha (TEF) and DNA-dependent RNA polymerase II subunit (RPB2) genes. The pathogenicity test was repeated two times, and re-isolation of the nine *Trichoderma* spp. from the fruiting bodies of *G. sichuanense* fulfilled Koch's postulates. Prochloraz manganese showed the best performance against most species. This research contributes to our understanding of green mold disease, reveals the phylogenetic relationships among *Trichoderma* species, and expands our knowledge of *Trichoderma* species diversity associated with green mold disease in *G. sichuanense*.

KEYWORDS

***Trichoderma* spp., *Ganoderma sichuansense*, green mold disease, pathogenicity, fungicides, prochloraz manganese, mushroom health**

Introduction

Ganoderma sichuanense is a widely distributed pore fungus that holds ecological and economic significance (Zhao et al., 1983; Wang et al., 2012). With its valuable medicinal properties, it has been cultivated for centuries in China, Japan, South Korea, and other regions (Zhu et al., 2019; Wang et al., 2020). In China, *G. sichuanense* has been cultivated for over

100 years, primarily in provinces such as Jilin, Heilongjiang, Shandong, Anhui, Guangdong, Guangxi, Fujian, Jiangxi, and Zhejiang. Recent studies have highlighted its medicinal benefits, including anti-tumor activity, antioxidant effects, blood sugar and lipid regulation, blood pressure reduction, antiviral activity, liver protection, and anti-aging effects (Xiao et al., 2016; Chiu et al., 2017; Rahman et al., 2018, 2020; Pan and Lin, 2019; Qiu et al., 2019; Wu et al., 2019; Krobthong et al., 2021).

The commercial expansion of *G. sichuanense* cultivation has become crucial due to limited wild germplasm resources. In 2020, China's *Ganoderma* production exceeded 189,000 tons, representing significant economic value (China Edible Fungi Association, 2020). However, this expansion has also led to increased disease occurrences, resulting in substantial economic losses by impacting the quality and yield of *G. sichuanense*. Among the various fungal pathogens affecting *G. sichuanense* production, *Trichoderma* spp., *Xylogone ganodermophthora*, and *Cladobotryum* spp. pose significant challenges (Kang et al., 2010; Zuo et al., 2016; Yan et al., 2019; Cai et al., 2020).

Green mold disease, primarily caused by *Trichoderma* species, is particularly concerning as it hampers the growth and productivity of *G. sichuanense* (Wang et al., 2016). While *Trichoderma* is known for its biocontrol effects, it can also act as a pathogen, posing a serious threat to edible fungi during cultivation (Shah et al., 2013; Kosanović et al., 2020). The occurrence of green mold disease caused by *Trichoderma* species in China has raised significant concerns, resulting in contamination and losses in yield and quality (Seaby, 1987; Choi et al., 1998; Wang et al., 2016; Seung et al., 2018). The impact of this disease on *G. sichuanense* cultivation in China is of particular concern given the economic importance of this valuable medicinal fungus (Pan and Lin, 2019; Rahman et al., 2020).

In the context of *Ganoderma* cultivation, *Trichoderma*-induced diseases are particularly problematic during the mycelial growth and emergence stages of *G. sichuanense*. However, limited research has been conducted on the diversity and pathogenicity of *Trichoderma* species isolated from *G. sichuanense* in China, and the establishment of effective control measures against *Ganoderma*-related diseases remains a challenge (Seaby, 1987; Chen and Zhuang, 2017; Yan et al., 2019; Cai et al., 2020; An et al., 2022). Therefore, identifying the causal agent and understanding its pathogenicity are crucial prerequisites for the development of effective disease management strategies.

Although fungicides are effective in controlling green mold disease, their use can lead to the development of resistance and pose environmental risks. Nevertheless, fungicides remain the most effective measure for disease control (Shah et al., 2013; Kosanović et al., 2015; Innocenti et al., 2019). Understanding the sensitivity of *Trichoderma* species to various fungicides can significantly contribute to disease management strategies. However, the fungicide sensitivities of *Trichoderma* isolates causing green mold disease in *G. sichuanense* in China have not been thoroughly investigated.

In this study, we aimed to investigate the *Trichoderma* species associated with *G. sichuanense* and their impact on disease development. Our findings revealed a disease incidence ranging from 3 to 15%, which significantly affected the growth and development of *G. sichuanense*, leading to direct economic consequences. The rapid germination and spread of *Trichoderma* spores underscored the potential for irreparable damage if the disease is not promptly controlled. We focused on the identification and characterization of these *Trichoderma* species, the assessment of their pathogenicity in *G. sichuanense*, and the evaluation of their sensitivity to fungicides. Through these comprehensive analyses, our objective was to provide valuable insights into disease management strategies for *G. sichuanense* cultivation.

Materials and methods

Sample collection and fungal isolation

During the period from 2021 to 2022, we collected fruiting bodies (basidiomata) of *G. sichuanense* displaying symptoms of green mold disease from three farms situated in Zhejiang, Hubei, and Jilin Province, China. The incidence of the disease ranged from 3 to 15%, significantly impacting the growth and development of *G. sichuanense*.

To conduct a comprehensive investigation of the disease, we isolated the fungus from the infected fruiting bodies using the tissue-isolation method. This involved carefully excising small pieces (0.3 cm) from the edges of the lesions on the diseased fruiting bodies using a sterile scalpel. The excised tissues were then subjected to surface sterilization by treating them with 75% ethanol (vol/vol) for 30 s, followed by 1% NaOCl (wt/vol) for 10 s. Subsequently, the tissues underwent three rinses with sterilized distilled water.

The tissues were placed onto dried and sterilized potato dextrose agar (PDA) plates and incubated in darkness at 25°C for three to 5 days. Regular inspections were carried out to monitor any fungal growth. Colonies that developed from the infected tissues were transferred to new PDA plates using the hyphal tip culture method to obtain pure cultures. All purified isolates were further subcultured on PDA medium for 3 days and preserved on PDA slants at 4°C.

Morphological characterization

To evaluate the characteristics of the isolates, mycelia plug with a diameter of 5.0 mm were obtained from the edges of actively growing cultures aged 5 days. These plugs were then placed at the center of agar plates containing potato dextrose agar (PDA), cornmeal dextrose agar (CMD), and synthetic low-nutrient agar (SNA). The plates were incubated at 25°C with a 12-h light/dark photoperiod for a duration of 5–7 days.

During the incubation period, careful observations and recordings were made on various colony characteristics, including color, shape, radial growth, and texture. The colony diameters were measured in two perpendicular directions. The daily growth rate was determined by calculating the average mean daily growth (mm/day).

For further analysis, one-week-old colonies cultivated on SNA plates were utilized to examine the conidia and conidiophores following the methods outlined by Chaverri et al. (2015). The shape and color of the conidia were observed, and the sizes of 20 randomly selected conidia from each isolate were measured under a Zeiss Axio lab. A1 microscope equipped with a differential interference contrast

(DIC) optics camera (Carl Zeiss Microscopy GmbH, Germany), utilizing 1,000× magnification.

DNA extraction and sequence analysis

To obtain DNA for analysis, mycelia were collected from colonies cultivated on potato dextrose agar (PDA) for 3–5 days. DNA extraction was performed using the NuClean Plant Genomic DNA Kit (Cowin Biotech Co., Ltd., Taizhou, China).

For amplification of the target genes, specific primer pairs were used. The primer pair fRPB2-5f and fRPB2-7cr (Liu et al., 1999) amplified a 1 kb fragment of the RNA polymerase II second largest subunit (RPB2) gene. Additionally, the primer pair EF1-728F and TEF1LLErev (Chaverri et al., 2003; Jaklitsch et al., 2005) amplified a 1.3 kb fragment of the translation elongation factor 1-alpha (TEF1-a) gene. PCR amplification was conducted in a 30 μL reaction system comprising 15 μL of 10× PCR mix, 1.5 μL of each primer, 1.5 μL of template DNA, and 10.5 μL of ddH_2O. For both RPB2 and TEF1-a genes, PCR conditions included an initial denaturation step at 95°C for 5 min, followed by 30 cycles of denaturation at 95°C for 1 min, annealing at 59°C for RPB2 or 55°C for TEF1-a for 90 s, extension at 72°C for 90 s, and a final extension at 72°C for 10 min. The PCR products were purified using the PCR Product Purification Kit, and gel electrophoresis was performed to confirm successful amplification.

Sequencing of the PCR products was carried out bidirectionally using the fRPB2-5f/fRPB2-7cr and TEF1/TEF2 primers (Jaklitsch, 2009) at Comate Biosciences Co. Ltd (Changchun, Jilin, China). The obtained sequences were assembled using CAP3 software (Huang and Madan, 1999) to generate consensus sequences. BioEdit software (version 7.0.0) was used to remove 20 to 30 bp from the terminal ends. Basic Local Alignment Search Tool (BLAST) analysis[1] was conducted for each gene locus to confirm the identity of the isolates. The consensus sequences were deposited in GenBank (Table 1).[2]

Phylogenetic analyses

After performing a BLAST search using the obtained ITS, RPB2, and TEF1-a sequences in the NCBI GenBank database, sequences that met specific criteria: ≥ 99% similarity for RPB2, ≥ 97% for TEF1-a, and ≥ 76% for ITS, were utilized to verify the identity of Trichoderma species in our phylogenetic analysis (Cai and Druzhinina, 2021). We retrieved homologous RPB2, TEF1-a, and ITS gene sequences of the isolates from GenBank. These sequences were aligned using the MUSCLE program (Edgar, 2004), and the resulting alignment was further refined using BioEdit 7.2.5 (Hall, 1999; Hall, 2011). Finally, we concatenated the gene sequences using Phylosuit V1.2.2 (Zhang et al., 2020). For the phylogenetic analysis, we employed the Maximum-Likelihood (ML) method using PhyML 3.0 (Guindon et al., 2010). The best substitution model was determined with PartitionFinder v2.1.1 (Lanfear et al., 2017). To assess statistical support, we conducted bootstrapping with 1,000 replicates (ML). Detailed lists of the fungal isolates used in this study can be found in Table 1 and Supplementary Table S1. The resulting ML tree was visualized using Figtree v1.4.4,[3] providing a clear representation of the phylogenetic relationships among the isolates.

Pathogenicity tests

Pathogenicity experiments were conducted following Koch's postulates, with each experiment replicated twice to ensure accuracy. Fully colonized substrate bags containing *G. sichuanense* were sourced from the Panshi Mushroom Base in Jilin Province, China. These bags were placed in a growth room with controlled conditions, including a temperature range of 25–30°C and humidity levels set between 80 and 90%, to promote fruiting. Once the fruiting bodies were formed, the bottom surface of the cap and the stipe were meticulously damaged using a sterilized needle. Subsequently, they were inoculated with a spore suspension of the isolates at a concentration of 1×10^5 spores per milliliter. As a comparison, the control group was inoculated with sterilized distilled water.

For each strain, six bags of *G. sichuanense* were inoculated. The development of symptoms was monitored daily for a period of 14 days. To confirm the causative agents of green mold disease, the pathogens were re-isolated from the inoculated *G. sichuanense* showing green mold symptoms. Identification was performed using the aforementioned morphological and molecular methods, considering strains that matched the original inoculum as the causative agents of green mold disease.

Effect of *Trichoderma* spp. on *G. sichuanense* mycelia in petri plates

To assess the aggressiveness of the isolates, a subset of nine isolates representing nine different species was selected from the total of 47 isolates. The experiments were performed with three replicates, following the procedure outlined below. Mycelial agar plugs with a diameter of 8 mm were obtained from the advancing edge of 10-day-old *G. sichuanense* colonies. These plugs were then inoculated onto potato dextrose agar (PDA) plates, positioned 1 cm from the edge of Petri plates with a diameter of 9 cm. After 7 days, mycelial plugs from *Trichoderma* cultures were inoculated in the same manner, but on the opposite side of the plate, 1 cm away from the edge. The growth of *Trichoderma* species in confrontation with *G. sichuanense* mycelia was carefully observed and recorded.

Fungicide sensitivity of isolates and *G. sichuanense*

To evaluate the efficacy of fungicides against green mold in mushrooms, a preliminary screening of six fungicides (mancozeb,

1 https://www.ncbi.nlm.nih.gov/BLAST/

2 http://www.ncbi.nlm.nih.gov/genbank

3 http://tree.bio.ed.ac.uk/software/figtree/

TABLE 1 Specimen Numbers, country and their corresponding GenBank accession numbers of sequences used for phylogenetic analyses.

Scientific name	Specimen numbers	Country	Substrate	GenBank accession numbers		
				RPB2	TEF1-a	ITS
T. anisohamatum	YMF1.00333 T	China	/	MH155272	MH177912	MH113926
T. anisohamatum	YMF1.00215	China	/	MH262576	MH236494	MH262583
T. asperellum	CBS 433.97 T	USA	Soil	EU248617	AY376058	/
T. asperellum	**T19**	**China**	**G. sichuanense**	**OR291404**	**OR291385**	**OR569146**
T. atroviride	CBS 142.95 ET	Slovenia	Decayed log	EU341801	AF456891	MH862505
T. atroviride	NECC21247	/	/	OL790433	OL790432	OL690567
T. ceramicum	CBS 114576 T	USA	Wood	FJ860531	FJ860628	FJ860743
T. ceramicum	GJS 88–70 T	USA	Wood	AF545510	AF534593	AY737764
T. citrinoviride	DAOM 172792 T	/	/	KJ842210	KJ713208	EU280098
T. citrinoviride	DEMf:TR4	Serbia	*Pinus sylvestris* bark	OK422202	OK422205	OK384603
T. citrinoviride	**T31**	**China**	**G. sichuanense**	**OR291411**	**OR291392**	**OR569153**
T. estonicum	GJS 96–129 T	Estonia	*Hymenochaete tabacina*	AF545514	AF534604	AY737767
T. ganodermatiderum	CCMJ5245 T	China	*G. sichuanense*	ON567189	ON567195	ON399102
T. ganodermatiderum	CCMJ5246	China	*G. sichuanense*	ON567190	ON567196	ON399103
T. ganodermatiderum	**T1**	**China**	**G. sichuanense**	**OR291399**	**OR291380**	**OR569141**
T. ganodermatiderum	**T2**	**China**	**G. sichuanense**	**OR291400**	**OR291381**	**OR569142**
T. ganodermatiderum	**T3**	**China**	**G. sichuanense**	**OR291401**	**OR291382**	**OR569143**
T. guizhouense	HGUP0038 T	China	Soil	JQ901400	JN215484	JN191311
T. guizhouense	S278	Croatia	/	KF134791	KF134799	/
T. guizhouense	**T41**	**China**	**G. sichuanense**	**OR291413**	**OR291394**	**OR569155**
T. guizhouense	**T42**	**China**	**G. sichuanense**	**OR291414**	**OR291395**	**OR569156**
T. hamatum	DAOM 167057 ET	Canada	/	AF545548	EU279965	EU280124
T. hamatum	KUFA 0088	/	/	OP250964	OP250957	OP218247
T. hamatum	**T28**	**China**	**G. sichuanense**	**OR291410**	**OR291391**	**OR569152**
T. harzianum	CBS 226.95 T	England	Soil	AF545549	AF348101	AJ222720
T. harzianum	GJS 05–107	Italy	*Ricinus communis*	FJ442708	FJ463329	/
T. harzianum	**T23**	**China**	**G. sichuanense**	**OR291407**	**OR291388**	**OR569149**
T. harzianum	**T24**	**China**	**G. sichuanense**	**OR291408**	**OR291389**	**OR569150**
T. koningiopsis	GJS 93–20 T	Cuba	Branch	EU241506	DQ284966	DQ313140
T. koningiopsis	CCMJ5254	China	*G. sichuanense*	ON567202	ON567188	ON385947
T. koningiopsis	**T26**	**China**	**G. sichuanense**	**OR291409**	**OR291390**	**OR569151**
T. koningiopsis	**T40**	**China**	**G. sichuanense**	**OR291412**	**OR291393**	**OR569154**
T. koningiopsis	**T43**	**China**	**G. sichuanense**	**OR291415**	**OR291396**	**OR569157**
T. koningiopsis	**T45**	**China**	**G. sichuanense**	**OR291416**	**OR291397**	**OR569158**
T. paratroviride	S385 T	Spain	/	KJ665321	KJ665627	/
T. paratroviride	PARC1012	/	/	MT454131	MT454115	MT448958
T. paratroviride	**T17**	**China**	**G. sichuanense**	**OR291402**	**OR291383**	**OR569144**
T. paratroviride	**T18**	**China**	**G. sichuanense**	**OR291403**	**OR291384**	**OR569145**
T. paratroviride	**T47**	**China**	**G. sichuanense**	**OR291417**	**OR291398**	**OR569159**
T. parestonicum	CBS 120636 T	Austria	*Hymenochaete tabacina*	FJ860565	FJ860667	FJ860803
T. virens	DIS 162	Costa Rica	*T. cacao*	FJ442696	FJ463367	FJ442669
T. virens	DIS 328A	Ecuador	*T. gileri*	FJ442738	FJ463363	FJ442670
T. virens	**T20**	**China**	**G. sichuanense**	**OR291405**	**OR291386**	**OR569147**
T. virens	**T21**	**China**	**G. sichuanense**	**OR291406**	**OR291387**	**OR569148**

Sequences produced in this study are in bold.

chlorothalonil, fludioxonil, carbendazim, prochloraz, and prochloraz-Mn) was conducted. Stock solutions of each fungicide at a concentration of 100 mg/mL were prepared by dissolving them in sterilized distilled water. The growth inhibition rate of the fungi was assessed through mycelial growth assays.

PDA medium plates with different concentrations of each fungicide were prepared by adding the appropriate volume of the stock solution to sterilized distilled water. Mycelial plugs with a diameter of 7 mm were obtained from the edges of 3-day-old colonies grown on PDA and placed at the center of the PDA plates containing varying fungicide concentrations. All plates were then incubated at 25°C for 3 days. The growth inhibition rate of the mycelia was calculated using the formula $i = \frac{(a1 - a2)}{a1} \times 100$, where "$i$" represents the growth inhibition rate, "a1" is the hyphae area of the untreated pathogen, and "a2" is the hyphae area of the treated pathogen (Etebarian et al., 2005).

Each fungicide treatment and the control were replicated on three plates, and the experiment was repeated twice. Based on the preliminary screening results of the six fungicides using the nine isolates, a suitable fungicide was selected. The sensitivity of *G. sichuanense* to these fungicides was further tested using the same method described above.

The sensitivity of the fungi to fungicides was determined by measuring the fungicide concentration that inhibited fungal development by 50% [half maximal effective concentration (EC50)] (Wong and Midland, 2007; Kim et al., 2020). The relative growth (RG) of the fungi at a specific fungicide concentration was calculated as a percentage of fungal growth compared to the control plates. The EC50 value was obtained by performing linear regression analysis on the probit-transformed relative inhibition values (1 - RG) at log10-transformed fungicide concentrations. The EC50 value for each isolate was calculated as the average of three experiments. The correlation coefficients (r) among EC50 values for different fungicides were determined using statistical algorithms provided by SAS software (version 9.4 for Windows; SAS Institute, Cary, NC, U.S.A.).

Results

Disease symptoms and fungal isolation

The fruiting bodies of *G. sichuanense* exhibited symptoms of green mold disease, which were visually distinct. Infected basidiomata displayed a layer of green mycelia, leading to decay and withering of the affected fruiting bodies (Figure 1). The severity of the disease was evident, as it progressed rapidly, particularly after watering flushes of the fruiting bodies. The development of symptoms followed a specific pattern: initially, white spots and mycelium appeared on the infected fruiting bodies. Under hot weather conditions or high humidity, there was a significant proliferation of green conidia within a short time, gradually covering the entire surface of the fruiting bodies. Subsequently, the spores dispersed through various means, such as water flow, human movement, or wind, resulting in the demise of *G. sichuanense* fruiting bodies and the loss of their ability to produce spores.

To investigate the pathogens responsible for green mold disease, we conducted fungal isolation from the infected fruiting bodies. A total of 47 pathogens were isolated and identified during the study (Tables 1, 2; Supplementary Table S1). Among the isolated pathogens, we identified one strain of *T. harzianum* in Zhejiang Province and three strains in Hubei Province, namely *T. koningiopsis*, *T. paratrovide*, and *T. virens*. Interestingly, in Jilin Province, we observed a diverse range of strains, with a total of nine different species identified (Table 2). These pathogens were characterized by their ability to induce the distinctive symptoms associated with green mold disease on *G. sichuanense*.

Morphological characteristics

Using the classification methods proposed by Bissett (1984), Gams and Bissett (1998), and Park et al. (2006), we conducted a meticulous examination of colony shape, conidia, conidiophore size, chlamydospores, and pigmentation (Figures 2, 3) to identify nine *Trichoderma* species. The isolated species include *T. ganodermatiderum* (Figures 2A–G), *T. citrinoviride* (Figures 2H–L), *T. hamatum* (Figures 2M–P), *T. asperellum* (Figures 2Q–U), *T. guizhouense* (Figures 2V–Z), *T. harzianum* (Figures 3A–C), *T. virens* (Figures 3D–F), *T. paratroviride* (Figures 3G–J), and *T. koningiopsis* (Figures 3K–O).

After 1 day of cultivation at 25°C, all strains displayed white villous colonies on PDA, SNA, and CMD media. By the fifth day, light green to dark green sporulation bands emerged on all media, gradually extending toward the center. CMD and SNA media supported the growth of relatively thin colonies. By the seventh day, green spores were dispersed throughout the entire plate, exhibiting a grayish green or chartreuse color (Figure 4). *T. citrinoviride* exhibited the production of a yellow pigment at a later stage (Figure 4B), and some exhibited concentric rings (Figure 4).

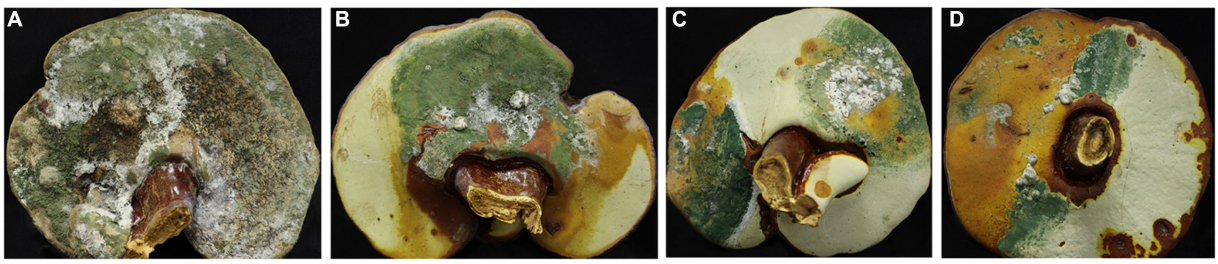

FIGURE 1
Ganoderma sichuanense fruiting bodies infected by *Trichoderma* **(A–D)**.

10.3389/fmicb.2023.1264699

TABLE 2 Number of *Trichoderma* isolates recovered from *G. sichuanense* with macroscopic symptoms of green mold disease collected.

Species	*T. ganodermatiderum*	*T. koningiopsis*	*T. paratroviride*	*T. harzianum*	*T. virens*	*T. guizhouense*	*T. hamatum*	*T. asperellum*	*T. citrinoviride*
Strains	T1-T16, T30, T32, T36, T37, T38, T46, T48	T26, T27, T33, T39, T40, T43, T44, T45	T17, T18, T34, T35, T47	T23, T24, T25	T20, T21, T22	T41, T42	T28	T19	T31
Total	23	8	5	3	3	2	1	1	1
[a]Percentage	48.93%	17.02%	10.64%	6.38%	6.38%	4.26%	2.13%	2.13%	2.13%

[a]Percentage = $n/N \times 100\%$, where n is the number of isolates for one species of Trichoderma, and N is the total number of isolates for all Trichoderma species.

Microscopic analysis unveiled notable distinctions in the morphology of conidiophores, phialides, and conidia among the *Trichoderma* species. *T. ganodermatedrum* (Figures 2A–G), *T. asperellum* (Figures 2Q–U), *T. harzianum* (Figures 3A–C), and *T. koningiopsis* (Figures 3K–O) exhibited dendriform branches and green spherical or ellipsoidal spores. While *T. ganodermatedrum* (Figures 2A–G) and *T. harzianum* (Figures 3A–C) shared similar spore sizes, the former displayed densely distributed conidiophores, whereas the latter had sparser conidiophore clusters. *T. asperellum* (Figures 2Q–U) and *T. koningiopsis* (Figures 3K–O) exhibited similar spore sizes, but there were significant differences in the sizes of their phialides. Specifically, *T. koningiopsis* had phialides measuring 5.0–7.5 × 3.0–4.8 µm (Figures 3K–M), while *T. asperellum* had phialides measuring 7–11 × 2–4 µm (Figures 2Q–S).

T. virens presented irregular branches at the top of its conidiophores, often accompanied by 3–6 closely arranged phialides, resulting in a more complex structure (Figures 3D–F). *T. hamatum* displayed highly branched conidiophores, primarily with opposite lateral branches and a few solitary branches (Figures 2M–P). The phialides of *T. hamatum* were densely packed, short, and round, measuring 5–7.5 × 3.0–4.4 µm (Figures 2M–N). In the case of *T. citrinoviride*, its conidiophores appeared either opposite or alternate, and it possessed small spores measuring 2.9–4.0 × 1.8–2.2 µm (Figures 2H–L). While *T. guizouense* (Figures 2V–Z) and *T. paratroviride* (Figures 3G–J) featured nearly spherical spores, the former exhibited conidiophores in pairs or whorls, with phialides typically arranged in groups of 2–4. Conversely, *T. guizouense* predominantly displayed conidiophores in 2–3 whorls, occasionally occurring solitary, and its phialides were symmetrically distributed (Figures 2V–X). Notably, *T. hamatum* (Figure 2P), *T. asperellum* (Figure 2U), *T. guizouense* (Figure 2Z), and *T. koningiopsis* (Figure 3O) exhibited abundant chlamydospores in later stages. For further details regarding the specific characteristics of each *Trichoderma* isolate, please consult Table 3.

Phylogenetic analysis

The TEF1-a and RPB2 gene sequences of all *Trichoderma* isolates were compared to the NCBI database using BLAST analysis. Matches exhibiting a high similarity level (≥90%) were chosen for subsequent analysis. A phylogenetic analysis was conducted using the concatenated sequences of the TEF1-a and RPB2 genes from all *Trichoderma* isolates. The analysis revealed that the *Trichoderma* isolates could be classified into nine distinct clades: *T. asperellum*, *T. citrinoviride*, *T. ganodermatiderum*, *T. guizhouense*, *T. hamatum*, *T. harzianum*, *T. koningiopsis*, *T. paratroviride*, and *T. virens* (Figure 5). The phylogenetic trees were constructed using a dataset consisting of 19 sequences derived from two gene loci (TEF1-a and RPB2) obtained from a total of 47 samples. Among these sequences, 38 were newly generated, including 19 TEF1-a sequences and 19 RPB2 sequences. For more detailed information on the specific characteristics of each *Trichoderma* isolate, please refer to Table 1 and Supplementary Table S1.

Pathogenicity tests

In the pathogenicity test, mechanical damage was induced on the fruiting bodies followed by *in vitro* inoculation using a spore

10.3389/fmicb.2023.1264699

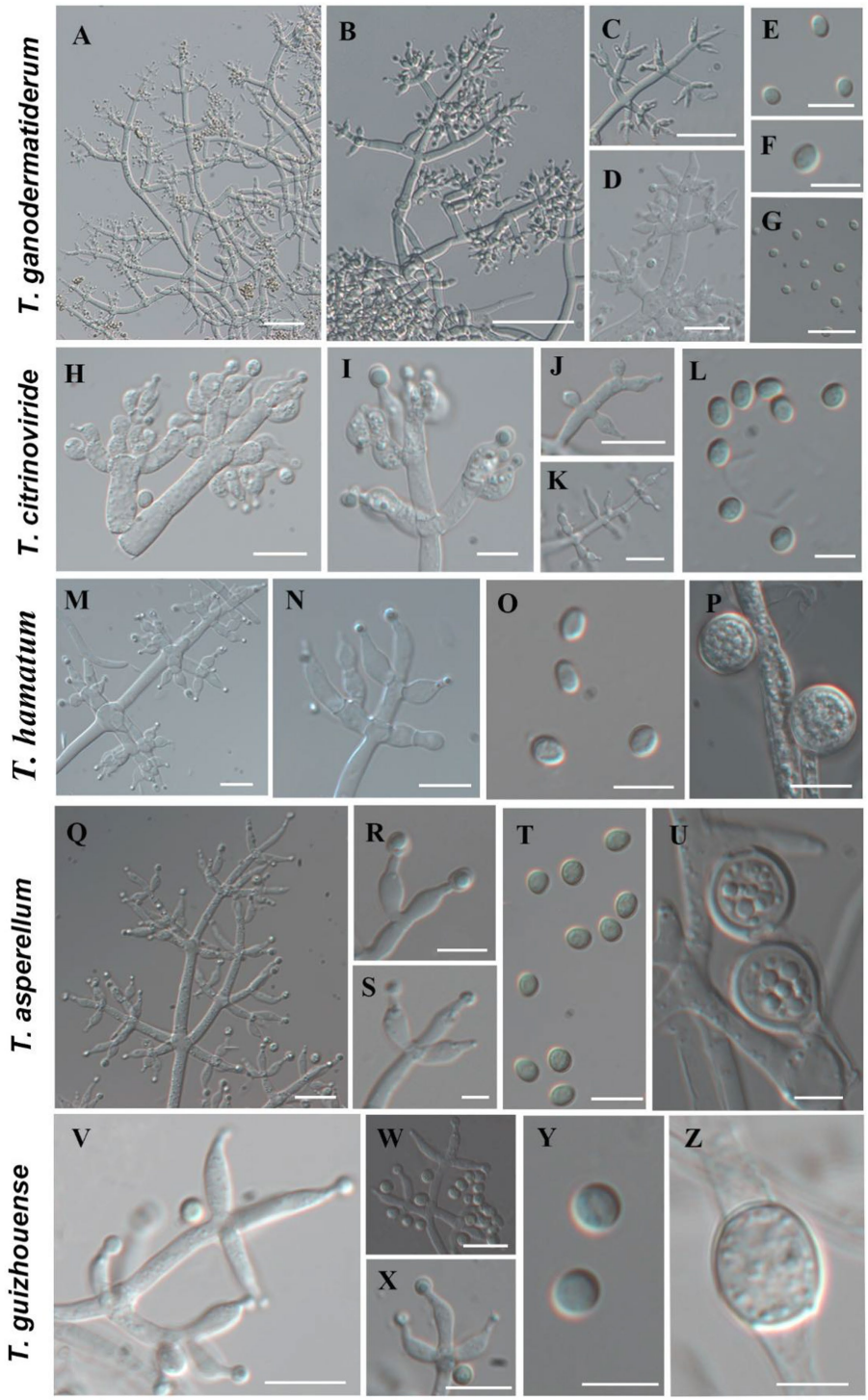

FIGURE 2
Morphological characteristics of *T. ganodermatiderum*, *T. citrinoviride*, *T. hamatum*, *T. asperellum*, *T. guizhouense*. (Scale bars: **A–D**, **J** = 40 μm; **G,K,M,N,Q** = 20 μm; **E,F,H,I,O,P,R–T,V–X** = 10 μm; **L,U,Y,Z** = 5 μm).

suspension. Two weeks after inoculation, all *Trichoderma* species showed similar green mold symptoms, as observed in Figure 6. Initially, small oval spots with white to pale green centers surrounded by a chlorotic area appeared on the *G. sichuanense* fruiting bodies 7 days post-inoculation. Over time, these lesions progressively increased in size and merged together. In severe cases, the infected fruiting bodies were completely covered by green spores. These symptoms observed under greenhouse conditions were consistent with the field symptoms of *G. sichuanense*. No symptoms were observed in the control group (Figure 6A).

Additionally, all *Trichoderma* species were consistently re-isolated and confirmed using morphological and molecular

10.3389/fmicb.2023.1264699

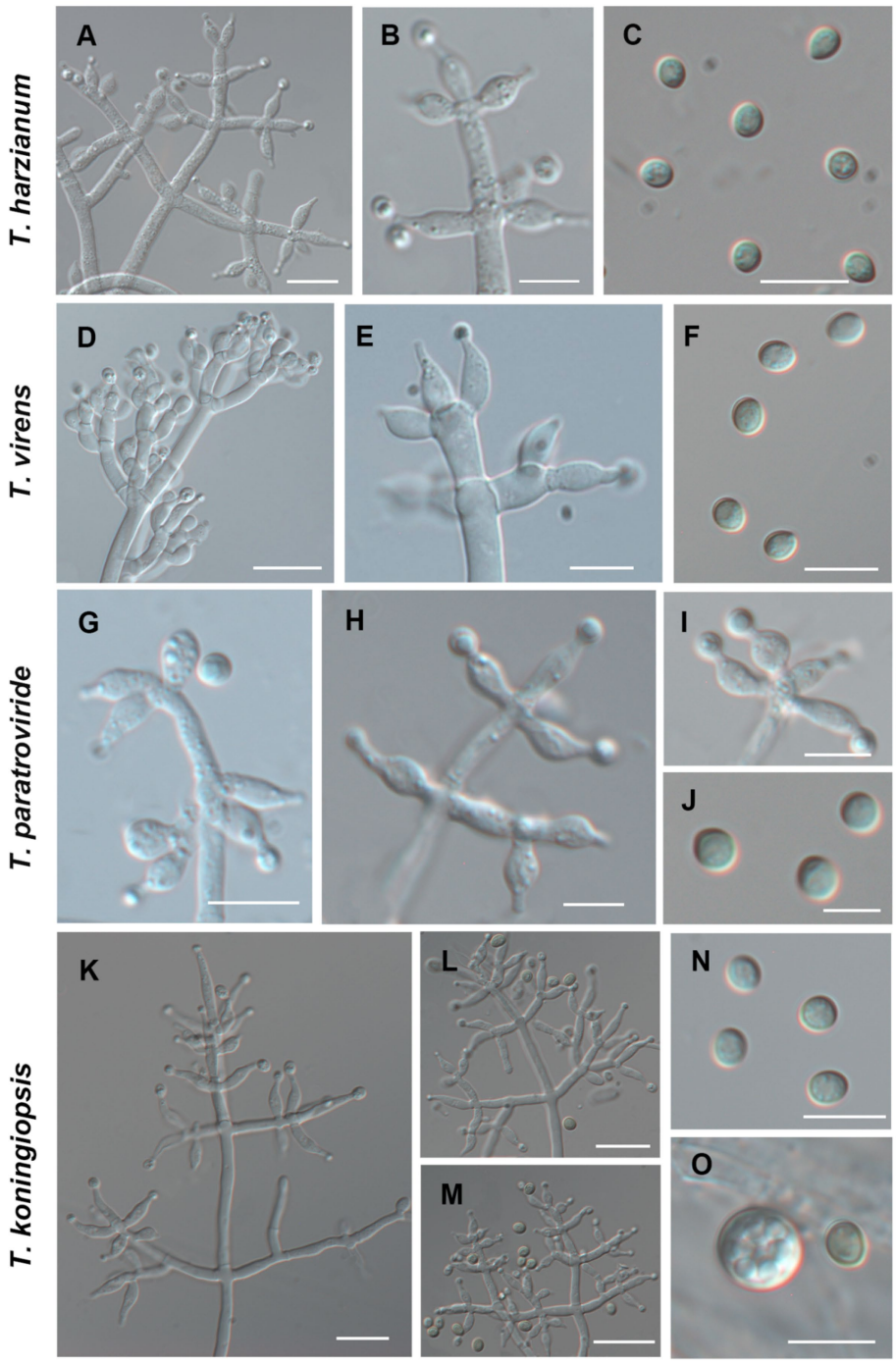

FIGURE 3
Morphological characteristics of *T. harzianum, T. virens, T. paratroviride, T. koningiopsis.* (Scale bars: **A,D,E,K–M** = 40 μm; **B,C,F,G–I,N,O** = 10 μm; **J** = 5 μm).

methods, while no *Trichoderma* isolates were obtained from the control group, satisfying Koch's postulates. The pathogenicity study demonstrated that all *Trichoderma* isolates induced green mold disease in *G. sichuanense* fruiting bodies upon inoculation. Among the isolates, *T. harzianum* exhibited the highest virulence (Figure 6J), followed by *T. citrinoviride* (Figure 6C), *T. paratroviride* (Figure 6H), *T. guizhouense* (Figure 6E), *T. ganodermatiderum* (Figure 6B), *T. asperellum* (Figure 6D), *T. virens* (Figure 6G), *T. koningiopsis* (Figure 6I), and *T. hamatum* (Figure 6F).

Effect of *Trichoderma* spp. on *G. sichuanense* mycelia

To assess the impact of different *Trichoderma* species on *G. sichuanense* mycelia, we conducted plate dual culture experiments. The results revealed that all *Trichoderma* species inhibited the growth of *G. sichuanense* mycelia and produced antagonistic lines. However, there were variations in the interactions between the nine *Trichoderma* species and *G. sichuanense* mycelia (Supplementary Figure S2).

10.3389/fmicb.2023.1264699

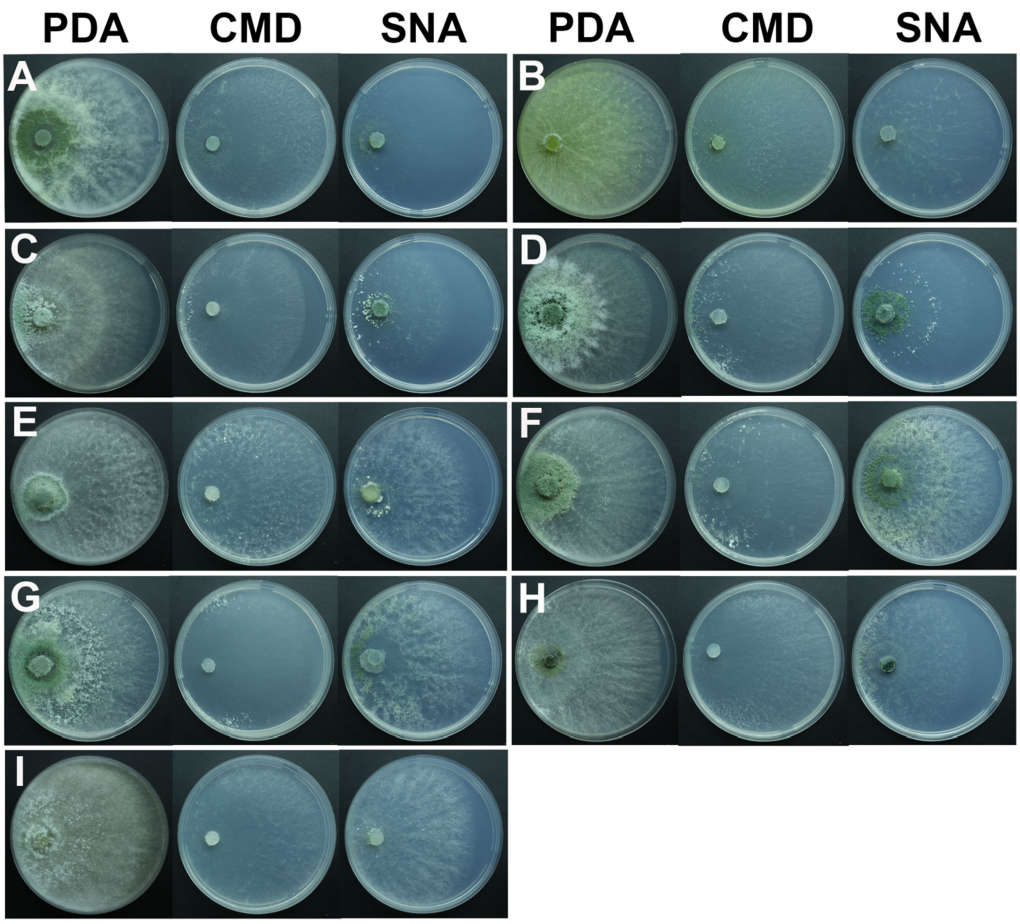

FIGURE 4
Colony appearance of representative isolates of 9 *Trichoderma* species. **(A)** *T. ganodermatiderum*; **(B)** *T. citrinoviride*; **(C)** *T. hamatum*; **(D)** *T. asperellum*; **(E)** *T. guizhouense*; **(F)** *T. harzianum*; **(G)** *T. virens*; **(H)** *T. paratroviride*; **(I)** *T. koningiopsis*.

Notably, *T. ganodermatiderum* (Supplementary Figure S2A), *T. citrinoviride* (Supplementary Figure S2B), *T. asperellum* (Supplementary Figure S2D), and *T. paratroviride* (Supplementary Figure S2H) exhibited significant inhibition on *G. sichuanense* mycelial growth, while *T. hamatum* (Supplementary Figure S2C), *T. guizhouense* (Supplementary Figure S2E), *T. harzianum* (Supplementary Figure S2F), *T. virens* (Supplementary Figure S2G) and *T. koningiopsis* (Supplementary Figure S2I) showed relatively milder inhibition.

In terms of mycelial morphology, *Trichoderma* mycelia demonstrated the ability to overgrow and spread on *G. sichuanense* mycelia, leading to the formation of irregular conidial clusters (Supplementary Figure S2). This resulted in the gradual withering of *G. sichuanense* mycelia. In some cases, certain *Trichoderma* strains completely covered the *G. sichuanense* mycelium with their spores. Additionally, we observed various pigments and antagonistic streaks on the back of the culture medium (Supplementary Figure S2).

Fungicide sensitivity of isolates and *G. sichuanense*

In order to assess the effectiveness of fungicides against green mold disease, we conducted tests using six different fungicides in this study. Initially, we selected nine *Trichoderma* isolates to evaluate their sensitivity to these fungicides. The results showed that the inhibitory effect of the fungicides on *Trichoderma* growth varied, with stronger inhibition observed at higher fungicide concentrations. Table 4 presents the results, highlighting that prochloraz-manganese exhibited the highest inhibitory effect among the tested fungicides, as indicated by its minimum EC50 value, while Mancozeb showed the weakest inhibition with the highest EC50 value.

Furthermore, we evaluated the inhibitory effects of the fungicides on the growth of *G. sichuanense* mycelium through extensive tests. Significant variations in the effects of the six fungicides on the growth of *G. sichuanense* mycelium were observed, which generally aligned with the effects observed on *Trichoderma* strains. Notably, prochloraz-manganese had the least impact on the growth of *G. sichuanense* mycelium, displaying the highest EC50 value while exhibiting the strongest inhibitory effect on *Trichoderma* mycelium (Table 4). These findings suggest that low concentrations of prochloraz-manganese can be effective in controlling *Trichoderma*. Additionally, prochloraz and carbendazim demonstrated good inhibitory effects on all *Trichoderma* strains (Supplementary Figures S3–S11).

TABLE 3 Microscopic characteristics of different *Trichoderma* isolates.

Species	Conidiophores and phialides	Conidia	Chlamydospores
T. ganodermatiderum	Tree-like, straight or slightly curved, with visible main axis and densely distributed branches. Phialides arranged in pairs or 3–5 wheels, 2.5–10.0 × 2.2–3.5 µm (Figures 2A–D)	Green, smooth-walled, subglobose to ellipsoidal, 3.0–4.8 × (2.5-) 2.8–3.8 µm (Figures 2E–G)	Not found
T. citrinoviride	Opposite or alternate, tree-like, with long main axis and short secondary branches. Phialides with 2–3 in 1 round, 3.5–5.2 × 1.8–3.5 µm (Figures 2H–K)	Chartreuse to green, smooth, ellipsoidal, 2.9–4.0 × 1.8–2.2 in size µm (Figure 2L)	Not found
T. hamatum	Main axis straight and highly branched, lateral branches opposite, few solitary. Phialides dense, short and chubby, 5–7.5 × 3.0–4.4 µm (Figures 2M,N)	Light green, smooth-walled, oblong, 4.1–5.0 × (2.5-) 3.0–3.5 µm (Figure 2O)	Spherical, terminal and intercalary, 8–12 × 6–10 µm (Figure 2P)
T. asperellum	Tree-like, lateral branches opposite, nearly perpendicular with main axios. Phialides symmetrically distributed, 7–11 × 2–4 µm (Figures 2Q–S)	Ellipsoidal, 3.5–5.0 × 3.0–4.2 µm (Figure 2T)	Subglobose, terminal or occasionally interstitial, smooth, 7–10 µm (Figure 2U)
T. guizhouense	Conidiophores in 2–3 whorls, occasional solitary growth. Phialides symmetrically distributed, conical, with a thin top, 5.5–11 × 2–3.5 µm (Figures 2V–X)	Spherical or subglobose, green, 2.0–3.2 × 2.0–3.0 µm (Figure 2Y)	Subglobose to ellipsoidal, intermediate, 5.5–8.6 × 4.7–7 µm (Figure 2Z)
T. harzianum	Tree-like, resembling a pyramid, main axis straight, many secondary branches. Phialides short, arranged in a circular pattern, usually in 3–4 whorls, occasionally opposite. (Figures 3A,B)	Spherical, subglobose, or obovate, smooth-walled, light green, 2.5–3.9 (−4.0) × 2.5–3.5 µm (Figure 3C)	Not found
T. virens	Irregular branching at the top, complex, with no branching at the base. Middle expansion of phialides, 4.0–6.5 × 3.0–5.0 µm (Figures 3D,E)	Green, smooth, broadly ellipsoid to obovate, 3.5–5.0 × 2.8–4.0 µm (Figure 3F)	Not found
T. paratroviride	Main axis is long, with branches in pairs or whorls, phialides usually arranged in 2–4 rounds, 5.0–8.5 × 2.5–3.0 µm (Figures 3G–I)	Subglobose, green, smooth, 3.0–4.0 × 3.0–3.5 µm (Figure 3J)	Not found
T. koningiopsis	Tree-like, longer main axis, branches growing alone or in pairs, at right angles to the main axis. Phialides slender, middle enlarged, 5.0–7.5 × 3.0–4.8 µm (Figures 3K–M)	Ellipsoidal, green, 4.0–5.0 × 2.8–3.2 µm (Figure 3N)	Spherical, green, 7.5–10.4 µm (Figure 3O)

Discussion

Green mold disease caused by *Trichoderma* species poses significant challenges in *G. sichuanense* cultivation, leading to economic losses and hindering industry growth (Lu et al., 2016; Huang et al., 2018; Zhang et al., 2018; Cai et al., 2020; An et al., 2022). This study aimed to comprehensively investigate *Trichoderma* species associated with *G. sichuanense*, focusing on their identification, characterization, pathogenicity assessment, and evaluation of fungicide efficacy. By addressing these objectives, we aimed to provide valuable insights into disease management strategies and the development of effective control measures for *G. sichuanense* cultivation.

Through morphological and molecular analyses, we successfully identified nine *Trichoderma* species associated with *G. sichuanense*: *T. asperellum, T. citrinoviride, T. ganodermatiderum, T. guizhouense, T. hamatum, T. harzianum, T. koningiopsis, T. paratroviride, and T. virens* (Lu et al., 2016; Huang et al., 2018; Zhang et al., 2018; Cai et al., 2020; An et al., 2022). These findings contribute to our understanding of the diversity and population dynamics of *Trichoderma* species associated with *G. sichuanense*, providing valuable insights for further research and disease management strategies.

A comprehensive understanding of the diversity and distribution of *Trichoderma* species in *G. sichuanense* cultivation is crucial for developing effective strategies to manage green mold disease. Our study revealed a wide range of *Trichoderma* species associated with green mold disease in *G. sichuanense*, including species known to affect mushrooms worldwide. Previous studies have also identified *Trichoderma* species as causative agents of green mold disease in various mushroom hosts, such as *Agaricus bisporus*, *Pleurotus ostreatus*, *Lentinula edodes*, *Flammulina filiformis*, *Tricholoma matsutake*, and *Dictyophora rubrovolvata* (Choi et al., 1998; Kosanović et al., 2015, 2020; Wang et al., 2016; Seung et al., 2018; Innocenti et al., 2019; Chen et al., 2021). These findings emphasize the broad host range of *Trichoderma* species and their significant economic impact on global mushroom cultivation.

Comparing our results with previous studies on *Trichoderma* species associated with *G. sichuanense*, we confirmed the presence of several previously reported species, including *T. asperellum*, *T. citrinoviride*, *T. guizhouense*, *T. hamatum*, *T. paratroviride*, and *T. virens* (Bissett et al., 2015; Zhu et al., 2017; An et al., 2022). However, our identification of *T. ganodermatiderum* in this specific cultivation system confirms its previously reported association as a pathogen on *G. sichuanense* (An et al., 2022). The incorporation of molecular data, specifically TEF1-a and RPB2 gene sequences, in our identification process significantly enhanced the accuracy and reliability of species identification. This approach contributes to a more comprehensive understanding of *Trichoderma* populations in *G. sichuanense* cultivation and adds to the growing body of knowledge on *Trichoderma* diversity associated with specific host plants.

The confrontation assay demonstrated that *Trichoderma* species effectively overgrow and spread on *G. sichuanense* mycelia, leading to the formation of irregular conidial clusters and the gradual withering

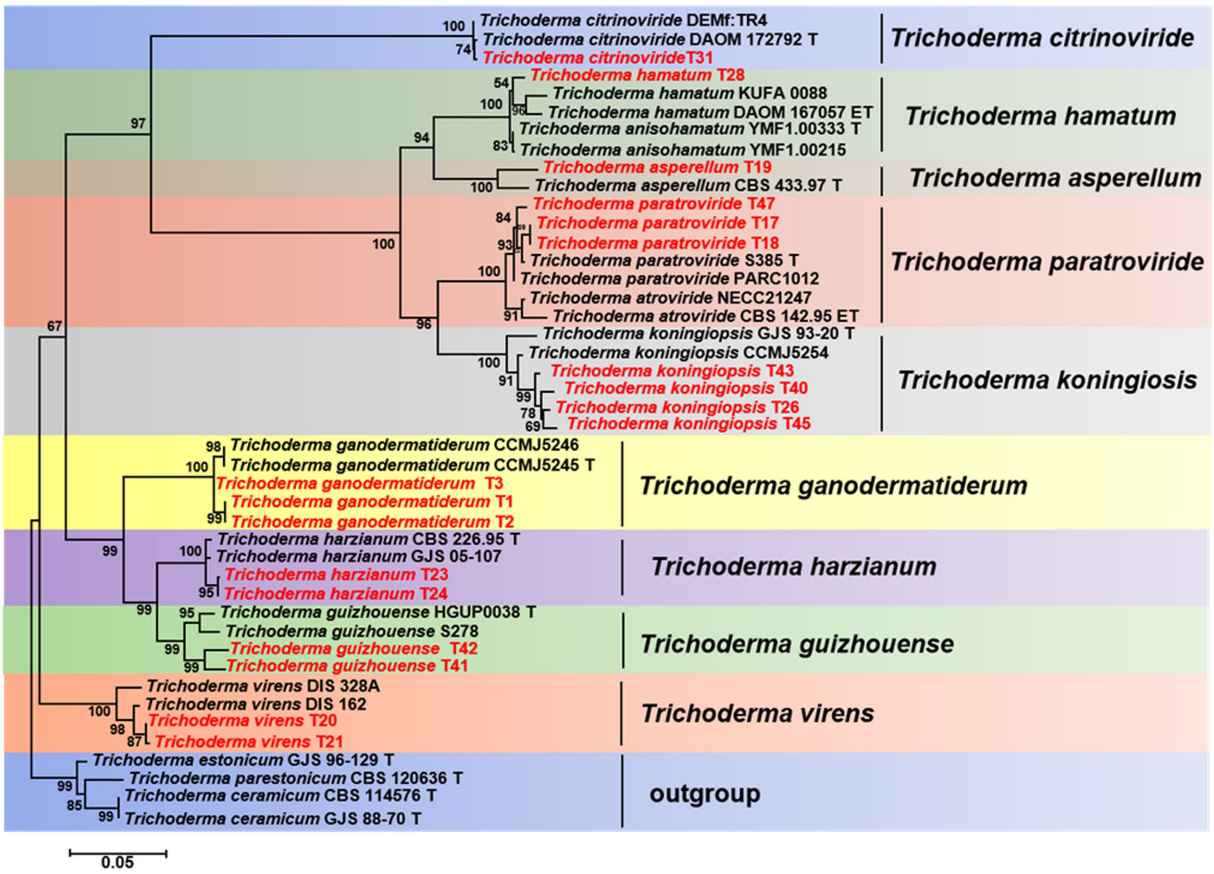

FIGURE 5
Phylogenetic tree illustrating the relationships among 19 *Trichoderma* isolates from *Ganoderma sichuanense* based on the combined TEF-1a and RPB2 genes using PhyML analysis. Bootstrap support values equal to or greater than 70% are shown at the nodes. *T. estonicum* and *T. ceramicum* were used as the outgroup. The isolates obtained in this study are highlighted in red.

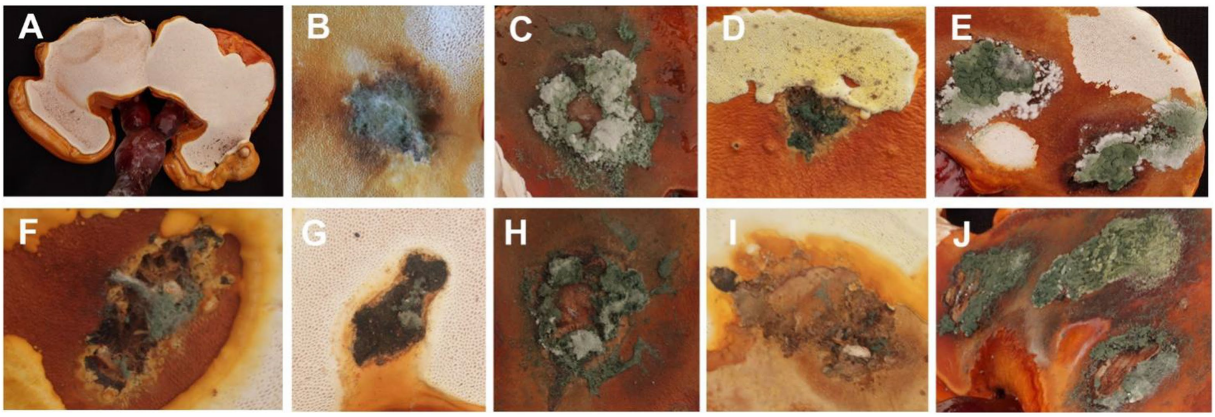

FIGURE 6
(A) CK; **(B)** *T. ganodermatiderum*; **(C)** *T. citrinoviride*; **(D)** *T. asperellum*; **(E)** *T. guizhouense*; **(F)** *T. hamatum*; **(G)** *T. virens*; **(H)** *T. paratroviride*; **(I)** *T. Koningiopsis*; **(J)** *T. harzianum.*

of the mycelia. Some *Trichoderma* strains completely covered the *G. sichuanense* mycelium with their spores. The presence of pigments and antagonistic streaks on the culture medium further confirmed the antagonistic behavior of *Trichoderma* species against *G. sichuanense*. These findings indicate that the identified *Trichoderma* species have the ability to suppress the growth of *G. sichuanense* mycelia and can be considered as pathogens causing green mold disease in *G. sichuanense*. The pigments produced by *Trichoderma* species may

TABLE 4 Mean effective concentration to cause inhibition of by 50% (EC50) values of nine *Trichoderma* isolates from China to six fungicides.

Isolates	EC50 (μg mL^{-1})					
	Mancozeb	Chlorothalonil	Fludioxinil	Prochloraz	Carbendazim	Prochlorza-Mn
T. ganodermatiderum	78.81 ± 0.0245	3.381 ± 0.00137	2.786 ± 0.0012	0.0069 ± 0.0001	0.0086 ± 0.0001	0.0013 ± 0.0001
T. citrinoviride	180.4 ± 0.7359	8.9910 ± 0.0008	0.0445 ± 0.0012	0.0519 ± 0.0010	0.0301 ± 0.0008	0.0040 ± 0.0008
T. hamatum	47.51 ± 0.3764	0.0469 ± 0.0009	0.0029 ± 0.0006	0.0033 ± 0.0005	0.0059 ± 0.0005	0.0014 ± 0.0006
T. asperellum	129.1 ± 0.3764	0.5085 ± 0.0006	0.0377 ± 0.0004	0.0342 ± 0.0008	0.0073 ± 0.0006	0.0051 ± 0.0005
T. guizhouense	4.375 ± 0.1256	4.907 ± 0.0006	103.4 ± 0.9908	0.7338 ± 0.0079	0.0107 ± 0.0071	0.0047 ± 0.0015
T. virens	29.04 ± 0.1059	0.3593 ± 0.0135	139.6 ± 0.1351	0.0125 ± 0.0078	0.0073 ± 0.0107	0.0031 ± 0.0061
T. paratroviride	101.9 ± 0.0522	0.0462 ± 0.0062	0.0286 ± 0.0069	0.8578 ± 0.0005	0.0131 ± 0.0023	0.0082 ± 0.0009
T. harzianum	114.2 ± 0.0482	0.0082 ± 0.0002	105.9 ± 0.0157	0.0061 ± 0.0002	0.0155 ± 0.0002	0.0045 ± 0.0001
T. koningiopsis	30.20 ± 0.0026	0.0067 ± 0.0001	0.0019 ± 0.0001	7.432 ± 0.0001	0.0683 ± 0.0002	0.0051 ± 0.0001
G. sichuanense	11.06 ± 0.0019	3.622 ± 0.0002	0.1211 ± 0.0002	3.443 ± 0.0003	8.573 ± 0.0002	17.22 ± 0.0002

play a role in their antagonistic behavior against *G. sichuanense* by acting as defense mechanisms, allowing *Trichoderma* to outcompete and suppress the growth of *G. sichuanense* mycelia (Kubicek et al., 2019; Robinson, 2022).

Further research should focus on investigating the specific mechanisms underlying the inhibition of *G. sichuanense* mycelial growth by *Trichoderma* species, as well as characterizing and understanding the role of the pigments and metabolites produced by *Trichoderma*. Such studies will provide valuable insights into the interaction between *Trichoderma* and *G. sichuanense* and contribute to the development of effective strategies for managing green mold disease.

The effectiveness of fungicides in controlling green mold disease caused by *Trichoderma* species is crucial for successful mushroom cultivation. In this study, we evaluated the efficacy of six different fungicides against *Trichoderma* growth and their inhibitory effects on *G. sichuanense* mycelium. Our results revealed varying levels of inhibition on *Trichoderma* growth by the tested fungicides. The inhibitory effect was stronger at higher fungicide concentrations (Table 4). Prochloraz-manganese exhibited the highest inhibitory effect, as evidenced by its minimum EC50 value (Shamshad et al., 2009), while Mancozeb showed the weakest inhibition with the highest EC50 value. These findings highlight the dependence of fungicide effectiveness on both the specific fungicide used and its concentration. Furthermore, we investigated the effects of the fungicides on the growth of *G. sichuanense* mycelium. Interestingly, the inhibitory effects of the six fungicides on *G. sichuanense* mycelium generally aligned with their effects on *Trichoderma* strains. Notably, despite exhibiting the strongest inhibitory effect on *Trichoderma* mycelium, prochloraz-manganese had the least impact on *G. sichuanense* mycelium growth (Table 4; Hatvani, 2008; Grogan and Jukes, 2010). This suggests that prochloraz-manganese can effectively control *Trichoderma* without severely affecting the growth of *G. sichuanense* mycelium, even at low concentrations.

The results indicate that prochloraz and carbendazim exhibited strong inhibitory effects on all tested Trichoderma strains (Supplementary Figure S3–S11), suggesting their potential as broad-spectrum fungicides for controlling *Trichoderma* species in mushroom cultivation (Innocenti et al., 2019). These findings underscore the importance of selecting fungicides based on their specific inhibitory effects on Trichoderma species, taking into account their compatibility with the growth of the mushroom host. Notably, prochloraz-manganese, prochloraz, and carbendazim have shown promise in effectively managing Trichoderma growth while minimizing their impact on *G. sichuanense* mycelium.

However, it is important to consider the potential development of fungicide resistance and the long-term sustainability of fungicide use in disease management strategies. To mitigate the economic losses associated with green mold disease while minimizing negative impacts on mushroom production and the environment (Potocnik et al., 2015), alternative control measures and integrated disease management approaches should be explored. These measures can incorporate cultural practices and biological control agents. Such approaches would enhance the sustainability of mushroom cultivation and reduce reliance on fungicides.

There are several limitations to consider in this study. Firstly, the survey was conducted in a specific geographic region of China, including Zhejiang, Hubei, and Jilin Province. Therefore, the findings may not be representative of the entire country or other regions where *G. sichuanense* is cultivated. Further studies in different regions and countries would provide a more comprehensive understanding of the prevalence and diversity of *Trichoderma* species causing green mold disease in *G. sichuanense*. Secondly, while morphological and phylogenetic analysis were employed to classify the isolated *Trichoderma* strains into different species, these methods have certain limitations. Additional molecular techniques, such as DNA sequencing or genotyping, would provide more precise identification and a deeper understanding of the genetic diversity and relationships among the *Trichoderma* pathogens.

Furthermore, this study focused primarily on the pathogenicity of the identified *Trichoderma* species through inoculation tests on healthy *G. sichuanense* fruiting bodies. The investigation of other factors influencing the disease development, such as environmental conditions, host resistance, or interactions with other microorganisms, was not extensively explored. A more comprehensive study incorporating these factors would provide a more holistic understanding of green mold disease in *G. sichuanense*. Lastly, the sensitivity of the *Trichoderma* species to fungicides was assessed using a limited number of commercially available fungicides. The evaluation of additional fungicides or alternative management approaches would contribute to a more comprehensive understanding of effective control measures for green mold disease. Addressing these limitations in future research

endeavors would help to enhance our understanding of the prevalence, genetic diversity, pathogenicity mechanisms, and effective management strategies for *Trichoderma* species causing green mold disease in *G. sichuanense*.

In summary, our study provides valuable insights into the host range of *Trichoderma* species associated with *G. sichuanense* and their susceptibility to *T. guizhouense*, *T. virens*, *T. hamatum*, *T. paratroviride*, *T. asperellum*, and *T. citrinoviride*. Furthermore, we have evaluated the effectiveness of selected fungicides in controlling green mold disease, offering valuable information for disease prevention and management in edible fungi. These findings are of significant importance for the effective control of green mold disease on *G. sichuanense* in China. our study also contributes to the existing knowledge on the effectiveness of fungicides against *Trichoderma* and their impact on *G. sichuanense* mycelium. These findings provide a foundation for the development of robust disease management strategies and underscore the importance of continued research to enhance the sustainability of mushroom cultivation. By understanding the sensitivity of *Trichoderma* strains and the efficacy of fungicides, we can develop targeted strategies for disease management. However, it is crucial to conduct further research to explore sustainable approaches that minimize potential fungicide resistance and environmental impacts in mushroom cultivation.

Data availability statement

The data presented in the study are deposited in the NCBI repository. TEF-1a sequence accession numbers: OR291383-OR291398; RPB2 sequence accession numbers: OR291399-OR291417; ITS sequence accession numbers: OR569141-OR569159.

Author contributions

XuL: Conceptualization, Data curation, Formal analysis, Investigation, Methodology, Resources, Software, Validation, Visualization, Writing – original draft, Writing – review & editing. FS: Formal analysis, Methodology, Resources, Software, Visualization, Writing – review & editing. YT: Data curation, Investigation, Methodology, Resources. JH: Conceptualization, Methodology, Resources, Software. QW: Methodology, Validation. SL: Methodology, Validation. NR: Methodology, Validation. MW-K: Formal analysis, Visualization. CL: Investigation, Resources, Visualization. BZ: Funding acquisition, Project administration, Supervision, Visualization, Writing – review & editing. XiL: Conceptualization, Investigation, Project administration, Resources, Supervision, Visualization, Writing – review & editing. YL: Conceptualization, Funding acquisition, Project administration, Supervision, Visualization, Writing – review & editing.

Funding

The author(s) declare financial support was received for the research, authorship, and/or publication of this article. This work was financed by the Diversity and conservation of characteristic macrofungi resources in different vegetation zones in Changbai Mountain of China (20230202119NC), Natural Science Foundation of China (nos. 31970020), the Scientific and Technological Tackling Plan for the Key Fields of Xinjiang Production and Construction Corps (no. 2021AB004), Research on the Creation of Excellent Edible Mushroom Resources and High Quality & Efficient Ecological Cultivation Technology in Jiangxi Province (20212BBF61002), Modern Agroindustry Technology Research System (CARS20), and 111 program (no. D17014).

Acknowledgments

We would like to express our gratitude to Xiulian Duan, Director of Jigu Biotechnology Co., Ltd. in Jilin Province, for kindly providing the mushroom bags of *G. sichuanense*. Additionally, we extend our thanks to Jianquan Zhu, Director of Fuzhidao Biotechnology Co., Ltd. in Jilin Province, for assisting us with the collection of green mold samples from *G. sichuanense* fruiting bodies.

Conflict of interest

The authors declare that the research was conducted in the absence of any commercial or financial relationships that could be construed as a potential conflict of interest.

Publisher's note

Supplementary material

The Supplementary material for this article can be found online at: https://www.frontiersin.org/articles/10.3389/fmicb.2023.1264699/full#supplementary-material

References

An, X. Y., Cheng, G. H., Gao, H. X., Li, X. F., Yang, Y., Li, D., et al. (2022). Phylogenetic analysis of *Trichoderma* species associated with green mold disease on mushrooms and two new pathogens on *Ganoderma sichuanense*. *J. Fungi* 8:704. doi: 10.3390/jof8070704

Bissett, J. (1984). A revision of the genus *Trichoderma*. I. Section *Longibrachiatum* sect. nov. *Can. J. Bot.* 62, 924–931. doi: 10.1139/b84-131

Bissett, J., Gams, W., Jaklitsch, W., and Samuels, G. J. (2015). Accepted *Trichoderma* names in the year 2015. *IMA Fungus* 6, 263–295. doi: 10.5598/imafungus.2015.06.02.02

Cai, F., and Druzhinina, I. S. (2021). In honor of John Bissett: authoritative guidelines on molecular identification of *Trichoderma*. *Fungal Divers.* 107, 1–69. doi: 10.1007/s13225-020-00464-4

Cai, M., Idrees, M., Zhou, Y., Zhang, C., and Xu, J. (2020). First report of green mold disease caused by *Trichoderma hengshanicum* on *Ganoderma lingzhi*. *Mycobiology* 48:427-430. doi: 10.1080/12298093.2020.1794230

Chaverri, P., Branco-Rocha, F., Jaklitsch, W., Gazis, R., Degenkolb, T., et al. (2015). Systematics of the *Trichoderma harzianum* species complex and the re-

identification of commercial biocontrol strains. *Mycologia* 107, 558–590. doi: 10.3852/14-147

Chaverri, P., Castlebury, L. A., Samuels, G. J., and Geiser, D. M. (2003). Multilocus phylogenetic structure within the *Trichoderma harzianum*/*Hypocrea lixii* complex. *Mol. Phylogenet. Evol.* 27, 302–313. doi: 10.1016/S1055-7903(02)00400-1

Chen, X. Y., Zhou, X. H., Zhao, J., Tang, X. L., Pasquali, M., Migheli, Q., et al. (2021). Occurrence of green mold disease on *Dictyophora rubrovolvata* caused by *Trichoderma koningiopsis*. *J. Plant Pathol.* 103, 981–984. doi: 10.1007/s42161-021-00861-x

Chen, K., and Zhuang, W. Y. (2017). Discovery from a large-scaled survey of *Trichoderma* in soil of China. *Sci. Rep.* 7:9090. doi: 10.1038/s41598-017-07807-3

China Edible Fungi Association (2020). Available at: http://www.cefa.org.cn/web/index.html

Chiu, H. F., Fu, H. Y., Lu, Y. Y., Han, Y. C., Shen, Y. C., Venkatakrishnan, K., et al. (2017). Triterpenoids and polysaccharide peptides-enriched *Ganoderma lucidum*: a randomized, double-blind placebo-controlled crossover study of its antioxidation and hepatoprotective efficacy in healthy volunteers. *Pharm. Biol.* 55, 1041–1046. doi: 10.1080/13880209.2017.1288750

Choi, I. Y., Lee, W. H., and Choi, J. S. (1998). Forest green mold disease caused by *Trichoderma pseudokoningii* in winter mushroom, *Flammulina velutipes*. *Korean J. Mycol.* 26, 531–537.

Edgar, R. C. (2004). MUSCLE: multiple sequence alignment with high accuracy and high throughput. *Nucleic Acids Res.* 32, 1792–1797. doi: 10.1093/nar/gkh340

Etebarian, H. R., Sholberg, P. L., Eastwell, K. C., and Sayler, R. J. (2005). Biological control of apple blue mold with *Pseudomonas fluorescens*. *Can. J. Microbiol.* 51, 591–598. doi: 10.1139/w05-039

Gams, W., and Bissett, J. (1998). Morphology and identification of *Trichoderma*. *Trichoderma Gliocladium* 1, 3–34.

Grogan, H. M., and Jukes, A. A. (2010). Persistence of the fungicides thiabendazole, carbendazim and prochloraz-Mn in mushroom casing soil. *Pest Manag. Sci.* 59, 1225–1231. doi: 10.1002/ps.759

Guindon, S., Dufayard, J. F., Lefort, V., Anisimova, M., Hordijk, W., and Gascuel, O. (2010). New algorithms and methods to estimate maximum-likelihood phylogenies: assessing the performance of PhyML 3.0. *Syst. Biol.* 59, 307–321. doi: 10.1093/sysbio/syq010

Hall, T. A. (1999). Bioedit: a user-friendly biological sequence alignment editor and analysis program for windows 95/98/Nt. *Nucleic Acids Symp.* 41, 95–98. doi: 10.1021/bk-1999-0734.ch008

Hall, T. A. (2011). BioEdit: an important software for molecular biology. *Gerf Bull Biosci.* 2, 60–61.

Hatvani, L. (2008). *Mushroom pathogenic Trichoderma species: occurrence, diagnosis and extracellular enzyme production*. PhD thesis. Szeged, Hungary: University of Szeged

Huang, X., and Madan, A. (1999). CAP3: a DNA sequence assembly program. *Genome Res.* 9, 868–877. doi: 10.1101/gr.9.9.868

Huang, X. W., Yan, Y. H., Zhang, T., Geng, L. J., Cheng, Z., et al. (2018). Isolation, identification and rapid detection of the pathogen causing green mold on *Ganoderma lingzhi*. *J. Plant Prot.* 45, 1435–1436. (in Chinese)

Innocenti, G., Montanari, M., Righini, H., and Roberti, R. (2019). *Trichoderma* species associated with green mould disease of *Pleurotus ostreatus* and their sensitivity to prochloraz. *Plant Pathol.* 68. doi: 10.1111/ppa.12953

Jaklitsch, M. W. (2009). European species of Hypocrea. Part I. The green-spored species. *Stud. Mycol.* 63, 1–91. doi: 10.3114/sim.2009.63.01

Jaklitsch, W. M., Komon, M., Kubicek, C. P., and Druzhinina, I. S. (2005). *Hypocrea voglmayrii* sp. nov. from the Austrian Alps represents a new phylogenetic clade in *Hypocrea*/*Trichoderma*. *Mycologia* 97, 1365–1378. doi: 10.3852/mycologia.97.6.1365

Kang, H. J., Sigler, L., Lee, J., Gibas, C. F., Yun, S. H., et al. (2010). *Xylogone ganodermophthora* sp. nov., an ascomycetous pathogen causing yellow rot on cultivated mushroom *Ganoderma lucidum* in Korea. *Mycologia* 102, 1167–1184. doi: 10.3852/09-304

Kim, C. H., Hassan, O., and Chang, T. (2020). Diversity, pathogenicity, and fungicide sensitivity of *Colletotrichum* species associated with apple anthracnose in South Korea. *Plant Dis.* 104, 2866–2874. doi: 10.1094/PDIS-01-20-0050-RE

Kosanović, D., Grogan, H., and Kavanagh, K. (2020). Exposure of *Agaricus bisporus* to *Trichoderma aggressivum* f. *europaeum* leads to growth inhibition and induction of an oxidative stress response. *Fungal Biol.* 124, 814–820. doi: 10.1016/j.funbio.2020.07.003

Kosanović, D., Potočnik, I., Vukojević, J., Stajić, M., Rekanović, E., Stepanović, M., et al. (2015). Fungicide sensitivity of *Trichoderma* spp. from *Agaricus bisporus* farms in Serbia. *J. Environ. Sci. Health B* 50, 607–613. doi: 10.1080/03601234.2015.1028849

Krobthong, S., Choowongkomon, K., Suphakun, P., Kuaprasert, B., and Yingchutrakul, Y. (2021). The anti-oxidative effect of Lingzhi protein hydrolysates on lipopolysaccharide-stimulated A549 cells. *Food Biosci.* 41:101093. doi: 10.1016/j.fbio.2021.101093

Kubicek, C. P., Steindorff, A. S., Chenthamara, K., Manganiello, G., Henrissat, B., et al. (2019). Evolution and comparative genomics of the most common *Trichoderma* species. *BMC Genomics* 20:485. doi: 10.1186/s12864-019-5680-7

Lanfear, R., Frandsen, P. B., Wright, A. M., Senfeld, T., and Calcott, B. (2017). PartitionFinder 2: new methods for selecting partitioned models of evolution for molecular and morphological phylogenetic analyses. *Mol. Biol. Evol.* 34, 772–773. doi: 10.1093/molbev/msw260

Liu, Y. J., Whelen, S., and Hall, B. D. (1999). Phylogenetic relationships among ascomycetes: evidence from an RNA polymerse II subunit. *Mol. Biol. Evol.* 1799-1808. doi: 10.1093/oxfordjournals.molbev.a026092

Lu, B. H., Zuo, B., Liu, X. L., Feng, J., Wang, Z. M., and Gao, J. (2016). *Trichoderma harzianum* causing green mold disease on cultivated *Ganoderma lucidum* in Jilin province, China. *Plant Disease* 100:2524. doi: 10.1094/PDIS-04-16-0422-PDN

Pan, Y., and Lin, Z. B. (2019). Anti-aging effect of *Ganoderma* (Lingzhi) with health and fitness. *Adv. Exp. Med. Biol.* 1182, 299–309. doi: 10.1007/978-981-32-9421-9_13

Park, M. S., Bae, K. S., and Yu, S. H. (2006). Two new species of *Trichoderma* associated with green mold of oyster mushroom cultivation in Korea. *Mycobiology* 34, 111–113. doi: 10.4489/MYCO.2006.34.3.111

Potocnik, I., Stepanovic, M., Rekanovic, E., Todorovic, B., and Milijasevic, M. S. (2015). Disease control by chemical and biological fungicides in cultivated mushrooms: button mushroom, oyster mushroom and shiitake. *Pestic. Phytomed* 30, 201–208. doi: 10.2298/PIF1504201P

Qiu, Z., Zhong, D., and Yang, B. (2019). Preventive and therapeutic effect of *Ganoderma* (Lingzhi) on liver injury. *Adv. Exp. Med. Biol.* 1182, 217–242. doi: 10.1007/978-981-32-9421-9_9

Rahman, M. A., Abdullah, N., and Aminudin, N. (2018). Evaluation of the anti-oxidative and hypocholesterolemic effects of Lingzhi or Reishi medicinal mushroom, *Ganoderma lucidum* (Agaricomycetes), in ameliorating cardiovascular diseases. *Int. J. Med. Mushrooms* 20, 961–969. doi: 10.1615/IntJMedMushrooms.2018028370

Rahman, M. A., Hossain, S., Abdullah, N., and Aminudin, N. (2020). Lingzhi or Reishi medicinal mushroom, *Ganoderma lucidum* (Agaricomycetes) ameliorates spatial learning and memory deficits in rats with hypercholesterolemia and alzheimer's disease. *Int J Med Mushrooms.* 22, 93–103. doi: 10.1615/IntJMedMushrooms.2020033383

Robinson, S. C. (2022). Colorants produced by *Penicillium murcianum* are a natural moldicide against *Trichoderma* and other *Penicillium* species. *Coatings* 12:821. doi: 10.3390/coatings12060821

Seaby, A. (1987). Infection of mushroom compost by *Trichoderma* species. *Mushroom J.* 179, 355–361.

Seung, Y. O., Myung, S. P., Hae, J. C., and Young, W. L. (2018). Diversity and effect of *Trichoderma* isolated from the roots of *Pinus densiflora* within the fairy ring of pine mushroom (*Tricholoma matsutake*). *PLoS One* 13:e0205900. doi: 10.1371/journal.pone.0205900

Shah, S., Nasreen, S., and Kousar, S. (2013). Efficacy of fungicides against *Trichoderma* spp. causing green mold disease of oyster mushroom (*Pleurotus sajor-caju*). *Res. J. Microbiol.* 8, 13–24. doi: 10.3923/jm.2013.13.24

Shamshad, A., Clift, A. D., and Mansfield, S. (2009). Imazalil, manganese prochloraz and carbendazim treatments do not affect the yield of *Agaricus bisporus*, hybrid strain Sylvan A15 in New South Wales. *Plant Prot. Quart.* 24, 50–54. doi: 10.1586/1744666X.2016.1133295

Wang, G. Z., Cao, X. T., Ma, X. L., Guo, M. P., Liu, C. H., Yan, L., et al. (2016). Diversity and effect of *Trichoderma* spp. associated with green mold disease on *Lentinula edodes* in China. *Microbiology* 5, 709–718. doi: 10.1002/mbo3.364

Wang, Y., Fan, X., and Wu, X. (2020). *Ganoderma lucidum* polysaccharide (GLP) enhances antitumor immune response by regulating differentiation and inhibition of MDSCs via a CARD9-NF-κB-IDO pathway. *Biosci. Rep.* 40:BSR20201170. doi: 10.1042/BSR20201170

Wang, X. C., Xi, R. J., Li, Y., Wang, D. M., and Yao, Y. J. (2012). The species identity of the widely cultivated *Ganoderma*, '*G. lucidum*' (Ling-zhi), in China. *PLoS One* 7:e40857. doi: 10.1371/journal.pone.0040857

Wong, F. P., and Midland, S. L. (2007). Sensitivity distributions of California populations of *Colletotrichum cereale* to the DMI fungicides propiconazole, myclobutanil, tebuconazole, and triadimefon. *Plant Dis.* 91, 1547–1555. doi: 10.1094/PDIS-91-12-1547

Wu, Q., Li, Y., Peng, K., Wang, X. L., Ding, Z. Y., et al. (2019). Isolation and characterization of three antihypertension peptides from the mycelia of *Ganoderma lucidum* (Agaricomycetes). *J. Agric. Food Chem.* 67, 1–11. doi: 10.1021/acs.jafc.9b02276

Xiao, C., Wu, Q., Zhang, J., Xie, Y., Cai, W., et al. (2016). Antidiabetic activity of *Ganoderma lucidum* polysaccharides F31 down-regulated hepatic glucose regulatory enzymes in diabetic mice. *J. Ethnopharmacol.* 196, 47–57. doi: 10.1016/j.jep.2016.11.044

Yan, Y., Xu, J., Zhang, C., Moodley, O., and Zhang, L. (2019). Green mold on *Ganoderma lingzhi* (Agaricomycetes) caused by *Trichoderma atroviride*. *Int. J. Med. Mushrooms* 21, 515–521. doi: 10.1615/IntJMedMushrooms.2019030352

Zhang, D., Gao, F., Jakovlić, I., Zou, H., Zhang, J., Li, W. X., et al. (2020). Phylosuite: an integrated and scalable desktop platform for streamlined molecular sequence data management and evolutionary phylogenetics studies. *Mol. Ecol. Resour.* 20, 348–355. doi: 10.1111/1755-0998.13096

Zhang, T., Lu, M. Z., Zhang, C. L., and Xu, J. Z. (2018). First report of *Trichoderma longibrachiatum* causing green mold disease on *Ganoderma lingzhi*. *Plant Dis.* 103. doi: 10.1094/PDIS-05-18-0818-PDN

Zhao, J. D., Xu, L. W., and Zhang, X. Q. (1983). Taxonomic studies on the family Ganodermataceae of China II. *Acta Mycol. Sin.* 2, 159–167. doi: 10.13346/j.mycosystema.1983.03.003 (In Chinese).

Zhu, Z. X., Xu, H. X., Zhuang, W. Y., and Li, Y. (2017). Two new green-spored species of *Trichoderma* (Sordariomycetes, Ascomycota) and their phylogenetic positions. *MycoKeys* 26, 61–75. doi: 10.3897/mycokeys.26.14919

Zhu, L. F., Yao, Y. F., Ahmad, Z., and Chang, M. W. (2019). Development of *Ganoderma lucidum* spore powder based proteoglycan and its application in hyperglycemic, antitumor and antioxidant function. *Process Biochem.* 2019, 103–111. doi: 10.1016/j.procbio.2019.05.025

Zuo, B., Lu, B. H., Liu, X. L., Wang, Y., Ma, G. L., and Gao, J. (2016). First report of *Cladobotryum mycophilum* causing cobweb on *Ganoderma lucidum* cultivated in Jilin Province, China. *Plant Dis.* 100:1239. doi: 10.1094/PDIS-12-15-1431-PDN

frontiers | Frontiers in Microbiology

TYPE Original Research
PUBLISHED 30 October 2023
DOI 10.3389/fmicb.2023.1280420

OPEN ACCESS

EDITED BY
Chenyang Huang,
Chinese Academy of Agricultural Sciences, China

REVIEWED BY
Wei Gao,
Chinese Academy of Agricultural Sciences (CAAS), China
Qiang Li,
Chengdu University, China
Yan Zhang,
Shandong Agricultural University, China

*CORRESPONDENCE
Xiao Li
✉ lxmogu@163.com
Bo Zhang
✉ zhangbofungi@126.com

RECEIVED 20 August 2023
ACCEPTED 09 October 2023
PUBLISHED 30 October 2023

CITATION
Qian K, Qi Z, Xu A, Li X, Zhang B and Li Y (2023) Interspecies hybridization between *Auricularia cornea* cv. Yu Muer and *Auricularia heimuer* cv. Bai Muer through protoplast fusion. *Front. Microbiol.* 14:1280420. doi: 10.3389/fmicb.2023.1280420

Interspecies hybridization between *Auricularia cornea* cv. Yu Muer and *Auricularia heimuer* cv. Bai Muer through protoplast fusion

Keqing Qian[1,2,3], Zhengxiang Qi[2], Anran Xu[2], Xiao Li[1,2,3]*, Bo Zhang[1,2,3]* and Yu Li[2]

[1]Northeast Asian Specialty Germplasm Resources Innovation Centre, Jilin Agricultural University, Changchun, China, [2]Engineering Research Center of Chinese Ministry of Education for Edible and Medicinal Fungi, Jilin Agricultural University, Changchun, China, [3]Joint International Research Laboratory of Modern Agricultural Technology, Ministry of Education, Jilin Agricultural University, Changchun, China

Color variations in cultivated edible mushrooms present novel and potentially valuable alternatives to the research and cultivation industries. We collected, identified, and domesticated a white strain of *Auricularia cornea* and a white strain of *Auricularia heimuer* from China. However, due to an unstable phenotype and stricter requirements on environment and management technology, the production and utilization of *Auricularia heimuer* cv. Bai Muer make slow progress. Outcrossing is an essential means to broaden the intraspecific genetic resources to expand the gene pool and compensate for the limitations of related species hybridization. In this study, interspecies hybridization between *Auricularia cornea* cv. Yu Muer and *Auricularia heimuer* cv. Bai Muer was conducted using polyethylene glycol (PEG)-induced double-inactivated protoplast fusion. Apart from the functional complementation of double-inactivated protoplasts, the hybrids were characterized by colony morphology, antagonistic test, primordial morphology, and polymerase chain reaction (PCR) fingerprinting. The results suggested that the hybrids and their parents showed significant differences in their colony morphology. Moreover, positive barrage reactions were observed between each parent and hybrid. Inter-simple sequence repeat (ISSR) and start codon targeted (SCoT) profile analysis of fusants and parents depicted that fusants contained polymorphic bands, which indicated the rearrangement and deletion of deoxyribonucleic acid (DNA) in the fusants. Yellowish-white primordia were obtained from two hybrids. Protoplast fusion may reinforce the genetic potential and provide an ideal alternative for breeding albino *Auricularia*.

KEYWORDS

edible mushrooms, color variations, interspecies hybridization, protoplast inactivation, *Auricularia*

1. Introduction

Auricularia Bull. (family Auriculariaceae, order Auriculariales) is an important wood-decaying fungal genus widely distributed worldwide (Wu et al., 2014). Moreover, it is one of the earliest cultivated mushrooms in the world and was first recorded in Tang Materia Medica, written by Gong Su (Yuan et al., 2019). It has traditionally been consumed as food and medicine for over 1,000 years in China (Miao et al., 2020). As the primary producer of cultivated

Auricularia in the world, China's output reached approximately 9.24 million tons in 2021, representing over 90% of the global production (China Edible Fungi Association, 2022). *Auricularia cornea* Ehrenb. and *Auricularia heimuer* F. Wu, B.K. Cui, and Y.C. Dai are the main species commercially cultivated in China.

Edible mushrooms with color variation have high research value and commercial value, such as Agaricus bisporus (J.E. Lange) Imbach, Flammulina filiformis (Z.W. Ge, X.B. Liu & Zhu L. Yang) P.M. Wang, Y.C. Dai, E. Horak & Zhu L. Yang, Hypsizygus marmoreus (Peck) H.E. Bigelow (Lee et al., 2008; Liu et al., 2013, 2016). *Auricularia cornea* cv. Yu Muer is an albino mutant strain of *A. cornea* with numerous biological activities, such as antidiabetic, antinephritic, antioxidant, anticoagulant, and hepatoprotective effects (Wang et al., 2019; Li et al., 2021). The pigment in the fruiting body of *A. cornea* was γ-glutaminyl-3,4-dihydroxy-benzoate. In the process of synthesizing pigment, the key enzymes were polyphenol oxidase and 20 other enzyme genes (Ma et al., 2023). In addition to its white color, the popularity of this mushroom is due to its high nutritional content and short production cycle (45–55 days). The mushroom is grown on an industrial scale in many regions of China because it has a high-yielding capacity and low output cost, is adaptable to a different environment, and is resistant to many pathogens (Chen et al., 2021).

In 2019, the white variety of *A. heimuer* was successfully domesticated and cultivated at Jilin Agricultural University (Li et al., 2019). According to the latest statistics, *A. heimuer* (ranks second in production) is more popular than *A. cornea* (ranks seventh in production) in China due to its flavor, slippery texture, and unique taste. However, *A. heimuer* cv. Bai Muer has a longer production cycle and higher output cost than *A. cornea* cv. Yu Muer, so it needs stricter requirements on environment and management technology. In addition, the color of the fruiting body is easily affected by light during the cultivation period. Therefore, selecting new strains of *Auricularia* with good characteristics is of great importance.

There are many ways to breed new strains, for example, artificial selection breeding, cross-breeding, protoplast fusion breeding, mutation breeding, and genetic engineering breeding. A lot of traditional mushroom breeding methods have been carried out intraspecifically. However, due to a lack of basic knowledge of the genetics and breeding system of this crop, advances in research on mushroom breeding and production are very limited compared with other crops. Moreover, the fruiting body of a mushroom is a complex organism with a series of complex characteristics. Many of these characteristics, especially those related to yield, are controlled by multiple genes (Chakravarty, 2011).

Gene transfer using protoplast fusion is a non-conventional method that is used to break down the natural barrier to gene exchange encountered in conventional breeding systems. Protoplast fusion technology can be performed intraspecifically, interspecifically, intergenerically, and even inter-hetero-generically (Dhitaphichit and Pornsuriya, 2005). The course of biological processes can be significantly influenced by protoplast fusion between different species. Through this process, gene control can be deregulated either positively or negatively, and metabolic pathways may be combined to create new metabolites. This can result in high yields, fast spawn runs, tolerance to adverse conditions, utilization of various agricultural waste, unique taste, attractive color, enhanced nutritive value, and medicinal properties in mushrooms (Selvakumar et al., 2015; Raman et al., 2021). Hybrids constructed by protoplast fusion in several mushrooms have been reported (Mallick and Sikdar, 2014). Interfamily hybrid strains with high biological efficiency and cold-tolerant ability have been obtained through protoplast fusion (He et al., 2018). A successful interspecific protoplast fusion has been carried out between the two edible mushroom strains *Lentinula edodes* (Berk.) Pegler and *Coriolus versicolor* (L.) Quél. (Kim et al., 1997). Somatic hybrids between *Calocybe indica* Purkay & A. Chandra and *Pleurotus fiorida* Singer showed a significant increase in bio-eficiency and γ-linoleic acid content (Chakraborty and Sikdar, 2010). The structural investigation of polysaccharides obtained from somatic hybrid mushrooms through protoplast fusion showed that they are different from the polysaccharides isolated from the fruit bodies of parental strains and exhibited strong immune activation of macrophages, splenocytes, and thymocytes (Patra et al., 2011; Maity et al., 2013; Maji et al., 2013; Sen et al., 2013). Therefore, distant hybridization can introduce important quantitative and qualitative traits, such as high bio-efficiency, good palatability, and a shorter cropping period, from either of the parents into their progeny. Interspecies hybridization between white *Auricularia* through protoplast fusion can enhance genetic potential and offer an excellent alternative for breeding edible mushrooms.

Thus, considering the beneficial characteristics of the two parents, the present study carried out the protoplast fusion between *A. heimuer* cv. Bai Muer and *A. cornea* cv. Yu Muer to obtain new intergeneric strains of albino *Auricularia* with improved characteristics. In our study, we successfully developed 10 hybrids, which were successfully characterized by microstructure, mycelial morphology, inter-simple sequence repeat (ISSR), and start codon targeted (SCoT) analysis.

2. Materials and methods

2.1. Strains and media

The *A. cornea* cv. Yu Muer strain (MC6), the *A. heimuer* cv. Bai Muer strain (JAUH-W-591), monokaryotic strains of *A. cornea* cv. Yu Muer (D-MC6), and *A. heimuer* cv. Bai Muer (D-JAUH-W-591) were preserved at Jilin Agricultural University (Changchun, China). Vegetative cultures of both strains were maintained on potato dextrose agar (PDA) medium, containing 20 g/L of glucose, 2 g/L of KH_2PO_4, 2 g/L of $MgSO_4{\cdot}7H_2O$, 1.5 g/L of agar, and 1 L of potato juice (He et al., 2018). Before protoplast isolation, the strains were grown in liquid malt yeast extract glucose (MYG) medium (10 g/L of malt, 4 g/L of yeast extract, and 10 g/L of glucose, pH = 6.2) under stationary conditions for 10 days at 30°C (Chakraborty and Sikdar, 2008; Xu et al., 2012). The same MYG medium supplemented with 0.6 M $MgSO_4$ and 2% agar was used as a regeneration medium.

2.2. Isolation of protoplasts

Monokaryotic mycelia derived from a single spore isolate of each species were incubated for 10 days at 28°C in 100 mL of liquid MYG medium for static culture. Cultures were harvested by the filter (0.22 μm), washed twice with distilled water, and dried with sterile paper. Then, 200–300 mg of mycelium was added to a 1 mL aliquot of lywallzyme solution (2%, purchased from the Guangdong Institute of Microbiology), which contained 0.6 M osmotic stabilizer and was incubated at 30°C for

7 h. The suspension was filtered and centrifuged at 3000 × g for 5 min. The obtained protoplasts were collected and washed twice with a 0.6 M osmotic stabilizer. The total yield was calculated using a hemocytometer (Wang et al., 2017). Finally, purified protoplast pellets were suspended in 200 μL of osmotic stabilizer solution for further use.

2.3. Inactivation of protoplasts

The protoplast suspensions of *A. heimuer* cv. Bai Muer and *A. cornea* cv. Yu Muer were inactivated by heat and ultraviolet (UV) radiation, respectively. For heat inactivation, the protoplasts were treated at 55, 60, and 65°C for 10, 20, and 30 min, respectively; for UV inactivation, protoplasts were placed 30 cm away under a 15 W UV lamp for 1, 3, 5, 8, and 10 min. After serial dilution, the inactivated protoplasts were plated on the regeneration MYG medium to check the inactivation effect (He et al., 2018). The medium was cultured at 28°C, and the number of regenerated colonies was recorded after 15 days. Protoplasts without inactivation were set as the control group. The inactivated protoplasts were then used for fusion (Zhao et al., 2011).

2.4. Fusion of protoplasts

An equivalent amount of inactive protoplasts of *A. heimuer* cv. Bai Muer and *A. cornea* cv. Yu Muer was mixed in a test tube and centrifuged at 1,000 × g for 5 min. The supernatant was rinsed off, and 1 mL of sterilized polyethylene glycol (PEG 4000; 30 g PEG in 100 mL 0.05 M $CaCl_2{\cdot}2H_2O$) was added to the protoplasts in the test tube and incubated at room temperature for 30 min (Moturi and Charya, 2009). During this period, protoplast fusion was followed by observation under the optical microscope (Nikon, Japan). The fused protoplasts were centrifuged at 1,000 × g for 5 min. The supernatant was rinsed off, and protoplasts were washed twice with the osmotic stabilizer and added 1 mL of osmotic stabilizer again. They were then serially diluted, and approximately 0.1 mL from the protoplast suspension was coated in MYG with 0.6 M $MgSO_4$ at 25°C until colonies developed (Zhao and Chang, 1996). Protoplasts from the same parent strains were also fused as controls. Only the progeny that continued growing on the regeneration medium were considered fusion hybrids. The nuclear phase of the putative hybrid stained with 4′,6-diamidino-2-phenylindole (DAPI) dye was observed by fluorescence microscopy. These procedures excluded the possibility of a dual culture.

2.5. Identification of hybrids

2.5.1. Antagonistic reactions

Hybrid mycelia, on slabs of PDA, were inoculated at a distance of 2 cm, with three in each Petri plate (i.e., the two parent cultures and a single hybrid). The plates were incubated at 25°C for 14 days, after which the point of contact zone was observed.

2.5.2. Spawning and fruiting test

All hybrids were subjected to a fruiting test in the laboratory. The spawn substrate, which consisted of (w/w) 40% flake hardwood sawdust (4 mm × 6 mm), 37.5% powdered hardwood sawdust, 11% bran, 10% corncob, 1% gypsum, 0.5% lime, pH = 7, and 58–60% water, was autoclaved at 121°C for 120 min. After spawning, when the mycelia showed complete colonization in the substrate, several "V" pores were made all over the surface of the polypropylene packet (approximately 2 cm apart). The temperature was then maintained at 22–28°C, and the relative humidity was adjusted to 85–90%. After pin head emergence through the pores on the polypropylene packets, high humidity was maintained by misting the room. Ventilation and light were required for healthy fruiting body development. If a strain did not form any primordia in all triplicate bags after 25 days, it was considered sterile. The morphology of the fruiting bodies of the hybrids was compared with that of the parents.

2.5.3. Inter-simple sequence repeat and start codon targeted analysis

Genomic deoxyribonucleic acid (DNA) was isolated from actively growing mycelia using a DNA Extraction Kit (Beijing CoWin Biotech Co., Ltd.). The ISSR primers used in the test are shown in Table 1. The ISSR amplification condition was as follows: 5 min initial denaturation at 94°C; 60 s initial denaturation at 94°C; 35 cycles consisting of 45 s denaturation at 52–58°C; 1 min extension at 72°C; and a final extension for 10 min at 72°C. Reaction termination was conducted at 4°C. ISSR-PCR

TABLE 1 Sequence and Annealing temperature of nine inter-simple sequence repeat (ISSR) primers.

Primer	Sequence	Annealing temperature (°C)
3	5′ (CA)8G 3’	55.5
4	5′ (ATG)6 3’	56
6	5’CCG ACTCGA GNN NNN NATGTGG 3’	57.5
p2	5’ BDB(ACA)5 3’	55
p4	5′ (CAC)4 SC 3’	58
p11	5′ (AC)8\u00B0C 3’	56
p13	5′ (GA)8 YG 3’	57
p14	5′ (AG)8 YT 3’	56
p15	5′ (AG)8 YC 3’	57.5

Note: B = (C,G,T); D = (A, G, T); S = (G, C); Y = (C, T); N = (A, T, C, G).

10.3389/fmicb.2023.1280420

reaction system (20 μL) was as follows: 10 μL of PCR Master Mix (2 X), 7.5 μL of dd H_2O, 1 μL of ISSR primer, and 1.5 μL of DNA. The final PCR products were separated by electrophoresis on a 1.0% (w/v) agarose gel (Chiu et al., 1995). According to Zhao et al. (2013), SCoT amplifications were performed with modifications. The SCoT primers used in the test are shown in Table 2.

3. Results

3.1. Preparation and regeneration of protoplasts

Sufficient protoplasts could be obtained by using mycelium aged 10 days under the conditions of an enzymatic hydrolysis temperature of 30°C, an enzymatic hydrolysis solution concentration of 2.0%, and an enzymatic hydrolysis time of 7 h. The protoplast yield was 7.84×10^7 CFU/mL in *A. heimuer* cv. Bai Muer and 7.36×10^7 CFU/mL in *A. cornea* cv. Yu Muer. The regeneration percentage of *A. heimuer* cv. Bai Muer protoplast was found to be 6.6%, while the rate of *A. cornea* cv. Yu Muer was 6.4%. The process of protoplasts being released from young hyphae was observed under a microscope (Figure 1A). Protoplast regeneration was observed in MYG medium containing 0.6 M $MgSO_4$ after 4 days.

TABLE 2 Sequence and Annealing temperature of five start codon targeted (SCoT) primers.

Primer	Sequence	Annealing temperature (°C)
7	5' CAACAATGGCTACCACGG 3'	51
8	5' CAACAATGGCTACCACGT 3'	51
9	5' CAACAATGGCTACCAGCA 3'	51
11	5' AAGCAATGGCTACCACCA 3'	51
28	5' CCATGGCTACCACCGCCA 3'	51

3.2. Heat and ultraviolet inactivation of protoplasts

Inactivation of *A. heimuer* CV. Bai Muer protoplasts at 60°C for 20 min yielded good results, as no protoplasts regenerated in the MYG medium with 0.6 M $MgSO_4$ after this treatment. After 3 min of UV inactivation, the inactivation rate of the *A. cornea* CV. Yu Muer protoplast was 100%, and the regeneration rate was 0.

3.3. Fusion and regeneration of protoplasts

The contact and fusion of protoplasts induced by PEG were observed under the microscope (Figure 1E). A total of 26 hybrid colonies were regenerated from five fusion experiments. No regenerated colonies were found in the control group. Sectors appearing in the protoplast fusion of distant hybrids are frequently observed when cultured in PDA, as shown in Figure 1H. This phenomenon is generally caused by the discordant

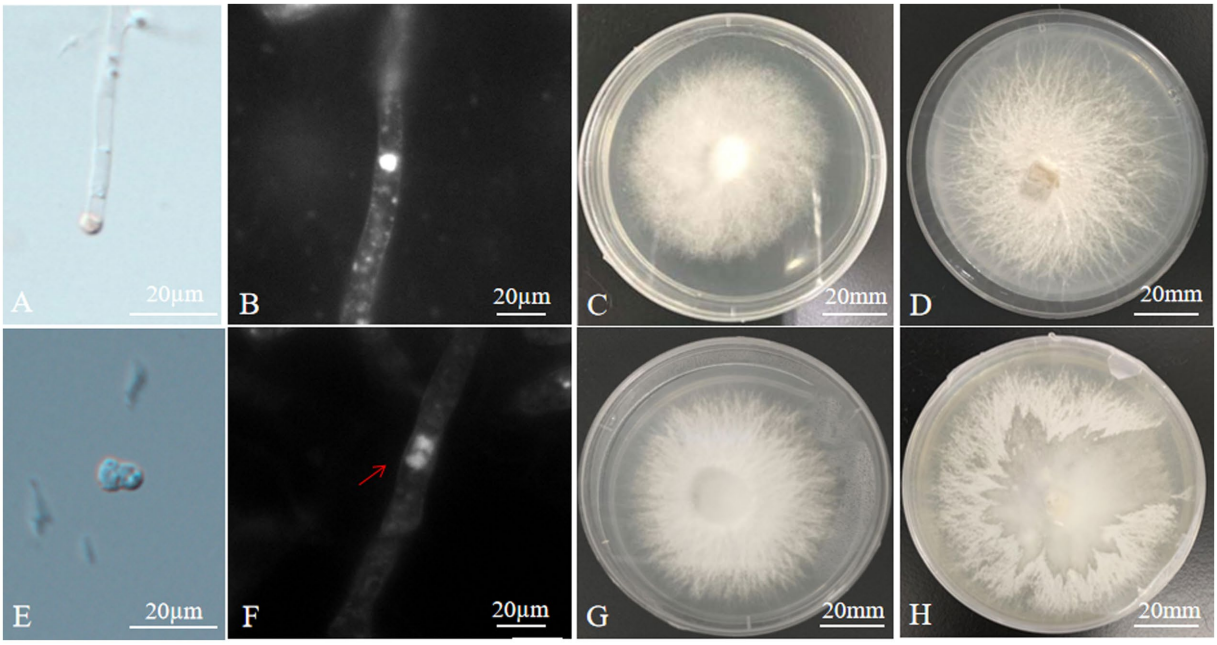

FIGURE 1
Microstructure and mycelial morphology of parents and hybrids **(A)** isolation of protoplast; **(B)** monokaryotic mycelium of *A. heimuer* cv. Bai Muer; **(C)** colony morphology of *A. heimuer* cv. Bai Muer; **(D)** colony morphology of *A. cornea* cv. Yu Muer; **(E)** protoplast fusion; **(F)** dikaryotic mycelium of hybrid; **(G)** colony morphology of hybrid strains R2; and **(H)** separation of one parent from unstable heterokaryons.

division of heterokaryons from different sources, which separates one parent from unstable heterokaryons. Sixteen hybrids exhibited this particular phenomenon in PDA culture. The remaining 10 fusions are confirmed as hybrid strains, renamed R1 ~ R10. There were no single protocols developed from any of the parental protoplasts in this regeneration medium because protoplasts were inactivated. Only hybrid protoplasts could regenerate in a regeneration medium due to the complementation of the parental genome. This confirmed that 10 hybrids had dikaryotic hyphae, while the parent strain had monokaryotic hyphae, as observed under the fluorescence microscope (Figures 1B,F).

The colony morphology of hybrids was different from that of their parents. The colony morphology of *A. heimuer* cv. Bai Muer showed a whitish colony with linear and centrally radiating mycelia; *A. cornea* cv. Yu Muer produced a whitish colony with fluffy mycelia. The colony morphology of hybrids had the characteristics of both parents (Figures 1C,D,G).

3.4. Identification of hybrids

3.4.1. Antagonistic reactions

The antagonistic reaction was a specific example of somatic incompatibility. The antagonist tests were conducted to confirm that the hybrids and parental strains had significant genetic differences. The antagonist test results showed that 10 hybrids and parental strains have a strong degree of antagonism resistance (Figure 2). This indicated that 10 strains generated through protoplast fusion are genetically different from the parental trains.

3.4.2. Fruiting test of somatic hybrids

In the cultivation study, hybrid mycelia grew thickly in a cultivation bag with sawdust as the main material. After 8 days of "V" pores being made, a yellowish-white primordium was observed in hybrid R2. Hybrid R4 required 11 days for primordial initiation, where parent *A. heimuer* cv. Bai Muer required 9 days and *A. cornea* cv. Yu Muer required 7 days. The results of lab-scale experiments indicated that all primordia of hybrids fail to differentiate even after 50 days. The fruit bodies of these parents and hybrids are shown in Figure 3.

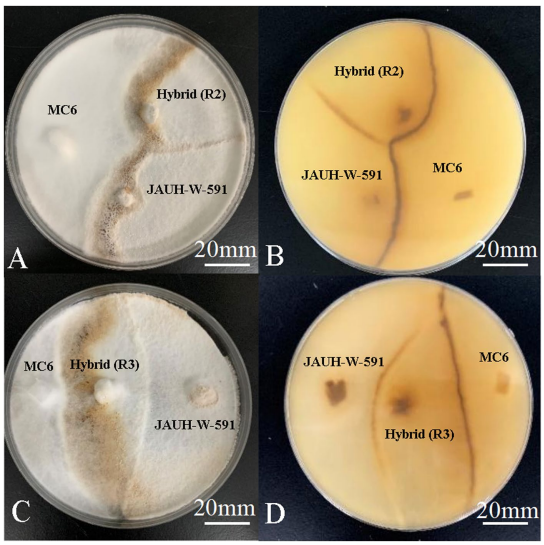

FIGURE 2
Antagonism of hybrids and parents. **(A-B)** The upper and reverse colony of JAUH-W-591, MC6, and R2; **(C-D)** the upper and reverse colony of JAUH-W-591, MC6, and R3.

3.4.3. Inter-simple sequence repeat and start codon targeted analysis

Genetic variations among parental strains and 10 *Auricularia* hybrids were determined by using ISSR and SCoT markers. The PCR band profiles of the hybrids were compared with those of the parental strains. If ISSR and SCoT bands are present (or absent) in the possible fusion but not in the parents, they are considered distinct fragments. For example, the ISSR-3 primer amplified and generated new bands of approximately 600 bp in the R2. The ISSR-4 primer amplified a band of approximately 400 bp in *A. heimuer* cv. Bai Muer, but this band was not present in R2. Similarly, ISSR-6 could generate polymorphic bands in the R2, R3, R5, R6, and R9 strains. However, the band of approximately 250 bp appeared in both parent strains but was not present in the R2 and R6 strains. R3, R5, and R9 strains were similar to *A. cornea* cv. Yu Muer, but bands of approximately 700 bp and 850 bp appeared in *A. cornea* cv. Yu Muer were not present in the R3, R5, and R9 strains. SCoT-28 could generate polymorphic bands in all hybrids. This indicated that ISSR and SCoT were efficient in analyzing the genetic diversity of *Auricularia*. Meanwhile, SCoT markers have high polymorphism, a large amount of information, and a wide evaluation range, which are more suitable for genetic diversity research (Zhao et al., 2013). However, it has not been reported yet whether SCoT molecular markers have been applied to study the genetic diversity of *Auricularia*. In this study, we applied SCoT molecular markers to the genetic diversity of *Auricularia*, aiming to provide a reference for the construction of *Auricularia* molecular fingerprints and the evaluation of strains of *Auricularia*. The moderated genetic transformation was observed, as shown in Figure 4, and the hybrids obtained were confirmed to be heterokaryotic.

4. Discussion

Selecting true hybrids was an essential step in breeding, which can directly affect breeding efficiency. The PEG-induced double-inactivated protoplast has been widely applied in protoplast fusion in edible mushrooms (He et al., 2020). PEG is widely used to mediate cell–cell fusion in the production of somatic cell hybrids. PEG can cause changes in electron distribution on the cell surface in the presence of calcium ions. Then, fusion points and recesses form in the plasma membrane, constituting a bridge of protoplasts. Finally, intercellular channels were formed and gradually expanded until protoplast fusion was completed (Zhu et al., 2016). In this study, the protoplast-regenerated mononuclear strain of the parents was used as the starting strain of interspecific fusion, and different inactivation methods were used for marking inactivation to ensure that only fusion products regenerated into colonies. In the regeneration medium, neither the *A. heimuer* cv. Bai Muer

10.3389/fmicb.2023.1280420

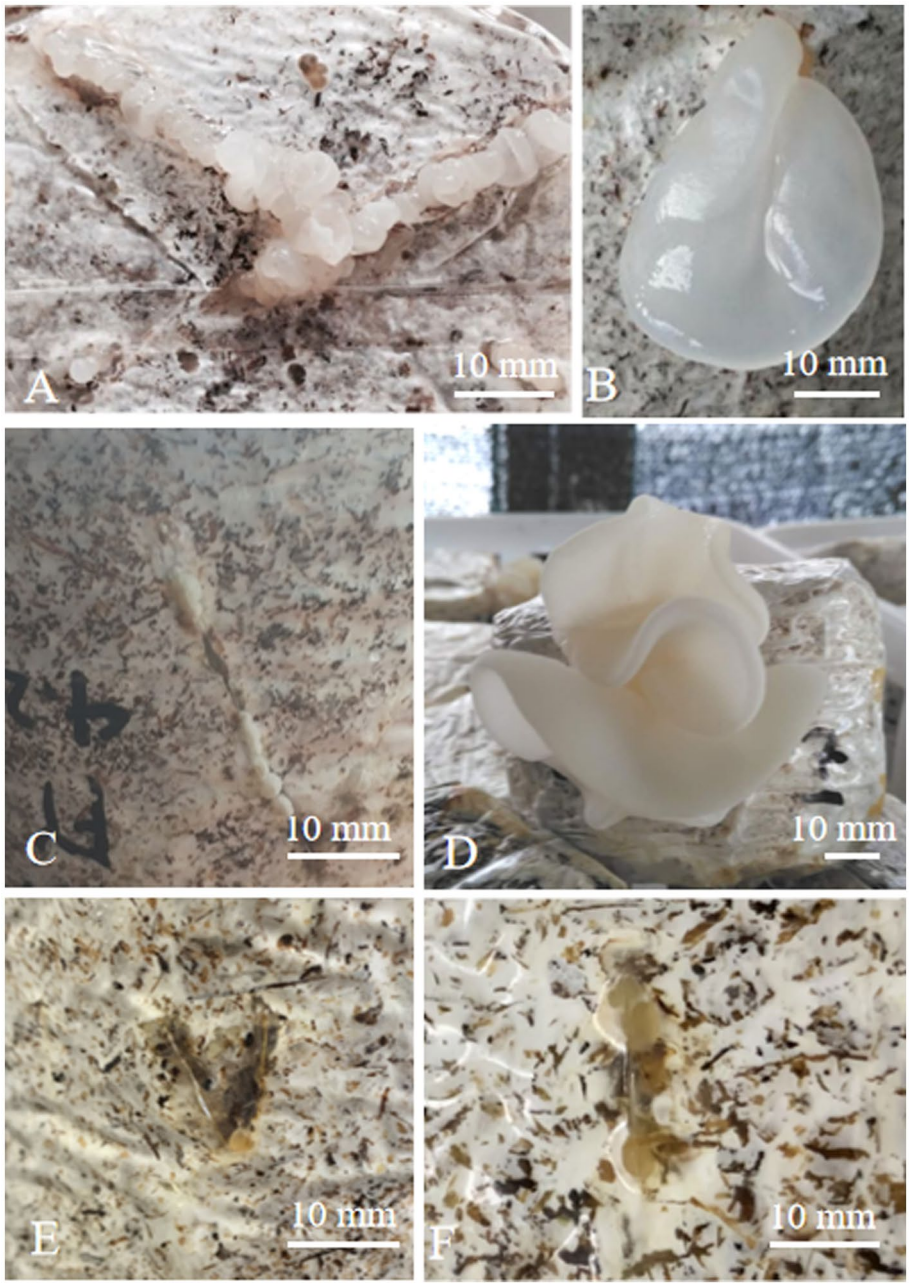

FIGURE 3
Morphology of fruiting bodies of hybrids **(A)** primordium of *A. heimuer* cv. Bai Muer; **(B)** fruiting body of *A. heimuer* cv. Bai Muer; **(C)** primordium of *A. cornea* cv. Yu Muer; **(D)** fruiting body of *A. cornea* cv. Yu Muer; and **(E,F)** primordium of hybrids.

protoplasts (due to heat inactivation) nor the *A. cornea* cv. Yu Muer protoplasts (due to UV inactivation) will grow. Hybrid protoplasts can grow due to the complementation of the parental genome or nuclear–cytoplasmic interactions (Mallick and Sikdar, 2014). The nuclear phase of the fused hybrid was observed as binucleate hypha under a fluorescence microscope, which showed that the genetic materials of both parents were complementarily repaired during the fusion process, and the heterokaryons were successfully obtained, which ruled out the possibility that the fused strain was the parent dikaryotic strain and monokaryon strain (Chiu et al., 1995).

This is the first time that interspecific protoplast fusion has been carried out among white varieties of *Auricularia* species. Yellowish-white primordia were obtained from two hybrids. The antagonistic line showed rejection between the fusion strain and its parents. The morphology of hybrids on the PDA medium had the characteristics of their parents. However, it may be due to the special mechanism of heterokaryon development after fusion or the change in environmental requirements of the fusion strain (Eyini et al., 2006); the primordia have not developed into a fruiting body, so it needs to be further domesticated and cultivated.

10.3389/fmicb.2023.1280420

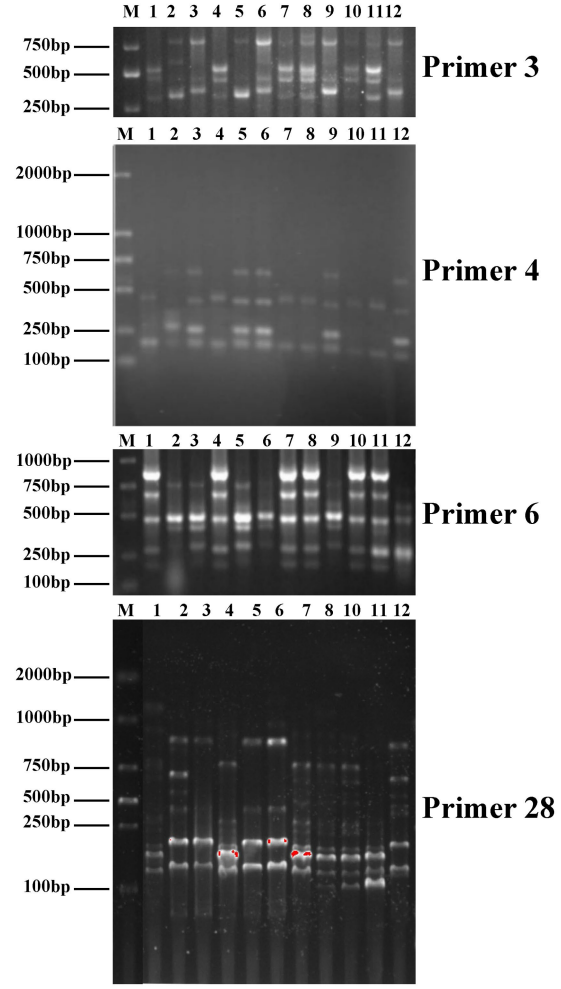

FIGURE 4
Inter-simple sequence repeat (ISSR) profiles of primers 3, 4, and 6 and start codon targeted (SCoT) profiles of primer 28 (1-R1, 2-R2, 3-R3, 4-R4, 5-R5, 6-R6, 7-R7, 8-R8, 9-R9, 10-R10, 11-*A. cornea* cv. Yu Muer, and 12-*A. heimuer* cv. Bai Muer).

There are reports of the hybrids exhibiting novel nutrient and biochemical characteristics even though they resembled any of their parents molecularly (Loveleen and Kapoor, 2014; Mallick and Sikdar, 2016). Many different molecular markers, such as simple sequence repeats (SSRs), randomly amplified polymorphic DNA (RAPD), and sequence-characterized amplified region (SCAR), were used to find evidence of gene recombination (Yoo et al., 2002; Su et al., 2008; Mallick et al., 2017). Therefore, it is necessary to establish an accurate and rapid PCR-based diagnostic system for hybrid strains of white *Auricularia* hybrids. Moreover, the ISSR and SCoT primers are suitable for *A. heimuer* cv. Bai Muer and *A. cornea* cv. Yu Muer that are screened to reveal high polymorphism, which helps distinguish individuals at the inter- and/or intra-species level.

Post-fusion incompatibility caused by heterokaryons is common in mushrooms and has been reported in several mushrooms (Peberdy and Fox, 2018). Separating one parent from unstable heteronuclear cells in PDA culture proves this point. This phenomenon of parental separation is caused by the disharmony of heterokaryotic nuclei in distant fusion. Although protoplast fusion can bypass the natural barriers of cytoplasmic fusion and achieve distant hybridization between different species, protoplast fusion cannot eliminate the hybridization barriers caused by post-fusion incompatibility during hybrid development. In our experiment, we observed that the primordia of hybrids failed to differentiate into fruiting bodies. How to maintain the stability of heterokaryons is a crucial problem during the development of distant hybrids (Kim et al., 1997). Regardless of the genetic mechanism, when two distant parents undergo protoplast fusion, the resulting hybrids can offer a range of benefits. These benefits include enhanced biological efficiency, increased fruiting body yield, higher polysaccharide content, enhanced enzyme production, and other improvements (Okamura et al., 2000; Khattab and Mohamed, 2012; Das et al., 2021). This method has been proven to be successfully used in the improvement of naturally incompatible strains (Chakraborty and Sikdar, 2010). In addition, protoplast fusion may result in interactions between nuclear and exonuclear genes, such as mitochondrial genes (Stasz and Harman, 1990; Harman and Stasz, 1991; Harman and Hayes, 1993). Fukuda has reported the successful mitochondrial DNA transmission in interspecific fusion protoplasts of *Pleurotus*, which increased the genetic variability of economically significant mushrooms (Fukuda et al., 2007). Because mitochondrial genomes may influence the phenotypic characteristics of edible mushrooms, this possibility is useful in mushroom breeding (Zhao and Chang, 1997).

In this study, the double-inactivated method, colony morphology, barrage reaction, ISSR, and SCoT strongly proved their hybrid nature. The somatic hybrids obtained through this study are not end products. Instead, the non-fruit body-generating somatic hybrid could serve as resource material for backcrossing with parents, and other further studies would give us insight into the basic genetics of Basidiomycetes mating-type genes, clamp formation, and mode of sexuality. Moreover, these hybrids could be used for further mushroom improvement programs.

Data availability statement

The original contributions presented in the study are included in the article, further inquiries can be directed to the corresponding authors.

Author contributions

KQ: Conceptualization, Data curation, Investigation, Methodology, Software, Writing – original draft, Writing – review & editing. ZQ: Conceptualization, Software, Writing – review & editing, Data curation, Formal analysis, Methodology, Supervision, Writing – original draft. AX: Supervision, Project

administration, Investigation, Methodology, Writing – review & editing, Conceptualization. BZ: Supervision, Project administration, Investigation, Methodology, Validation, Writing – review & editing. XL: Supervision, Project administration, Validation, Investigation, Writing – review & editing, Funding acquisition, Methodology, Resources. YL: Methodology, Supervision, Validation, Writing – review & editing.

Funding

The author(s) declare financial support was received for the research, authorship, and/or publication of this article. This work is supported by Demonstration and Promotion of Key Agricultural Core Technologies in Jilin Province (Industrial Technology System 202300601), the Jilin Province Science and Technology Development Plan Project (No. 20230202114NC), and the Scientific and Technological Tackling Plan for the Key Fields of Xinjiang Production and Construction Corps (No. 2021AB004).

Acknowledgments

The authors would like to thank Zong Liu for his kind help in the cultivation studies.

Conflict of interest

The authors declare that the research was conducted in the absence of any commercial or financial relationships that could be construed as a potential conflict of interest.

Publisher's note

References

Chakraborty, U., and Sikdar, S. R. (2008). Production and characterization of somatic hybrids raised through protoplast fusion between edible mushroom strains *Volvariella volvacea* and *Pleurotus florida*. *World J. Microbiol. Biotechnol.* 24, 1481–1492. doi: 10.1007/s11274-007-9630-1

Chakraborty, U., and Sikdar, S. R. (2010). Intergeneric protoplast fusion between *Calocybe indica* (milky mushroom) and *Pleurotus florida* aids in the qualitative and quantitative improvement of sporophore of the milky mushroom. *World J. Microbiol. Biotechnol.* 26, 213–225. doi: 10.1007/s11274-009-0162-8

Chakravarty, B. (2011). Trends in mushroom cultivation and breeding. *Aust. J. Agric. Eng.* 2, 102–109.

Chen, Y. Q., Sossah, F. L., Lv, Z. W., Lv, Y. C., Tian, L., Sun, X. Z., et al. (2021). Effect of wheat bran and maize straw substrates on the agronomic traits and nutritional content of *Auricularia cornea* cv. *Yu Muer*. *Sci. Hortic.* 286:110200. doi: 10.1016/j.scienta.2021.110200

China Edible Fungi Association. (2022). Analysis of the results of the 2021 national edible fungi statistical survey. Available at: https://mp.weixin.qq.com/s/M6ZQN5IYkkMCOmsojfLtUw (Accessed October 18, 2023).

Chiu, S. W., Chen, M., and Chang, S. T. (1995). Differentiating homothallic *Volvariella* mushrooms by RFLPs and AP-PCR. *Mycol. Res.* 99, 333–336. doi: 10.1016/s0953-7562(09)80909-x

Das, P., Sikdar, S. R., and Samanta, A. (2021). Nutritional analysis and molecular characterization of hybrid mushrooms developed through intergeneric protoplast fusion between *Pleurotus sajor-caju* and *Calocybe indica* with the purpose to achieve improved strains. *World J. Microbiol. Biotechnol.* 37:69. doi: 10.1007/s11274-021-03032-3

Dhitaphichit, P., and Pornsuriya, C. (2005). Protoplast fusion between *Pleurotus ostreatus* and *P. Djamor. Warasan. Songkhla. Nakharin.* 27, 975–982.

Eyini, M., Rajkumar, K., and Balaji, P. (2006). Isolation, regeneration and PEG-induced fusion of protoplasts of *Pleurotus pulmonarius* and *Pleurotus florida*. *Mycobiology.* 34, 73–78. doi: 10.4489/MYCO.2006.34.2.073

Fukuda, M., Wakayama, M., Uchida, M., Fukumasa-Nakai, Y., and Matsumoto, T. (2007). Introduction of mitochondrial DNA from *Pleurotus ostreatus* into *Pleurotus pulmonarius* by interspecific protoplast fusion. *J. Wood Sci.* 53, 339–343. doi: 10.1007/s10086-006-0861-9

Harman, G. E., and Hayes, C. K. (1993). The genetic nature and biocontrol ability of progeny from protoplast fusion in *Trichoderma*. *Biotechnol. Plan. Dis. Control.* 42, 237–255.

Harman, G. E., and Stasz, T. E. (1991). Protoplast fusion for the production of superior biocontrol Fungi. *Microb. Control. Weeds.* 10, 171–186. doi: 10.1007/978-1-4615-9680-6-10

He, B. L., You, L. R., Ye, Z. W., Guo, L. Q., Lin, J. F., Wei, T., et al. (2018). Construction of novel cold-tolerant strains of *Volvariella volvacea* through protoplast fusion between *Volvariella volvacea* and *Pleurotus eryngii*. *Sci. Hortic.* 230, 161–168. doi: 10.1016/j.scienta.2017.12.003

He, P. X., Yu, M., Wang, K., Cai, Y. L., Li, B., and Liu, W. (2020). Interspecific hybridization between cultivated morels *Morchella importuna* and *Morchella sextelata* by PEG-induced double inactivated protoplast fusion. *World J. Microbiol. Biotechnol.* 36:58. doi: 10.1007/s11274-020-02835-0

Khattab, A. A., and Mohamed, S. A. (2012). Mutation induction and protoplast fusion of *Streptomyces* spp. for enhanced alkaline protease production. *J. Appl. Sci. Res.* 8, 807–814.

Kim, C., Choi, E. C., and Kim, B. K. (1997). Protoplast fusion between *Lentinula edodes* and *Coriolus versicolor*. *Arch. Pharm. Res.* 20, 448–453. doi: 10.1007/BF02973938

Lee, Y. L., Jian, S. Y., Lian, P. Y., and Mau, J. L. (2008). Antioxidant properties of extracts from a white mutant of the mushroom *Hypsizigus marmoreus*. *J. Food Compos. Anal.* 21, 116–124. doi: 10.1016/j.jfca.2007.09.005

Li, X., Qian, K. Q., and Han, W. W. (2021). Prediction of hyaluronic acid target on sucrase-isomaltase (SI) with reverse docking and molecular dynamics simulations for inhibitors binding to SI. *PLoS One* 16:e0255351. doi: 10.1371/journal.pone.0255351

Li, X., Qian, K. Q., and Xu, A. R. (2019). Studies on the breeding of albino *Auricularia heimuer*. *Acta Edulis Fungi.* 26, 24–30. doi: 10.16488/j.cnki.1005-9873.2019.02.004

Liu, X. B., Feng, B., Li, J., Yan, C., and Yang, Z. L. (2016). Genetic diversity and breeding history of winter mushroom (*Flammulina velutipes*) in China uncovered by genomic SSR markers. *Gene* 591, 227–235. doi: 10.1016/j.gene.2016.07.009

Liu, J., Jia, L., Kan, J., and Jin, C. H. (2013). *In vitro* and *in vivo* antioxidant activity of ethanolic extract of white button mushroom (*Agaricus bisporus*). *Food Chem. Toxicol.* 51, 310–316. doi: 10.1016/j.fct.2012.10.014

Loveleen, K., and Kapoor, S. (2014). Protoplast electrofusion for development of somatic hybrids between *Pleurotus florida* and *Pleurotus sajor-caju*. *Int J Pharm. Bio. Sci.* 5, 507–519.

Ma, X., Lu, L., Yao, F., Fang, M., Wang, P., Meng, J., et al. (2023). High-quality genome assembly and multi-omics analysis of pigment synthesis pathway in *Auricularia cornea*. *Front. Microbiol.* 14:1211795. doi: 10.3389/fmicb.2023.1211795

Maity, K. K., Patra, S., Dey, B., Bhunia, S. K., Mandal, S., Bahera, B., et al. (2013). A β-glucan from the alkaline extract of a somatic hybrid (PfloVv5FB) of *Pleurotus florida* and *Volvariella volvacea*: structural characterization and study of immunoactivation. *Carbohydr. Res.* 370, 13–18. doi: 10.1016/j.carres.2013.01.016

Maji, P. K., Sen, I. K., Devi, K. S. P., Maiti, T. K., Sikdar, S. R., and Islam, S. S. (2013). Structural elucidation of a biologically active heteroglycan isolated from a hybrid mushroom of *Pleurotus florida* and *Lentinula edodes*. *Carbohydr. Res.* 368, 22–28. doi: 10.1016/j.carres.2012.12.008

Mallick, P., Chattaraj, S., and Sikdar, S. R. (2017). Molecular characterizations of somatic hybrids developed between Pleurotus florida and Lentinus squarrosulus through inter-simple sequence repeat markers and sequencing of ribosomal RNA-ITS gene. *Biotech* 7:298. doi: 10.1007/s13205-017-0931-2

Mallick, P., and Sikdar, S. R. (2014). Production and molecular characterization of somatic hybrids between *Pleurotus florida* and *Lentinula edodes*. *World J. Microbiol. Biotechnol.* 30, 2283–2293. doi: 10.1007/s11274-014-1652-x

Mallick, P., and Sikdar, S. R. (2016). Restriction fragment length polymorphism and sequence analysis of rRNA-ITS region of somatic hybrids produced between *Pleurotus florida* and *Lentinula edodes*. *Ann. Microbiol.* 66, 389–395. doi: 10.1007/s13213-015-1121-2

Miao, J., Regenstein, J. M., Qiu, J., Zhang, J., Zhang, X., Li, H., et al. (2020). Isolation, structural characterization and bioactivities of polysaccharides and its derivatives from *Auricularia*-a review. *Int. J. Biol. Macromol.* 150, 102–113. doi: 10.1016/j.ijbiomac.2020.02.054

Moturi, B., and Charya, M. A. (2009). Strain improvement in dye decolourising mutants of *Mucor mucedo* by protoplast fusion. *Afr. J. Biotechnol.* 8, 6908–6912. doi: 10.4314/ajb.v8i24.68774

Okamura, T., Takeno, T., Dohi, M., Yasumasa, I., Hayashi, T., Toyoda, M., et al. (2000). Development of mushrooms for thrombosis prevention by protoplast fusion. *J. Biosci. Bioeng.* 89, 474–478. doi: 10.1016/s1389-1723(00)89099-4

Patra, S., Maity, K. K., Bhunia, S. K., Dey, B., Mandal, S., Maiti, T. K., et al. (2011). Structural characterization and study of immunoenhancing properties of heteroglycan isolated from a somatic hybrid mushroom (PfloVv1aFB) of *Pleurotus florida* and *Volvariella volvacea*. *Carbohydr. Res.* 346, 1967–1972. doi: 10.1016/j.carres.2011.06.014

Peberdy, J. F., and Fox, H. M. (2018). *Protoplast technology and edible mushrooms genetics and breeding of edible mushrooms*. UK: Routledge: 125–155.

Raman, J., Jang, K. Y., Oh, Y. L., OH, M., Im, J. H., Lakshmanan, H., et al. (2021). Interspecific hybridization between *Ganoderma lingzhi* and *G. Applanatum* through protoplast fusion. *World J. Microbiol. Biotechnol.* 37, 114–117. doi: 10.1007/s11274-021-03084-5

Selvakumar, P., Rajasekar, S., Babu, A. G., Periasamy, K., Raaman, N., and Reddy, M. S. (2015). Improving biological efficiency of *Pleurotus* strain through protoplast fusion between *P. Ostreatus* var. *florida* and *P. Djamor* var. *roseus*. *Food Sci. Biotechnol.* 24, 1741–1748. doi: 10.1007/s10068-015-0226-5

Sen, I. K., Maji, P. K., Behera, B., Mallick, P., Maiti, T. K., Sikdar, S. R., et al. (2013). Structural characterization of an immunoenhancing heteroglycan of a hybrid mushroom (pfls1h) of *Pleurotus florida* and *Lentinus squarrosulus* (Mont.) singer. *Carbohydr. Res.* 371, 45–51. doi: 10.1016/j.carres.2013.02.004

Stasz, T. E., and Harman, G. E. (1990). Nonparental progeny resulting from protoplast fusion in *Trichoderma* in the absence of parasexuality. *Exp. Mycol.* 14, 145–159. doi: 10.1016/0147-5975(90)90073-3

Su, H. Y., Wang, L., Ge, Y. H., Feng, E., Sun, J., and Liu, L. (2008). Development of strain-specific SCAR markers for authentication of *Ganoderma lucidum*. *World J. Microbiol. Biotechnol.* 24, 1223–1226. doi: 10.1007/s11274-007-9579-0

Wang, S. H., Duan, M. G., Liu, Y. L., Fan, S., Lin, X. S., and Zhang, Y. (2017). Enhanced production of fructosyltransferase in *aspergillus oryzae* by genome shuffling. *Biotechnol. Lett.* 39, 391–396. doi: 10.1007/s10529-016-2254-5

Wang, D., Jiang, X., Teng, S. S., Zhang, Y. Q., Liu, Y., Li, X., et al. (2019). The antidiabetic and antinephritic activities of *Auricularia cornea* (an albino mutant strain) via modulation of oxidative stress in the db/db mice. *Front. Immunol.* 10:1039. doi: 10.3389/fimmu.2019.01039

Wu, F., Yuan, Y., Malysheva, V. F., Du, P., and Dai, Y. C. (2014). Species clarification of the most important and cultivated *Auricularia* mushroom "Heimuer": evidence from morphological and molecular data. *Phytotaxa.* 186, 241–253. doi: 10.11646/phytotaxa.186.5.1

Xu, J. Z., Zhang, J. L., Zhang, W. G., and Hu, K. H. (2012). The novel role of fungal intracellular laccase: used to screen hybrids between *Hypsizigus marmoreus* and *Clitocybe maxima* by protoplasmic fusion. *World J. Microbiol. Biotechnol.* 28, 2625–2633. doi: 10.1007/s11274-012-1072-8

Yoo, Y. B., Lee, K. H., and Kim, B. G. (2002). Characterization of somatic hybrids with compatible and incompatible species by protoplast fusion in genera *Pleurotus* (Fr.) P. Karst. and *Ganoderma* P. Karst. by RAPD-PCR analysis. *Int. J. Med. Mushrooms* 4, 147–157. doi: 10.1615/IntJMedMushr.v4.i2.80

Yuan, Y., Wu, F., Si, J., Zhao, Y. F., and Dai, Y. C. (2019). Whole genome sequence of *Auricularia heimuer* (Basidiomycota, Fungi), the third most important cultivated mushroom worldwide. *Genomics* 111, 50–58. doi: 10.1016/j.ygeno.2017.12.013

Zhao, J., and Chang, S. T. (1996). Intergeneric hybridization between *Pleurotus ostreatus* and *Schizophyllum commune* by PEG-induced protoplast fusion. *World J. Microbiol. Biotechnol.* 12, 573–578. doi: 10.1007/bf00327717

Zhao, J., and Chang, S. T. (1997). Interspecific hybridization between *Volvariella volvacea* and *V. Bombycina* by PEG-induced protoplast fusion. *World J. Microbiol. Biotechnol.* 13, 145–151. doi: 10.1023/A:1018519827561

Zhao, M. R., Chen, Q., Zhang, J. X., Wu, X. L., and Huang, C. Y. (2013). Comparison studies of genetic diversity of *Pleurotus eryngii* var. *tuoliensis* by IGS2-RFLP, SCoT and ISSR markers. *Mycosystema* 32, 682–689. doi: 10.13346/j.mycosystema.2013.04.002

Zhao, K., Sun, L., Ma, X., Li, X., Wang, X., Ping, W., et al. (2011). Improved taxol production in Nodulisporium sylviforme derived from inactivated protoplast fusion. *Afr. J. Biotechnol.* 10, 4175–4182.

Zhu, Z. P., Wu, X., Lv, B. B., Wu, G. G., Chen, J. Z., Chen, M. G., et al. (2016). A new approach for breeding low-temperature-resistant *Volvariella volvacea* strains: genome shuffling in edible fungi. *Biotechnol. Appl. Biochem.* 63, 605–615. doi: 10.1002/bab.1420

frontiers | Frontiers in Microbiology

TYPE Original Research
PUBLISHED 24 January 2024
DOI 10.3389/fmicb.2024.1287641

OPEN ACCESS

EDITED BY
Chenyang Huang,
Institute of Agricultural Resources and Regional Planning, Chinese Academy of Agricultural Sciences, Beijing, China

REVIEWED BY
Qiang Li,
Chengdu University, China
Bingzhi Chen,
Fujian Agriculture and Forestry University, China
Hosein Salehian Dehkordi,
Chinese Academy of Sciences (CAS), China

*CORRESPONDENCE
Xu Zhao
✉ zhaoxu02@caas.cn

†These authors have contributed equally to this work

RECEIVED 02 September 2023
ACCEPTED 08 January 2024
PUBLISHED 24 January 2024

CITATION
Cao L, Yang D, Zhang Q, Ni Y, Li W, Feng R, Mu W and Zhao X (2024) Population genetic structure of *Hymenopellis radicata* germplasm resources based on genome re-sequencing.
Front. Microbiol. 15:1287641.
doi: 10.3389/fmicb.2024.1287641

Population genetic structure of *Hymenopellis radicata* germplasm resources based on genome re-sequencing

Luping Cao[1,2,3†], Delong Yang[3†], Qin Zhang[1,2], Yanqing Ni[4], Wensheng Li[4], Rencai Feng[1,2], Wen Mu[5] and Xu Zhao[1,2*]

[1]Institute of Urban Agriculture, Chinese Academy of Agricultural Sciences, Chengdu, China, [2]Chengdu National Agricultural Science and Technology Center, Chengdu, China, [3]College of Life Science and Technology, Gansu Agricultural University, Lanzhou, China, [4]College of Food and Biological Engineering, Chengdu University, Chengdu, China, [5]College of Agronomy and Biotechnology, Southwest University, Chongqing, China

Through whole-genome re-sequencing of 18 *Hymenopellis radicata* germplasm resources collected from diverse regions in China, we identified significant variations in the form of Single Nucleotide Polymorphisms (SNPs) and Insertions and Deletions (InDels). These variations were comprehensively annotated, shedding light on the mutation types present in the entire genome of the *H. radicata* germplasm. This analysis revealed the number and position information of each mutation and provided insights into the overall genomic landscape of *H. radicata* germplasm. Utilizing SNP data, we delved into the population structure of the 18 *H. radicata* germplasm resources. The results indicated the presence of 2,335,179 Indel sites and 12,050,448 SNP sites. The population structure analysis unveiled two distinct subgroups among the *H. radicata* germplasm resources. Phenotypic statistics, principal component analysis, and phylogenetic tree results echoed the findings of the population structure analysis. Different strains of *H. radicata* from various regions in China exhibited notable differences in genetic diversity, mycelial growth rate, yield, and fruiting body characteristics. Significant disparities were observed between the two subgroups, while strains within each subgroup shared common characteristics. This research establishes a solid foundation for integrating *H. radicata* into diverse breeding programs. The data underscore the potential of *H. radicata* for genetic improvement and exploitation in breeding initiatives, paving the way for future advancements in this field.

KEYWORDS

***Hymenopellis radicata*, whole genome resequencing, SNP, INDEL, population genetic structure**

1 Introduction

The Physalacricea *Hymenopellis radicata* mushroom, commonly known as Changgengu, belongs to the Basidiomycota, Agaricales, and Physalacriceae families (Yang et al., 2009). As a delectable and nutritionally rich rare edible fungus, it predominantly thrives in Sichuan, Yunnan, and Guizhou provinces (Hou et al., 2022). The fruiting body of *H. radicata* contains active components such as polysaccharides (Wang et al., 2018; Pan et al., 2022) and flavonoids

(Zhang et al., 2022), making it a valuable source of natural antioxidants and medicinal supplements for food, pharmaceuticals, and health products. Despite efforts in optimizing cultivation methods (Xiao et al., 2021) and extracting bioactive components (Zhang et al., 2021) from domesticated strains, the existing cultivated strains have low yields and inconsistent quality. The breeding of *H. radicata* has proven to be comparatively inefficient, compounded by issues of disorganized strain management in the market, leading to challenges such as the presence of the same species and name. The industry's growth is intricately tied to the quality of *H. radicata* strains. Given its widespread presence in the wild across our country, we can effectively harness these excellent resources to enhance the genetic diversity of the strains, facilitating the breeding of high-yield, superior, and unique *H. radicata* strains in China.

In *H. radicata* cultivation, the fruiting body characteristics often exhibit high variability, with phenotypic traits closely linked to genotype and environment. The unstable phenotypic characteristics pose challenges to genetic improvement in *H. radicata*. The utilization of existing genomic resources and the generation of additional genomic data can help unravel the molecular basis of phenotypic variation. In recent years, molecular resources for *H. radicata* have expanded, including *de novo* transcriptome assembly (Zhu et al., 2023), ISSR labeling (Lian et al., 2023), and fingerprint construction (Gong et al., 2022). However, these studies primarily focused on genome structure analysis, strain identification, and classification, lacking a comprehensive discussion on the genetic diversity of *H. radicata* strains.

In the exploration of genetic diversity, resequencing technology is often employed, in addition to molecular markers, to detect genetic variation in samples. Whole-genome resequencing, a high-throughput sequencing technique, it is possible to sequence the genomes of various members of a species whose genome sequence is known and compare the variations between individuals or populations (Ley et al., 2008). Comparing whole-genome re-sequenced individuals with reference genome sequences allows for the discovery of numerous Single Nucleotide Polymorphisms (SNPs) and Insertions and Deletions (InDels) sites. A notable example is the analysis conducted by Shen et al. (2020), which explored the genetic diversity and population genetic structure of 28 strains of *Flammulina filiformis*. Another study by Shi et al. (2019) involved the preliminary resequencing investigation of 18 *Agaricus bisporus* strains, leading to the identification of the largest hybrid strains in the world through SNP, InDel, and SV detection.

This study undertakes the complete genome resequencing of 18 *H. radicata* strains to detect, filter, and subtype SNP and InDel locations. Group genetic structure analysis, utilizing SNP data, is employed to construct a systematic development tree and perform principal component analysis. Simultaneously, the study seeks the theoretical basis for the protection and utilization of *H. radicata* resources, genetic localization of important agricultural characteristics, and polymorphic breeding based on molecular markers. These objectives are pursued in conjunction with the physiological epithetic indicators of all strains. This research aims to contribute valuable insights to the genetic variation in edible fungi, paving the way for the development of new molecular markers to assist in breeding, aligning with the advancements brought about by resequencing technology in this domain.

2 Materials and methods

2.1 Source of the tested strains

The Institute of Urban Agriculture, Chinese Academy of Agricultural Sciences, supplied 18 specimens of *H. radicata* collected from diverse provinces and cities across China. Based on their respective origins, the 18 strains were categorized into three groups: A, B, and C. Strains in Group A originated from the eastern coastal area, those in Group B were sourced from central China, and Group C comprised strains from southwest China. Details regarding their names and locations are presented in Table 1.

2.2 Strain culture and sample collection

Solid medium (Potato Dextrose Agar, PDA) was prepared using 1 L of distilled water, 200 g of potato, 20 g of glucose, and 15 g of agar. The mycelium and medium were separated using cellophane. The mycelium was cultivated on a complete plate for subsequent DNA extraction and sequencing. Specifically, it was cultured in a 9 cm diameter petri dish containing 20 mL of PDA.

2.3 DNA extraction and genome sequencing of *H. radicata*

DNA extraction was carried out using the CTAB method (Zhang et al., 2010) following the crushing of an appropriate amount of mycelial tissue with liquid nitrogen. The purity of the extracted DNA was assessed using a spectrophotometer (K5800, Kaiao, Beijing, China). DNA samples with distinct electrophoretic bands and 260/280 nm values falling between 1.6 and 1.8 were selected for further analysis. High-quality DNA samples meeting these criteria were sent to Wuhan Hope Group Biotechnology Co., Ltd. for sequencing on the Illumina platform. The DNA sample underwent subsequent processes, including fragmentation, purification, terminal repair, 3′ terminal adenylation, junction head, fragment screening, and fragment enrichment through PCR.

2.4 Sequencing quality control

Raw data obtained through sequencing is processed using base recognition to generate clean data. The initial sequencing data may contain adapter sequences and low-quality sequences. To ensure the quality of subsequent data analysis, the fastp (Chen et al., 2018) program is employed to enhance the quality of the original data. Data noise is then reduced through data filtering. The clean data undergoes rigorous filtering, resulting in high-quality data suitable for subsequent information analysis. This high-quality data is essential for generating reliable results in the subsequent information analysis.

The filtering steps include: (1) filtering Reads that contain the adapter (for paired-end sequencing, both ends of the Reads are removed if one end contains the adapter); (2) removing low-quality Reads (bases with quality values below Q15 in Reads constitute more than 40% of all bases; for paired-end sequencing, if one end is

TABLE 1 Breed number and origin of 18 *H. radicata* strains.

Number	Strains	Origin	Group	Number	Strains	Origin	Group
1	Or015	Fuzhou, Fujian	A	10	Or007	Linyi, Shandong	A
2	Or024	Fuzhou, Fujian	A	11	Or019	Biyang, Henan	B
3	Or022	Fuzhou, Fujian	A	12	Or020	Jiayu, Hubei	B
4	Or001	Zhangzhou, Fujian	A	13	Or017	Wuhan, Hubei	B
5	Or002	Zhangzhou, Fujian	A	14	Or023	Changsha, Hunan	B
6	Or004	Zhangzhou, Fujian	A	15	Or018	Xijiu, Guizhou	C
7	Or009	Gaoyou, Jiangsu	A	16	Or012	Chengdu, Sichuan	C
8	Or003	Jining, Shandong	A	17	Or013	Chengdu, Sichuan	C
9	Or034	Junan, Shandong	A	18	Or014	Chengdu, Sichuan	C

low-quality Reads, both ends of the Reads will be removed); (3) eliminating Reads with more than 5; and removing Reads with more than 1.

2.5 Compared with the reference genome

Following data filtering, the clean data underwent alignment with the reference genome utilizing the BWA-mem (Bolger et al., 2014) program, yielding alignment results in SAM format. Subsequently, the alignment findings were converted to BAM format and sorted according to chromosomal order using the SAMtools (Li et al., 2009) software. To ensure the quality of the data, duplicate reads were identified and removed using Picard software. After eliminating duplicates, the alignment results were scrutinized using Qualimap 2 (Okonechnikov et al., 2016).

2.6 Genomic variation detection and annotation

Based on the alignment results, the GATK (McKenna et al., 2010) software was employed to identify SNPs and InDels. Subsequently, the ANNOVAR (Wang et al., 2010) software was utilized to annotate the detected SNPs and InDels. The annotation results were then leveraged for subsequent analysis and interpretation. Finally, the outcomes were utilized to discern genetic variations and explore their potential biological roles.

2.7 Population analysis

Based on SNP data, the population structure of *H. radicata* was investigated through the ADMIXTURE (Alexander et al., 2009) program. The optimal subpopulation number, K, was determined via cross-validation error. The precise procedure involves studying the population structure across various K values. We employed 10 different seeds for 10 repetitions of the analysis. The outcomes were clustered using Pong (Behr et al., 2016) in 10 iterations, and the most representative results were chosen for visualization. For all samples, the IBS matrix was computed using PLINK (Purcell et al., 2007). Subsequently, a phylogenetic tree was constructed using the neighbor-joining algorithm in PHYLIP (Shimada and Nishida, 2017). Principal component analysis based on SNP divergence was then conducted using EIGENSTRAT (Price et al., 2006).

2.8 Statistics of biological characters of different strains

Firstly, activated strains were inoculated onto a solid PDA medium using a 5 mm punch. Subsequently, they were placed in a constant temperature incubator at 25°C to avoid light during cultivation. A "cross" method was employed to mark the starting line and date on the back of the plate with a pen when the mycelium made contact with the medium surface. As the mycelium reached approximately 1 cm from the dish edge, the ending line and date were marked. The distance between the starting and ending lines was measured to calculate the average growth rate of mycelium. Each strain had three parallels, and the average value was determined for comparison and analysis. The formula for calculating the average growth rate (V, mm/d) is: $V = D/d$.

Secondly, mushroom cultivation was conducted in Pengzhou, Sichuan province, using the soil covering method in small areas. Each strain was set up in three identical replicate areas, each comprising 15 bags. The mature bag cultivation method was employed in production, involving substrate mixing, bagging, inoculation, and mushroom development management. In each small area, 20 harvested fruiting bodies were collected for quantitative trait statistics. The quantitative trait testing method followed the Guidelines for the conduct of tests for distinctness, uniformity, and stability rooting shank mushroom [*Oudemansiella raphanipes* (Berk.) Pegler & T.W.K. Young] (National Plant New Variety Test Standardization Technical Committee, 2020), with specific methods outlined in Table 2. Fresh fruiting bodies were harvested daily when the mushroom caps were fully expanded but not yet curled upwards. The weight of the fruiting bodies was recorded for each small area, and the total yield for the entire cultivation period was calculated to determine the yield per bag.

3 Results and analysis

3.1 Genome sequencing analysis

In this investigation, 18 strains of *H. radicata* were sequenced utilizing the Illumina platform (Table 3). Raw reads ranged from

TABLE 2 Methods for determining quantitative traits of fruiting bodies.

Number	Characters	Method
No. 1	Pileus diameter	Measure the length of number 1 in Figure 1, 20 replicates
No. 2	Pileus thickness	Measure the length of number 2 in Figure 1, 20 replicates
No. 3	Stipe length	Measure the length of number 3 in Figure 1, 20 replicates
No. 4	Stipe diameter	Measure the length of number 4 in Figure 1, 20 replicates

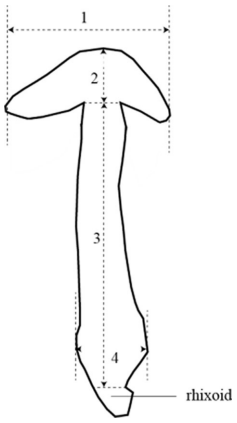

FIGURE 1
Schematic diagram of various parts of the fruiting body.

142,018,200 M to 32,595,990 M. After filtering, the reads were refined to a range of 325,866,758 M to 14,196,060 M. Clean databases range in size from 4.89 GB to 2.13 GB, while raw databases also fall within the 4.89 GB to 2.13 GB range. The sequencing results met the criteria for re-sequencing data analysis because the clean data Q20 ranged from 93.26% to 98.64%, the clean data Q30 ranged from 85.33% to 96.09%, and the GC content ranged from 45.59% to 48.50%.

H. radicata IJFM A160 (GenBank accession: GCA_015501595.1) was used the reference genome for this study. Table 4 presents a comparison of the resequencing results from 18 *H. radicata* samples with the reference genome. More than 57.62% of the entire dataset successfully aligned to the reference genome in a double-ended manner, while over 32.90% of the total data showed precise matches with the reference genome. Moreover, over 67.21% of the total data were mapped to the reference genome. These findings highlight discrepancies between the experimental material and the reference genome, suggesting the need for further investigation to accurately characterize the genetic differences among these 18 samples. Such an analysis could offer valuable insights into the genetic variability of *H. radicata*.

3.2 SNP and InDel sites of the strain of *H. radicata*

After aligning with the reference genome, we identified 12,050,448 SNP sites and 2,335,179 InDel sites (refer to Table 5). Strain Or020 exhibited the fewest SNPs (502,973), while strain Or024 presented the highest count (692,787). The transitions ranged between 359,326 and 488,733, and transversions were observed between 143,627 and 204,054. InDel sites varied from the lowest in strain Or020 (92,542) to the highest in strain Or024 (136,963). Insertion sites ranged from 43,041 to 63,571, and deletion sites were observed between 49,501 and 73,392. Additionally, ANNOVAR software annotated the identified SNPs and InDels, and the annotations are displayed in Figure 2. Among the 18 *H. radicata* strains, SNPs located in the exon region constituted 53% of all identified SNPs. Among these, 70% were synonymous mutations, and 30% were non-synonymous mutations (Figure 2A). Regarding InDels, 22% of the total were located in the exon region, 27% in the intronic region, and 12% in the intergenic region (Figure 2B).

3.3 Analysis of the population genetic structure of *H. radicata*

PLINK 1.9 was employed to filter SNPs across the entire genome using the parameter "-Indep-pairwise 50 5 0.5", based on the outcomes of the preceding investigation. For population stratification, 176,640 SNPs with loose linkages were utilized. The population structure was examined using ADMIXTURE version 1.3.0 for K values ranging from 2 to 5, and the ideal K value was determined through cross-validation error (CV). It is important to note that the model has higher reliability when the error rate at K = 2 is low, indicating that the most appropriate number of subgroups is two. Additionally, Figure 3A displays the result of the simulation analysis at different K values. At K = 2, the 18 germplasms were divided into two subgroups (red and blue), with strains Or004 and Or020 showing different levels of mixing between these two subgroups. This is speculated to be the result of genetic drift. When K = 3, strains Or004 and Or020 were categorized into a distinct subgroup, while strains Or001 and Or002 exhibited genetic elements from both subgroups, marking the beginning of further divergence between the two groups. At K = 4, strain Or020 branched off into its own subset, and at K = 5, strain Or002 also formed a new subgroup. The stable and genetically similar breeds were generally divided into two subgroups. Strains Or001, Or002, Or004, and Or020 are examples of strains that possess genetic components from two or more subgroups. As the number of subgroups increased, the phenomenon of genetic drift became more pronounced.

3.4 Comparison of mycelial growth rate between two subgroups of strains

The mycelial growth rate of strains in subgroup I ranged from 1.23 ± 0.074 cm/d to 1.53 ± 0.172 cm/d, while that of strains in subgroup II varied from 1.55 ± 0.086 cm/d to 1.77 ± 0.165 cm/d. The specific mycelial growth rates of each strain are shown in Figure 4. Statistical analysis revealed that strains in subgroup I grew significantly slower than those in subgroup II ($p < 0.0001$). This indicates that under identical culture conditions, strains in

TABLE 3 Quality of re-sequencing data for 18 strains of *H. radicata*.

Sample	Raw reads number (M)	Raw data bases (G)	Clean reads number (M)	Clean data bases (G)	Clean data Q20	Clean data Q30	Clean data GC%
Or001	292,246,120	4.39	290,622,120	4.35	97.7930	93.5679	47.9731
Or002	276,714,300	4.15	274,909,180	4.12	97.9459	93.9989	48.1457
Or003	305,329,340	4.58	303,543,200	4.55	97.6902	93.3225	48.3862
Or004	284,761,740	4.27	283,114,880	4.24	97.6404	93.1906	48.0073
Or007	289,265,420	4.34	287,622,600	4.31	97.8011	93.5098	48.3826
Or009	286,800,600	4.30	285,116,860	4.27	97.5997	93.1156	48.5011
Or012	323,283,200	4.85	323,283,200	4.84	98.1250	94.6436	46.7751
Or013	325,831,840	4.89	325,831,840	4.88	97.3662	92.4603	46.5693
Or014	325,203,040	4.88	325,203,040	4.87	97.7535	93.5750	47.2989
Or015	325,959,900	4.89	325,959,900	4.89	98.3398	95.1298	46.6987
Or017	310,126,920	4.65	310,126,920	4.65	98.3387	95.1136	46.6430
Or018	309,087,860	4.64	309,087,860	4.63	98.4040	95.3102	46.7836
Or019	308,710,460	4.63	308,710,460	4.63	98.6416	96.0939	46.7383
Or020	309,491,240	4.64	309,491,240	4.64	98.1612	94.6065	46.3452
Or022	308,801,140	4.63	308,802,140	4.63	97.2164	92.0595	46.3672
Or023	309,706,700	4.65	309,706,700	4.64	98.2581	94.8948	46.7202
Or024	309,290,740	4.64	309,290,740	4.64	98.4996	95.5830	46.6569
Or034	142,018,200	2.13	142,018,200	2.13	93.2582	85.3306	45.5942

subgroup II have a significant advantage in terms of the mycelial growth rate index.

3.5 Comparison of single bag yield of two subgroups of strains

We collected yield data for all strains throughout their growth period and calculated the yield per bag, as shown in Figure 5. The yield of strains in subgroup I ranged from 64.10 ± 22.513 g/bag to 222.9 ± 13.930 g/bag, while the yield of strains in subgroup II varied from 47.08 ± 11.267 g/bag to 197.55 ± 51.631 g/bag. Although the average yield of strains in subgroup I was higher than in subgroup II, both subgroups contained strains with both high and low yields. Overall, the yield of strains within the two subgroups varied widely, showing no significant differences between them ($p = 0.0593$).

3.6 Comparison of the quantity and characteristics between two subgroups of strains

As shown in Figure 6, the pileus diameter, pileus thickness, stipe diameter, and stipe length were measured for each strain. The strains from subgroup II had significantly larger pileus diameters ($p < 0.001$), pileus thickness ($p < 0.01$), and stipe diameter ($p < 0.05$) compared to those from subgroup I. However, there was no significant difference in stipe length between the two subgroups. On the whole, the strains in subgroup II exhibited larger pileus diameters, thicker pilei, and larger stipe diameters than those in subgroup I.

3.7 Population principal component analysis of *H. radicata*

Based on the extent of SNP differences detected in individual genomes, individuals were clustered into different subgroups and groups according to principal components, as depicted in Figure 7. Each point in the figure represents a sample, with greater distances between two points indicating more significant differences in the genetic backgrounds of the corresponding samples. The categorization of strains into two distinct groups, as determined by their locations and distances on the two-dimensional graph, aligns well with the results of the population genetic structure analysis (see Figure 8).

3.8 Cluster analysis of strain resources of *H. radicata*

The SNP identification data were used to construct a phylogenetic tree, which aided in understanding the evolutionary relationships among *H. radicata* populations from various geographical locations. According to the data, the strains in the two subgroups originated from four main branches. The first significant branch includes Or009, Or012, Or013, Or014, Or017, Or018, Or019, Or023, and Or024, which are present in Sichuan, Henan, Jiangsu, Hubei, Hunan, and Guizhou provinces. The second major branch comprises five strains: Or007, Or022, Or015, Or034, and Or003, found in Shandong and Fujian provinces. The third branch consists of strains Or001, Or002, and Or004, all located in Zhangzhou, Fujian Province. The unique strain Or020 originates from Jiayu, Hubei Province. As observed, strains conserved within the same region are closely related. There is

TABLE 4 Statistics of genome alignment and coverage.

Sample	Total reads	Total mapped	Total pair reads	Total pair mapped	Properly paired	1X (%)	10X (%)
Or001	43,523,934	72.64%	25,479,978	58.54%	41.43%	54.32	42.04
Or002	40,743,576	72.50%	24,054,682	59.04%	41.54%	54.40	41.64
Or003	45,288,738	73.60%	26,094,136	57.62%	42.20%	54.31	42.33
Or004	41,780,177	71.56%	24,588,954	58.85%	39.86%	54.57	41.50
Or007	42,900,214	73.48%	31,521,273	73.48%	32.90%	54.11	41.76
Or009	43,575,939	74.16%	25,250,443	57.95%	42.89%	54.84	42.52
Or012	49,810,653	71.64%	31,494,048	63.23%	45.06%	54.72	43.34
Or013	50,909,618	71.48%	31,588,549	62.05%	42.83%	55.27	43.78
Or014	50,939,786	72.84%	31,552,918	61.94%	44.94%	55.17	43.90
Or015	50,193,035	71.87%	31,569,266	62.90%	44.25%	54.56	43.53
Or017	48,622,702	71.98%	30,072,205	61.85%	43.11%	55.16	43.65
Or018	48,138,851	72.01%	30,038,907	62.40%	44.00%	55.00	43.49
Or019	47,755,567	71.81%	30,009,770	62.84%	44.57%	54.65	43.07
Or020	48,798,468	70.84%	29,955,844	61.39%	40.89%	55.05	42.99
Or022	47,053,933	69.91%	29,973,347	63.70%	41.77%	54.62	42.90
Or023	48,393,451	71.93%	30,054,633	62.10%	43.32%	55.14	43.64
Or024	48,056,660	71.77%	30,055,329	62.54%	43.84%	54.94	43.39
Or034	20,877,936	67.21%	13,943,666	66.79%	40.34%	52.09	32.89

TABLE 5 SNP and InDel variation of 18 strains of *H. radicata* in comparison with the reference genome.

Sample	SNP			InDel		
	Transition	Transversion	Total	Deletion	Insertion	Total
Or001	477,282	198,026	675,308	68,233	60,511	128,744
Or002	480,300	198,969	679,269	68,640	60,319	128,959
Or003	478,923	199,418	678,341	69,966	61,529	131,495
Or004	446,140	182,689	628,829	62,148	54,803	116,951
Or007	479,231	199,379	678,610	69,794	61,274	131,068
Or009	485,903	202,872	688,775	72,221	62,693	134,914
Or012	487,966	203,843	691,809	73,192	63,186	136,378
Or013	487,839	203,783	691,622	73,065	63,322	136,387
Or014	488,423	203,966	692,389	73,361	63,598	136,959
Or015	479,016	199,415	678,431	70,238	61,552	131,790
Or017	488,053	203,822	691,875	73,013	63,241	136,254
Or018	488,383	204,034	692,417	73,325	63,559	136,884
Or019	488,012	203,803	691,815	73,156	63,357	136,513
Or020	359,326	143,627	502,953	49,501	43,041	92,542
Or022	479,768	199,655	679,423	70,064	61,484	131,548
Or023	487,935	203,731	691,666	73,117	63,434	136,551
Or024	488,733	204,054	692,787	73,392	63,571	136,963
Or034	441,988	182,141	624,129	60,797	53,482	114,279

minimal genetic difference between the strain populations from Shandong Province and Fujian Province. Strains from Hunan Province and Guizhou Province, as well as those from adjacent provinces, are genetically closer to those from Sichuan Province. Overall, the genetic analysis reveals a close relationship between the strains and their geographic distribution.

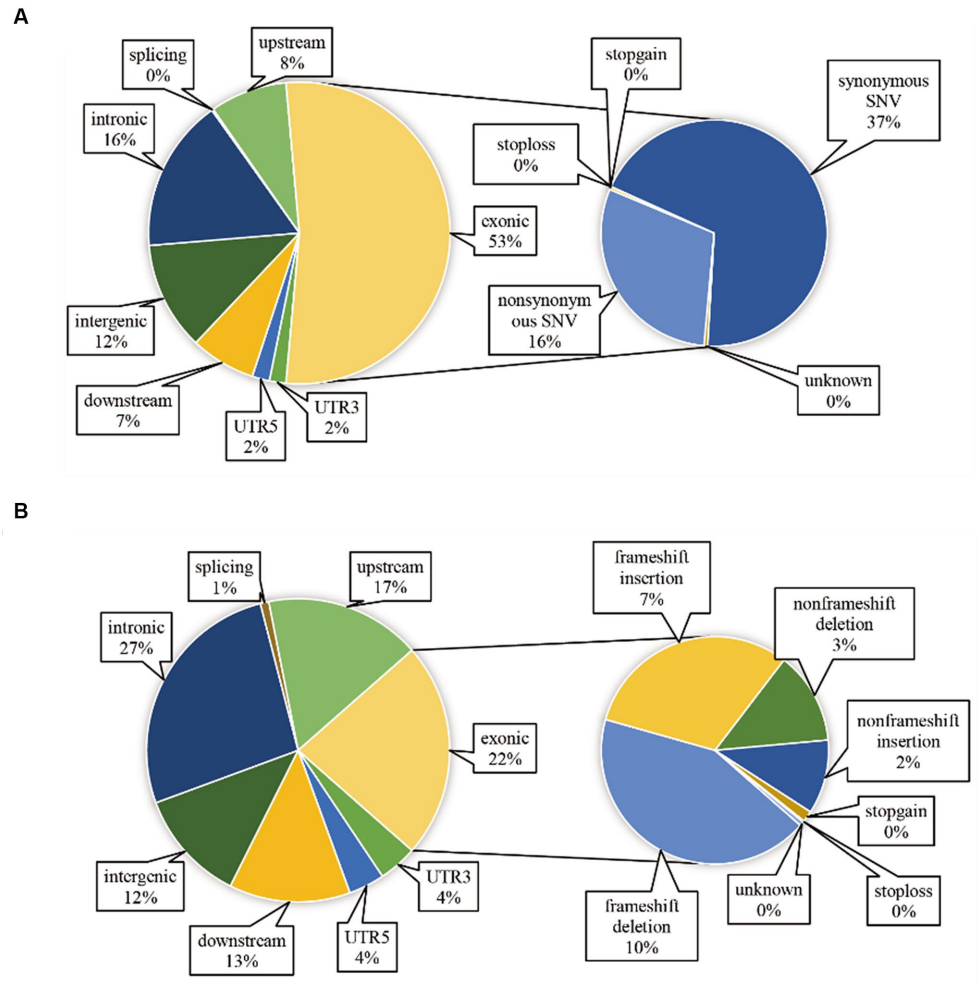

FIGURE 2
Localization and functional annotation of genetic variations in *H. radicata* strains. SNP functional annotation **(A)**; InDel functional annotation **(B)**.

4 Discussion

We re-sequenced strains from various regions and successfully obtained a minimum of 2.3GB of clear data, with a Q30 exceeding 85.33% for each strain. The average genome coverage reached 71.93%. All strains were identified with a reference genome ratio of 12,050,448 SNP sites and 2,335,179 InDel sites. Using the SNP data for group genetic structure, principal component analysis, and constructing a systematic evolutionary tree, 18 strains were categorized into two subgroups. Furthermore, a statistical analysis of the growth rate, yield and fruiting body characteristics of the germ strains in the two subgroups revealed similarities within each subgroup and significant differences between them. The acquisition of this data contributes to understanding the genetic evolution of *H. radicata*.

The study of the evolution of edible fungi is a burgeoning topic. Numerous variables influence the diversification of mushroom populations, including geographical location. Several studies indicate that resequencing technology significantly enhance the effectiveness and accuracy of analysis by exploring the genetic diversity of germplasm resources of edible fungi in different regions (Bao and Xie, 2020). Branco et al. (2017) re-sequenced 55 strains of *Suillus brevipes* to analyze the differentiation process of these strains from different parts of the United States. They found that temperature was related to the genetic evolution of these strains, and some genes responsive to low-temperature stress were also discovered. Re-sequencing 33 *Pleurotus eryngii* populations from Europe and the Gobi Desert environment in China, Dai et al. (2024) discovered several genes involved in stress response and DNA repair connected to the adaptation to the Gobi Desert environment. Re-sequencing *Agaricus bisporus* strains from the Tibetan Plateau and the United States revealed significant independent divergence, as reported by Sun et al. (2019). Additionally, scientists identified a few crucial genes related to the cell wall and membrane that may play a role in the mushroom's growth and development as well as its defensive mechanism against a hostile environment. The genes identified in the study employed to enhance the mushroom's ability to adapt and survive in extreme environments. Moreover, the genetic diversity of the strains was analyzed at the later stages of mushroom molecular breeding. Zhu et al. (2019) re-sequenced *Ganoderma lucidum* isolates from South Korea and China and found many altered genes. The cultivation practices of mushrooms also impacted mushroom populations differently. Wild and domesticated Chinese *Lentinula edodes* were re-sequenced by Xiao et al. (2016). They separated the strains into three subgroups and filtered out 18 genes causing population

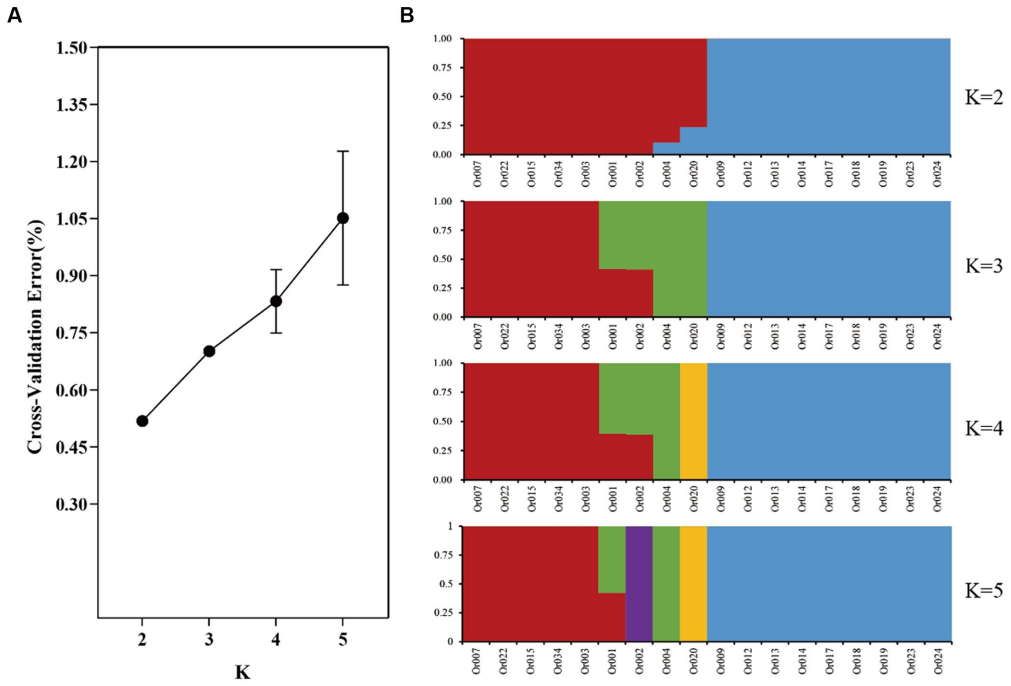

FIGURE 3
Cross-validation error rates **(A)** and the genetic structure of the *H. radicata* population **(B)** simulated by different K values.

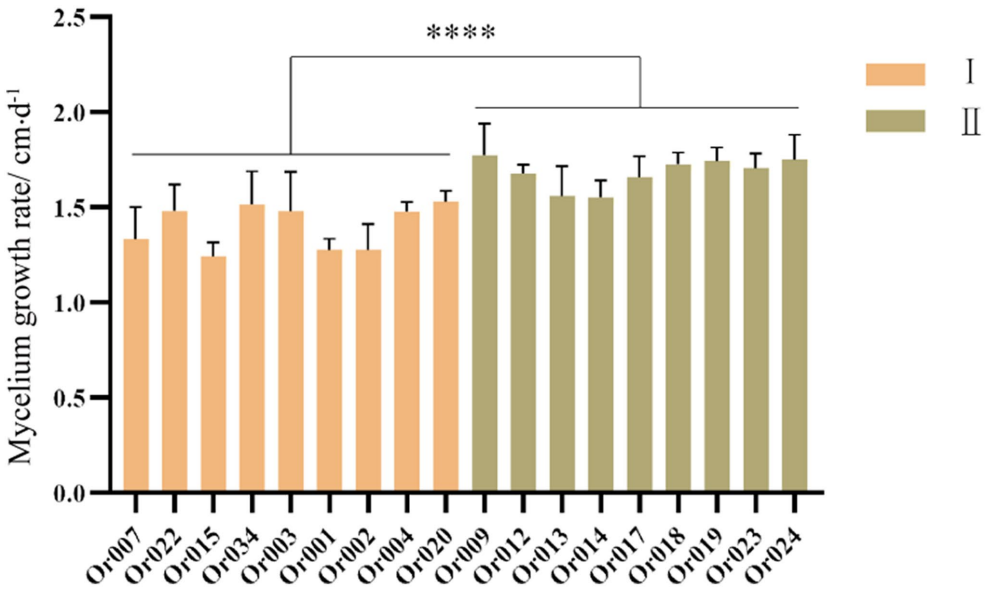

FIGURE 4
Comparison of mycelium growth rate among different strains of *H. radicata*. The value bar with **** indicates $p < 0.0001$.

variations, some of which were connected to stress responses. Re-sequencing 26 strains of *Sarcomyxa edulis* by Tian (2019). The results showed that the genetic distance between wild strain T24 and many cultivated strains was close, and there was gene exchange. It is speculated that these cultivated strains may have evolved from T24 strains. Shen et al. (2020) re-sequenced 28 wild and domesticated strains of *Flammulina filiformis* into five subgroups that were compatible with the breeding history of *F. filiformis*. Resequencing offers the benefit of obtaining information on variant genes as well as variable loci, crucial for environmental adaptation and population divergence. This has the potential to provide insight into the development of new varieties and offer new genetic resources for future breeding. It is also useful for understanding species genetic diversity.

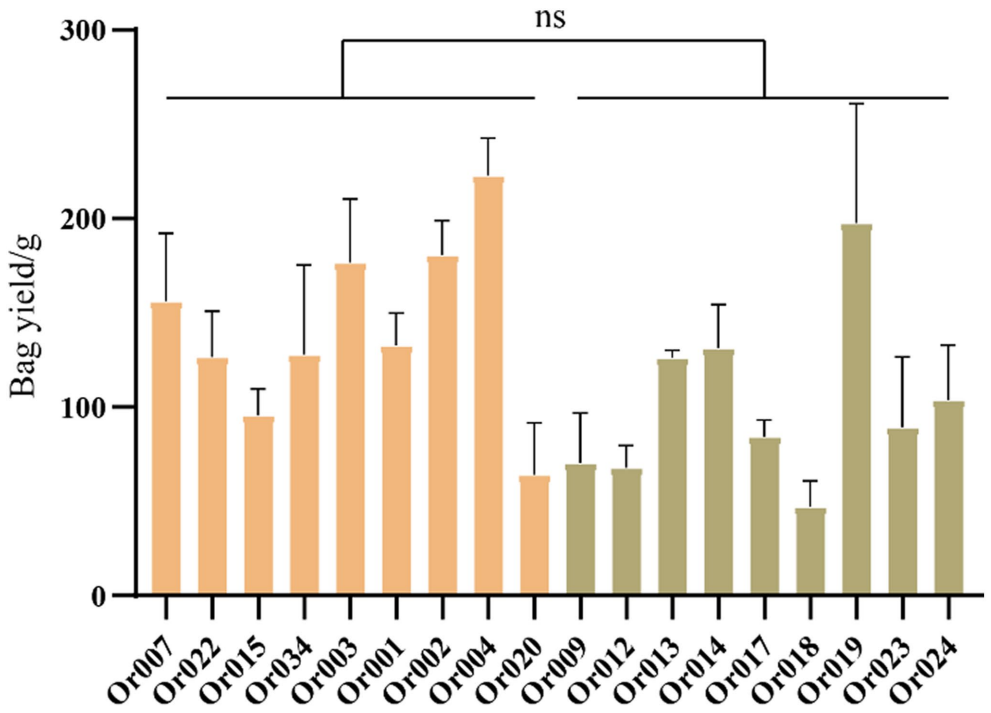

FIGURE 5
Comparison of yield between two subgroups of *H. radicata*. The symbol "ns" indicates not significant.

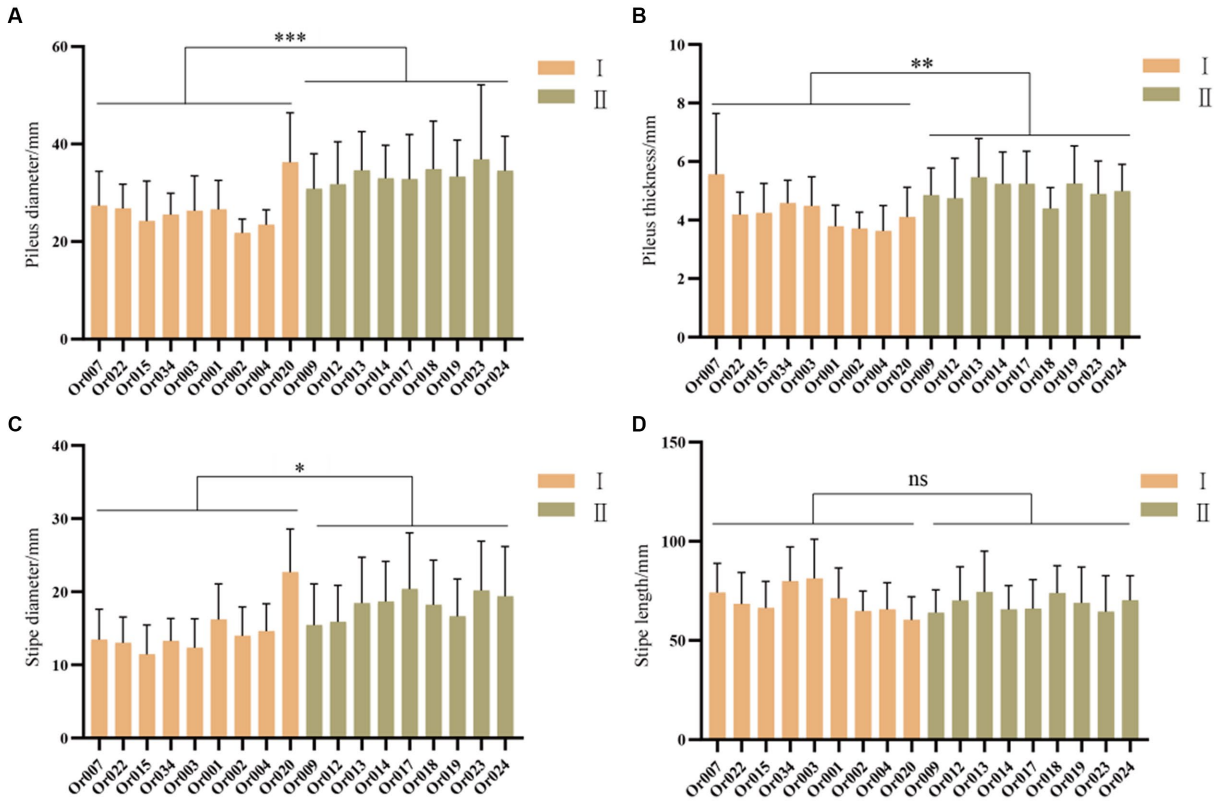

FIGURE 6
Comparison of fruiting body characteristics between two subgroups of *H. radicata*. **(A)** comparison of pileus diameter ($p < 0.001$); **(B)** comparison of pileus thickness ($p < 0.01$); **(C)** comparison of stipe diameter ($p < 0.05$); **(D)** comparison of stipe length ($p = 0.4174$). The symbol "ns" indicates not significant, the symbol "*" indicates $p < 0.05$; the symbol "**" indicates $p < 0.01$; the symbol "***" indicates $p < 0.001$.

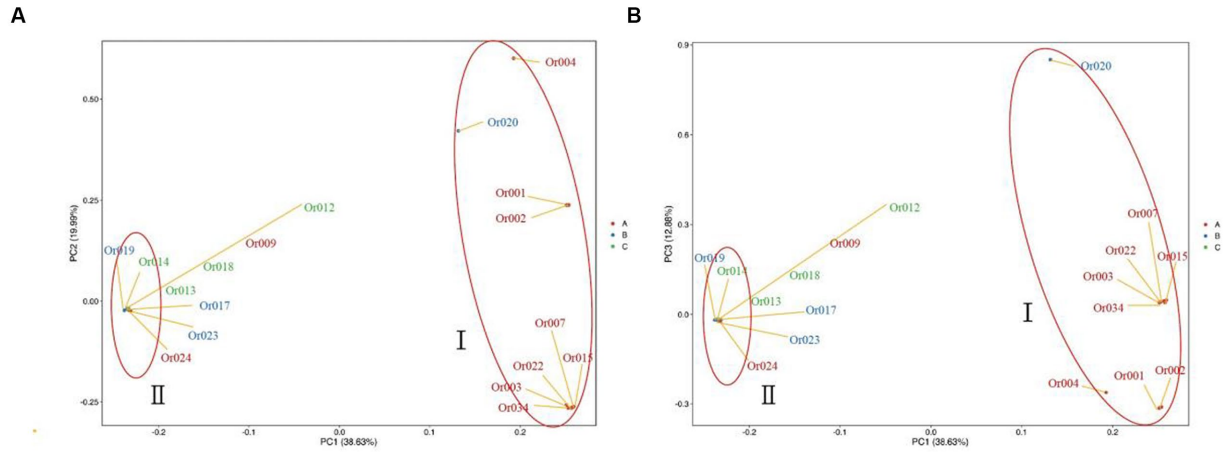

FIGURE 7
Principal component analysis (PCA) of 18 *H. radicata* strains. The numerical colors in the figure represent the strain names, and identical colors indicate similar geographical locations of the strain sources.

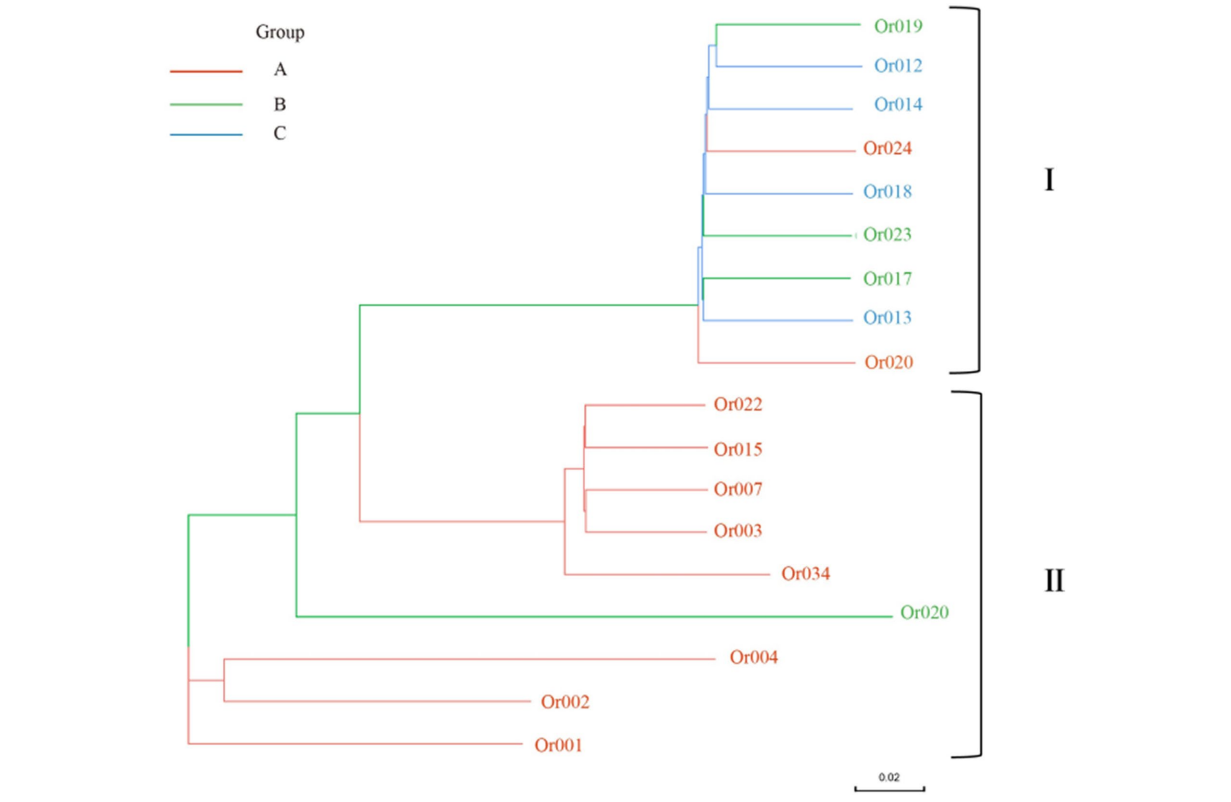

FIGURE 8
Phylogenetic tree of *H. radicata* based on SNP data. Red line A represents strains from Fujian, Jiangsu, and Shandong provinces; Green line B includes strains from Henan, Hubei, and Hunan provinces; blue line C comprises strains from Guizhou and Sichuan provinces.

4.1 Genetic diversity analysis of strains

Currently, numerous articles explore the genetic diversity of edible fungi, such as Agaricus blazei (Wan et al., 2021), Pleurotus eryngii (Lin et al., 2023), Lentinula edodes (Wu et al., 2023), and Agaricus bisporus (Gu et al., 2013). These studies employ SSR, ISSR and other molecular marker technologies to cluster strains. In contrast, our study utilizes resequencing technology to analyze individual differences between strains at the genomic level. Our findings demonstrate that resequencing technology is highly effective in analyzing the genetic diversity of strains.

In our study, significant differences in genetic variation between different strains were observed. Through sequencing analysis, we identified substantial variations in genetic makeup among breeds.

Notably, strain Or020 exhibited significantly fewer SNPs and InDels compared to other strains, followed by strains Or004 and Or034. The presence of fewer mutation sites suggests more conserved sequences in the evolutionary process, indicating higher genetic stability. These strains may be better suited as primary cultivars. Simultaneously, it is noteworthy that among the detected SNPs, variations in all transmutation types were almost twice as many as in transversion types. This variation predominantly occurred in the exon region (53%) and intronic region (16%), encompassing crucial information for protein synthesis and covering most functional variations related to individual phenotypes. Increased variation in these two regions may resulted in greater phenotypic differences between strains, warranting further investigation into this variation. Regarding the detected InDel variants, the number of deletions and insertions was similar. Mutations in the coding region may lead to changes in protein structure and function, thereby influencing the properties of *H. radicata*. The SNP data were utilized for a group genetic structure analysis dividing the test strains into two subgroups (Figure 3B).

The blue-marked subgroups primarily consisted of strains from Fujian and Shandong, including the main Shandong variety Or034. The number of mutations detected in these subgroups was slightly higher than in the other population, suggesting a higher degree of variability in evolution. Strains with greater variability may hold greater potential for molecular breeding. Conversely, the red-marked subgroups mainly comprised strains from inland areas such as Sichuan and Hunan. The number of variations detected in these strains was slightly lower, indicating a more conservative evolution and stable inheritance of desirable traits. In future breeding efforts, we propose crossbreeding strains from the two subpopulations to obtain heterosis strains, playing a significant role in future production. Additionally, it is essential to collect more varieties for domestication, and expand the germplasm bank of *H. radicata*.

4.2 Diversity analysis of fruiting body characters

A comprehensive statistical analysis of yields and fruiting body characteristics across all strains revealed significant differences between the two subgroups in multiple aspects. Thile there is more similarity among strains within the same subgroup, notable differences exist between the two subgroups. Subgroup II demonstrated significant advantages in terms of mycelial growth rate and fruiting body characteristics. However, there was no significant difference in yield traits between the two subpopulations, possibly attributed to greater strain yield variation within subpopulations. In subsequent studies, we recommend hybridizing strains from the two subgroups to select superior strains.

Although the fruiting body characteristics exhibited remarkable quality, the average yield was slightly lower. The comprehensive analysis of cultivation data and biological results demonstrated good consistency, indicating that the selected traits in this study effectively represent the differences and commonalities among strains. These distinctions and similarities are primarily derived from the genetic material of the strains. The study revealed genetic differences among strains but commonalities in yield and fruiting body traits within the same subpopulation. These strains share a common background, potentially representing different strains of the same variety even the same variety. Apart from genetic material, these phenotypic differences and commonalities may also be linked to gene expression and metabolic pathways, which will be the focal point of our future research in analyzing the association between genotype and phenotype.

Furthermore, we observed that strain Or019 exhibits characteristics such as fast mycelial growth, high yield and good fruiting body traits, suggesting its potential as a major cultivar. Similar studies conducted by Lin et al. (2023) on *Pleurotus eryngii* have shown a strong correlation between SNP markers and fruiting body traits, aligning with our findings. In upcoming research, we plan to conduct multi-year cultivation experiments across various regions to investigate the stability of strain yield and fruiting body characteristics. We aim to collect more trait indicators through phenotypic analysis and develop molecular markers for association analysis using the detected variation sites. This will provide essential technical support for variety identification, trait prediction and crossbreeding. Additionally, testing strains' tolerance to biological and abiotic stresses, screening dominant strains, and optimizing cultivation techniques are envisioned to enhance *H. radicata* quality and yield.

5 Conclusion

In this study, we conducted whole-genome re-sequencing on 18 strains of *H. radicata* sourced from different regions in China. The integration of bioinformatics analysis with population genetics allowed us to extract quantitative and positional information about SNPs and InDels. Additionally, the mycelial growth rate, yield, and fruiting body characteristics of the strains were collectively considered to explore commonalities and differences within the population. The 18 materials were categorized into two subgroups, each demonstrating its own set of advantages. Notably, strains within the same subgroup exhibited consistency in both yield and fruiting body characteristics.

For future endeavors, strains from each of the two subgroups can be chosen as parents and crossbred according to breeding objectives, aiming to obtain strains with excellent traits from both subgroups. The molecular markers we identified stand as valuable tools for genetic diversity analysis, gene localization of desirable traits, and the selection of high-quality germplasm in *H. radicata.*

Data availability statement

The original contributions presented in the study are included in the article/supplementary material, further inquiries can be directed to the corresponding author.

Author contributions

LC: Conceptualization, Formal analysis, Investigation, Methodology, Writing – original draft. DY: Investigation, Methodology, Resources, Writing – review & editing. QZ: Data curation, Formal analysis, Methodology, Writing – review & editing. YN: Data curation, Formal analysis, Software, Writing – review & editing. WL: Data curation, Investigation, Project administration, Writing – review & editing. RF: Formal analysis, Software, Supervision,

Writing – review & editing. WM: Formal analysis, Project administration, Software, Writing – review & editing. XZ: Funding acquisition, Resources, Validation, Visualization, Writing – review & editing.

Funding

The author(s) declare financial support was received for the research, authorship, and/or publication of this article. This work was supported by Scientific and Technological Innovation Talents of Sichuan Province (no. 2022JDRC0034), the Agricultural Science and Technology Innovation Program (no. ASTIP-IUA-2023005), Local Financial Funds of National Agricultural Science and Technology Center, Chengdu (no. NASC2021KR06) and Technology Innovation Guidance Program (no. 22CX8NH219).

Conflict of interest

The authors declare that the research was conducted in the absence of any commercial or financial relationships that could be construed as a potential conflict of interest.

The reviewer QL declared a shared affiliation with the authors YN and WL to the handling editor at the time of review.

Publisher's note

References

Alexander, D. H., Novembre, J., and Lange, K. (2009). Fast model-based estimation of ancestry in unrelated individuals. *Genome Res.* 19, 1655–1664. doi: 10.1101/gr.094052.109

Bao, D. P., and Xie, B. G. (2020). Some research directions worthy of attention in the genetics of edible mushrooms in China. *Mycosystema* 39, 971–976. doi: 10.13346/j.mycosystema.200168

Behr, A. A., Liu, K. Z., Liu-Fang, G., Nakka, P., and Ramachandran, S. (2016). Pong: fast analysis and visualization of latent clusters in population genetic data. *Bioinformatics* 32, 2817–2823. doi: 10.1093/bioinformatics/btw327

Bolger, A. M., Lohse, M., and Usadel, B. (2014). Trimmomatic: a flexible trimmer for Illumina sequence data. *Bioinformatics* 30, 2114–2120. doi: 10.1093/bioinformatics/btu170

Branco, S., Bi, K., Liao, H. L., Gladieux, P., Badouin, H., Ellison, C. E., et al. (2017). Continental-level population differentiation and environmental adaptation in the mushroom *Suillus brevipes*. *Mol. Ecol. Resour.* 26, 2063–2076. doi: 10.1111/mec.13892

Chen, S., Zhou, Y., Chen, Y., and Gu, J. (2018). Fastp: an ultra-fast all-in-one FASTQ preprocessor. *Bioinformatics* 34, i884–i890. doi: 10.1093/bioinformatics/bty560

Dai, Y., Sun, L., Yin, X., Gao, M., Zhao, Y., Jia, P., et al. (2024). *Pleurotus eryngii* genomes reveal evolution and adaptation to the Gobi Desert environment. *Front. Microbiol.* 10:10. doi: 10.3389/fmicb.2019.02024

Gong, N., Ma, X. Y., Chen, X., Liu, G. L., Zhao, Y., Xiao, J., et al. (2022). Study on classification of *Oudemansiella raphanipes* based on HPLC and mult gene combined sequence identification. *Northern Horticul.* 18, 117–123. doi: 10.11937/bfyy.1001-0009(2022)18-0117-07

Gu, M., Shen, Y., Jin, Q., Feng, W., Song, T., Tian, F., et al. (2013). Development and application of SSR markers in *Agaricus bisporus*. *Acta Agriculturae Zhejiangensis.* 25, 987–993. doi: 10.3969/j.issn.1004-1524.2013.05.14

Hou, Y. C., Ye, S. C., Liang, J. M., Yan, D. X., Wanyan, H. Y., Cao, B. H., et al. (2022). Extraction technology and in vitro antioxidant activity of polysaccharides from *Oudemansiella radicata*. *Food Sci. Technol.* 47, 203–208. doi: 10.13684/j.cnki.spkj.2022.04.019

Ley, T. J., Mardis, E. R., Ding, L., Fulton, B., McLellan, M. D., Chen, K., et al. (2008). DNA sequencing of a cytogenetically normal acute myeloid leukaemia genome. *Nature* 456, 66–72. doi: 10.1038/nature07485

Li, H., Handsaker, B., Wysoker, A., Fennell, T., Ruan, J., Homer, N., et al. (2009). The sequence alignment/map format and SAMtools. *Bioinformatics* 25, 2078–2079. doi: 10.1093/bioinformatics/btp352

Lian, Y. P., Zhao, G. H., Wu, Z. Q., Yuan, B., Ke, L. N., Zhang, Z. H., et al. (2023). Antagonistic and ISSR molecular markers of *Oudemansiella raphanipes* strains. *Chin. J. Trop. Agric.* 43, 15–20. doi: 10.12008/j.issn.1009-2196.2023.1.004

Lin, J. B., Yan, J. J., Han, X., Zhao, J., Gan, Y., Miao, R. Y., et al. (2023). Population diversity and characters of *Pleurotus eryngii* strains based on whole genome resequencing. *Southwest China J. Agric. Sci.* 36, 1–12. Available at: https://link.cnki.net/urlid/51.1213.S.20230921.1500.066

McKenna, A., Hanna, M., Banks, E., Sivachenko, A., Cibulskis, K., Kernytsky, A., et al. (2010). The genome analysis toolkit: a map reduce framework for analyzing next-generation DNA sequencing data. *Genome Res.* 20, 1297–1303. doi: 10.1101/gr.107524.110

National Plant New Variety Test Standardization Technical Committee. *NY/T 3715–2020 agricultural industry standard of the People's Republic of China*. Beijing: China Agriculture Press, (2020).

Okonechnikov, K., Conesa, A., and Garcia-Alcalde, F. (2016). Qualimap 2: advanced multi-sample quality control for high-throughput sequencing data. *Bioinformatics* 32, 292–294. doi: 10.1093/bioinformatics/btv566

Pan, W. J., Shi, L. L., Ren, Y. R., Yao, C. Y., Lu, Y. M., and Chen, Y. (2022). Polysaccharide ORP-1 isolated from *Oudemansiella raphanipes* ameliorates age-associated intestinal epithelial barrier dysfunction in Caco-2 cells monolayer. *Food Res. Int.* 162:112038 (PA): 112038-112049. doi: 10.1016/j.foodres.2022.112038

Price, A. L., Patterson, N. J., Plenge, R. M., Weinblatt, M. E., Shadick, N. A., and Reich, D. (2006). Principal components analysis corrects for stratification in genome-wide association studies. *Nat. Genet.* 38, 904–909. doi: 10.1038/ng1847

Purcell, S., Neale, B., Todd-Brown, K., Thomas, L., Ferreira, M. A., Bender, D., et al. (2007). PLINK: a tool set for whole-genome association and population-based linkage analyses. *Am. J. Hum. Genet.* 81, 559–575. doi: 10.1086/519795

Shen, Y. Y., Jin, Q. L., Cai, W. M., Fan, L. J., Feng, W. L., Song, T. T., et al. (2020). Analysis of population diversity and structure of *Flammulina filiformis* strains based on whole genome resequencing data. *Mycosystema* 39, 1016–1028. doi: 10.13346/j.mycosystema.200041

Shi, X. K., Cai, Z. X., Guo, Z. J., Lu, Y. P., Chen, M. Y., Liao, J. H., et al. (2019). A preliminary report on resequencing 18 representative strains of *Agaricus bisporus*. *Fujian J. Agric. Sci.* 34, 1167–1172. doi: 10.19303/j.issn.1008-0384.2019.10.008

Shimada, M. K., and Nishida, T. (2017). A modification of the PHYLIP program: a solution for the redundant cluster problem, and an implementation of an automatic bootstrapping on trees inferred from original data. *Mol. Phylogenet. Evol.* 109, 409–414. doi: 10.1016/j.ympev.2017.02.012

Sun, L., Fu, Y., Yang, Y., Wang, X., Cui, W., Li, D., et al. (2019). Genomic analyses reveal evidence of independent evolution, demographic history, and extreme environment adaptation of Tibetan plateau *Agaricus bisporus*. *Front. Microbiol.* 10:1786. doi: 10.3389/fmicb.2019.01786

Tian, F. H. *Evaluation of germplasm resources and genes related to triterpene synthetic pathway of Sarcomyxa edulis in Northeast China*. Changchun: Jilin Agricultural University, (2019).

Wan, C., Li, L. J., Xiong, X., Luo, W. M., and Wang, Y. (2021). Genetic diversity of *Agricus blazei* Murrill germplasm resources. *Edible Fungi China* 40, 11–16. doi: 10.13629/j.cnki.53-1054.2021.09.003

Wang, Y., Jia, J., Ren, X., Li, B., and Zhang, Q. (2018). Extraction, preliminary characterization and in vitro antioxidant activity of polysaccharides from *Oudemansiella radicata* mushroom. *Int. J. Biol. Macromol.* 120, 1760 (PB): 1760-1769–1769. doi: 10.1016/j.ijbiomac.2018.09.209

Wang, K., Li, M., and Hakonarson, H. (2010). ANNOVAR: functional annotation of genetic variants from high-throughput sequencing data. *Nucleic Acids Res.* 38:e164. doi: 10.1093/nar/gkq603

Wu, X. Y., Bao, H. C., Li, X. L., Yu, H. B., Wang, H. X., Yu, C. Z., et al. (2023). ISSR analysis of genetic diversity of 26 *Lentinula edodes* strains. *Seed* 42, 63–67. doi: 10.16590/j.cnki.1001-4705.2023.05.063

Xiao, Y., Cheng, X., Liu, J., Li, C., Nong, W., Bian, Y., et al. (2016). Population genomic analysis uncovers environmental stress-driven selection and adaptation of *Lentinula edodes* population in China. *Sci. Rep.* 6, 1–12. doi: 10.1038/srep36789

Xiao, Z. T., Lin, H. T., Zeng, L. X., He, H. Q., Lin, X., Peng, Y. Y., et al. (2021). Efficient annual cultivation technique of *Oudemansiella raphanipes* (Heipijizong) without soil cover in factory. *China Veg.* 6, 112–114. doi: 10.19928/j.cnki.1000-6346.2021.3026

Yang, Z. L., Zhang, L. F., Mueller, G. M., Kost, G. W., and Rexer, K. H. (2009). A new systematic arrangement of the genus *Oudemansiella* s. str. (Physalacriaceae, Agaricales). *Mycosystema* 28, 1–13. doi: 10.13346/j.mycosystema.2009.01.002

Zhang, Z. F., Wu, C., Cai, W. M, Song, T. T., and Lv, G. Y. (2021). Effects of dehydration and extraction techniques on the physicochemical properties and antioxidant activities of *Oudemansiella radicata* polysaccharides. *J. Food Meas. Charact.* 16, 180–190. doi: 10.1007/s11694-021-01154-8

Zhang, Y. J., Zhang, S., Liu, X. Z., Wen, H. A., and Wang, M. (2010). A simple method of genomic DNA extraction suitable for analysis of bulk fungal strains. *Lett. Appl. Microbiol.* 51, 114–118. doi: 10.1111/j.1472-765X.2010.02867.x

Zhang, C., Zhao, J., Yan, J. J., Mioa, R. Y., Lin, J. B., Li, X., et al. (2022). Optimization of extraction process of total flavonoids from *Oudemansiella raphanipes* by response surface methodology. *China Condiment* 47, 138–143. doi: 10.3969/j.issn.1000-9973.2022.11.026

Zhu, L., Gao, X., Zhang, M., Hu, C., Yang, W., Guo, L., et al. (2023). Whole genome sequence of an edible mushroom *Oudemansiella raphanipes* (Changgengu). *J. Fungi* 9, 266–281. doi: 10.3390/jof9020266

Zhu, F. L., Xu, X. L., Chen, T. Q., Shi, L. C., Miao, X. Q., Lan, J., et al. (2019). The analysis of whole-genome resequencing of *Ganoderma lucidum* originated from South Korea. *World Sci. Technol.* 21, 764–774. doi: 10.11842/wst.2019.04.032

10.3389/fmicb.2024.1287641

Appendix

Agarose gel electrophoresis of the DNA. M: 1 Kb plus DNA ladder marker; 1–18: 18 strains of *H. radicata*.

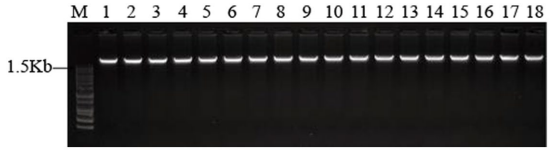

Frontiers in Microbiology

Explores the habitable world and the potential of microbial life

The largest and most cited microbiology journal which advances our understanding of the role microbes play in addressing global challenges such as healthcare, food security, and climate change.

Discover the latest Research Topics

See more →

Frontiers

Avenue du Tribunal-Fédéral 34
1005 Lausanne, Switzerland
frontiersin.org

Contact us

+41 (0)21 510 17 00
frontiersin.org/about/contact